10-22-2018

Electrochemical Behaviors of the Electrodes for Proton Conducting Intermediate Temperature Solid Oxide Fuel Cells (IT-SOFC)

Shichen Sun
ssun006@fiu.edu

FLORIDA INTERNATIONAL UNIVERSITY

Miami, Florida

ELECTROCHEMICAL BEHAVIORS OF THE ELECTRODES FOR PROTON CONDUCTING INTERMEDIATE TEMPERATURE SOLID OXIDE FUEL CELLS (IT-SOFC)

A dissertation submitted in partial fulfillment of

the requirements for the degree of

DOCTOR OF PHILOSOPHY

in

MATERIALS SCIENCE AND ENGINEERING

by

Shichen Sun

2018

To: Dean John L. Volakis
College of Engineering and Computing

This dissertation, written by Shichen Sun and, entitled Electrochemical Behaviors of the Electrodes for Proton Conducting Intermediate Temperature Solid Oxide Fuel Cells (IT-SOFC), having been approved in respect to style and intellectual content, is referred to you for judgment.

We have read this thesis and recommend that it be approved.

_____
Arvind Agarwal

_____
Norman Munroe

_____
Yu Zhong

_____
Anil Virkar

_____
Zhe Cheng, Major Professor

Date of Defense: Oct 22, 2018

The dissertation of Shichen Sun is approved.

_____
Dean John L. Volakis
College of Engineering and Computing

_____
Andrés G. Gil
Vice President for Research and Economic Development
and Dean of the University Graduate School

Florida International University, 2018

DEDICATION

I dedicate this thesis to my parents, Yafen Wang and Yaobo Sun and my girlfriend, Xiuyuan Yang for their consistent support and patience along all these years.

ACKNOWLEDGMENTS

I would like to express my deepest gratitude to my adviser Dr. Zhe Cheng for his continuous support, guidance and encouragement during the project. Working with him has been a constant learning experience for me. Also, I would like to extend my appreciation to Dr. Arvind Agarwal, Dr. Norman Munroe, Dr. Yu Zhong and Dr. Anvil Virkar for serving as my committee members and providing insightful suggestions and guidance throughout the course of this research.

I like to take this opportunity and thank the support of Advanced Materials Engineering Research (AMERI) and Center for Study of Matter at Extreme Conditions (CeSMEC) at FIU for providing facilities.

I am thankful to University Graduate School, FIU for supporting me through Dissertation Year Fellowship (DYF) awards. Last but not the least; I would like to thank my parents and my girlfriend for having faith in me and motivating me in pursuing my goal.

ABSTRACT OF THE DISSERTATION

ELECTROCHEMICAL BEHAVIORS OF THE ELECTRODES FOR PROTON CONDUCTING INTERMEDIATE TEMPERATURE SOLID OXIDE FUEL CELLS (IT-SOFC)

by

Shichen Sun

Florida International University, 2018

Miami, Florida

Professor Zhe Cheng, Major Professor

Proton conducting intermediate temperature (600^{o}C-400^{o}C) solid oxide fuel cells (IT-SOFC) have many potential advantages for clean and efficient power generation from readily available hydrocarbon fuels. However, it still has many unsolved problems, especially on the anode where the fuel got oxidized and the cathode where oxygen got reduced.

In this study, for the anode, the effects of hydrogen sulfite (H_2S) and carbon dioxide (CO_2) as fuel contaminants were studied on the nickel (Ni) based cermet anode of proton conducting IT-SOFC using proton conducting electrolyte of $BaZr_{0.1}Ce_{0.7}Y_{0.1}Yb_{0.1}O_3$ (BZCYYb). Both low-ppm level H_2S and low-percentage level CO_2 caused similar poisoning effects on the anode reaction. The H_2S poisoning effect was also found to be much less than on oxide-ion conducting SOFC, which is attributed to the absence of water

evolution for the anode reaction in proton conducting SOFC. In addition, the H_2S/CO_2 poisoning mechanisms were investigated using X-ray diffraction, energy dispersive spectroscopy (EDS), Raman spectroscopy, and secondary ion mass spectroscopy (SIMS). For H_2S, other than possible sulfur dissolution into BZCYYb, no bulk reaction was found, suggesting sulfur adsorption contributes to the reduced performance. For CO_2, reaction with BZCYYb to form $BaCO_3$ and CeO_2 is identified and is believed to be the reason for the sudden worsening in CO_2 poisoning as temperature drops below ~550^oC.

For the cathode, several representative SOFC cathodes including silver (Ag), $La_{0.6}Sr_{0.4}Co_{0.2}Fe_{0.8}O_{3-\delta}$ (LSCF), LSCF-BZCYYb composite, and $Ba_{0.5}Sr_{0.5}Co_{0.8}Fe_{0.2}O_{3-\delta}$ (BSCF) were evaluated based on BZCYYb electrolyte. LSCF give similar high interfacial resistance as Ag, while LSCF-BZCYYb composite cathode shows lower interfacial resistance, suggesting LSCF behaves like pure electronic conductor cathode in this case. For BSCF, it shows smallest interfacial resistance and the charge transfer process appears to accelerate with the introduction of H_2O, while oxygen adsorption/transport seem to slow down due to adsorbed H_2O. Furthermore, CO_2 was shown to cause poisoning on the BSCF cathode, yet the poisoning was significantly reduced with the co-presence of water. The results suggest that although BSCF seem to display mixed proton-electronic conduction, its strong affinity to H_2O may inhibit the oxygen reduction reaction on the cathode and new cathode materials still need to be designed.

TABLE OF CONTENTS

CHAPTER PAGE

LIST OF TABLES

TABLES PAGE

LIST OF FIGURES

FIGURE PAGE

1 Chapter I: Introduction

1.1 Motivation of the Research

Solid oxide fuel cells (SOFC) are a type of electrochemical energy conversion devices that offer various advantages such as high overall combined heat and electrical efficiency (80-90%), wide range of scales (100W-100MW) and high stack volumetric power density (10 W/cm^3) as well as high specific energy (~1 kWh/kg) over conventional power generation systems. [1-10] However, several problems have been discovered for conventional SOFC based on oxide-ion conducting electrolyte, such as high degradation rate during long-term operation, and high cost for the sealing and interconnect materials. [3, 11, 12] These problems are mainly due to the high operating temperature (at or above 750^oC) for conventional oxide-ion conducting SOFC and have so far interfered with wide adoption of SOFC.

As a result, increasing interest has been drawn to intermediate temperature SOFC (IT-SOFC), the type of SOFC that can operate at intermediate temperature range of 400^oC to 600^oC which is much lower than the operating temperature of conventional oxide-ion conducing SOFC. To achieve reduced operating temperature, proton conducting ceramics (PCC) are found to be promising electrolyte materials due to their high ionic conductivity at intermediate temperature compared to conventional oxide-ion conducting electrolyte materials. [11-15] For example, $BaZr_{0.1}Ce_{0.7}Y_{0.1}Yb_{0.1}O_{3-\delta}$ (BZCYYb) which is one of the leading PCC, shows conductivity of ~$10^{-2}\Omega^{-1}\cdot cm^{-1}$ at 450^oC which is much higher than the conductivity of Yttria-stabilized zirconia (YSZ) (~$2*10^{-4}$ $\Omega^{-1}\cdot cm^{-1}$), which is the most

widely used oxide-ion conducting electrolyte material for conventional SOFC. [15] However, the electrodes (anode and cathode) reaction mechanism have significantly changed as the electrolyte material changes from oxide-ion conductor (e.g. YSZ) to proton conductor, leading to many unsolved questions in the system of proton conducting IT-SOFC.

For conventional SOFC based on oxide-ion conducting electrolyte, the structure typically consists of porous anode (typically a mixture of oxide-ion conducting oxides (e.g. YSZ) and metal catalyst (e.g. nickel (Ni)), dense solid oxide electrolyte (e.g. YSZ) and porous cathode (typically mixed oxide-ion and electron conducting oxides (e.g. $La_{0.6}Sr_{0.4}Co_{0.2}Fe_{0.8}O_{3-\delta}$ (LSCF))). [4, 7, 11]

On the anode side of conventional oxide-ion conducting SOFC, the reaction can be written as follows:

$$H_2 + O_O^{\times} = H_2O + V_O^{\cdot\cdot} + 2e^- \qquad \text{Equation 1.1}$$

As shown in Figure 1. 1 (a), the overall anode reaction pathway involves water evolution and is composed of several other elementary steps including (i) hydrogen (H_2) adsorption on the metal catalyst (e.g. Ni) surface, (ii) dissociation of hydrogen on the metal catalyst surface and diffusion of adsorbed dissociated hydrogen atoms over metal catalyst surface onto the triple-phase boundary (TPB), which is the region between the ion-conducting electrolyte phase (e.g. YSZ), the electron conducting metal phase (e.g. Ni), and the gas phase reaction sites, and (iii) charge transfer on the TPB, including creation of oxide ions (i.e. oxygen vacancies $V_O^{\cdot\cdot}$ or the O^{2-}), generation of water molecule and electrons, and (iv) desorption of water molecules from the TPB.

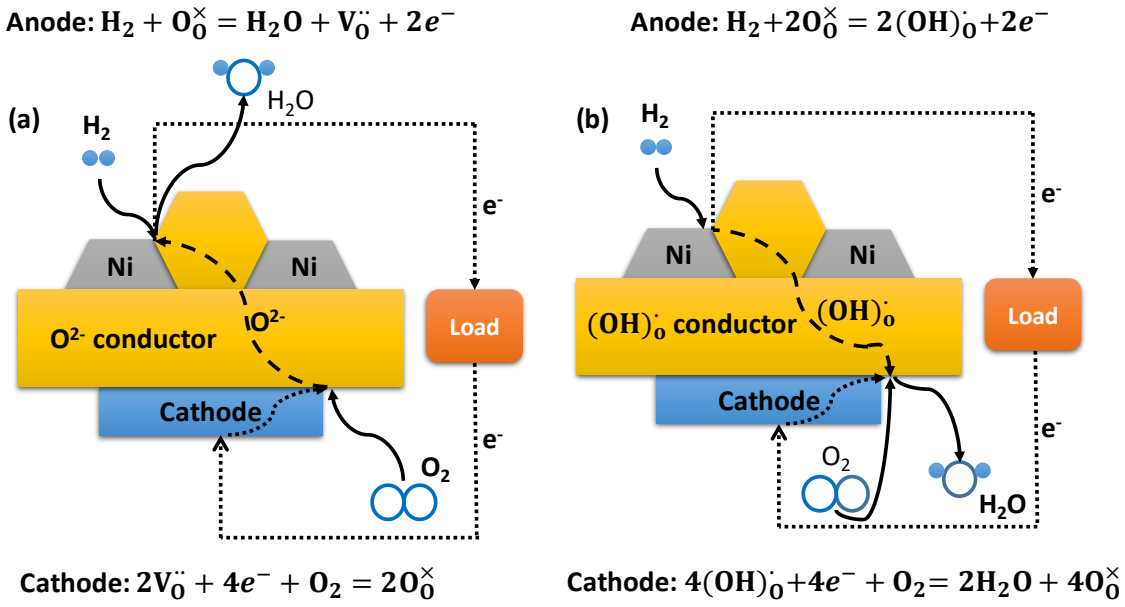

Figure 1. 1 Schematics showing (a) electrodes reaction route for a conventional oxide-ion conducting SOFC, and (b) electrodes reaction route for a proton conducting SOFC.

On the cathode side of conventional oxide-ion conducting SOFC, the overall reaction can be written as following:

$$2V_O^{\cdot\cdot} + 4e^- + O_2 = 2O_O^{\times} \qquad \text{Equation 1.2}$$

As shown in Figure 1. 1 (a), the overall reaction pathway in the cathode also consists of multiple elementary steps including (i) oxygen (O_2) adsorption on the cathode (e.g. LSCF) surface, (ii) dissociation of oxygen on the cathode surface and diffusion to the TPB of cathode; (iii) charge transfer including incorporation of dissociated oxygen and electrons and generation of lattice oxygen.

In comparison, for the ideal reaction process in proton conducting IT-SOFC, the reaction route is different from that for conventional oxide-ion conducting SOFC as shown in Figure 1. 1 (b).

First and most importantly, the conducting species for proton conducting SOFC are protons ($(OH)_O^{\cdot}$) instead of oxide ions (O^{2-}) as in oxide-ion conducting SOFC. In this case, the overall anode reaction can be written as:

$$H_2 + 2O_O^{\times} = 2(OH)_O^{\cdot} + 2e^- \qquad \text{Equation 1.3}$$

Such an anode reaction pathway consists of multiple elementary steps including (i) hydrogen adsorption, (ii) dissociation of adsorbed hydrogen and diffusion of dissociated hydrogen atoms to TPB, and (iii) charge transfer step involving the proton incorporation and generation of electrons in TPB region, *without generation of water*.

For the cathode reaction in proton conducting SOFC, it can be written as following:

$$4(OH)_O^{\cdot} + 4e^- + O_2 = 2H_2O + 4O_O^{\times} \qquad \text{Equation 1. 4}$$

Similarly, the overall cathode reaction pathway consists of several elementary steps as the following: (i) oxygen (O_2) adsorption on the cathode surface, (ii) dissociation of oxygen on the cathode surface and diffusion to the TPB of cathode, and (iii') charge transfer including the generation of water molecule near TPB and lattice oxygen remains and (iv') desorption of generated water on the TPB of cathode.

Even though there have been some studies on the reaction mechanisms for proton conducting IT-SOFC, various issues remain unsolved.

For conventional oxide-ion conducting SOFC, the Ni metal catalyst is the only electrocatalytic active part for hydrogen oxidation in the anode reaction, i.e. step (i) H_2 adsorption, (ii) H_2 dissociation and surface diffusion and are believed to only happen on the metal catalyst surface (e.g. nickel Ni) while oxide-ion conductor (e.g. YSZ) participate only in step (iii) and (iv). On the other hand, previous studies seem to show certain electrocatalytic activity for PCC in hydrogen oxidation [16-19] as in proton conducting IT-SOFC.

Besides that, considering the change in anode reaction process that no longer involve water evolution on the anode, how the anode for proton conducting IT-SOFC respond to different fuel contaminants such as H_2S and CO_2 is still unknown.

On the other hand, for the cathode of proton conducting IT-SOFC, factors that limit the cathode reaction rate, such as material choice and cathode microstructure including grain size, are not well studied yet. Additionally, since H_2O evolution is involved in the cathode reaction for proton conducting IT-SOFC, [20] understanding concerning the H_2O effect on the cathode is required for further improving the cathode materials for proton conducting IT-SOFC. Besides that, CO_2, which is generally not a concern for the cathode of conventional oxide-ion conducting SOFC, should be taken into consideration since PCC, which have high affinity to CO_2 are involved in the cathode reaction for proton conducting IT-SOFC. [21-23]

Studying the issues outlined above is expected to generate new understandings and help optimize the anode and cathode for proton conducting IT-SOFC that operate at temperature down to ~400^{o}C would be designed.

1.2 Research Objectives and Methods

The objectives of this research are to (i) characterize the electrochemical behaviors of the anode for proton conducting intermediate temperature (~400-750^{o}C) solid oxide fuel cells (IT-SOFC) against low-ppm level H_2S and low-percentage level CO_2, and develop new understanding about the underlying reaction mechanism including what role proton conducting ceramics (PCC) play in the anode reaction for proton conducting IT-SOFC (ii) characterize the electrochemical behaviors of several different types of cathode materials for proton conducting IT-SOFC including BSCF, Ag, LSCF and LSCF-BZCYYb facing different atmospheres (e.g. various pH_2O, pO_2 and CO_2) and design better cathode for proton conducting IT-SOFC based on the insight gained above.

In order to achieve the first objective, electrochemical experiments were carried out using low concertation fuel contaminants of H_2S and CO_2 for proton conducting IT-SOFC.

In detail, H_2S, which will cause severe poisoning on the anode for conventional oxide-ion conducting (e.g. Ni/YSZ mixture as anode) due to its strong adsorption on Ni surface with low concentration down to ppm(v)-level, [24-38] and CO_2, which is believed to have strong adsorption on PCC surface while no affinity and reactivity to the Ni surface, [39-42] were used to determine the electrocatalytic role of PCC in the anode reaction for proton conducting IT-SOFC.

The controlled poisoning experiments were carried out on anode-supported and electrolyte-supported full cells with the configuration of Ni-BZCYYb/BZCYYb/LSCF. Electrochemical behaviors of the anode for proton conducting IT-SOFC under typical

operation conditions (e.g. temperature of 750-450^{o}C, atmosphere of 3% H_2O+H_2, etc.) were recorded using electrochemical impedance spectroscopy (EIS) and voltage monitoring under constant current. Furthermore, in order to study the reaction mechanism for the anode reaction without the complexity originated from the cathode and enlarge the poisoning effect on the anode, anode symmetrical cells with the configuration of Ni-BZCYYb/BZCYYb/Ni-BZCYYb were used in this study. Besides that, conventional oxide-ion conducting anode symmetrical cell with the configuration of Ni-YSZ/YSZ/Ni-YSZ will be subjected to similar poisoning conditions for comparison purpose. Characterization techniques such as X-Ray diffraction (XRD), energy dispersive X-Ray spectroscopy (EDS) and secondary-ion mass spectroscopy (SIMS) are applied following the electrochemical response tests on the post-exposure anode or samples under similar reaction circumstances for achieving better understanding the fundamental interaction mechanism between fuel poisons (H_2S and CO_2) and the cermet anode for proton conducting IT-SOFC.

For the second task, cathode materials such as BSCF, Ag, LSCF, and LSCF-BZCYYb composite were studied using proton conducting cathode symmetrical cells based on BZCYYb electrolyte to eliminate possible influence from the anode. Such symmetrical cells were subjected to atmosphere with different pH_2O, pO_2 and pCO_2 in the of 750-450^{o}C. Electrochemical behaviors of various cathode symmetrical cells were recorded under these conditions and the results offer useful insights about the fundamental cathode reaction mechanism for the proton conducting IT-SOFC that are not available before. New cathode

materials and microstructures for proton conducting IT-SOFC are also explored based on the insights gained above.

1.3 Thesis Outline

This dissertation is organized into 7 chapters. Chapter I provides a general introduction to proton conducting intermediate temperature solid oxide fuel cells (IT-SOFC) and some of the remaining challenges and the corresponding motivations for this sudy. Chapter II details the reason for adopting proton conducting IT-SOFC, followed by a review on the unsolved problems for the anode and cathode of proton conducting IT-SOFC and the need for our research. Chapter III and Chapter IV discusses the H_2S and CO_2 poisoning effect on the anode of proton conducting IT-SOFC and their implications on the electrochemical catalytic role of proton conducting ceramics played in the anode reaction. Chapter V discusses the electrochemical responses of several different types of cathode materials to H_2O vapor effect and their implications on understanding cathode reaction mechanism for proton conducting IT-SOFC. Chapter VI discusses the H_2O and CO_2 effect on the $Ba_{0.5}Sr_{0.5}Co_{0.8}Fe_{0.2}O_3$ (BSCF) cathode for proton conducting IT-SOFC and the corresponding explanations. Summary of the major findings in this work and recommendations for future work are provided in Chapter VII.

2 Chapter II: Literature Review

2.1 Proton Conducting Intermediate Temperature Solid Oxide Fuel Cells (IT-SOFC)

2.1.1 Components and Structure of SOFC

Solid oxide fuel cells are a type of energy conversion devices that produce electricity by combining the fuel (e.g. H_2) and the oxidant (typically O_2 in air) through electrochemical reactions. They have a solid electrolyte, which conducts oxide-ion or proton. [1, 2, 4, 7, 8] As shown in Figure 2. 1, the dense electrolyte is located between the porous anode and the cathode, and the anode/electrolyte/cathode trilayer is typically referred to as a single cell or full cell. [3, 4, 9, 10, 43, 44] Fuel gas, typically H_2, is fed to the anode, undergoes oxidation, and releases electrons to the external circuit. On the other hand, oxidant is fed to the cathode, undergoes reduction and accept the electrons from the external circuit. The electricity is produced by the electron flow from the anode to the cathode in the external circuit.

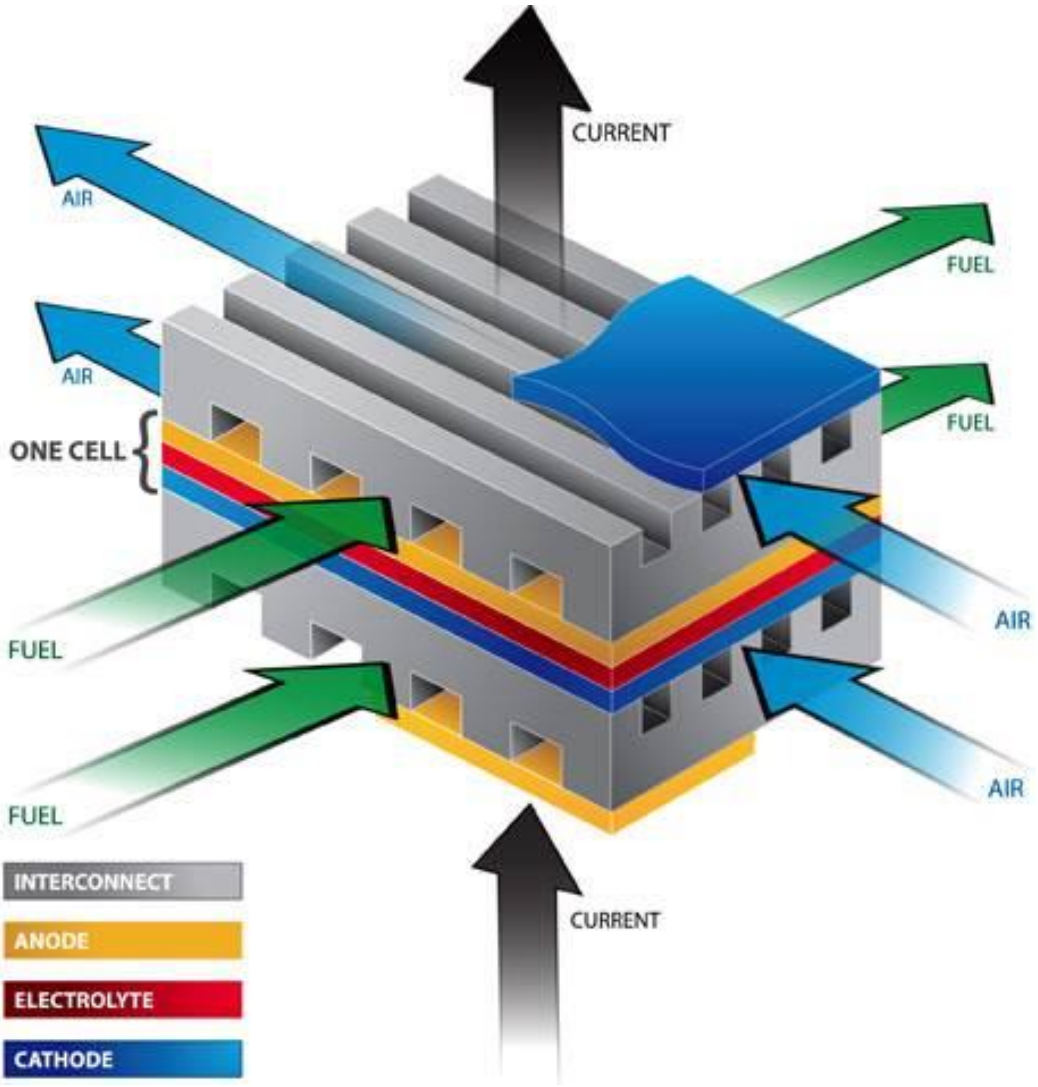

Figure 2. 1 Materials and related issues for SOFC. From Mahato et al. [9]

In an SOFC stack, single cells are connected in electrical series via a component called interconnect as shown in Figure 2. 1, which is typically doped lanthanum chromite or high-temperature metal alloys. [8, 45, 46]

2.1.2 From High Temperature SOFC (HT-SOFC) to Intermediate Temperature SOFC (IT-SOFC)

So far, typical operating temperature for conventional SOFC is relatively high in the range from 1000°C to 700°C, and they are called high-temperature SOFC (HT-SOFC).[11] These HT-SOFC are based on oxide-ion conducting electrolyte, for which the most commonly used is yttria-stabilized zirconia (YSZ) because of its adequate oxide-ion conductivity, and excellent stability in both oxidizing and reducing atmosphere. [1, 2, 11, 43, 47-50] The oxide-ion conductivity for YSZ comes from its high concentration of oxygen vacancies, which are introduced when the Zr^{4+} cations in ZrO_2 is replaced by Y^{3+} cations due to Y_2O_3 doping in ZrO_2, as shown in equation 2.1. [47, 51-54]

$$Y_2O_3 \xrightarrow{ZrO_2} 2Y'_{Zr} + V_O^{\cdot\cdot} + 3O_O^X \qquad \text{Equation 2. 1}$$

For conventional oxide-ion conducting SOFC, Ni-YSZ cermet is widely used as the anode. Ni, which serves as the electronic conductor and fuel (e.g. H_2) oxidation electro-catalyst, is suitable for HT-SOFC operation due to its low cost (comparing with Co and noble metals), reasonable stability against oxidation in fuel mixture even with high H_2O and CO_2 concentration at high temperature of ~1000°C, [47, 55] as well as sufficient electronic conductivity and high electroactivity for fuel (e.g. H_2) oxidation. The YSZ in the cermet anode provides mechanical support for the Ni particles, assures that the anode has similar thermal expansion coefficient (TEC) to other cell components, and inhibits Ni coarsening. [56, 57] In addition, the YSZ also serves as the oxide-ion conductor, which transports oxide-ion to the triple phase boundary of anode and expand the anode reaction

zone. [58] YSZ has been considered to be not electrocatalytic active in fuel oxidation reaction. [47]

For the cathode of HT-SOFC, perovskite (ABO_3) structured oxides are commonly used. Many of them offer low cost, great oxide-ion conductivity, reasonable stability and compatibility, as well as similar thermal expansion coefficient as the electrolyte material (e.g. YSZ). [56, 59, 60] Among those doped perovskite oxides cathodes, Strontium doped Lanthanum Manganite $(La_{1-x}Sr_x)_{1-y}MnO_{3-\delta}$ (LSM), [48, 61-66] Strontium and Iron co-doped Lanthanum Cobaltite $La_{1-x}Sr_xCo_{1-y}Fe_yO_{3-\delta}$ (LSCF) [67-69] and Strontium and Iron co-doped Barium Cobaltite $Ba_{1-x}Sr_xCo_{1-y}Fe_yO_{3-\delta}$, [70-74] show high electrocatalytic activity for oxygen reduction, and high mixed ionic (oxide-ion) and electronic conductivity (MIEC).

The advantages of HT-SOFC comes from its high combined heat and power (CHP) efficiency (~>85%), good modularity, fuel flexibility (meaning both pure H_2 and many hydro-carbon fuels can be used), very low levels of SO_x and NO_x emissions as well as low noise during operation. [3, 5-7, 11]

However, there are still several major issues with the HT-SOFC that have limited the development and deployment of this technology associated with its high operating temperature. Among those issues, the most important ones are the high cost originated from the expensive sealing and interconnect materials that need to tolerate high temperature, high performance degradation rates due to unwanted reactions/diffusions at high temperature, as well as potential mechanical failure due to repeated thermal cycling.

Thus, lowering the operating temperature of SOFC seems attractive, and possibly, necessary for their wider applications. This is because the lowered temperature is expected to slower the degradation due to slower diffusion and interactions between the components. The lower operating temperature may also enable the use of cheaper sealing and interconnect materials that are stable at ~400-600^{o}C (e.g. stainless steel or even graphite). Besides that, the reduced operating temperature could also enhance the durability during long-term thermal cycling due to less thermal stress and lower thermal mismatch. [12, 13, 75]

However, for SOFC to operate at lower temperature in the range of ~400 - 600^{o}C, the main challenges are related to high electrolyte resistivity and electrode polarization loss.[13] For common oxide-ion based electrolyte material in HT-SOFC, dramatic decrease in ionic conductivity was observed at intermediate temperature: For the example of YSZ elecrolyte, its ionic conductivity is only ~10^{-4} ohm^{-1}cm^{-1} at 450^{o}C comparing with ~10^{-2} ohm^{-1}cm^{-1} at 750^{o}C. [15] Therefore, in order to still use YSZ as the electrolyte at intermediate temperature, tremendously reduced YSZ thickness (by ~10-100 times) is required to compensate for its low ionic conductivity. However, this may lead to significant decrease in durability and high cost (associated with <1um thin-film deposition).

Alternatively, electrolyte material with higher ionic conductivity at intermediate temperature range could be adopted. For example, other oxide-ion conducting electrolytes such as gadolinium-doped ceria (GDC) shows higher ionic conductivity at reduced temperature. However, the ionic conductivities of those electrolyte materials are still not high enough, and for GDC the open circuit voltage (OCV) is low due to electronic leakage.

Thus, electrolyte materials that have even higher ionic conductivity with lower electronic leakage are required.

2.1.3 From Proton Conducting Ceramics to Proton Conducting IT-SOFC

2.1.3.1 Proton Conducting Ceramics: Conductivity and Stability

Recently, proton conducting ceramics (PCC), mainly acceptor doped barium or strontium cerates or zirconates, [76-86] are found to be promising electrolyte materials for IT-SOFC due to their high ionic conductivities and low electronic leakage at intermediate temperature. For example, the ionic conductivity of $BaZr_{0.1}Ce_{0.7}Y_{0.1}Yb_{0.1}O_{3-\delta}$ (BZCYYb) is ~10^{-2}ohm^{-1}cm^{-1} at 450^{o}C as shown in Figure 2. 2, [15] which matches the conductivity of YSZ at 750^{o}C. The high ionic conductivity of PCC in principle allows much lower operation temperature of SOFC towards 450^{o}C. [15, 79, 82, 83, 85, 87-89]

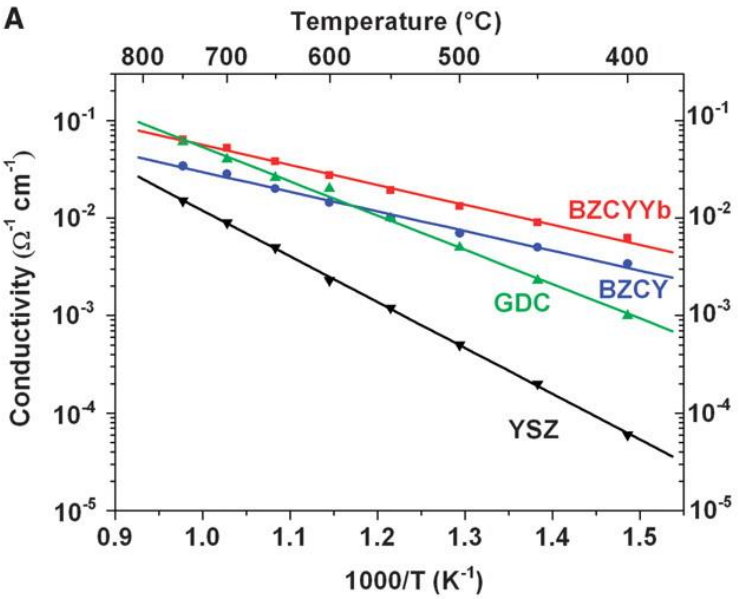

Figure 2. 2 Ionic conductivities of BZCYYb, $BaZr_{0.1}Ce_{0.7}Y_{0.2}O_{3-\delta}$ (BZCY), Gadolinium doped ceria (GDC), and YSZ as measured at 400° to 750°C in wet oxygen (with ~3 vol % H_2O). From Yang et al. [15]

The high ionic conductivity for such PCC is mainly due to the conduction of proton ($H_i^{\cdot}$ or $OH_O^{\cdot}$) instead of the oxide-ion ($V_{\ddot{o}}$ or O^{2-}), especially in atmospheres with high partial pressure of water and at temperature lower than 700°C. [15, 88, 90] Such proton conduction is based on the creation of proton defects from oxygen vacancies and water adsorbed from surrounding atmosphere, and the defect reaction can be written as following: [77]

$$O_o^x + V_{\ddot{o}} + H_2O \leftrightarrow 2OH_O^{\cdot} \text{ or } V_{\ddot{o}} + H_2O \leftrightarrow OH_O^{\cdot} + H_i^{\cdot} \qquad \text{Equation 2. 1}$$

The proton can migrate or transfer from one lattice oxygen atom to a neighboring lattice oxygen, as illustrated in Figure 2. 3 below. [81, 91, 92]

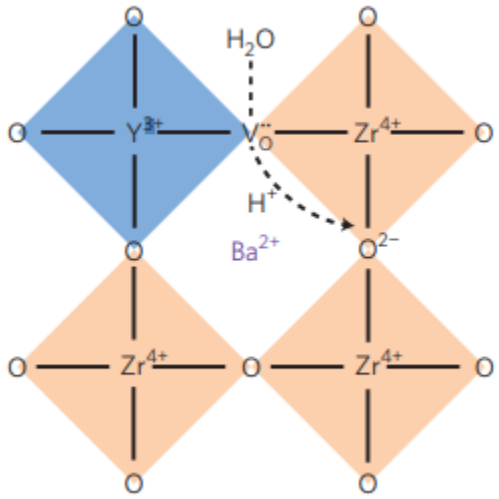

Figure 2. 3 Proton incorporation and conduction mechanisms in conventional perovskite proton conductors (for example, Y-doped $BaZrO_3$). From Zhou et al. [92]

It's worth mentioning that PCC may display both proton conductivity and oxide-ion conductivity, especially when the surrounding water partial pressure is low (e.g. $pH_2O < 10^{-4}$) or operation temperature is too high (T > 700°C). [76, 77, 90] However, proton conductivity is reported to dominate for PCC in humidified atmosphere with water concentration at or above 3% and at temperature significantly below 700°C. The implication is that oxide-ion conductivity can be neglected, and PCC would demonstrate pure proton conduction under most IT-SOFC operation conditions ($T \leq 600$°C with humidified fuel fed to the anode and ambient air containing ~2-3% H_2O fed to the cathode). [76, 77, 80, 88]

The stability of PCC has been reported to depend on various factors. For example, PCC with high concentration of Ce are found to be reactive to high concentration of CO_2.[41, 79, 89]. Those with high Zr content show better stability against CO_2 as well as H_2S. [41] On the other hand, when CO_2 concentration is low, the materials can be stable.

The compatibility between PCC and other cell components, mainly the electrodes also depends on specific materials and conditions. For the cathode, reaction involving the diffusion of Ba^{2+} from $BaCe_{0.9}Y_{0.1}O_{2.95}$ to $Ba_{0.5}Sr_{0.5}Co_{0.8}Fe_{0.2}O_{3-\delta}$ was observed for co-firing temperature above 950°C. [72]

2.1.3.2 Proton Conducting IT-SOFC

When using proton conducing ceramics (PCC) as the electrolyte materials for IT-SOFC, they are called proton conducting IT-SOFC. Typical proton conducting IT-SOFC

also consists of three parts (anode/electrolyte/cathode) similar as oxide-ion conducting SOFC as mentioned in section 1.1.

Apart from the general advantages for conventional oxide-ion SOFC such as high efficiency, high power density and modularity as well as low emission, proton conducting IT-SOFC also possess a few unique benefits. For example, there is in principle no anode-side fuel dilution in proton conducting IT-SOFC because the water is generated on the cathode or air side during operation, which could increase fuel utilization. In addition, when hydrocarbon fuels (e.g. methane) are used, the co-production of electricity and high-value hydro-carbons such as ethylene might be achieved. [93] Furthermore, CO_2 capture and sequestration will also be much easier in proton conducting IT-SOFC because, as stated, H_2O is generated in the cathode side and naturally separated from CO_2. Additionally, recently studies suggest that proton conducting IT-SOFC may display enhanced resistance to fuel contaminants such as H_2S. [12, 13, 75, 94]

Despite the advantages that proton conducting IT-SOFC offers, as stated in section 1.1 there are still many challenges and unknowns, especially about the anode and cathode reaction processes. The following sections will present some of the previous studies on the anode and cathode reaction processes for proton conducting IT-SOFC related to this study and when applicable, how they compare with conventional oxide-ion conducting SOFC.

2.2 Anode for Proton Conducting IT-SOFC

2.2.1 Anode Reaction Process for Oxide Ion Conducting SOFC and Proton Conducting IT-SOFC

The anode materials for proton conducting IT-SOFC are similar to oxide-ion conducting SOFC: both are cermets consisting of metal catalyst (typically Ni) and ceramic electrolyte as the ion conductor (e.g., BZCYYb as PCC electrolyte versus YSZ as the oxide-ion conducting electrolyte). However, due to the change in the ionic species in the electrolyte there are significant differences in anode reaction processes between these two types of SOFC, which will be briefly reviewed below.

For the oxide-ion conducting SOFC, the overall anode reaction as described in section 1.1 ($O_O^x + H_2(g) \leftrightarrow V_O^{\cdot\cdot} + H_2O + 2e^-$) can be separated into several elementary steps as shown in Figure 2. 4. [95, 96]

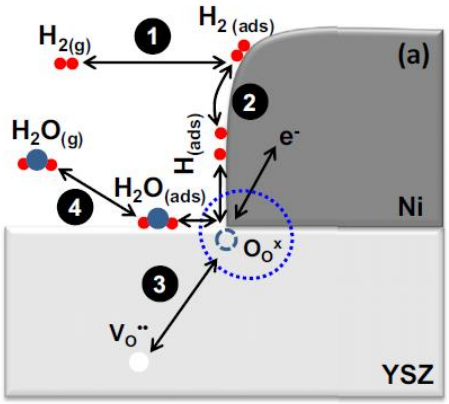

Figure 2. 4 Schematic diagram of the anodic reaction process for H_2 electrochemical oxidation around the anode (Ni)/electrolyte (YSZ) interfaces for a conventional oxide-ion conducting SOFC.

Specifically, step (1) represents the gas phase diffusion and adsorption of H_2 that occur near the surface of the metal (e.g. Ni) catalyst, which can be written as Equation 2.4.

$$H_2(g) \leftrightarrow H_2(ads)$$ Equation 2.4

Steps (2) is the dissociation of adsorbed H_2 and the diffusion of dissociated hydrogen atoms onto triple phase boundary (TPB), which is believed to happen on the surface of the metal catalyst and can be written as:

$$H_2(ads) \leftrightarrow 2H(ads)$$ Equation 2.5

Steps (3) is the charge transfer step, which includes combining the adsorbed hydrogen atoms with the lattice oxygen in the oxide-ion conducting electrolyte (e.g. YSZ) to form H_2O while generating oxygen vacancy and releasing electrons. [97, 98] This step can be written as:

$$2H(ads) + O_O^x \leftrightarrow V_O^{\cdot\cdot} + H_2O(ads) + 2e^-$$ Equation 2. 6

The last step (4) is the desorption of the water generated on the TPB of anode to the atmosphere, which can be written as:

$$H_2O(ads) \leftrightarrow H_2O(g)$$ Equation 2. 7

In comparison, for proton conducting SOFC, especially when it is operated at intermediate temperature (≤~600^{o}C), the major carrier will be protons. [99] The overall anode reaction changes to $H_2 + 2O_O^x \leftrightarrow 2(OH)_O^{\cdot} + 2e^-$. Similar to oxide-ion conducting SOFC, this reaction can still be separated into several elementary steps as shown in Figure 2. 5.

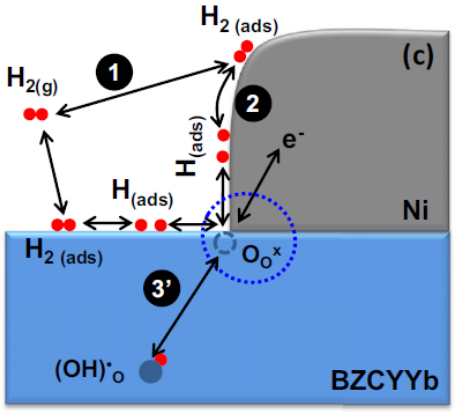

Figure 2. 5 Schematics showing anode reaction steps for ideal pure PC-SOFC at intermediate temperature. Note that the anode reaction mechanism for PC-SOFC is greatly simplified and the exact process including the dominating pathway still needs to be studied. In addition, BZCYYb stands for the $BaZr_{0.1}Ce_{0.7}Y_{0.1}Yb_{0.1}O_{3-\delta}$ PCC electrolyte.

Similar to oxide-ion conducting SOFC, step (1) and (2) are still hydrogen gas phase diffusion then adsorption and dissociation of adsorbed hydrogen then diffusion to TPB, respectively. However, in proton conducting SOFC, apart from Ni surface, these two steps might also occur over PCC surface as suggested from earlier studies. For example, power density of ~100mW/cm^2 was achieved by Hirabayashi et al. using $BaCe_{0.76}Y_{0.2}Pr_{0.04}O_{3-\delta}$ based proton conducting electrolyte-supported full cell without conventional anode. [16] In another study by Tomita et al., power density of ~60mW/cm^2 was achieved using anode-less $BaCe_{0.8}Y_{0.2}O_{3-\delta}$ (BCY20) based electrolyte-supported cell. [17]

Step (3') is the anode charge transfer step for proton conducting IT-SOFC, which involves the incorporation of adsorbed hydrogen atoms into lattice oxygen to form proton defects (labeled as $(OH)_O^{\bullet}$ or $H_i^{\bullet}$) and the release of electrons. This step can be written as:

$$H(ads) + O_O^x \leftrightarrow (OH)_O^{\cdot} + e^- \quad \text{Equation 2.9}$$

Step (3') is different from the anode charge transfer step in oxide-ion conducting SOFC in the sense that no water generation is involved, and the defects created are protons instead of oxygen vacancies.

Lastly, unlike the anode reaction in oxide-ion conducting SOFC, there will be no subsequent water desorption because no water is generated in the anode reaction for proton conducting IT-SOFC.

However, despite the knowledge gained on general anode reaction process for proton conducting IT-SOFC, very little is known about the effects of major fuel contaminants in hydro-carbon fuel (e.g. H_2S and CO_2) on the anode reaction of proton conducting IT-SOFC. Because of the change in overall anode reaction process for proton conducting IT-SOFC compared to oxide-ion conducting SOFC, different responses to these fuel contaminants can be expected and are worth investigating. Such studies are important since in the near term, the primary fuel for proton conducting IT-SOFC will still be readily available hydro-carbon fuels instead of pure hydrogen.

2.2.2 Anode H_2S Poisoning Effect on Oxide-ion Conducting SOFC and Proton Conducting IT-SOFC

Among all fuel contaminants, H_2S is always encountered because it is either contained directly in the hydro-carbon fuels such as bio gas and natural gas or formed through the fuel reforming process during the operation. Since Ni is the metal catalyst in the cermet anode of proton conducting IT-SOFC (as well as oxide-ion conducting SOFC) and it is

known to be very sensitive to H_2S poisoning, [24-38] studies focusing on the H_2S poisoning effect on the anode of proton conducting IT-SOFC will be needed.

For proton conducting IT-SOFC, as stated, very few studies have been carried out on the H_2S poisoning effect. On the other hand, hydrogen permeation membrane based on Ni-PCC cermet material shows great similarity to the anode of proton conducting IT-SOFC in terms of material (Ni-PCC), conducting species (proton) and operating atmosphere (reducing atmosphere containing H_2). Thus, studies about the H_2S effect on hydrogen permeation membrane is expected to offer some insights for the H_2S effect on Ni-PCC cermet anode in proton conducting IT-SOFC and will be described as below. Thus, the following summarizes the existing studies on H_2S poisoning effect on both proton conducting IT-SOFC and hydrogen permeation membranes.

- Tomita et al. (2006) [17]

Tomita et al. were the first to report the H_2S effect on proton conducting SOFC. The authors studied the H_2S effect on the proton conducting cell with painted Pt cathode and BCY electrolyte with the thickness of 1mm, as well as Au current collector on the anode side (no other metal).

For such a cell, no change in impedance spectra was observed with the introduction of up to 10ppm H_2S at 800^oC as shown in Figure 2. 6. The authors attributed the high tolerance to H_2S to the Ce-rich phase on the surface of the heat-treated BCY, which has low reactivity to H_2S.

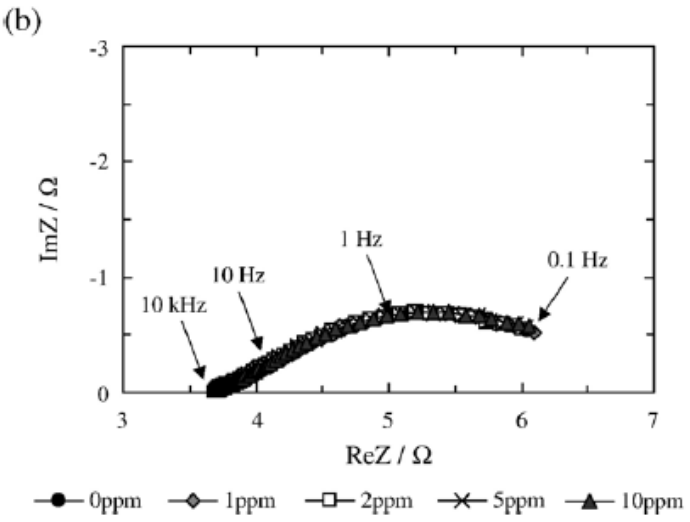

Figure 2. 6 Impedance spectra of the cell using heat-treated BCY20 with 0–10 ppm H2S and 80% H_2 at 800 °C. The frequency range was 0.1–105 Hz. From Tomita et al. [17]

However, there were many questions remain unsolved in this study. For example, such a cell lacks typical anode structure consisting of Ni and PCC for proton conducting IT-SOFC and thus the knowledge gained in this study cannot be directly applied to proton conducting IT-SOFC. Secondly, the exact composition/structure for the BCY electrolyte was not clear. This is because the authors mentioned the BCY electrolyte was heat-treated in air at 1700^{o}C for 10 hours before the cell fabrication presumably following the reaction 2.10 as described below:

$$BaCe_{0.2}Y_{0.2}O_{3-\delta} \rightarrow BaO(g) + Ce_{0.8}Y_{0.2}O_{1.9} \qquad \text{Equation 2.10}$$

However, since no phase characterization results for different parts of the cell was provided, the actual cell structure was doubtable given the complexity of the reactivity for the BCY system. [89] In addition, how the system will perform at 600-400^{o}C, which is the

targeted operating temperature for proton conducting IT-SOFC, is not clear. Moreover, electrochemical measurements other than impedance spectroscopy such as discharge under constant current are also required for achieving solid understanding of the H_2S effect on the anode reaction for proton conducting IT-SOFC.

- Fang et al. (2008,2009) [100, 101]

Fang et al. studied the H_2S poisoning effect on the Ni-$BaZr_{0.1}Ce_{0.7}Y_{0.2}O_{3-\delta}$ (BZCY) hydrogen permeation membrane with the thickness of ~0.5 mm. As shown in Figure 2. 7, at 700^oC, the hydrogen permeation flux quick decreased by about 20% when 30ppm of H_2S was first introduced to the feed gas consisting of ~1.5% H_2O+ 58%N_2+40% H_2 and then slowly degraded until steady state. Further decrease of the hydrogen flux by about 10% was also observed with the increase of H_2S concentration to 60ppm. In comparison, at higher temperature of 900^oC, almost no degradation in hydrogen flux with the introduction of 30-60ppm of H_2S in the feed gas was observed as shown in Figure 2. 8. On the other hand, when the H_2S concentration was further increased to 80-300 ppm, the decreases in hydrogen flux were much larger as shown in Figure 2. 7 (b).

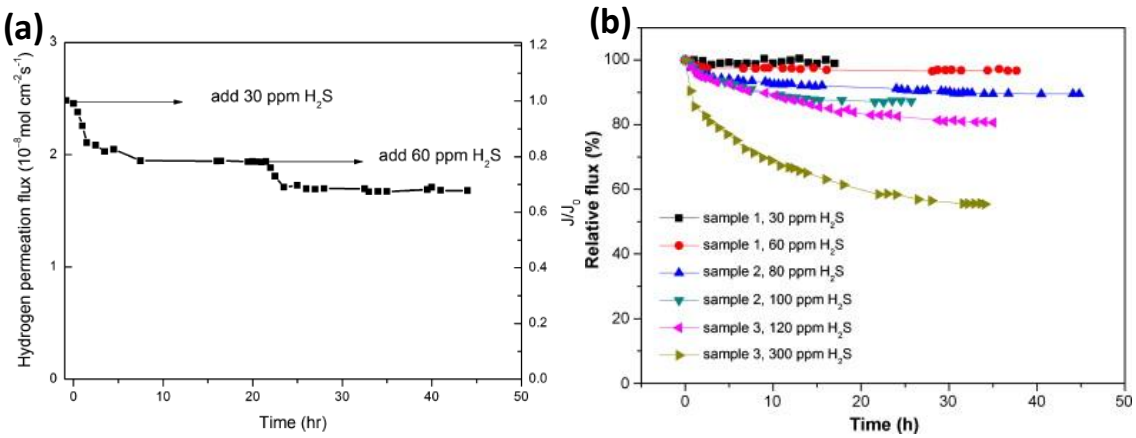

Figure 2. 7 Change in hydrogen permeation flux through Ni–BZCY hydrogen permeation membrane with the introduction of 30-60ppm H_2S in gas mixture of ~1.5% H_2O+ 58%N_2+40% H_2 at 700°C. Adapted from Fang et al. [100]

The authors also studied the regeneration behavior of the Ni-BZCY membrane after H_2S poisoning. As shown in Figure 2. 8 (b), the hydrogen permeation flux largely recovered after the removal of 60ppm H_2S from feed gas at 700°C. At 900°C, complete recovery was observed for the hydrogen flux after the removal of 120 ppm H_2S.

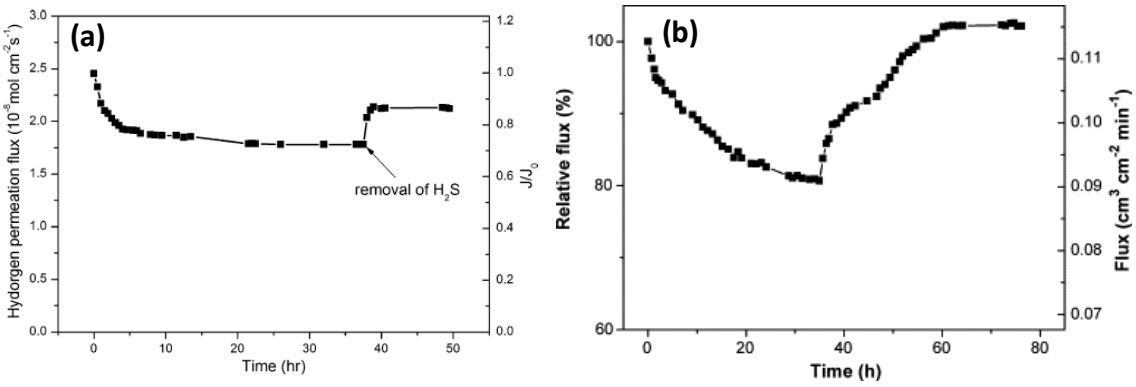

Figure 2. 8 Sulfur poisoning and regeneration behavior of Ni–BZCY in the feed gas (~1.5% H_2O+ 58%N_2+40% H_2) containing 60ppm H_2S at 700°C and 120ppm H_2S at 900°C. Adapted from Fang et al. [101]

Besides the hydrogen permeation measurements, XRD was used on the Ni-BZCY membrane before and after exposing to H_2S in the feed gas (~1.5% H_2O+ 58%N_2+40% H_2) as shown in Figure 2. 9. At 700^oC, very little amount of Ni_3S_2, doped CeO_2 and BaS were found in the post-exposure sample by XRD, suggesting very limited reaction between the Ni-BZCY and H_2S. [100, 102] EDX results indicated that around 5% atomic ratio of sulfur species on the surface of BZCY. Because if all of the BZCY on the surface was transformed into BaS and doped CeO_2, the sulfur content would be ~20%, this indicates the reaction between BZCY and H_2S was incomplete.

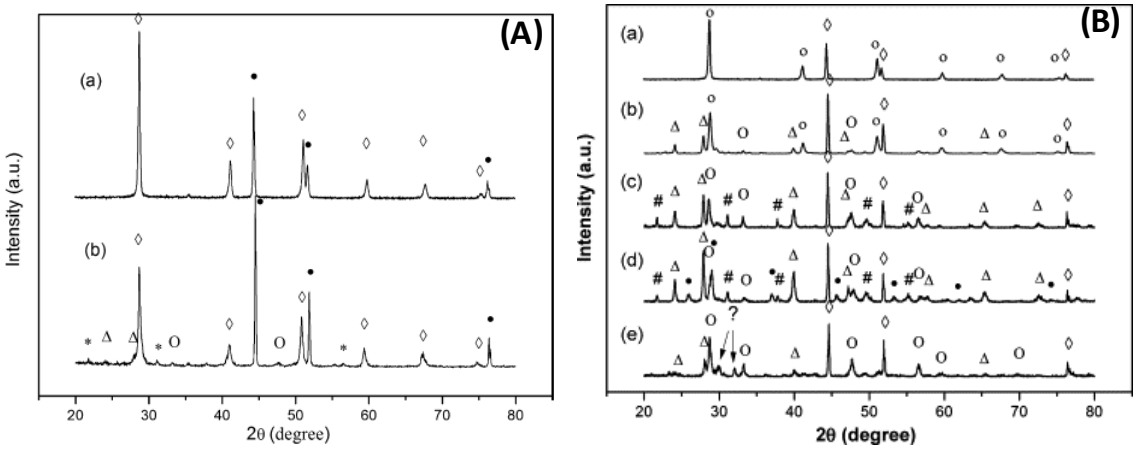

Figure 2. 9 XRD patterns of Ni-BZCY obtained from (A) a polished surface after sintering, (B) feed side surface after testing in 60ppm H_2S at 700^oC. Secondary pahses are: (◊) BZCY, (●) Ni, (*) Ni3S2, (O) doped CeO_2, (Δ) BaS. Adapted with change from Fang et al. [100]

The authors attributed the H_2S poisoning effect on the Ni-BZCY membrane to the bulk phase reaction between H_2S and BZCY at high temperature of ~900^oC. In fact, thermodynamic calculation was carried out in the study, and the results suggested the driving force for the reaction becomes larger as the change in Gibbs free energy gets

more negative at lower temperature as shown in Figure 2. 10 (A). In addition, the dependence of the critical H_2S concentration for the reaction 2.11 also decreases as the temperature falls as shown in Figure 2. 10 (b). This indicates that the reaction is thermodynamically more favored at higher H_2S concentrations or lower temperatures.

$$H_2S(g) + BaCeO_3(s) = H_2O(g) + BaS(s) + CeO_2(s) \qquad \text{Reaction 2.11}$$

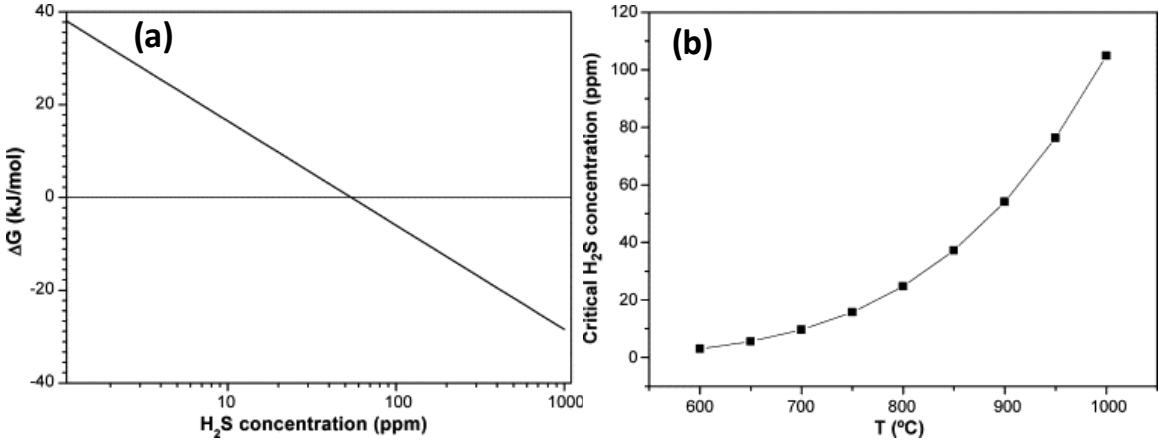

Figure 2. 10 Dependence of Gibbs free energy change for reaction (1) on H_2S concentrations with 0.015 atm H_2O at 900 °C. Temperature dependence of critical H_2S concentration for reaction (1) with 0.015 atm H_2O. Adapted from Fang et al. [101]

On the other hand, when the temperature was low of ~700ºC, very little reaction was observed between the BZCY and H_2S. Since the bulk reaction was thermodynamically more favorable at lower temperature, the limited reaction observed at 700ºC was attributed to the slow kinetics such as slow diffusion. Thus, the poisoning effect of H_2S on Ni-BZCY at 700ºC was attributed by the authors to the adsorption of H_2S over Ni and BZCY surfaces.

However, this study was carried out on Ni-BZCY hydrogen permeation membrane which has certain difference compared to the anode of proton conducting IT-SOFC. In addition, studies at even lower temperature of 600-400^{o}C is still needed. Moreover, more sensitive surface characterization of Ni-PCC sample after exposing to H_2S is also required to achieve better understanding about the origin of the H_2S poisoning effect and the nature of interactions between sulfur and PCC such as BZCY.

- Yang et al. (2009) [15]

Yang et al. (2009) studied the influence of low-ppm level H_2S on the Ni-BZCYYb/BZCYYb/BZCY-LSCF anode-supported full cells. The observations are that at 750^{o}C with a current density of 700mA/cm^2, there are no change in cell voltages with the introduction of up to 30ppm H_2S in 3%humidified (labeled as wet) H_2 fuel for both cells at as shown in Figure 2. 11 (A).

Moreover, similar sulfur tolerance was observed for Ni-BZCYYb/SDC/LSCF anode-supported full cell and the impedance data showed no increase in interfacial resistance in 3%humidified H_2 containing 20ppm H_2S as shown in Figure 2. 11 (B). However, when the water was absent in the fuel stream, significant increase of ~80% in interfacial resistance was observed for that cell with the introduction of 20ppm H_2S into dry H_2 as shown in Figure 2. 11 (C).

The authors hypothesized water may adsorb on the BZCYYb surface to facilitate the oxidation of H_2S or elemental sulfur to SO_2 at or near active sites, which can easily desorb. [103]

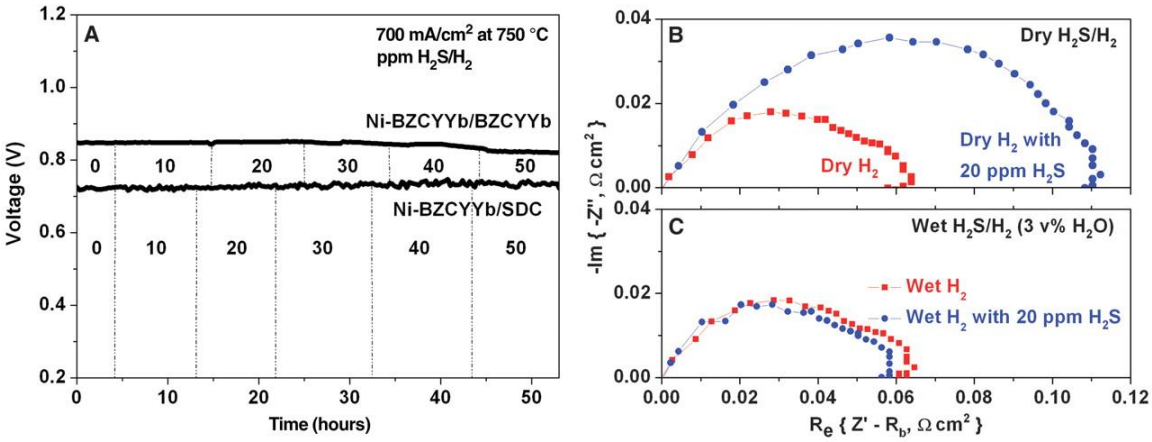

Figure 2. 11 (A) The change in cell voltage at 750°C for two cells with the configuration of Ni-BZCYYb/ BZCYYb/ BZCY-LSCF and Ni-BZCYYb/ SDC/ LSCF operated at 750^{o}C under the constant current density of 700 mA/cm^2 as 10-50ppm of H2S was introduced to the 3%humidified H_2 fuel stream, (B and C) Impedance spectra measured under OCV conditions at 750°C for the Ni-BZCYYb/ SDC/ LSCF anode-supported full cell in both (B) dry H_2 and dry H_2 containing 20 ppm H_2S and (C) wet H_2 and wet H_2 containing 20ppm H_2S. from Yang et al. (2009) [15]

However, no information about the impedance of the Ni-BZCYYb/BZCYYb/LSCF anode-supported full cell was showed. The response to low-ppm level H_2S for such cell at intermediate temperature of 400-600^{o}C is still not clear. Moreover, two of the cells used in the study was based on thin electrolyte (~20um) of SDC and YSZ, which may react with the BZCYYb in the anode and form proton conducting phases. [89]

For better understanding of the H_2S effect on the anode reaction of proton conducting IT-SOFC, it will be helpful to refer to the similar studies on H_2S effect of the conventional oxide-ion conducting SOFC, especially those operated at relatively low temperature (~750^{o}C). This is because as stated before, despite the change in the anode reaction process, both the anode in proton conducting IT-SOFC and oxide-ion conducting SOFC contain Ni as metal catalyst and is sensitive to H_2S. The similarity and also the difference between

these two types of cells are expected to provide some insight for the H_2S poisoning effect on proton conducting IT-SOFC. Because the problem of H_2S poisoning for conventional oxide-ion conducting SOFC has been extensively studied and well documented, there are many available reviews, and will not be repeated here. Only one representative study at relevant temperature of 750°C by Yang et al. is given below as an example.

- Yang et al. (2010) [35]

Yang et al. studied the H_2S poisoning effect on the Ni-YSZ/YSZ/LSCF oxide-ion conducting anode-supported full cell. At 750°C, increases in interfacial resistance of ~40%-80% were observed with the introduction of 1ppm H_2S into H_2 fuel at different current density in the range of 800-200mA/cm^2, as shown in Figure 2. 12.

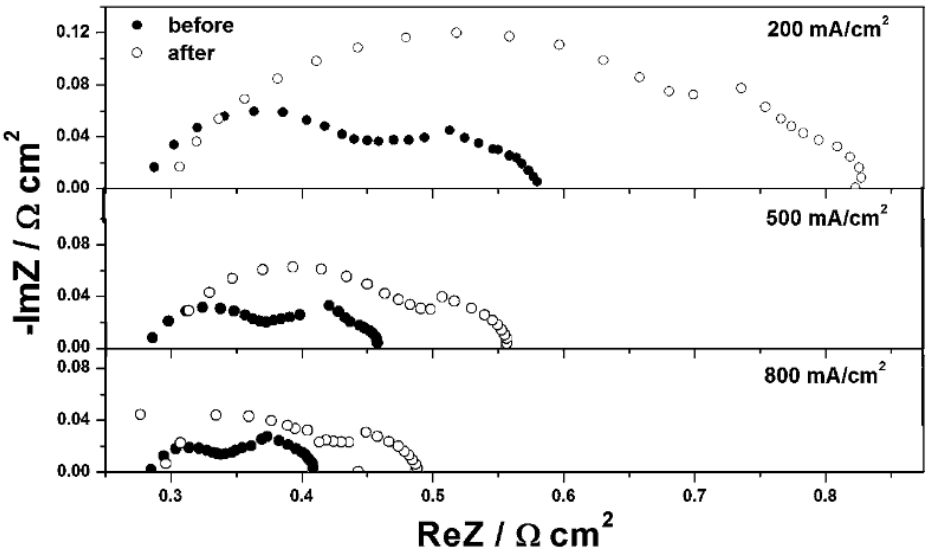

Figure 2. 12 Impedance spectra of Ni-YSZ/YSZ/LSCF anode-supported full cells operated at a constant current density of 200, 500, and 800 mA/cm^2 before and after 1 ppm H_2S was introduced into the fuel at 750^{o}C. From Yang et al. [35]

In addition, instant drops in the cell power output of ~10-15% upon the exposure to 0.8-1.1 ppm H_2S in H_2 at the current density of 200 and 400mA/cm^2 was observed as shown in Figure 2. 13 (a). On the other hand, when 10 ppm H_2S was introduced to the H_2 fuel at the current density of 200 and 400 mA/cm^2, slightly larger decreases were observed for the cell voltage as shown in Figure 2. 13 (b).

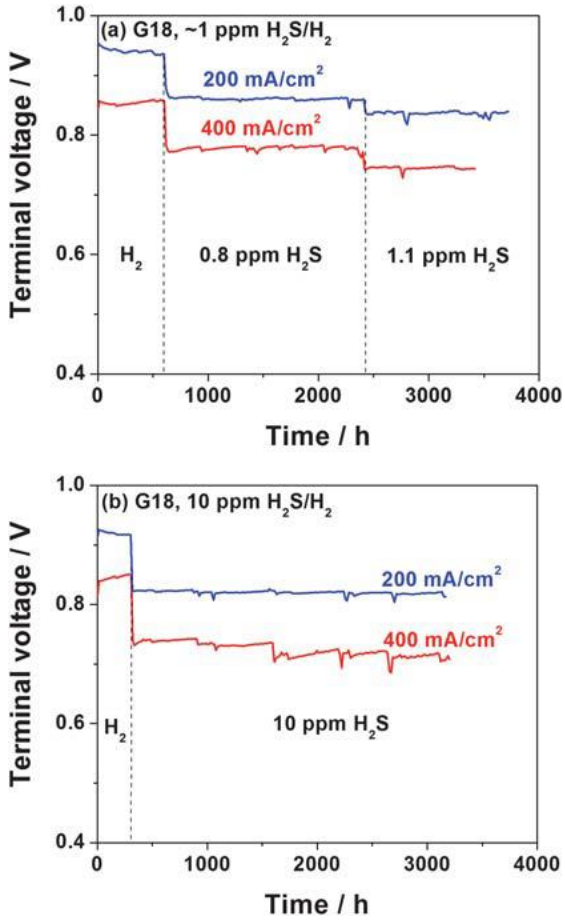

Figure 2. 13 Performances of the Ni-YSZ/YSZ/LSCF anode supported full cells operated at 750C at a constant current density of 200 and 400 mA/cm^2 in hydrogen for the first

~600 h and then in hydrogen with (a) 0.8-1.1 ppm H_2S, and (b) 10ppm H_2S. From Yang et al. [35]

In summary, even though there have been several studies reflecting the H_2S poisoning effect on the proton conducting electrode as mentioned above, most of these researches were carried out at relatively high temperature (≥700^oC). In addition, from the comparison, the H_2S poisoning on proton conducting IT-SOFC appears very different from conventional oxide-ion conducting SOFC, suggesting significant change in the poisoning process and the underlying mechanism. Thus, systematic studies focusing on H_2S poisoning of proton conducting IT-SOFC, especially at intermediate temperature of 400-600^oC is required. Detailed investigation on the interaction between the H_2S and proton conducting cermet anode is also expected to help understand the fundamental poisoning mechanism.

2.2.3 Anode CO_2 Poisoning Effect on Proton Conducting IT-SOFC

Unlike the widely-studied poisoning effect of H_2S on the anode reaction for SOFC, the CO_2 effect has rarely been studied as CO_2 typically is believed to be harmless for the anode reaction of conventional oxide-ion conducting SOFC. The chemisorption between the Ni catalyst and CO_2 is thought to be insignificant in fuel atmosphere and there is no reaction between the conventional oxide-ion conductor of YSZ and CO_2. [104]

On the other hand, certain extent of CO_2 poisoning could be expected for the cermet anode of proton conducting IT-SOFC, which contains PCC that are known to be vulnerable

to CO_2. So far, there are numerous studies on the reactivity of proton conducting ceramics (PCC) electrolyte with CO_2 as stated in section 2.1.3.1. [39-42] However, electrochemical behaviors of proton conducting IT-SOFC upon exposure to CO_2 as an anode fuel contaminant are not clear.

Similar to H_2S poisoning effect, existing studies about the CO_2 effect on Ni-PCC is mainly in the field of hydrogen permeation membrane and no study is available on proton conducting IT-SOFC. Nevertheless, due to the similarity between the hydrogen reaction for those two types of devices, these studies are expected to offer useful background information about the CO_2 poisoning effect on the cermet anode for proton conducting IT-SOFC and are described below.

- Zuo et al. (2005, 2006) [105, 106]

Zuo et al. studied the percentage-level CO_2 poisoning effect on Ni-$BaZr_{0.8-x}Ce_xY_{0.2}O_3$ ($0.4 \leq x \leq 0.8$) membranes with the thickness of ~0.5-0.75 mm at 900°C. As shown in Figure 2. 14 (a), instant drops in hydrogen flux were observed for the Ni-BZCY6 (x=0.6) membrane with the introduction of 10-30% CO_2 into the wet feed gas of 40%H_2 balanced by He. The decrease in hydrogen flux is proportional to the concentration of CO_2 in feed gas. The initial quick drops were followed by saturation after exposure to CO_2 for ~20 hours under all concentrations. Similar poisoning effect was observed for Ni-BZCY8 (x=0.8) membrane with the introduction of 10% CO_2 in feed gas as shown in Figure 2. 14 (b). However, as CO_2 concentration further increased to 20%-30%, much more severe poisoning effect was observed for Ni-BCY20 membrane with decrease of ~80%-100%

after more than 20 hours of exposure. This dramatic CO_2 poisoning for Ni-BCY20 membrane was attributed to the bulk phase reaction between BCY20 and CO_2 with concentration ≥20% to form $BaCO_3$.

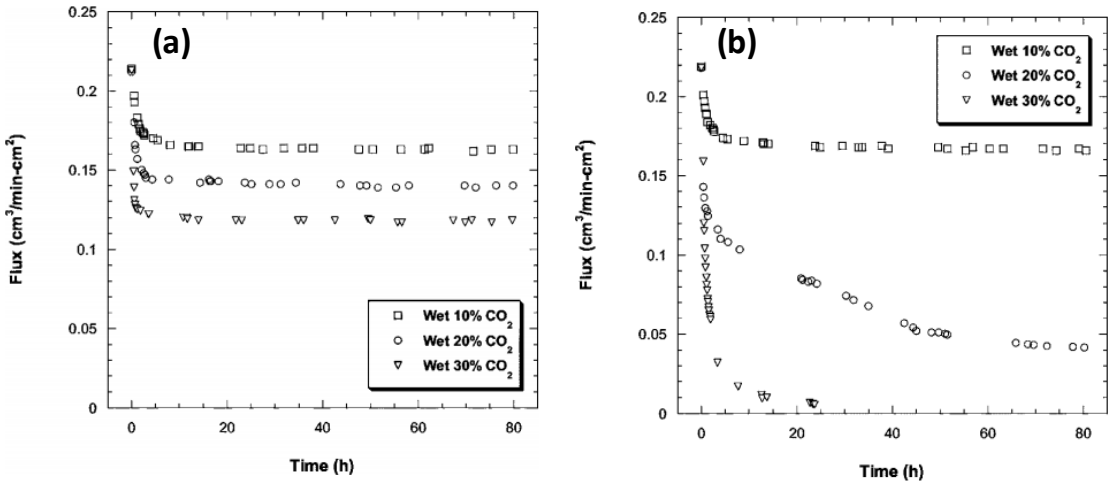

Figure 2. 14 Hydrogen flux through (a) Ni-BZCY6 and (b) Ni-BZCY8 membranes in wet feed gas (40% H_2/He) containing different concentrations of 10-30%CO_2 at 900°C. From Zuo et al. [105]

Zuo et al. also studied the influence of Zr doping concentration on the CO_2 poisoning effect for hydrogen permeation through Ni-BZCY membranes as shown in Figure 2. 15. The relative drop in hydrogen permeation flux decreased with increasing Zr concentration, meaning the substitutional doping of Zr in Yttrium-doped barium cerate can significantly increase the stability against CO_2 poisoning.

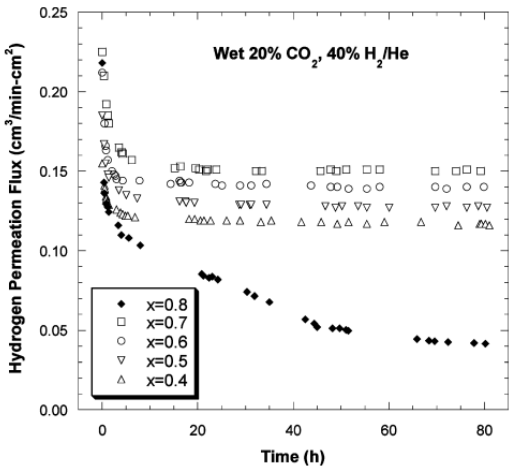

Figure 2. 15 Time dependence of hydrogen flux through Ni-$BaZr_{0.8-x}$ $Ce_xY_{0.2}O_3$ ($0.4 \leq x \leq 0.8$) membranes in a feed gas of wet 20% CO_2 (balance 40% H_2/He) at 900 °C. From Zuo et al. [106]

However, the origin of the observed CO_2 poisoning had not been well illustrated using convincing experiments in this study. Moreover, no information was provided at testing temperature lower than 900^{o}C.

- Fang et al. (2013, 2014) [107, 108]

Fang et al. studied the CO_2 poisoning effect on Ni-BZCYYb as hydrogen permeation membrane with the thickness of 0.4mm at 900^{o}C. When the feed gas contains no water, significant increases in hydrogen flux were observed with the introduction of 5-60% CO_2 into feed gas consisting of 20%H_2+75-15% He as shown in Figure 2. 16. The authors attributed such enhanced hydrogen permeation to the co-presence of CO_2 and H_2 and the occurrence of reverse water-gas shift (RWGS) reaction as below:

$$H_2(g) + CO_2(g) = H_2O(g) + CO(g)$$ Reaction 2. 12

This was supported by the large increase in the moisture content with the introduction of CO_2 into feed gas as also shown in Figure 2. 16.

The water generated from RWGS reaction was believed to increase the proton conductivity of the BZCYYb membrane and thus promoted the hydrogen permeation under these conditions.

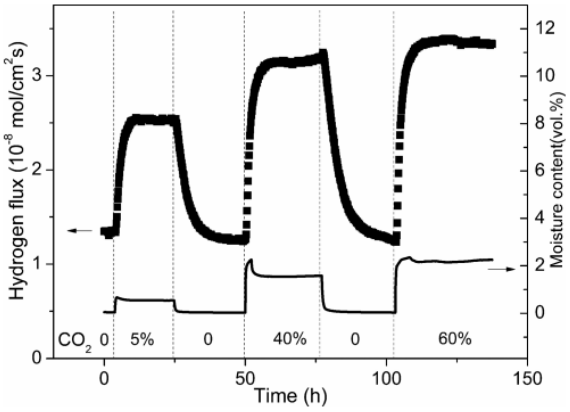

Figure 2. 16 Hydrogen permeation fluxes of the Ni-BZCYYb membrane (lower line) and absolute humidity in feed gas passing through the reactor (upper line). The feed gas consisted of 20% H_2, 5-60% CO_2, and 75-20% He. From Fang et al. [107]

However, when the feed gas already contains 3% H_2O, then the response of Ni-BZCYYb composite membrane to the introduction of CO_2 was complex as shown in Figure 2. 17. When 30% CO_2 was introduced, initial increases in the hydrogen permeation fluxes were observed in all conditions. However, after the initial increases, subsequent behaviors depend on H_2 concentration: when H_2 was high at 60%, similar enhancement in hydrogen flux was observed as the steady-state flow was higher than that prior to CO_2 introduction; when H_2 was low at 40% and 20%, the steady-state fluxes

were lower than those prior to CO_2 introduction, indicating CO_2 poisoning, which is consistent with earlier study by Zuo et al. [105, 106]

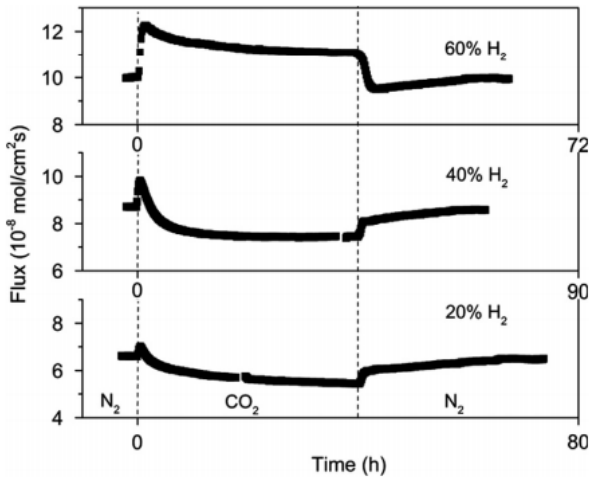

Figure 2. 17 Time dependence of hydrogen flux of the Ni-BZCYYb membrane in 20-60% H_2 balanced with 3% H_2O, 30% CO_2, and 47-7% He, respectively. From Fang et al. [108]

The degradation was attributed to the formation of secondary phases such as $BaCO_3$, doped-CeO_2, and carbon on the Ni-BZCYYb surface that inhibited the hydrogen flux which was confirmed by the XRD and Raman spectroscopy on the Ni-BZCYYb membrane after exposing to up to 60% CO_2 and recovering in wet 40% H_2+N_2+He at 900^{o}C for 912 h followed by fast cooling in the same atmosphere. As shown in Figure 2. 18, secondary phases such as $BaCO_3$, doped-CeO_2, and carbon were detected by XRD for the sample. In addition, Raman spectroscopy also identified the existence of $BaCO_3$, CeO_2 or $BaCeO_3$ and carbon, which correspond to the Raman peaks labeled as CO_3^{2-}

(140, 220, 700 and 1065 cm^{-1}), Ce-O (478cm^{-1}) or Ce-O (353cm^{-1}), and C (1353 and 1582 cm^{-1}), respectively in Figure 2. 20.

The authors attributed the formation of these secondary phases to the reaction between the CO_2 with BZCYYb. The reason why CO_2 showed poisoning effect in humidified feed gas is because the RWGS reaction was limited by the existing high H_2O content, and the CO_2 concentration would be higher than that in dry feed gas.

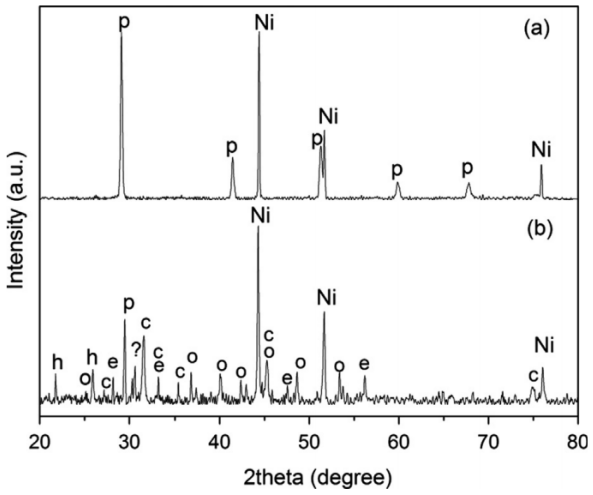

Figure 2. 18 XRD patterns obtained from the fresh (a) and tested (b) Ni–BZCYYb membrane. p: BZCYYb, h: hexagonal $BaCO_3$, o- orthorhombic $BaCO_3$, c: carbon, e: doped-CeO_2, ?: unknown phase. From Fang et al. [108]

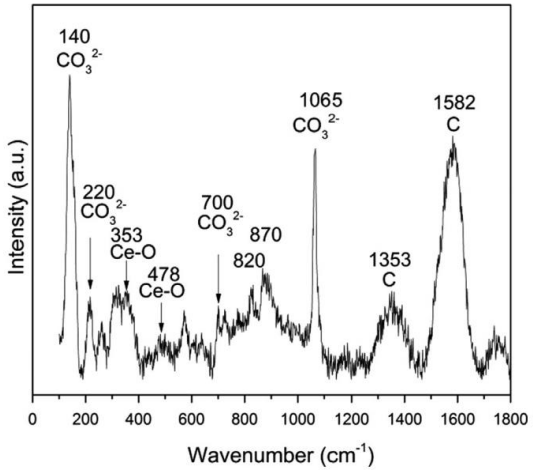

Figure 2. 19 Raman spectrum obtained from feed side surface of Ni–BZCYYb membrane after exposure to wet CO_2 and recovery without CO_2. From Fang et al. [108]

However, at intermediate temperature of 400-600^oC, since the RWGS reaction is thermodynamically unfavorable, how would the system will respond to CO_2 effect is not clear. In addition, as stated, since the Ni-BZCYYb hydrogen permeation membrane is not an SOFC, how the knowledge gained in this study can be leveraged to proton conducting IT-SOFC is of interest.

2.3 Cathode for Proton Conducting IT-SOFC

2.3.1 Cathode Reaction Process for Oxide-ion Conducting SOFC versus Proton Conducting IT-SOFC

Similar to the anode reaction process, the cathode reaction process will also change according to the electrolyte material. For the conventional oxide-ion conducting SOFC, the overall reaction of $O_2 + 2e^- + 2V_O^{\cdot\cdot} \leftrightarrow 2O_O^x$, as mentioned in section 1.1, can also be separated into several elementary steps as shown in Figure 2. 20 below. [109-119]

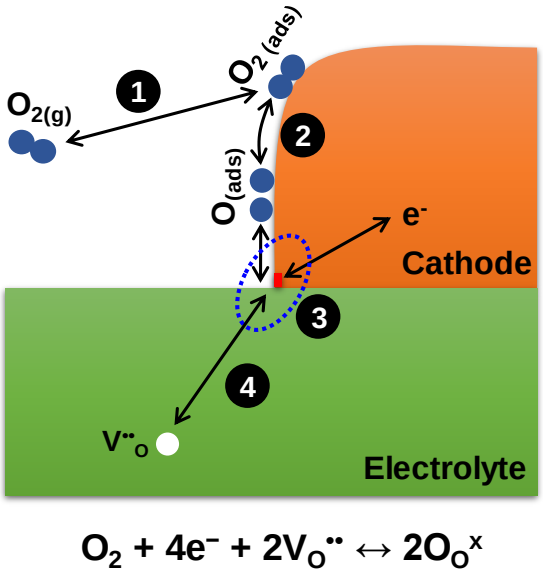

Figure 2. 20 Schematics showing the reaction species involved and the elementary steps for the cathode reactions for oxide-ion conducting SOFC when mixed ionic and electronic conducting material is used as cathode.

Step (1) is the oxygen adsorption reaction occurring on the surface of the cathode, which can be written as:

$$O_2(g) \leftrightarrow O_2(ads) \quad \text{Equation 2. 13}$$

Step (2) is the dissociation of oxygen molecules into adsorbed oxygen atoms occurring on the surface of cathode, which can be written as:

$$O_2(ads) \leftrightarrow 2O(ads) \quad \text{Equation 2. 14}$$

Step (3) represents the charge transfer step occurring over the cathode surface when mixed ionic-electronic conducting (MIEC) materials, such as LSCF and BSCF, are used as the cathode. [120] The dissociated oxygen atoms will accept electrons and incorporate into

oxygen vacancies in the MIEC cathode and become lattice oxygen during this step, which can be written as:

$$O(ads) + 2e^- + V_O^{\cdot\cdot}(cathode) \leftrightarrow O_O^x(cathode) \quad \text{Equation 2.15}$$

Step (4) represents the mass transfer step between the MIEC cathode and the electrolyte, which can be written as:

$$V_O^{\cdot\cdot}(cathode) \leftrightarrow V_O^{\cdot\cdot}(electrolyte) \quad \text{Equation 2.16}$$

For the cathode reaction in the proton conducting IT-SOFC, due to the change of ionic species from oxide-ion to proton, the cathode reaction is through a different process of $O_2 + 4e^- + 4(OH)_O^{\cdot} \leftrightarrow 2O_O^x + 2H_2O$ as mentioned in section 1.1 [20, 118, 121, 122]

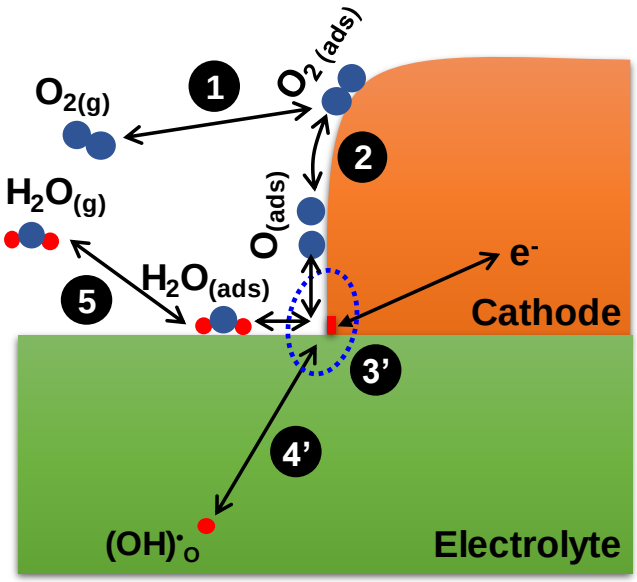

Figure 2. 21 Schematics showing the reaction species involved and the elementary steps for the cathode reactions for proton conducting IT-SOFC.

Similarly, this reaction process can also be divided into several elementary steps as shown in Figure 2. 21, including step (1) adsorption of oxygen molecules and (2) dissociation of adsorbed oxygen molecules into adsorbed oxygen atoms. Both steps are identical to the step (1) and (2) in the cathode reaction process for oxide-ion conducting SOFC.

On the other hand, the charge transfer step (3') would be different: It involves the combination of proton (or hydroxide group), electrons and adsorbed oxygen atoms to generate water on the TPB between cathode, electrolyte and atmosphere. This step can be written as:

$$O(ads) + 2e^- + 2(OH)_O^{\cdot}(TPB) \leftrightarrow 2O_O^x(TPB) + H_2O(ads) \quad \text{Equation 2. 17}$$

Step (4') is the mass transfer of proton from TPB of cathode through electrolyte, which can be written as:

$$(OH)_O^{\cdot}(electrolyte) \leftrightarrow (OH)_O^{\cdot}(TPB) \quad \text{Equation 2. 18}$$

Step (5) is the desorption of generated water from TPB of cathode, which can be written as:

$$H_2O(ads) \leftrightarrow H_2O(g) \quad \text{Equation 2. 19}$$

The obvious difference between the cathode reaction process for the proton conducting IT-SOFC versus oxide-ion conducting SOFC suggests major change in the cathode material choice. However, no agreement has been reached on the most suitable cathode for proton conducting IT-SOFC, and the cathode reaction mechanism has not well studied yet.

In the following section, some of the representative studies on the cathode materials adopted for proton conducting IT-SOFC were described.

2.3.2 Different Cathodes on Proton Conducting IT-SOFC

It has been well accepted that in intermediate-temperature SOFC, oxygen reduction at the cathode is the main rate limiting factor to the performance of the whole system. [61, 114, 123-125] Part of the reason is that the cathode materials are not optimized specifically for proton conducting IT-SOFC and thus high cathodic overpotential was observed. [119, 121, 125-127] Thus, previous studies are presented below in groups of pure electronic conductor, MIEC, and mixed electronic and protonic conductor.

2.3.2.1 Electronic Conducting Cathode for Proton Conducting IT-SOFC

Electronic conducting cathode, which typically is metal with great stability in oxidating atmosphere, has high electronic conductivity but negligible ionic conductivity. The most commonly used electronic conducting cathodes are silver (Ag) and platinum (Pt) metal. There were many studies about adopting the metal as the cathode for proton conducting IT-SOFC and some of the representatives were described below.

- Taherparvar et al. (2003) [128]

Taherparvar et al. studied the performance of the Pt/ $SrCe_{0.95}Yb_{0.05}O_3$ (SCYb)/ Pt proton conducting electrolyte-supported full cell at the temperature range of 800-600^{o}C

including the response to H_2O on the Pt cathode. Power densities of only ~8-2 mW/cm^2 were observed from 800-600^{o}C for the cell as shown in Figure 2. 22, suggesting Pt is not an efficient electrode for proton conducting IT-SOFC.

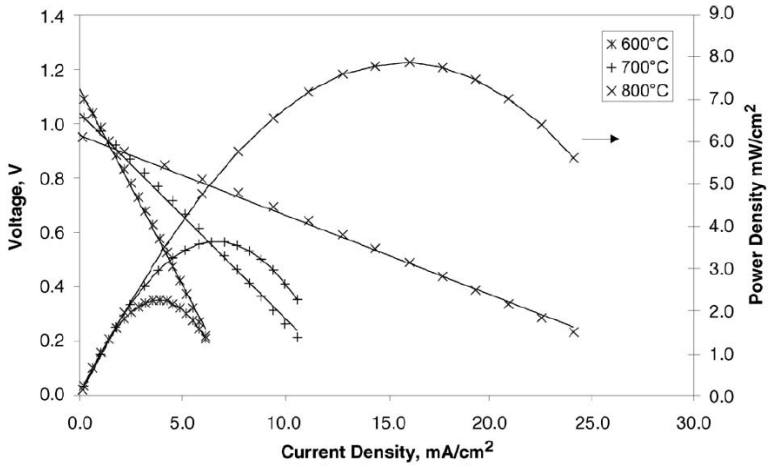

Figure 2. 22 Voltage-current and power density-current curves of Pt/ $SrCe_{0.95}Yb_{0.05}O_3$ (SCYb)/ Pt full cell at temperature of 800-600^{o}C in 3% humidified fuel (10% H_2 balanced by Ar) at anode and dry air at cathode. From Taherparvar et al. [128]

On the other hand, when 3-12% moisture was introduced to the Pt cathode side of the cell, drops in both cell voltage and power density for the cell were observed at 800-600^{o}C as shown in Figure 2. 23.

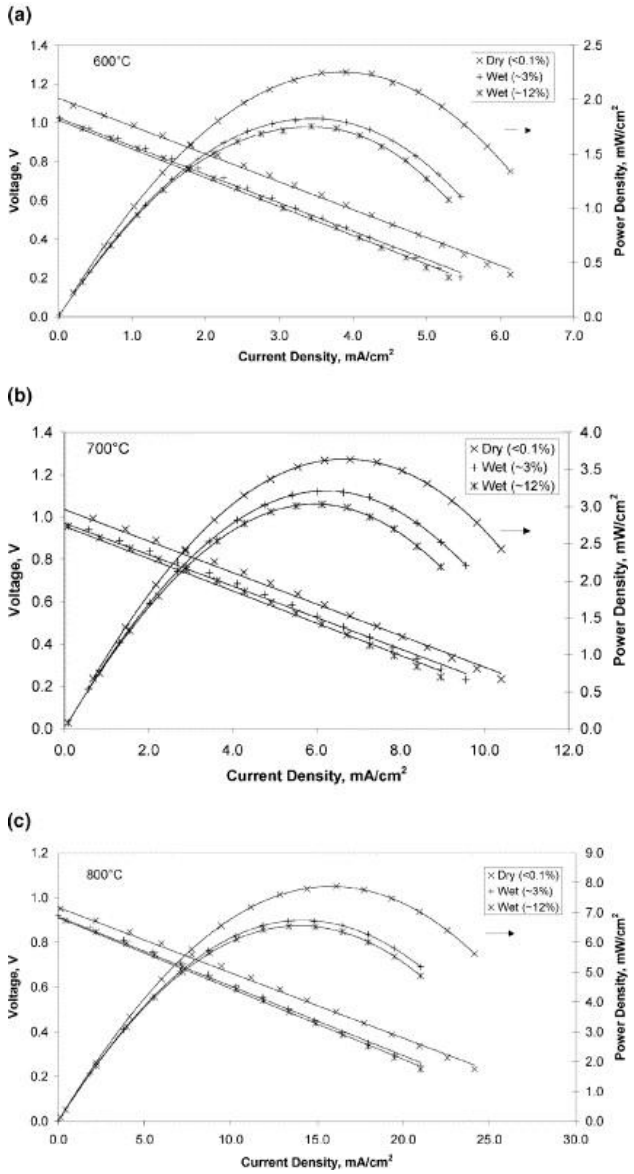

Figure 2. 23 (a) Fuel cell performance for Pt/ SCYb/ Pt full cell with varying pH_2O at the cathode at (a) 600 ^oC (b) 700^oC and (c) 800^oC with 3% humidified fuel consisted of 10% H_2+Ar. From Taherparvar et al. [128]

The authors hypothesized the H_2O effect was due to the suppressed oxygen reduction reaction on the TPB of cathode by the hydration reaction between water and the SCYb electrolyte.

However, the performance of Pt/ SCYb/ Pt is very low that the information gained in this study is hard to be leveraged for typical proton conducting IT-SOFC. In addition, more electrochemical measurements such as impedance spectroscopy would be needed for examining the humidification effect on metal cathode for proton conducting IT-SOFC.

- Potter et al. (2006) [129]

Potter et al. studied the microstructure and impedance spectra of Pt/ SCYb/ Pt proton conducting cathode symmetrical cell at 350^{o}C. The authors found that the porosity of the Pt electrode in the cell was low and the grain size was small of ~50-100nm as shown in Figure 2. 24.

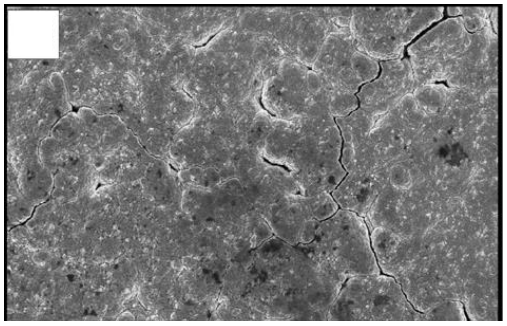

Figure 2. 24 SEM images of the morphology of the Pt electrode in Pt/ SCYb/ Pt cell. From Potter et al. [129]

The H_2O effect on the Pt cathode was tested using impedance spectroscopy at 350^{o}C. Significant decrease in interfacial resistance was observed with the introduction of ~3% H_2O as show in Figure 2. 25. On the other hand, huge interfacial resistance larger than 10kohm was observed for the cell, suggesting Pt behaved as a very poor cathode on

proton conducting SOFC based on SCYb electrolyte at 350ºC. The decrease in interfacial resistance with the introduction of moisture was not consistent with the observed decrease in power output by Taherparvar et al. [128]

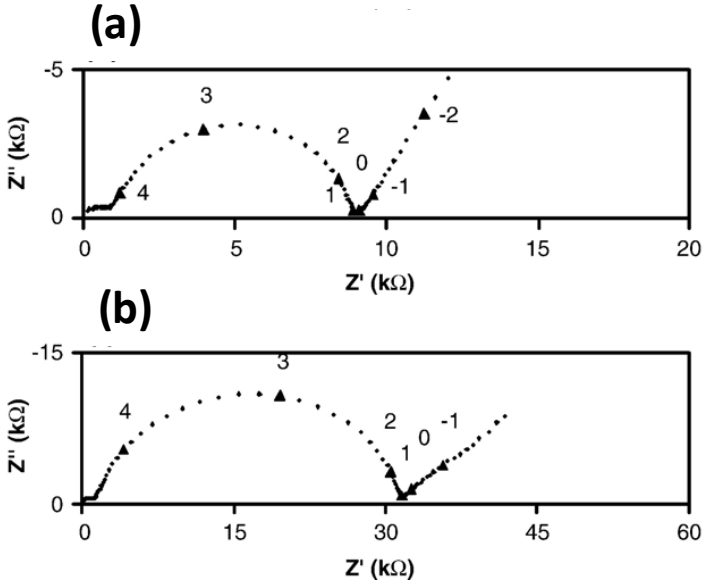

Figure 2. 25 Impedance spectra of Pt/ SCYb/ Pt cell at 350ºC in (a) humidified air and (b) dry air Numerical labels indicate log10 of applied frequency. Adapted from Potter et al. [129]

However, no explanation was given on the origin of such H_2O effect on the Pt/ SCYb/ Pt cell. Moreover, the impedance loops provided were only at the temperature of 350ºC. Thus, testing at intermediate temperature of 600-400ºC will be needed to achieve systematic understanding about the H_2O effect on the proton conducting IT-SOFC with electronic conducting cathode.

- Akimune et al. (2007) [130]

Akimune et al. studied the influence of cathode grain size on the cell performance using proton conducting electrolyte-supported full cell with the configuration of Ag cathode/ BCY/ Pt anode at the temperature range 500-300^{o}C. The grain size of the Ag cathode was modified by using several different types of Ag paste with various particle size (5 nm, 0.1 μm and 6 to 13 μm) as well as two different firing temperatures of 700^{o}C and 500^{o}C. It was found that the final grain size of Ag cathode increases with initial particle size and firing temperature as shown in Figure 2. 26. For example, the smallest grain size of ~0.85 um was observed in the Ag cathode with the smallest initial particle size of 5nm and lowest firing temperature of 500^{o}C.

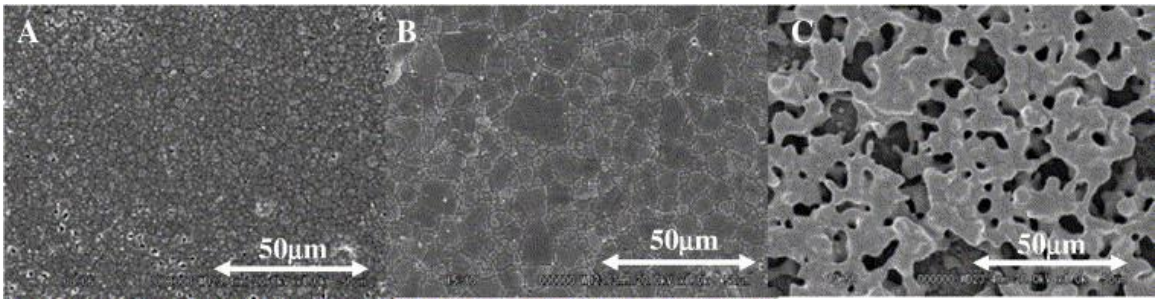

Figure 2. 26 Ag cathode surface with the initial particle of (A) 5nm, (B) 0.1um, and (C) 6-13 um after firing at 500^{o}C. From Akimune et al. [130]

It was found that the cell with smallest grain size of Ag cathode (smallest initial particle size, fired at 500^{o}C) delivered the best power density in the temperature range of 500-300^{o}C (773K-573K) as shown in Figure 2. 27. The enhanced performance of the cell was

attributed to the relatively small gain size of Ag cathode that extends the number of TPB on the cathode.

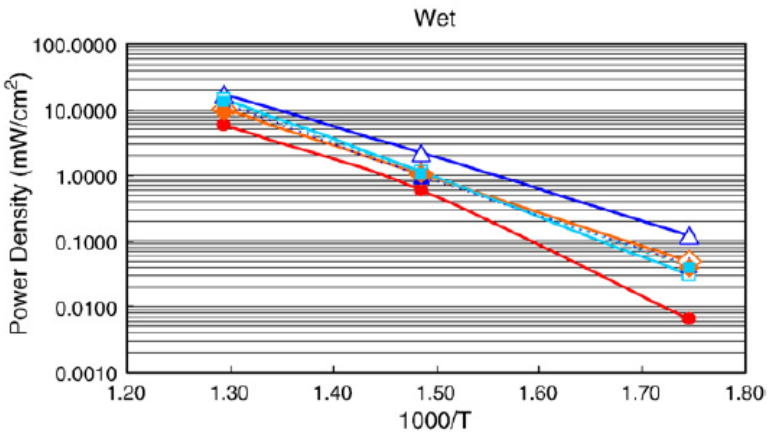

Figure 2. 27 Power density of cell using (●) Pt cathode, and Ag cathode fired at 500ºC with initial particle size of (Δ)5nm, (◊) 0.1um, and (□) 6-13um, and Ag cathode fired at 700ºC with initial particle size of (▲) 5nm, (♦) 0.1um and (■) 6-13um. From Akimune et al. [130]

However, the performance of Ag/BCY/Pt cell showed in this study was still too low to be leveraged.

2.3.2.2 Mixed Ionic and Electronic Conducting (MIEC) and Mixed Electronic and Protonic Conducting Cathodes for Proton Conducting IT-SOFC

Mixed ionic and electronic conducting (MIEC) cathode, which typically is doped perovskite materials, has high oxide-ionic and electronic conductivity. In the following, several representative studies using different cathode materials are described. Among those materials, the focus is on strontium and iron co-doped lanthanum cobaltite ($La_{1-x}Sr_xCo_{1-}$

$_yFe_yO_{3-\delta}$ (LSCF)) and barium cobaltite ($Ba_{1-x}Sr_xCo_{1-y}Fe_yO_{3-\delta}$ (BSCF)), because both are regarded as the state-of-art MIEC cathodes for conventional oxide-ion conducting SOFC and have a good balance between chemical stability, thermal expansion and electrochemical activity.

- LSCF and LSCF related cathodes

Fabbri et al. (2009) studied LSCF and related composite cathodes for $BaCe_{0.9}Yb_{0.1}O_{3-\delta}$ (10YbBC) based proton conducting electrolyte-supported full cells (thickness of 1mm) with the configuration of LSCF/10YbBC/Pt and LSCF-10YbBC/10YbBC/Pt. [93] The author found that the LSCF-10YbBC (1:1 weight ratio) composite cathode showed ~30% smaller interfacial resistance compared to the pure LSCF cathode on proton conducting IT-SOFC at 600^{o}C as shown in Figure 2. 28. The authors attributed the decrease in total interfacial resistance to the extended reaction zone, i.e. TPB area with the introduction of YbBC in the cathode.

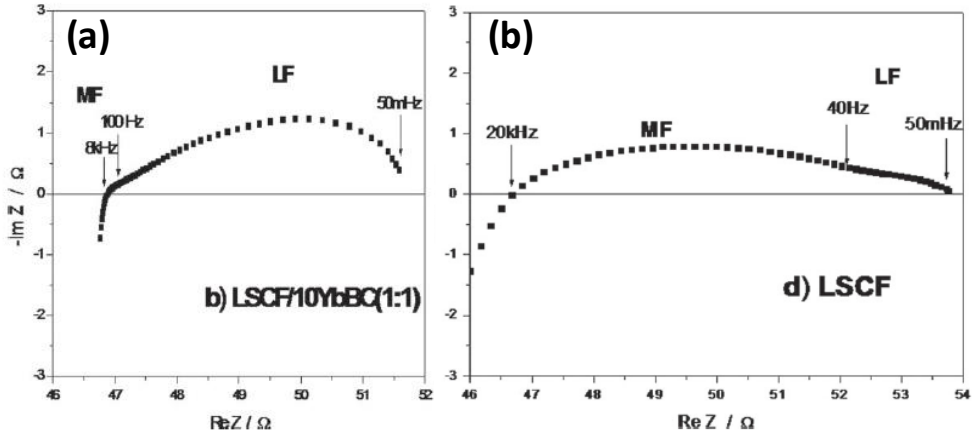

Figure 2. 28 Impedance spectra acquired in wet air at 600 °C for the (b) LSCF composite cathode with 10YbBC (weight ratio 1:1), and (d) and pure phase LSCF as cathode on YbBC electrolyte-supported cell. Adapted from Fabbri et al. [93]

The authors also compared the I-V, I-P and impedance spectra for proton conducting cells with LSCF-10YbBC cathode versus Pt cathode (anode stays the same as Pt) at 700^{o}C as shown in Figure 2. 29. The cell with LSCF-10YbBC cathode showed higher power density and lower interfacial resistance compared to that with Pt cathode at 700^{o}C.

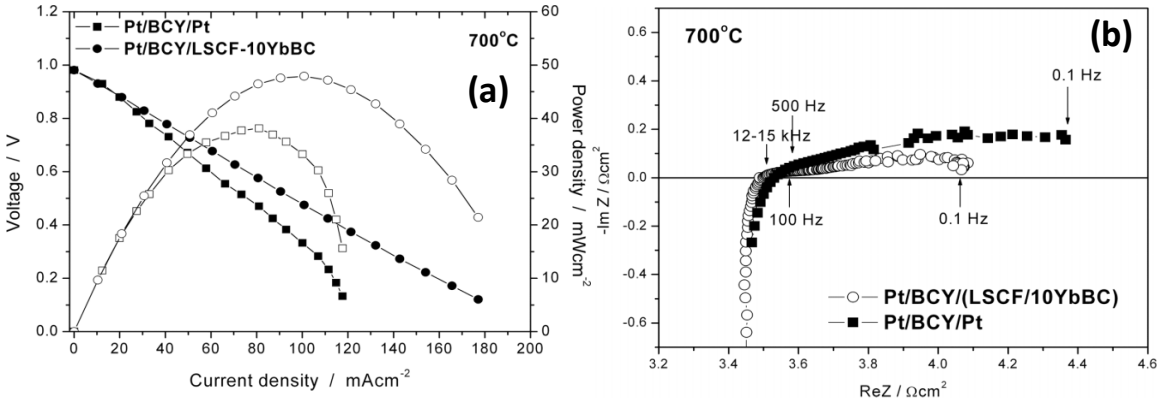

Figure 2. 29 (a) I–V and I-P curves, and (b) impedance spectra for the Pt/BCY/Pt and Pt/BCY/LSCF-10YbBC cell tested at 700 °C. Adapt from Fabbri et al. [93]

Similarly, Yang et al. (2010) also compared the cell performance and impedance of $BaZr_{0.1}Ce_{0.7}Y_{0.2}O_{3-\delta}$ (BZCY) based anode-supported proton conducting SOFC (electrolyte thickness of ~20 um) with pure LSCF cathode versus LSCF-BZCY composite cathode at the temperature range of 750-550^{o}C. [121] As shown in Figure 2. 30, with the introduction of BZCY in LSCF cathode, increase in cell power density and decrease in interfacial resistance was observed at various temperatures. High maximum power density of ~900mW/cm^2 was achieved at 750^{o}C in BZCY based proton conducting anode-supported

cell with LSCF-BZCY composite cathode, suggesting LSCF-BZCY composite cathode is a good cathode for proton conducting IT-SOFC.

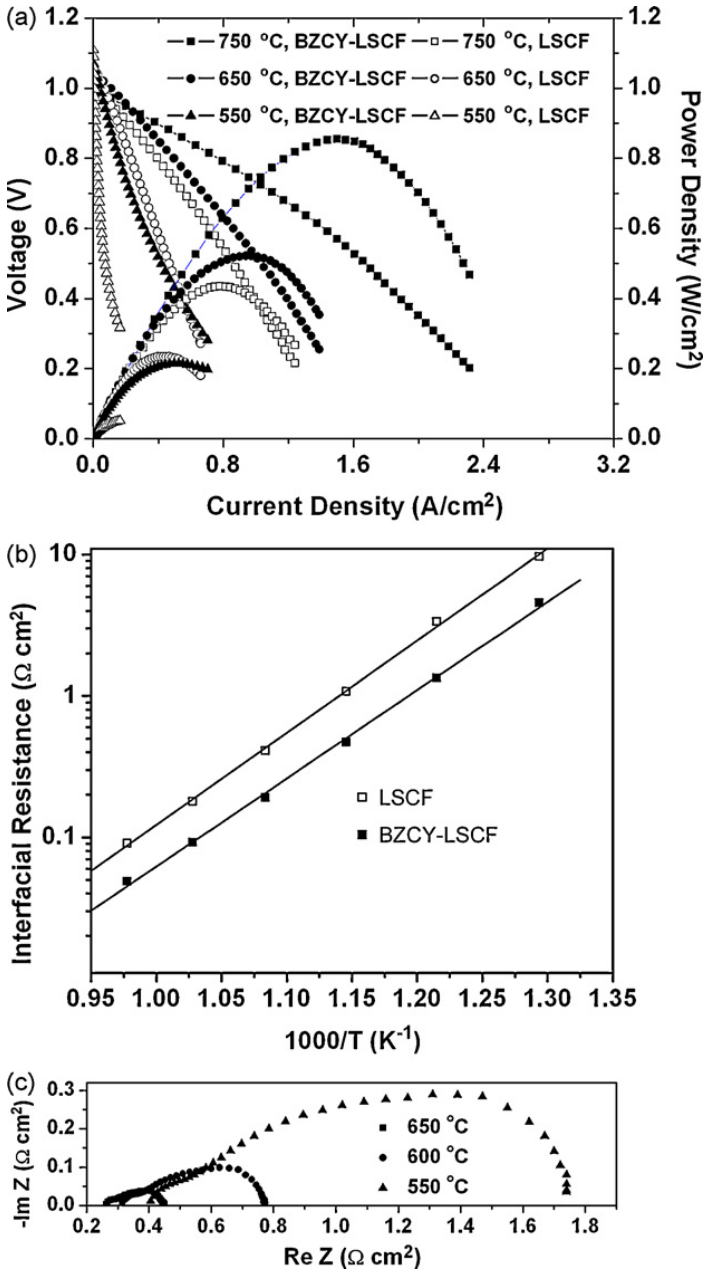

Figure 2. 30 (a) I-V curves, (b) interfaical resistances, for BZCY-based anode-supported cells with BZCY–LSCF and LSCF cathodes and (c) impedance spectra of the cell with LSCF-BZCY composite cathode at various temperatures. From Yang et al. [121]

- BSCF cathode

Lin et al. (2008) studied the microstructure and performance of BSCF cathode for anode-supported proton conducting IT-SOFC with the configuration of BSCF/ $BaCe_{0.9}Y_{0.1}O_{2.95}$ (BCY)/ Ni-BCY. [72] The influence of firing temperature on the BSCF cathode were examined using two different temperatures of 950^{o}C and 1100^{o}C. It was found that the BSCF with lower firing temperature of 950^{o}C showed slightly smaller grain size and higher porosity as shown in Figure 2. 31.

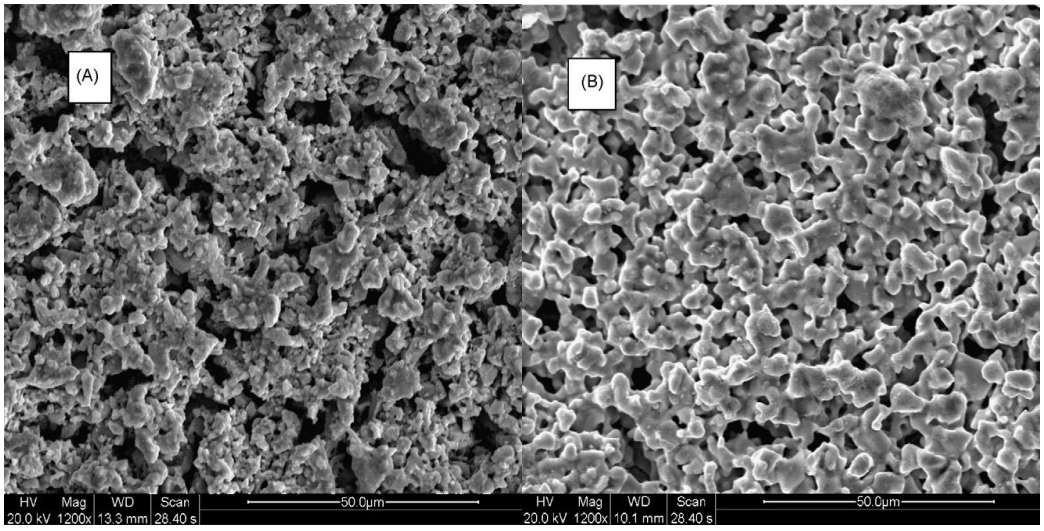

Figure 2. 31 SEM morphologies of the cathodes surface fired at: (A) 950^{o}C and (B) 1100^{o}C. From Lin et al. [72]

In addition, the cell fired at 950^{o}C showed better maximum power density (e.g ~550mW/cm^2 at 700^{o}C and ~130mW/cm^2 at 400^{o}C), higher open circuit voltage and lower interfacial resistance (e.g. ~0.15ohm cm^2 at 700^{o}C) in the temperature range of 700-400^{o}C than the cell fired at 1100^{o}C as shown in Figure 2. 32. The high power output

suggests the BSCF is a good cathode for proton conducting IT-SOFC based on BCY electrolyte.

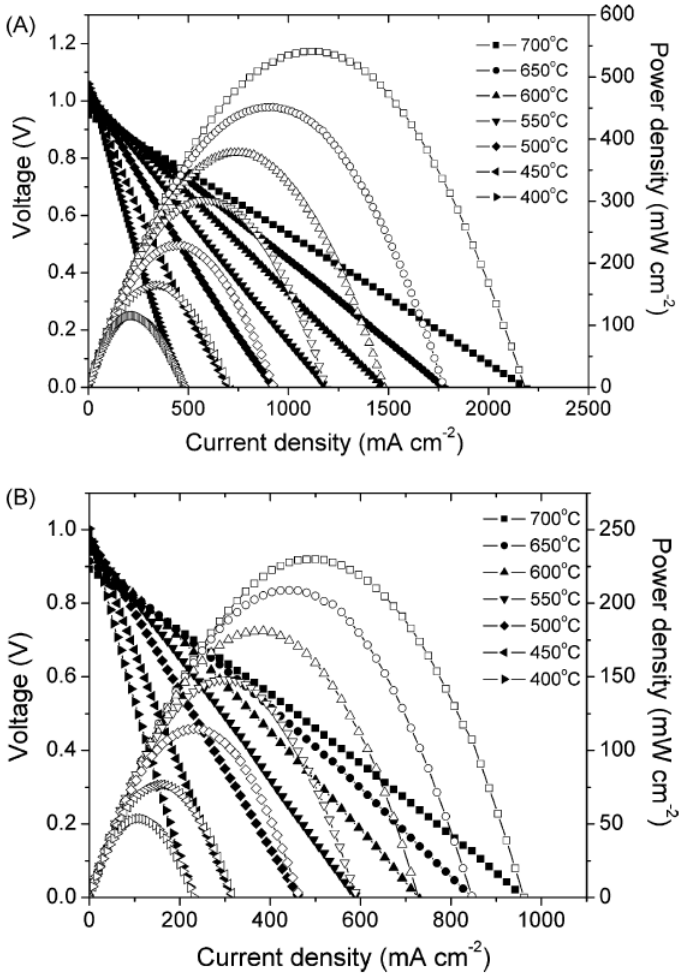

Figure 2. 32 I-V and I-P curves for the cell with BSCF cathode fired at (A) 950ºC, and (B) 1100 ºC at various temperatures of 700-400ºC. From Lin et al. [72]

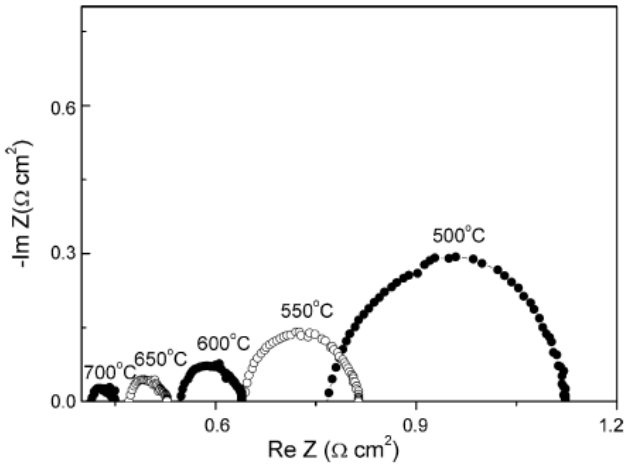

Fig. 8. EIS of the anode-supported fuel cell with 950°C fired BSCF cathode at various temperatures under OCV conditions. From Lin et al. [72]

Grimaud et al. (2012) studied the water uptake for BSCF and compared with LSCF using thermal gravimetric analysis (TGA). [20] The BSCF and LSCF powders were pre-hydrated in air containing 10% H_2O at 500°C for 12 hours followed by slow cooling in the same atmosphere before TGA measurement starting at room temperature towards 1000°C and then cool down to room temperature in dry air. (During the heating, weight loss come from both the oxygen loss and water loss, if any, while during the cooling, the weight gain is due to oxygen incorporation. The difference between heating and cooling gives the information about water content.) As shown in Figure 2. 33, the relative molar ratio of incorporated water to BSCF is ~1:10, while it was negligible for LSCF, indicating that strong hydration reaction occurred in BSCF with possible proton conduction similar to typical PCC.

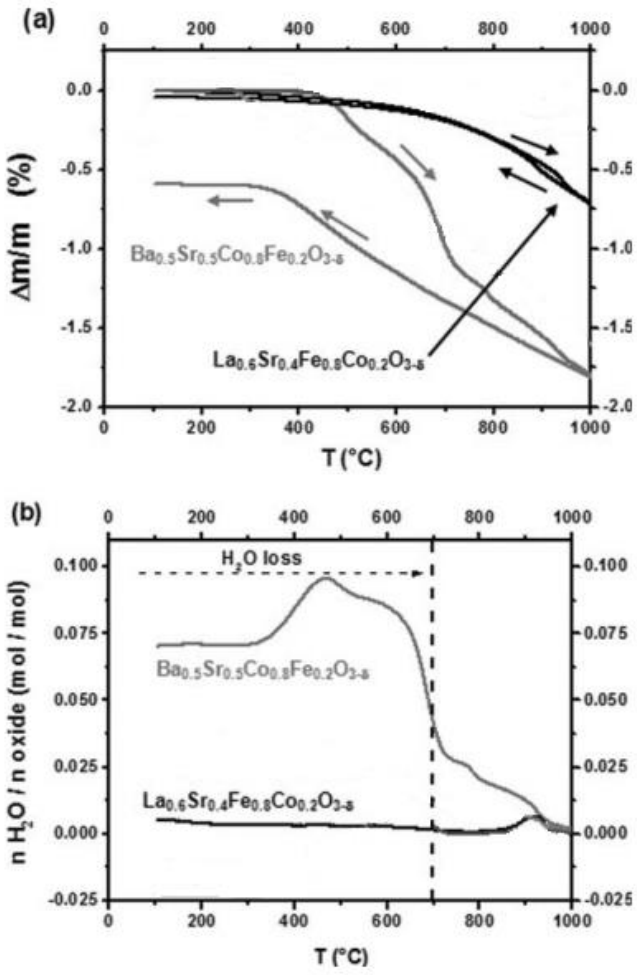

Figure 2. 33 Thermal variation in dry air of a) the relative weight loss of hydrated $La_{0.6}Sr_{0.4}Fe_{0.8}Co_{0.2}O_{3-\delta}$ and $Ba_{0.5}Sr_{0.5}Co_{0.8}Fe_{0.2}O_{3-\delta}$ samples, b) the calculated amount of inserted water (in mol. per mol. of oxide). Adapted with modification from Grimaud et al. [20]

Moreover, the microstructure of BSCF cathode was compared with LSCF. As shown in Figure 2. 34, the BSCF cathode fired at 1000^{o}C showed much larger grain size of ~2-10um compared to LSCF cathode of ≤~1um fired at same temperature. When BSCF cathode firing temperature was increased to 1100^{o}C, it got coarsen.

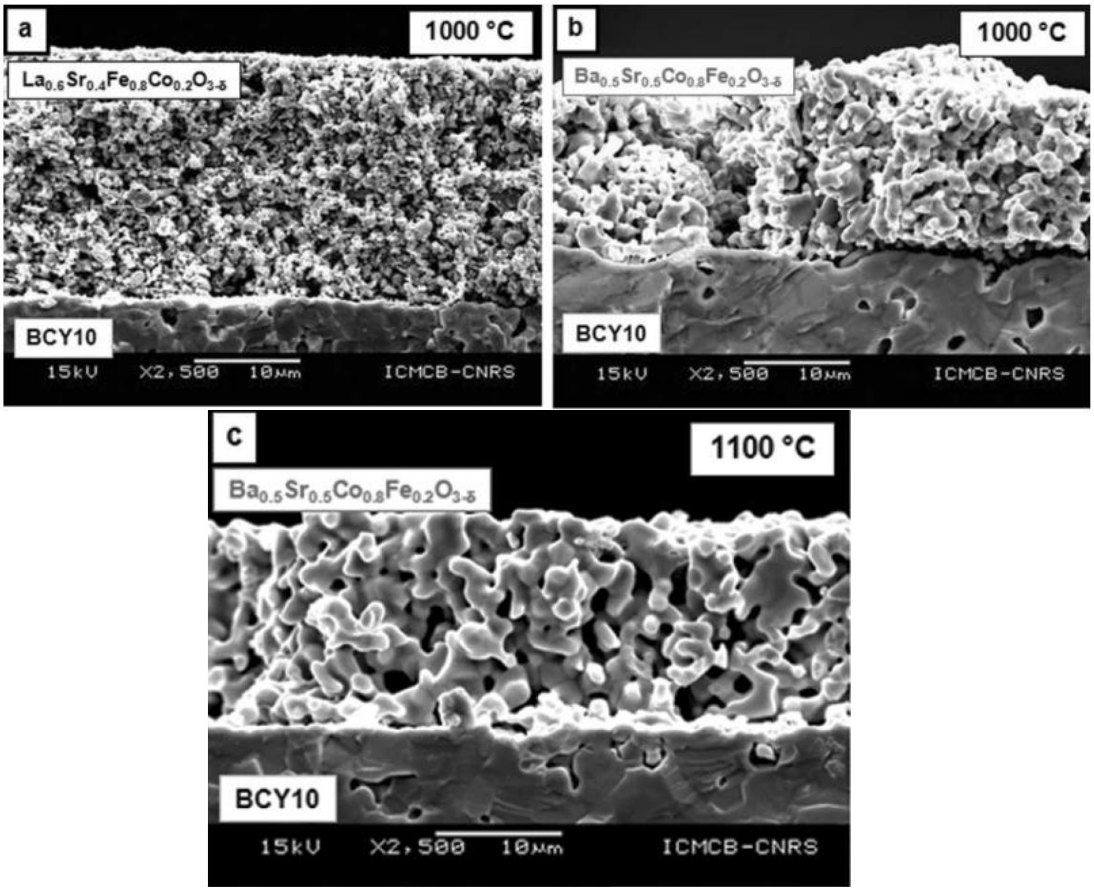

Figure 2. 34 SEM micrographs of (a) LSFC sintered at 1000ºC, (b) BSCF sintered at 1000ºC (c) BSCF sintered at 1100ºC. Adapted from Grimaud et al. [20]

Furthermore, the electrochemical response of BSCF cathode to H_2O was studied and compared with LSCF cathode using proton conducting cathode symmetrical cells based on $BaCe_{0.9}Y_{0.1}O_{3-\delta}$ (BCY10) electrolyte with pH_2O of 0.03-0.30 bar at 600ºC. As shown in Fig 2.X, decrease in interfacial resistance for 1000ºC fired BSCF cathode symmetrical cell with increasing pH_2O from 0.03 bar to 0.30 bar was observed, while the opposite trend (increasing interfacial resistance with increasing pH_2O) was observed for LSCF cathode

symmetrical cell. In addition, much smaller interfacial resistance of BSCF cathode symmetrical cells was observed compared to that for LSCF cell.

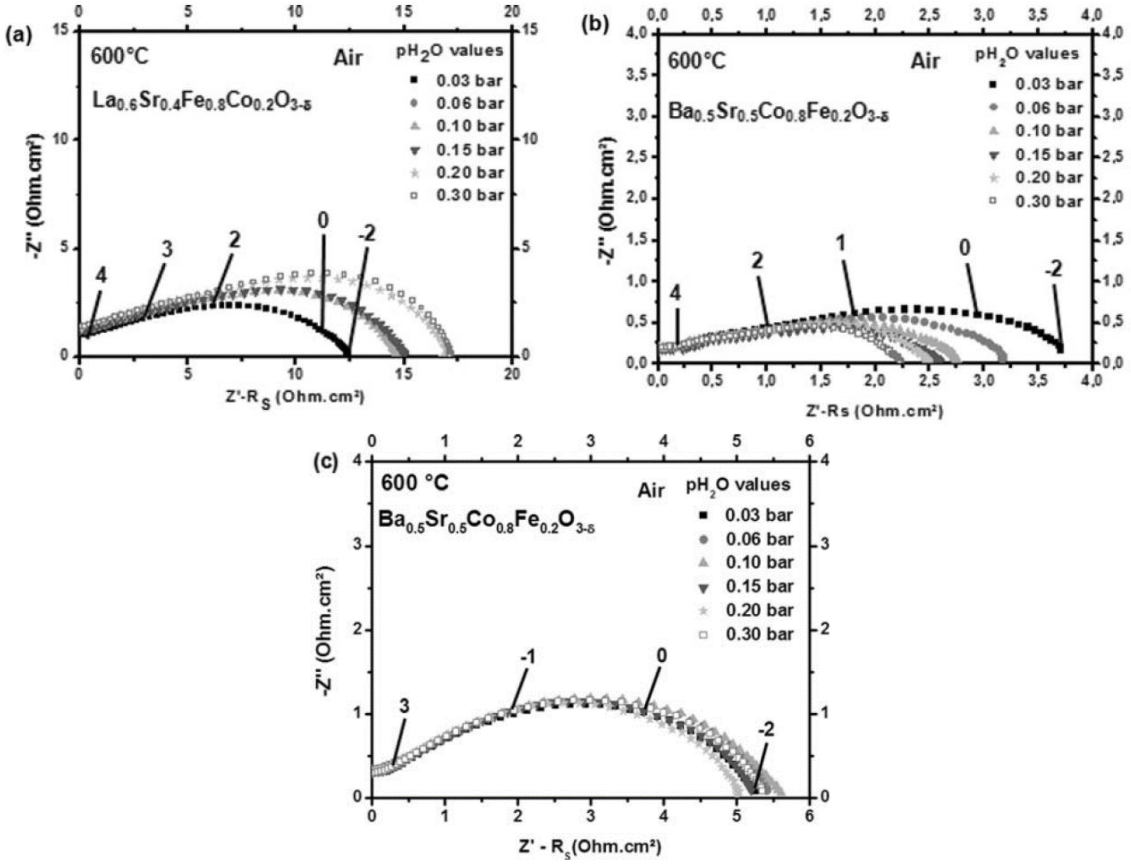

Figure 2. 35 Impedance spectra of the cathode symmetrical cell with (a)LSCF and (b) 1000ºC fired BSCF and (c) 1100ºC fired BSCF in air containing 0.03 to 0.30 bar of H_2O at 600◦C. (Note for BSCF, the water response is different when it was fired at higher temperature probably due to the reaction/ mutual diffusion between BSCF and BCY electrolyte). Adapted from Grimaud et al. [20]

The decrease in cathode interfacial resistance for 1000ºC fired BSCF cathode symmetrical cell with increasing pH_2O was attributed by the authors to the acceleration of cathode reaction by the water insertion to the BSCF cathode. Such water insertion for BSCF was hypothesized to be similar to the hydration process in typical proton conducting

ceramics and thus suggested that BSCF is a possible proton conductor. In comparison, LSCF, which showed negligible water uptake, was believed to be only an oxide-ion conductor. The cathode reaction was observed to slow down upon increasing water concentration, this was attributed to the water adsorption near TPB of cathode that blocked oxygen adsorption and transport.

On the other hand, it was noticed that when BSCF was fired at higher temperature of 1100^{o}C, the electrochemical response to water concentration seems to change: almost no decrease in interfacial resistance was observed with increasing pH_2O. Such behavior was attributed to the limited diffusion of water molecules inside the coarser cathode by the authors. However, another possibility is that there might be reaction or mutual diffusion between BSCF and BZCYYb at higher temperature of 1100^{o}C. [72]

Lim et al. (2016) studied the influence of pO_2 and pH_2O on BSCF cathode using proton conducting anode-supported full cell with the configuration of BSCF/ $BaZr_{0.4}Ce_{0.45}Y_{0.15}O_{3-\delta}$ (BZCY40)/ Ni-BZCY40 at 700^{o}C. [131] The BSCF cathode was fired at 1100^{o}C in this study. As shown in Figure 2. 36, the power output of the cell increased with increasing pO_2, and both the bulk and interfacial resistance decreased with the increasing pO_2 at cathode side. This was attributed to the accelerated oxygen reduction reaction in cathode.

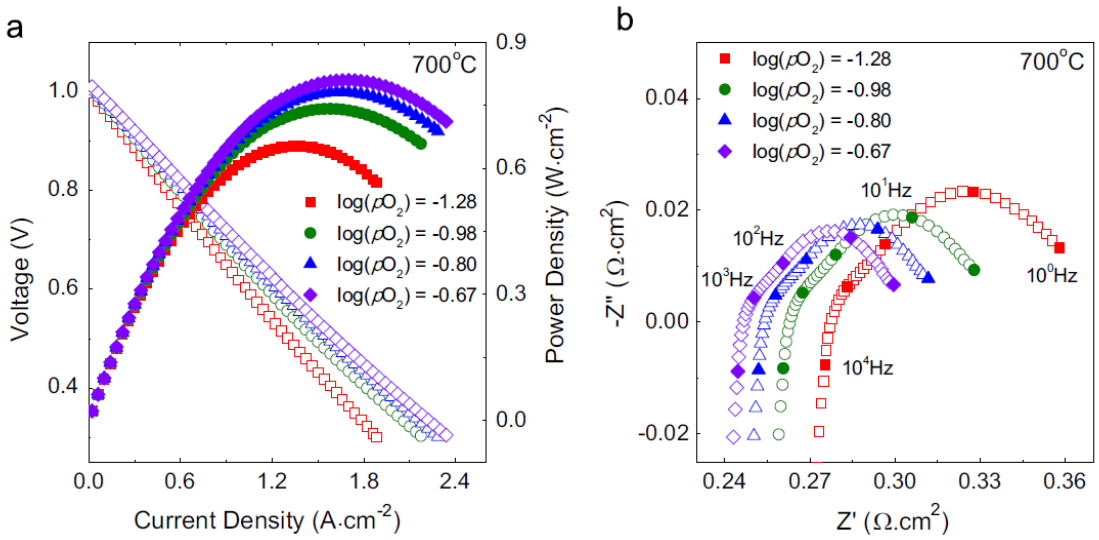

Figure 2. 36 (a) I–V and I–P curves and (b) impedance spectra of the BSCF/ $BaZr_{0.4}Ce_{0.45}Y_{0.15}O_{3-\delta}$ (BZCY40)/ Ni- BZCY40 cell with various pO_2 at BSCF cathode side at 700°C. [131]

In addition, decreases in power density was observed for the cell with the introduction of 2.3% H_2O on cathode at 700°C as shown in Figure 2. 37 (a), which was consistent with the increase in interfacial resistance as shown in Figure 2. 37 (b). The decrease in open circuit voltage with the introduction of H_2O was also observed. On the other hand, almost no further change in cell voltage, power density and interfacial resistance was observed when pH_2O was increased from 0.023 atm to 0.054 atm, which was consistent with the observation in previous study by Grimaud et al. at 600°C using same 1100°C fired BSCF cathode. The decrease in cell performance with the introduction of water was attributed by the authors to the suppressed water release reaction (step (5')) and reduced cathode reaction sites with adsorbed water on TPB of cathode. It's noteworthy that high power density of

~800mW/cm^2 was achieved for the cell in dry atmosphere at 700^{o}C, which suggests that BSCF is a good cathode on proton conducting IT-SOFC, especially in dry condition.

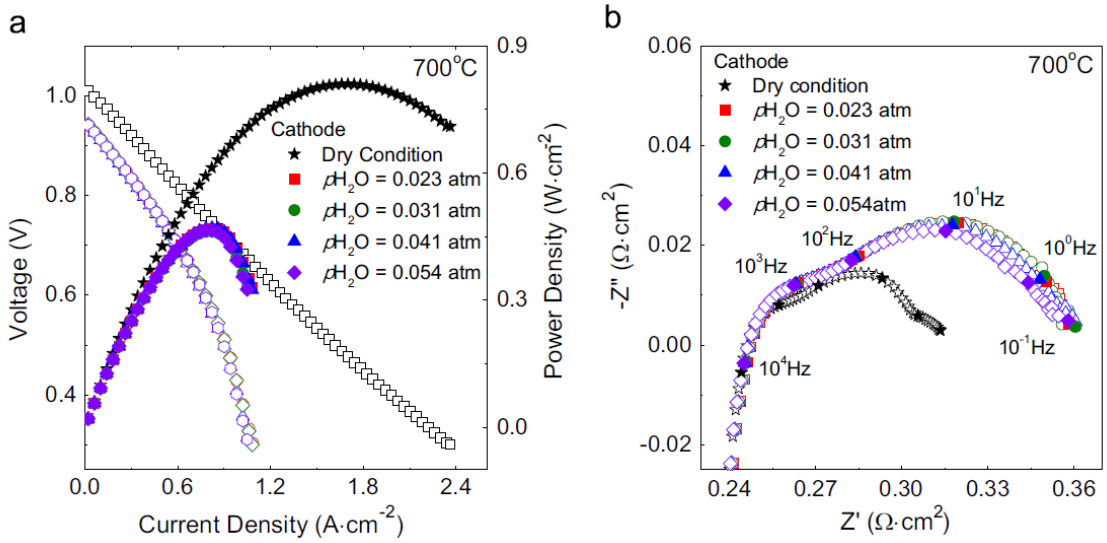

Figure 2. 37 (a) I–V and I–P curves and (b) impedance spectra of the BSCF/ $BaZr_{0.4}Ce_{0.45}Y_{0.15}O_{3-\delta}$ (BZCY40)/ Ni- BZCY40 cell with various pH_2O at BSCF cathode side at 700^{o}C. From Lim et al. [131]

These studies suggest BSCF appears to be a good cathode on proton conducting IT-SOFC and the H_2O effect on the proton conducting cell with BSCF cathode is complicated and thus worth investigating, especially at temperature below 600^{o}C. In addition, BSCF is known to have affinity to CO_2 and how it will be impacted by air containing CO_2 in proton conducting IT-SOFC is worth studying.

- Recent alternative cathodes

Additionally, some recent alternative cathodes, including transition-metal–doped derivative of the PCC (e.g. $BaZr_xY_{1-x}O_{3-\delta}$ (BZY)), are believed to be mixed electronic and protonic conductive due to the existence of transition-metal cations (Co and Fe) dopants and protonic conductivity due to the original PCC material. Several representative studies are described below.

Shang et al. (2013) studied $BaCo_{0.4}Fe_{0.4}Zr_{0.2}O_{3-\delta}$ (BCFZ) as a possible mixed electronic and protonic conducting cathode using both proton conducting cathode symmetrical cell and anode-supported full cell based on BZCYYb electrolyte. [132] In addition, cells with LSCF cathode were adopted as the comparison. As shown in Figure 2. 38, the BCFZ cathode symmetrical cell showed the lowest interfacial resistances in air containing 3%H_2O at 650-400^oC compared to the same cell in dry air and the LSCF cathode symmetrical cell. The reduced interfacial resistance of BCFZ cathode with the introduction of water was attributed to the enhancement in cathode conductivity with the introduced protonic conductivity from hydration reaction.

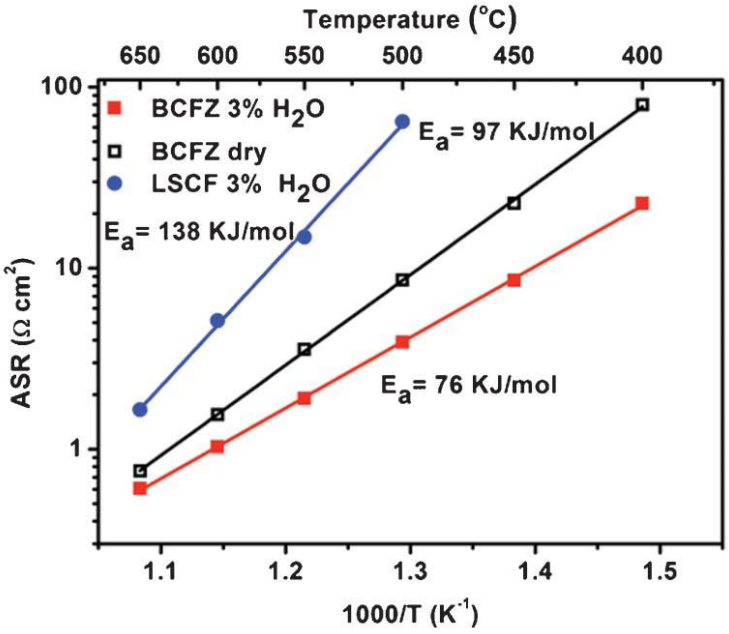

Figure 2. 38 ASR temperature dependence for BCFZ (with water and without water) vs. LSCF. From Shang et al. [132]

In addition, the power output of both BCFZ/ BZCYYb/ Ni-BZCYYb and LSCF/BZCYYb/Ni-BZCYYb proton conducting anode-supported cells were tested. The cell with BCFZ cathode showed much higher maximum power density compared to the cell with LSCF cathode as shown in Figure 2. 39. However, it's noteworthy that the power density of the cell with LSCF cathode in studies is much lower than the similar anode-supported full cell (with the configuration of LSCF/BZCY/Ni-BZCY) as mentioned above by Yang et al.

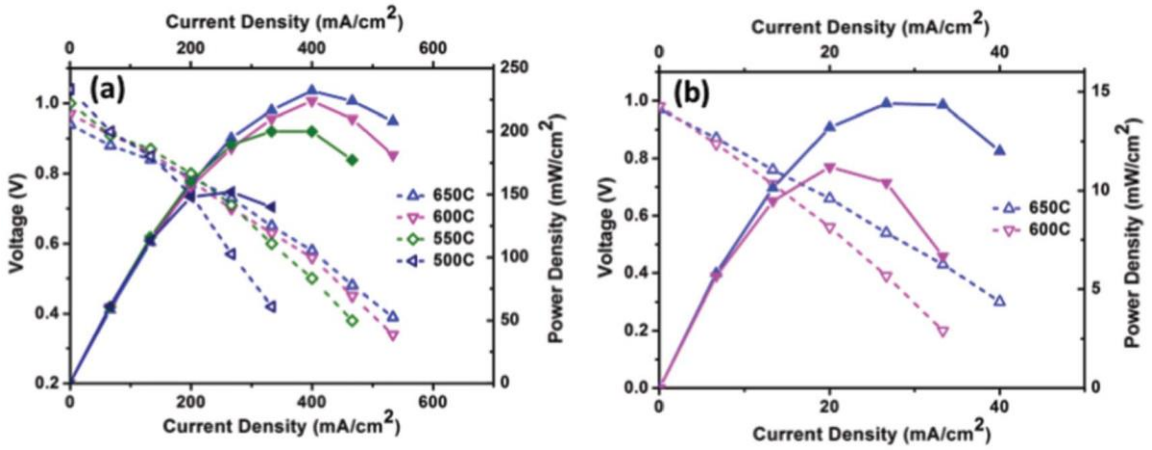

Figure 2. 39 Performance of the as-prepared single cells under hydrogen/air at different temperatures. (a) Cell with BCFZ cathode; (b) cell with LSCF cathode. From Duan et al. [132]

Duan et al. (2015) studied another cathode $BaCo_{0.4}Fe_{0.4}Zr_{0.1}Y_{0.1}O_{3-\delta}$ (BCFZY) for proton conducting IT-SOFC based on BZCYYb electrolyte. [133] As shown in Figure 2. 40, high power density of ~650mW/cm^2 was achieved at 600^{o}C, suggesting BCFZY is a good cathode on BZCYYb proton conducting IT-SOFC. In addition, very fine grain size of ~100nm was observed for the 900^{o}C fire BCFZY cathode even after 1100 hours of operation. The great performance of the cell can be partially attributed to the fine microstate of the BCFZY cathode, which significantly increase the reaction sites on the cathode.

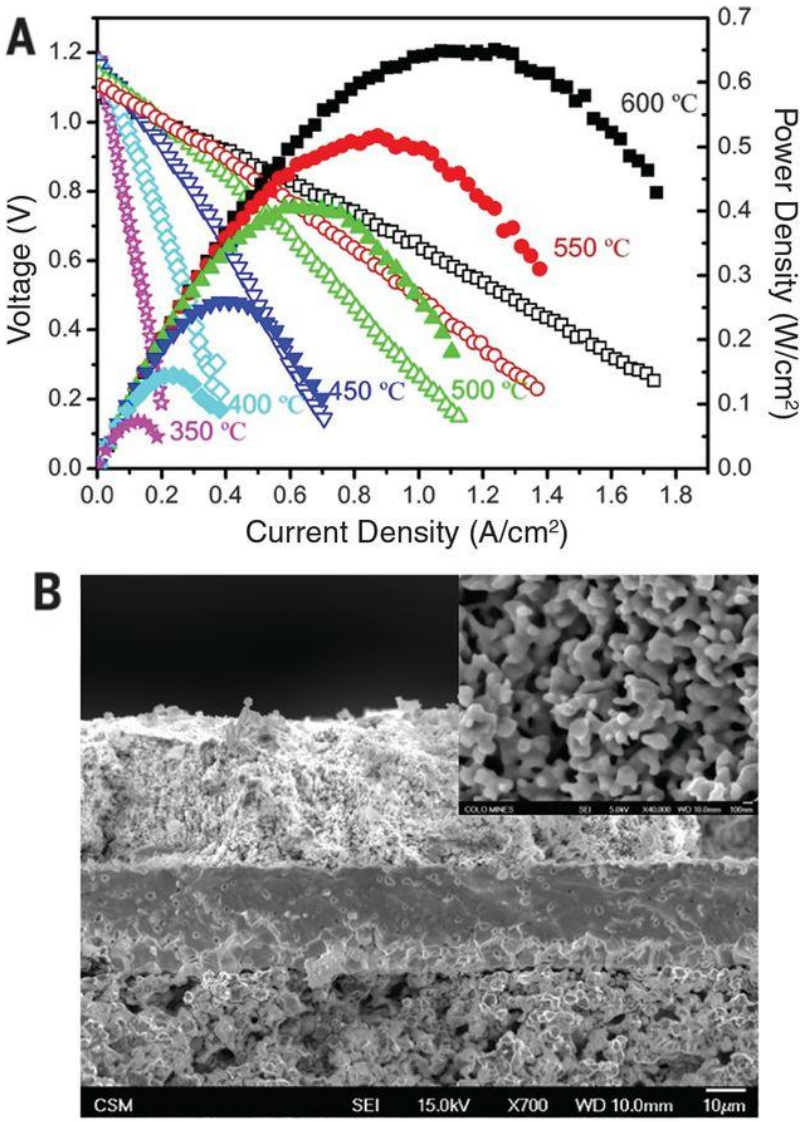

Figure 2. 40 (A) I-V and power density of the BCFZY/BZCYYb/Ni-BZCYYb anode-supported cell at 600-350ºC (B) a cross-sectional view of the cell after operation for over 1100 hours (inset figure is the high-magnification view of BCFZY0.1 cathode after 1100 hours operation). Adapted from Duan et al. [133]

3 Chapter III: H_2S Poisoning Behavior for the Anode of Proton Conducting IT-SOFC

This chapter details the study on the H_2S poisoning behavior for the anode of proton conducting IT-SOFC. This chapter is based on published paper by Shichen Sun, Osama Awadallah, and Zhe Cheng. Title of "Poisoning of Ni-based anode for proton conducting SOFC by H2S, CO2, and H2O as fuel contaminants." in Journal of Power Sources 378 (2018): 255-263 and published paper by Shichen Sun, and Zhe Cheng. Title of "H2S Poisoning of Proton Conducting Solid Oxide Fuel Cell and Comparison with Conventional Oxide-Ion Conducting Solid Oxide Fuel Cell." in Journal of The Electrochemical Society 165.10 (2018): F836-F844.

3.1 Introduction

Solid oxide fuel cell (SOFC) has shown great potential as an alternative power source due to its high energy conversion efficiency, high power density, and the ability to utilize readily available hydrocarbon fuels such as natural gas and coal gas, which are easier than pure hydrogen to transport and store in most areas. Recently intermediate temperature SOFC (IT-SOFC) has drawn growing attention due to higher overall thermodynamic efficiency and the possibility for lower cost and slower degradation from expanded choices of low-cost interconnect and sealing materials and reduced rate of corrosion and other unwanted reactions when the operating temperature is reduced from ~750-1000^{o}C for conventional SOFC to the range of ~400-600^{o}C. [12, 13, 134-136]

Among various types of possible electrolyte materials for IT-SOFC, proton conducting ceramics (PCC), for example, $BaZr_{0.1}Ce_{0.7}Y_{0.2-x}Yb_xO_{3-\delta}$ (BZCYYb), [15, 82, 84, 87-89] have become popular due to their high ionic conductivity at intermediate temperatures compared to conventional oxide-ion conducting electrolytes and the absence of anode-side fuel dilution. However, the change in anode reaction mechanism from oxide-ion conducting SOFC to proton conducting IT-SOFC has not been well studied yet. For example, previous studies have revealed that the anode for proton conducting IT-SOFC, which are based on cermet anodes consisting of Ni and PCC electrolyte material, seem to show better tolerance against poisoning by low parts-per-million (ppm)-level H_2S than conventional oxide-ion conducting SOFC. [15, 38, 100, 137] In particularly, for the cermet anode of conventional oxide-ion SOFC based on Ni and oxide-ion conducting electrolyte material (e.g. YSZ), the H_2S poisoning effect was severe: as little as 0.05 ppm-level of H_2S in H_2 could cause significant poisoning at 750^{o}C. [138] While for the cermet anode of proton conducting IT-SOFC, no significant poisoning behavior was observed with the introduction of 5ppm of H_2S into humidified H_2 fuel. [15] The reason for such change in poisoning behavior has not been systematically studied, especially at intermediate temperatures of ~400-600^{o}C.

Therefore, in this study, the electrochemical behaviors of the anode for proton conducting IT-SOFC upon exposure to ppm-level H_2S as contaminants in hydrogen fuel are investigated based on both anode-supported and electrolyte-supported proton conducting SOFC (PC-SOFC) full cell, and Ni-based anode symmetrical cells using both proton conducting electrolyte (BZCYYb) and oxide-ion conducting electrolyte (YSZ).

The aim is to gain a better understanding of the electrochemical responses of proton conducting IT-SOFC to H_2S poison and the differences in H_2S poisoning behaviors between PC-SOFC versus conventional oxide-ion conducting SOFC (OC-SOFC).

Besides that, series of chemical exposure tests on both loose Ni-BZCYYb powder and dense Ni-BZCYYb composite pellets were carried out to simulate the interaction between H_2S and the cermet anode for proton conducting IT-SOFC under various conditions followed by characterization techniques such as X-Ray Diffraction (XRD), scanning electron microscopy (SEM), energy dispersive spectroscopy (EDS) and secondary ion mass spectroscopy (SIMS).

The results from these experiments will be presented and their implications on the anode reaction mechanism and kinetics, as well as the possible electrocatalytic role PCC play in the anode reaction for proton conducting IT-SOFC will be discussed.

3.2 Experimental

3.2.1 Powder Synthesis and Cell Fabrication

In this study, $BaZr_{0.1}Ce_{0.7}Y_{0.1}Yb_{0.1}O_{3-\delta}$ (BZCYYb) was chosen as the proton conducting ceramic (PCC) electrolyte, which was synthesized by glycine nitrate process (GNP) process. [89] Briefly, salts of $Ba(NO_3)_2$ (#A11305, Alfa Aesar, 99%), $ZrO(NO_3)_2 \cdot xH_2O$ (#43224, Alfa Aesar, 99.9%), $Ce(NO_3)_3 \cdot 6H_2O$ (#11329, Alfa Aesar, 99.5%), $Y(NO_3)_3 \cdot 6H_2O$ (#12898, Alfa Aesar, 99.9%), and $Yb(NO_3)_3 \cdot xH_2O$ (#12901, Alfa Aesar, 99.9%) were dissolved in hot DI water (set at ~100^oC) together with glycine (#G8898,

Sigma Aldrich, 99+ %). The molar ratio was 1: 1 between glycine and total metal ions. The solution was then heated up on a hotplate set at ~540^{o}C. After the self-combustion process, the fine powder produced was collected and then calcined in ambient air at 1100^{o}C for 5 hours to form the pure perovskite phase. The cathode material used in this study is $La_{0.6}Sr_{0.4}Co_{0.2}Fe_{0.8}O_{3-\delta}$ (LSCF) and the synthesis steps are similar to that for BZCYYb except the starting materials were changed to $La(NO_3)_3$ (#A11305, Alfa Aesar, 99%), $Sr(NO_3)_2$ (#31633, Alfa Aesar, 99%), $Fe(NO_3)_3 \cdot 9H_2O$ (#216828, Alfa Aesar, 99%), $Co(NO_3)_2 \cdot 6H_2O$ (#239267, Alfa Aesar, 99%). After self-combustion, the powder was calcined at 1000^{o}C for 2 hours in ambient air to form the pure perovskite phase. [139]

Anode-supported PC-SOFC full cells with the configuration of Ni-BZCYYb/BZCYYb/LSCF-BZCYYb were fabricated. First, anode precursor/electrolyte bilayer was prepared via dry-pressing using 0.2 g NiO-BZCYYb-starch powder mixture with weight ratio of 5.5: 3.5: 1 and 10 mg BZCYYb electrolyte powder in a 10 mm diameter die at a pressure of 250 MPa. The pellets of anode precursor/electrolyte bilayer were then sintered at 1400^{o}C for 5 hours with heating and cooling rate of 5^{o}C/min (anode side facing down touching alumina crucible support while electrolyte side facing up). [89] The cathode slurry was prepared by mixing powders of LSCF and BZCYYb and polymer binder solution (containing 8wt% polymer) with LSCF: BZCYYb: polymer binder solution weight ratio of 7: 3: 15, followed by ball-milling for 24 hours. The cathode was brush-painted onto the electrolyte side of the sintered anode/electrolyte bilayer pellets using the LSCF-BZCYYb slurry. The painted cathode area was ~0.16 cm^2, and it was dried in an air oven at 150^{o}C and then calcined at 1100^{o}C for 2 hours in ambient air with heating and

cooling rate of 5°C/min. Finally, silver mesh and wires were attached to the electrodes using pure silver paste for current collection.

For the electrolyte-supported PC-SOFC full cells with the configuration of Ni-BZCYYb/BZCYYb/LSCF-BZCYYb, the fabrication process is described as following: First, an electrolyte pellet was prepared via dry-pressing 0.2 g BZCYYb powder in a 10 mm diameter die at a pressure of 250 MPa followed by sintering at 1550°C for 5 hours in air with heating and cooling rate of 5°C/min in a so called "protected sintering" configuration. [89] Second, the anode slurry was brushed-painted onto one side of the sintered electrolyte pellet. The anode slurry was made by mixing NiO, BZCYYb and organic binder solution (with polymer concentration of 8 wt.%, same for below) at a weight ratio of 3: 2: 5 followed by heat treatment in air at 1400°C for 2 hours at a heating and cooling rate of 5°C/min. Finally, LSCF-BZCYYb cathode slurry, with a LSCF: BZCYYb : organic binder solution weight ratio of 6.5 : 3.5 : 10 was brush-painted onto the other side of the pellet and then calcined at 1100°C for 2 hours in ambient air with a heating and cooling rate of 5°C/min. [138] Both the cathode and anode area were ~0.16 cm^2. For subsequent electrochemical test, silver mesh and wires were attached to the electrodes using pure silver paste for current collection.

In addition, both anode symmetrical PC-SOFC with the configuration of Ni-BZCYYb/BZCYYb/Ni-BZCYYb and anode symmetrical OC-SOFC with the configuration of Ni-YSZ/YSZ/Ni-YSZ were fabricated as described below. The anode symmetrical PC-SOFC were fabricated by first dry pressing 0.1 g of BZCYYb powder into 10 mm diameter pellets at a pressure of 250 MPa. The electrolyte pellets were then sintered

at 1550^{o}C for 5 hours under "protected condition" with heating and cooling rate of 5^{o}C/min. [38] Then, the anode slurry was made by mixing NiO, BZCYYb, and polymer binder solution (polymer content of 8%) at weight ratio of 5.5 : 3.5 : 9. After that, symmetrical anodes were painted onto both sides of the sintered electrolyte pellet followed by drying in an air oven at 100^{o}C and then calcination at 1400^{o}C for 2 hours in ambient air with heating and cooling rate of 5^{o}C/min. For the anode symmetrical OC-SOFC, first, 0.1 g of YSZ powder (#312022, FuelCellMaterials, 8 mol.%Y_2O_3 doping, USA) was dry pressed into a 10 mm diameter pellet at a pressure of 120 MPa. Then, the YSZ electrolyte pellet was sintered in air at 1550^{o}C for 5 hours with a heating and cooling rate of 5^{o}C/min. Anode slurry was made by mixing NiO, YSZ, and polymer binder solution at a weight ratio of 3 : 2 : 5. After that, symmetrical anodes were painted onto both sides of the sintered YSZ electrolyte pellet followed by drying in an air oven at 100 ^{o}C and then calcination at 1400^{o}C for 2 hours in ambient air with a heating and cooling rate of 5 ^{o}C/min. For both anode symmetrical cells, silver meshes were attached onto both electrodes using pure silver paste for current collection.

3.2.2 Testing of the Effects of H_2S on Electrochemical Cells

For electrochemical testing of PC-SOFC full cells (anode-supported and electrolyte-supported), the cells were first sealed onto one end of an alumina support tube using ceramic sealant (Aremco 552, USA) and placed in the hot zone of a tube furnace. [140] Then the cell was heated up to 750^{o}C, during which the anode-side was purged with pure nitrogen (N_2) (UHP grade, Airgas, USA) while the cathode side was exposed to ambient

air. At 750°C, clean dry hydrogen (H_2) (UHP grade, Airgas, USA) was introduced into the anode side at a flow rate of 40 mL/min, and NiO in the anode was reduced to Ni. After the anode reduction, electrochemical measurements including electrochemical impedance spectroscopy (EIS) measurements and cell voltage measurement under constant current were carried out using a potentiostat (Interface 1000, Gamry, USA). For EIS measurements, the frequency range was set from 10^{-2} Hz to 10^{6} Hz with AC amplitude of 0.1mA.

To characterize the effects of H_2S on the electrochemical responses of the anode-supported PC-SOFC, low ppm-level H_2S was introduced into the H_2 fuel while keeping the total fuel flow rate the same. (In particular, 38.7-36 mL/min of H_2 gas was passed through a water bubbler at room temperature and then 1.3-4 mL/min of 100 ppm H_2S balanced by H_2 gas mixture (Airgas, USA) was combined with the humidified H_2 stream before being introduced into the anode chamber to get the corresponding concentration of H_2S, All fuel gas concentrations mentioned in this study for various gas mixtures are by volume at room temperature before entering the anode chamber.) For anode-supported SOFC full cells, the change in cell voltage was monitored continuously at a constant current density of 125 mA/cm^2, and EIS was recorded before, after 2 hours of exposure to ppm-level H_2S, and after removal of H_2S for 24 hours under both open circuit condition and biased condition of 0.7V. In addition, in order to reveal the impact of H_2O including how H_2O influences the H_2S poisoning behavior, in some cases, H_2 gas was passed through a water bubbler at room temperature before being introduced into the anode chamber.

To characterize the effects of H_2S on the electrochemical responses of the electrolyte-supported PC-SOFC, at each temperature (750, 650, 550 and 450^oC), 3-10 ppm H_2S was introduced into the humidified H_2 fuel while keeping the total fuel flow rate the same. The changes in cell voltage under constant currents densities (35, 35, 6 and 2 mA/cm^2 at testing temperatures of 750, 650, 550 and 450^oC, respectively) were recorded. In addition, EIS spectra were recorded before and after 2 hours of exposure to low ppm-level H_2S.

For testing of both anode-symmetrical PC-SOFC and OC-SOFC, they were placed in the hot zone inside a one-end closed ceramic tube with gas fed directly to the cell. The symmetrical cells were also heated up in N_2 to 750^oC and then reduced in pure H_2 at 750^oC. EIS under open circuit condition were recorded in humidified H_2 (~3% moisture, labelled as wet H_2 in this study) and in wet H_2 containing 10 ppm of H_2S at temperatures of 750, 650, and 550^oC. The detailed testing sequence was as following: EIS was first recorded in clean wet H_2 from 750^oC all the way to 550^oC, and the cell was then heated up to 750^oC in wet H_2. After that, 10 ppm H_2S was introduced into the wet H_2 and EIS was recorded again after 2 hours of holding at each temperature (750, 650, and 550^oC).

3.2.3 Stability Tests of Ni-BZCYYb Mixed Powders

To study the chemical stability of Ni-BZCYYb cermet anode under relevant testing conditions and understand the observed electrochemical responses to H_2S, a series of experiments were carried out by exposing NiO-BZCYYb loose powder mixtures (5.5: 3.5 weight ratio) after hydrogen reduction to ppm-level H_2S as fuel contaminants in both ~3%

humidified and dry H_2. In each set of tests, 10 mg of NiO-BZCYYb powder mixture was placed in an alumina boat in a one-end closed tube with fuel gas mixture directly fed to the sample surface. As in electrochemical testing, the samples were first heated up in N_2 to 750^{o}C. Then NiO in the mixture was reduced to Ni in dry H_2 for 30 minutes. After that, the samples were cooled down to 550^{o}C, and 10 ppm H_2S was introduced into the hydrogen fuel (3% humidified or nominal dry with ~10 ppm H_2O) stream for 24 hours. For comparison purpose, one sample was treated in the same way without the introduction of H_2S. All post-exposure samples were cooled rapidly (by quickly removing the sample tube from the furnace) in clean N_2 to avoid any additional reaction. X-Ray diffraction (SIEMENS diffractometer D5000) was taken for all samples after the exposure tests for phase identification. Besides that, some samples were analyzed using energy dispersive spectroscopy (EDS) equipped on a field emission scanning electron microscope (FE-SEM, JEOL JSM 6330F) for determining the distribution of elements of interest such as Ba, Ni and S.

3.2.4 SIMS Analysis on Ni-BZCYYb Pellet after H_2S Exposure

Since the poisoning process and related mechanism for conventional oxide-ion conducting SOFC with Ni-YSZ cermet anode and YSZ electrolyte are well studied and documented in the literature, [26, 28, 29, 31, 33, 137, 138]the focus here in this study is on the sulfur-anode interaction for PC-SOFC.

Considering the fact that sulfur is well known to adsorb strongly over Ni surface without formation of bulk nickel sulfides under these conditions with different extent of coverage depending on the exact temperature and H_2S concentration, [25, 28] the issue of particular interest here is the interaction between the BZCYYb PCC electrolyte and H_2S under the testing condition. SIMS is very sensitive and will be complementary to XRD and EDS for the analysis on the surface of Ni-BZCYYb.

To simulate the H_2S poisoning effect on Ni-PCC cermet anode, dense Ni-BZCYYb pellets were prepared by mixing Ni (99.8%, -300 mesh, Alfa Aesar, USA) and BZCYYb powder with the weight ratio of 6: 4 and pressing into a 10 mm diameter pellet at the pressure of 100 MPa. The pressed pellet was then sintered at 1350^{o}C in 4% H_2 balanced by argon (Ar) (UHP grade, Airgas, USA) for 5 hours to avoid possible oxidation. For further characterizations, the sintered pellets were ground and polished to achieve a smooth surface. After that, the polished pellet was exposed to 10 ppm(v) H_2S balanced by ~3% humidified H_2 at 550^{o}C for 24 hours with subsequent rapid cooling in clean wet H_2. Secondary-ion Mass Spectroscopy (SIMS) was then conducted on the post H_2S-exposure sample surface using an ion time of flight (Ion TOF) - SIMS instrument utilizing Bismuth (III) cation (Bi^{3+}) for measurement on fields of view (FOV) between 20-100μm. Barium, sulfur, nickel and their corresponding oxides and hydroxides ion species were detected under both positive and negative ion modes for elemental distribution identification and depth profiling.

3.3 Results

3.3.1 H_2S Effect on Ni-BZCYYb/BZCYYb/LSCF Anode-supported PC-SFOC Full Cell

The impedance spectra at 750°C for the Ni-BZCYYb/BZCYYb/LSCF anode-supported PC-SOFC full cell under open circuit condition before and after the introduction of 5 ppm H_2S into the H_2 fuel is shown in Figure 3. 1. There is very little change in either ohmic resistance (R_O) or apparent interfacial resistance (R_{ai}, which is the difference between the high frequency and low frequency intercepts in the impedance curve) with the introduction of 5 ppm H_2S to the dry H_2 fuel (the so-called "dry" H_2 in this study was directly from UHP grade H_2 cylinder with pH_2O of ~10 ppm). The addition of 3% moisture to the H_2 fuel does not seem to change the overall electrochemical response with respect to introduction of 5 ppm H_2S poison, as shown also in Figure 3. 1.

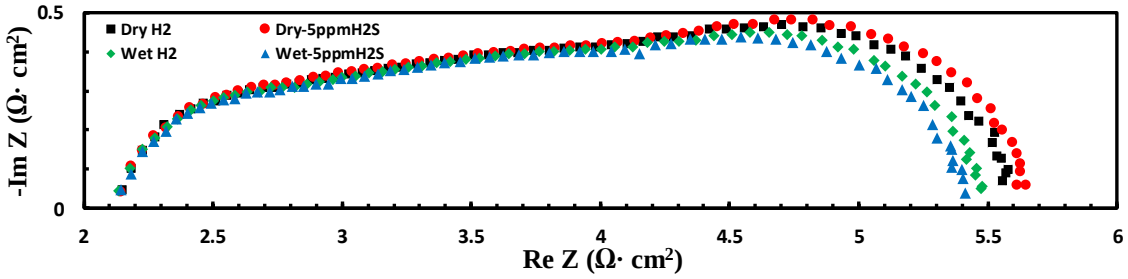

Figure 3. 1 Impedance spectra for a Ni-BZCYYb/BZCYYb/LSCF-BZCYYb anode supported proton-conducting SOFC full cell at 750°C showing the effect of introducing 5 ppm H_2S as fuel contaminant to the dry H_2 (UHP grade H_2 with $pH_2O \approx 10$ ppm; same for all subsequent figures) and 3% humidified H_2 (i.e. ~3% H_2O + 97% H_2, labelled as wet H_2 or simply wet in subsequent figures).

Figure 3. 2 (a) and (b) show the change of cell voltage of the anode-supported full cell under constant current at 750°C as a function of time when 5 ppm H_2S was introduced into and then later removed from the fuels of dry H_2 and 3% humidified H_2, respectively. The PC-SOFC with Ni-BZCYYb anode and BZCYYb electrolyte, despite the gradual degradation (probably due to non-ideal cell fabrication), appears to show no obvious poisoning by the low ppm H_2S introduced. Such tolerance to low ppm H_2S for proton conducting SOFC is consistent with earlier observations such as that by Yang et al. who reported Ni-BZCYYb/BZCYYb/LSCF anode-supported cells show sulfur tolerance up to ~20 ppm H_2S at 750^{o}C (see Figure 2. 11).[15]

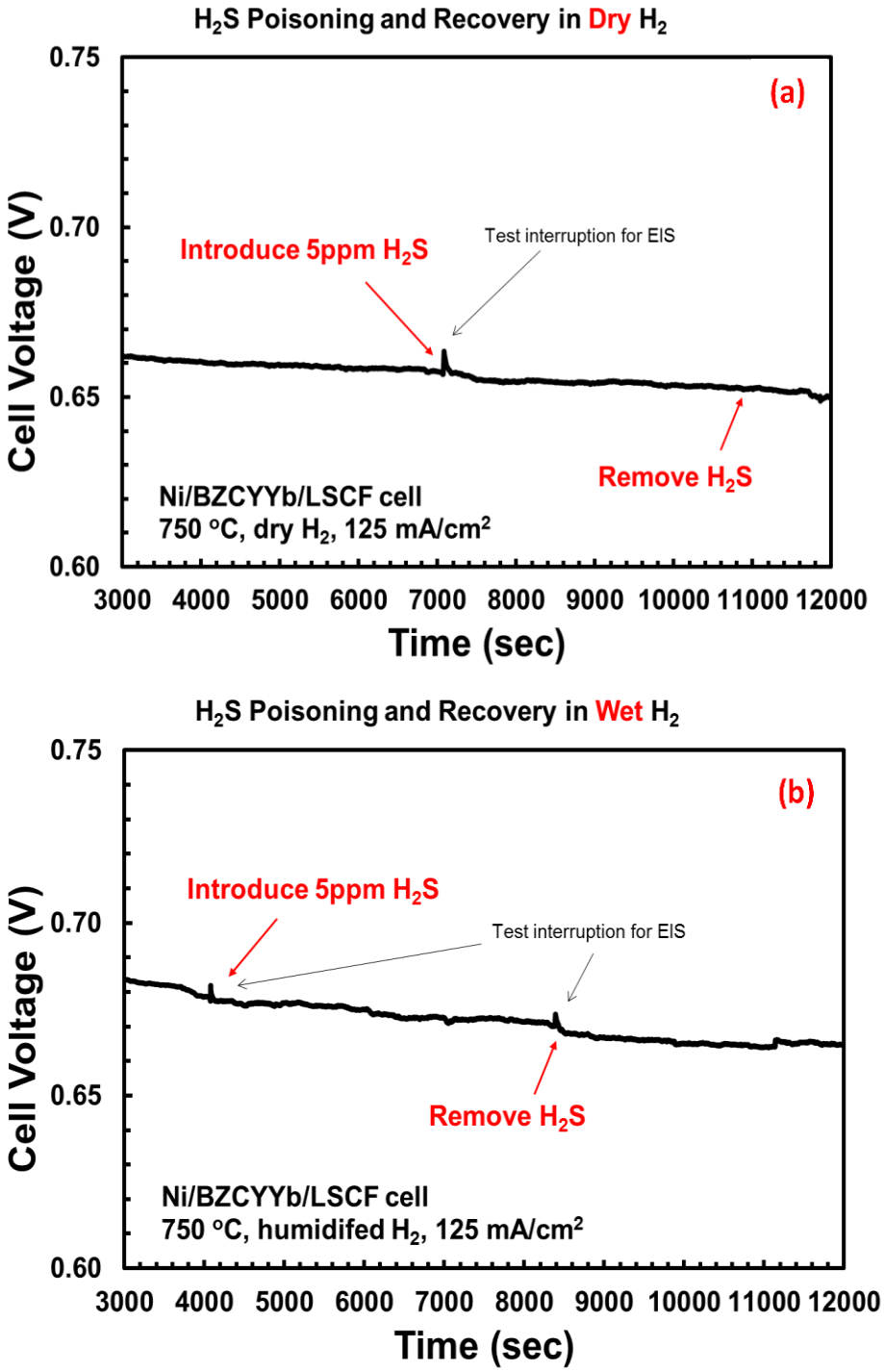

Figure 3. 2 Plots of cell voltage versus time for the Ni-BZCYYb/BZCYYb/LSCF-BZCYYb anode-supported PC-SOFC full cell at 750°C when 5 ppm of H_2S is introduced into and later removed from the fuel of (a) dry H_2 ($pH_2O \approx 10$ ppm) and (b) 3% humidified H_2.

3.3.2 H_2S Effect on Ni-BZCYYb/BZCYYb/LSCF Electrolyte-supported PC-SOFC Full Cell

The impedance spectra for the Ni-BZCYYb/BZCYYb/LSCF-BZCYYb electrolyte-supported PC-SOFC full cell under open circuit condition with 10 mV AC bias before and after the introduction of 3-10 ppm H_2S into the 3% wet H_2 fuel from 750ºC to 450ºC are shown in Figure 3. 3. At 750ºC (Figure 3. 3 (a)), with the introduction of 3 ppm H_2S, a small increase (from 1.18 $\Omega \cdot cm^2$ to 1.25 $\Omega \cdot cm^2$ or 6% relative) in the total electrode apparent interfacial resistance (R_{ai}) was observed but no change in cell ohmic resistance (R_O), which are similar to the observations for anode-supported PC-SOFC. As H_2S concentration increased from 3 ppm to 10 ppm, the poisoning effect got slightly more severe. Furthermore, it's noteworthy that the increase in R_{ai} is mainly due to the increase in the middle and low frequency (MF and LF, 10^4 to 10^{-2} Hz) semicircles, while almost no change was observed for the high frequency (HF, 10^6 to 10^4 Hz) semicircles.

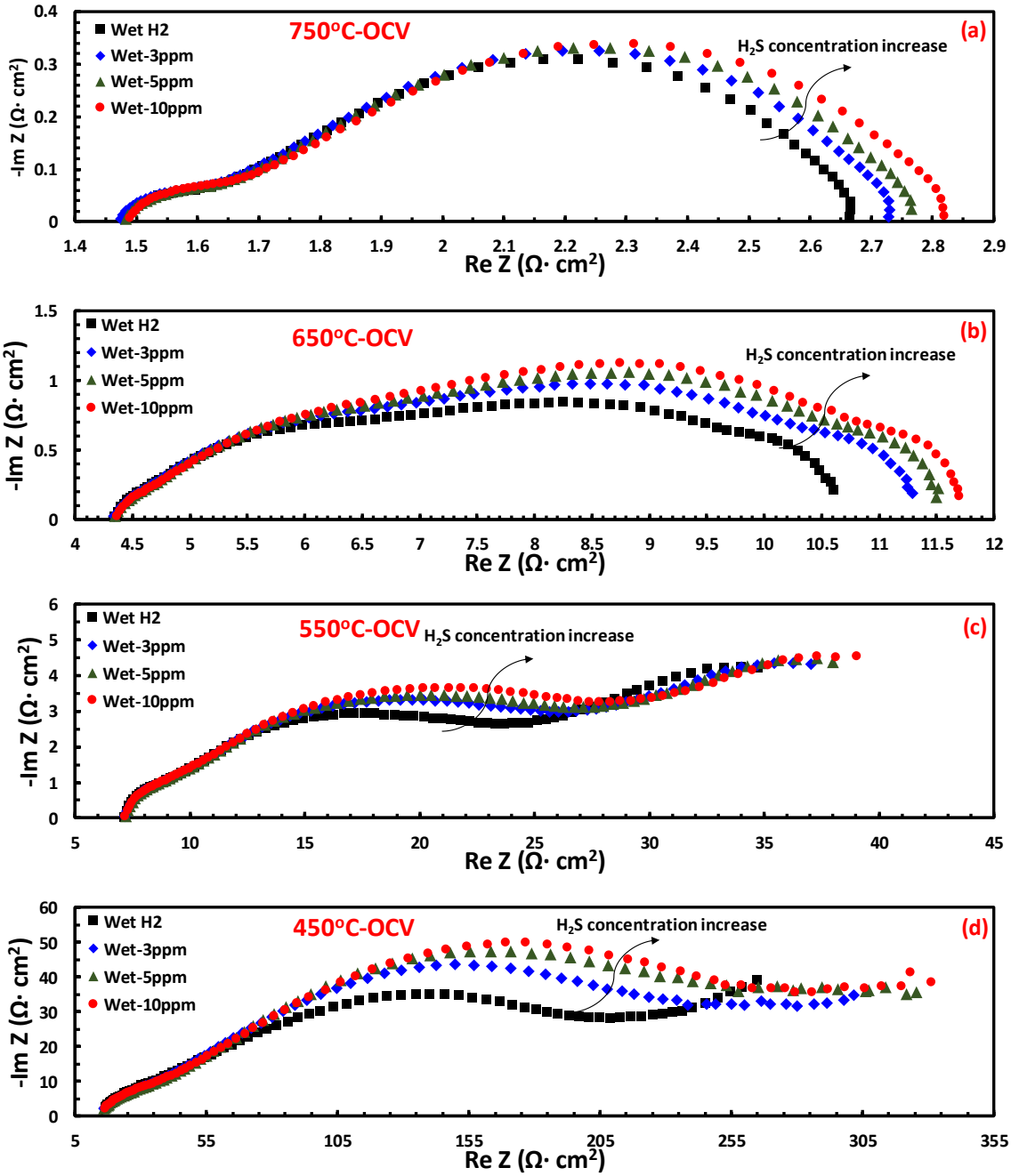

Figure 3. 3 Impedance spectra measured under open circuit condition for a Ni-BZCYYb/BZCYYb/LSCF-BZCYYb electrolyte-supported PC-SOFC full cell at (a) 750°C, (b) 650°C, (c) 550°C, and (d) 450°C showing the effect of introducing 3-10 ppm (by volume) H_2S as fuel contaminant to the ~3% wet H_2.

As temperature decreased to 650, 550 and 450°C, the observed poisoning behaviors by 3-10 ppm H_2S of the electrolyte-supported PC-SOFC full cell largely remain unchanged with a small (~10 to 20%) yet observable increase in electrode apparent interfacial resistance R_{ai} but no change in ohmic resistance R_O, and the increase in R_{ai} is limited to the MF-LF semicircles (see Figure 3. 3(b to d)).

Additionally, as shown in Figure 3. 4, the impedance spectra measured under constant current (e.g., 35 mA/cm^2) mode do not show obvious difference comparing with those measured under open circuit conditions.

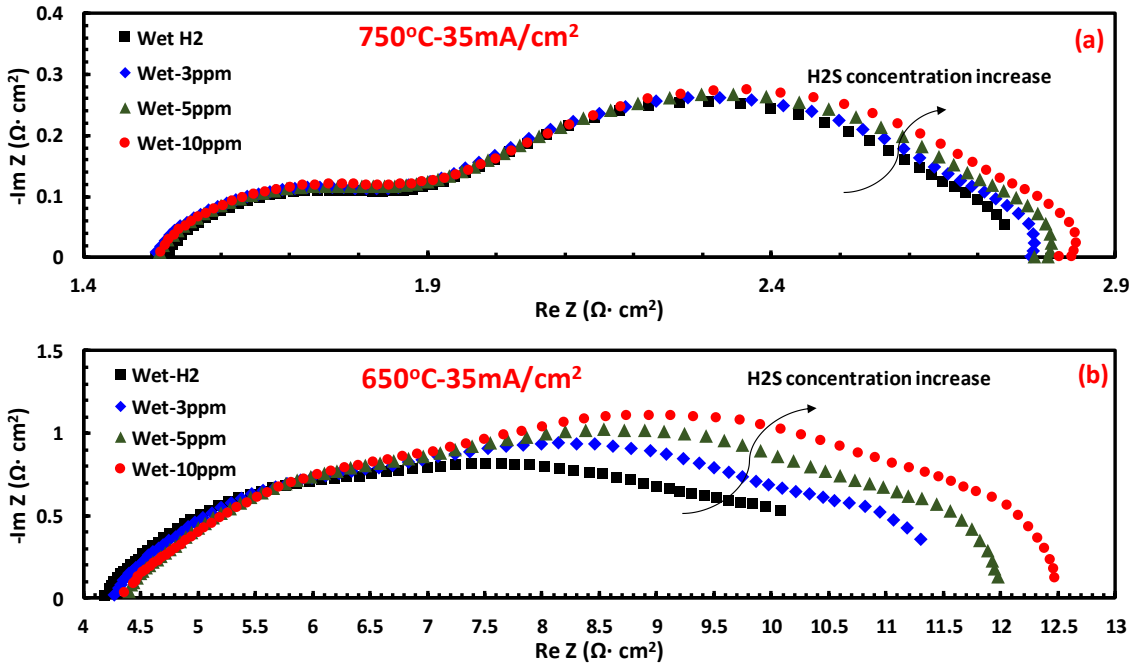

Figure 3. 4 Impedance spectra for a Ni-BZCYYb/BZCYYb/LSCF-BZCYYb electrolyte-supported PC-SOFC full cell operated with constant current of 5.5 mA/cm^2 at (a) 750°C and (b) 650°C showing the effect of introducing 3-10 ppm H_2S as fuel contaminant to the wet H_2.

Figure 3. 5 shows the cell voltage for an electrolyte-supported PC-SOFC full cell under constant current before, after the introduction of 3-10 ppm H_2S, and after the removal of H_2S in the wet hydrogen fuel. At 750°C, the decrease in cell voltage due to the introduction of ppm-level H_2S was almost negligible (Figure 3. 5(a)), which is in line with the observations (no change in cell voltage upon H_2S introduction to H_2) for anode supported PC-SOFC full cell at this temperature as shown in Figure 3. 1. As temperature dropped to 650-450°C range, the decrease in cell voltage with the introduction of H_2S becomes more obvious. Upon the removal of H_2S, cell voltage recovered slowly and also only partially at 650°C, while at lower temperature of 550 and 450°C, the recovery was not significant.

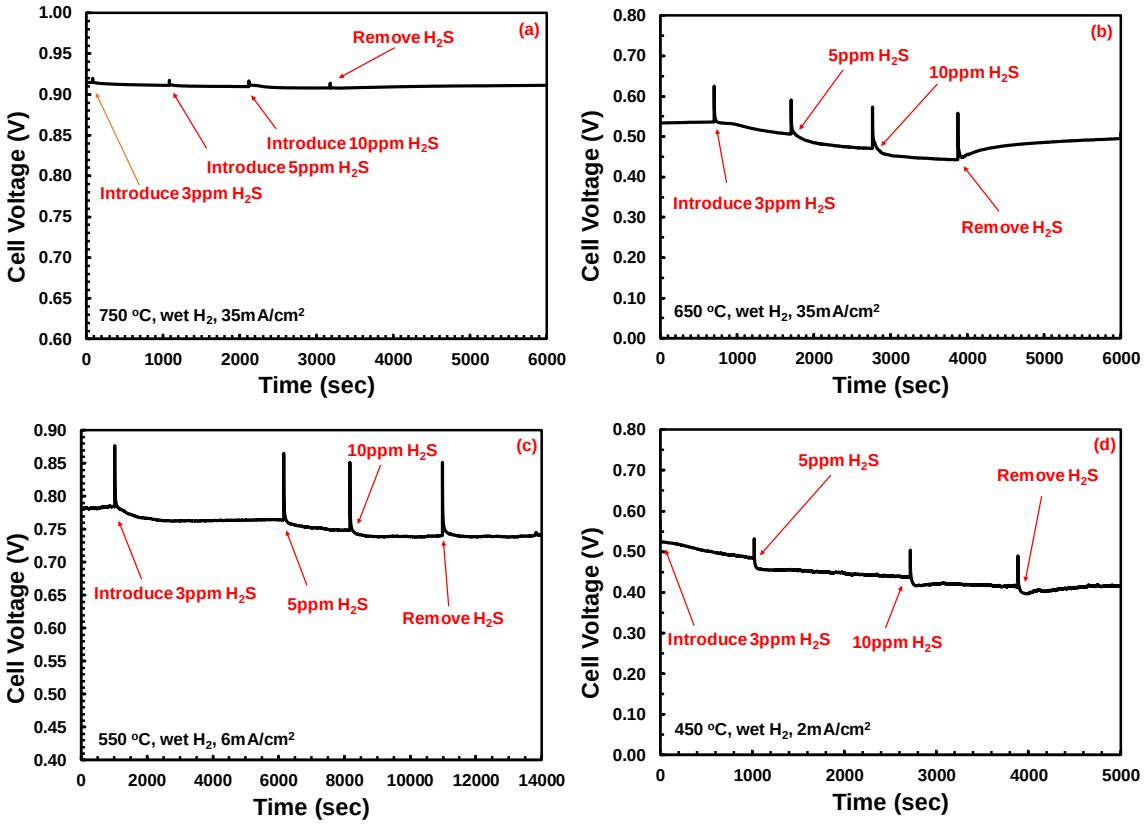

Figure 3. 5 Plots of cell voltage versus time under constant current for the Ni-BZCYYb/BZCYYb/LSCF-BZCYYb electrolyte-supported PC-SOFC full cell at (a)

750°C, (b) 650°C, (c) 550°C, and (d) 450°C when 3-10 ppm of H_2S is introduced into and later removed from the fuel of 3% humidified H_2.

3.3.3 H_2S Effect on Ni-BZCYYb/BZCYYb/Ni-BZCYYb Anode Symmetrical PC-SOFC

The impedance spectra of the Ni-BZCYYb/BZCYYb/Ni-BZCYYb anode symmetrical PC-SOFC were measured at 750°C under open circuit condition with 10 mV AC bias in dry H_2 and H_2 containing 3, 5, and 10 ppm of H_2S are shown in Figure 3. 6 (a). Different from the anode-supported and electrolyte-supported PC-SOFC full cell, for the anode symmetrical PC-SOFC, low ppm H_2S leads to clear increase in the total electrode apparent interfacial resistance R_{ai} but no change in cell ohmic resistance R_O. With increasing concentration of H_2S from 3 ppm to 5 ppm, the poisoning effect seems to get more severe. However, when H_2S concentration was further increased to 10 ppm, no further change in R_{ai} was observed, suggesting possible saturation of the H_2S poisoning effect. Examination of the impedance spectra suggests that the increase in R_{ai} is mainly due to the increase in the middle and low frequency (MF and LF) semicircles, while the high frequency (HF) semicircle remains largely unchanged after the introduction of 3-10 ppm of H_2S.

The influence of water vapor on the H_2S poisoning effect for the anode symmetrical cell is shown in Figure 3. 6 (b). It shows similar poisoning behavior by 3-10 ppm H_2S in ~3% humidified H_2 as that in dry H_2. This suggests that presence of significantly increased concentration of water vapor from ~10 ppm in the so-called dry H_2 to ~3% in the H_2 fuel

does not seem to dramatically change the electrochemical response of Ni-cermet anode to low-ppm level H_2S poison for PC-SOFC.

The results of low-ppm level H_2S poisoning effect on the Ni-BZCYYb/BZCYYb/Ni-BZCYYb symmetrical cell at reduced temperature of 650^{o}C and 550^{o}C were shown in Figure 3. 6 (c), (d), (e) and (f). It's obvious that, similar to 750^{o}C, no change in the HF semicircle or R_O was observed under both dry and wet H_2 conditions. On the other hand, at 650^{o}C and 550^{o}C, the increase in LF loops caused by H_2S becomes more obvious than at 750^{o}C, while no saturation of H_2S poisoning effect was observed up to 10 ppm of H_2S at those temperatures.

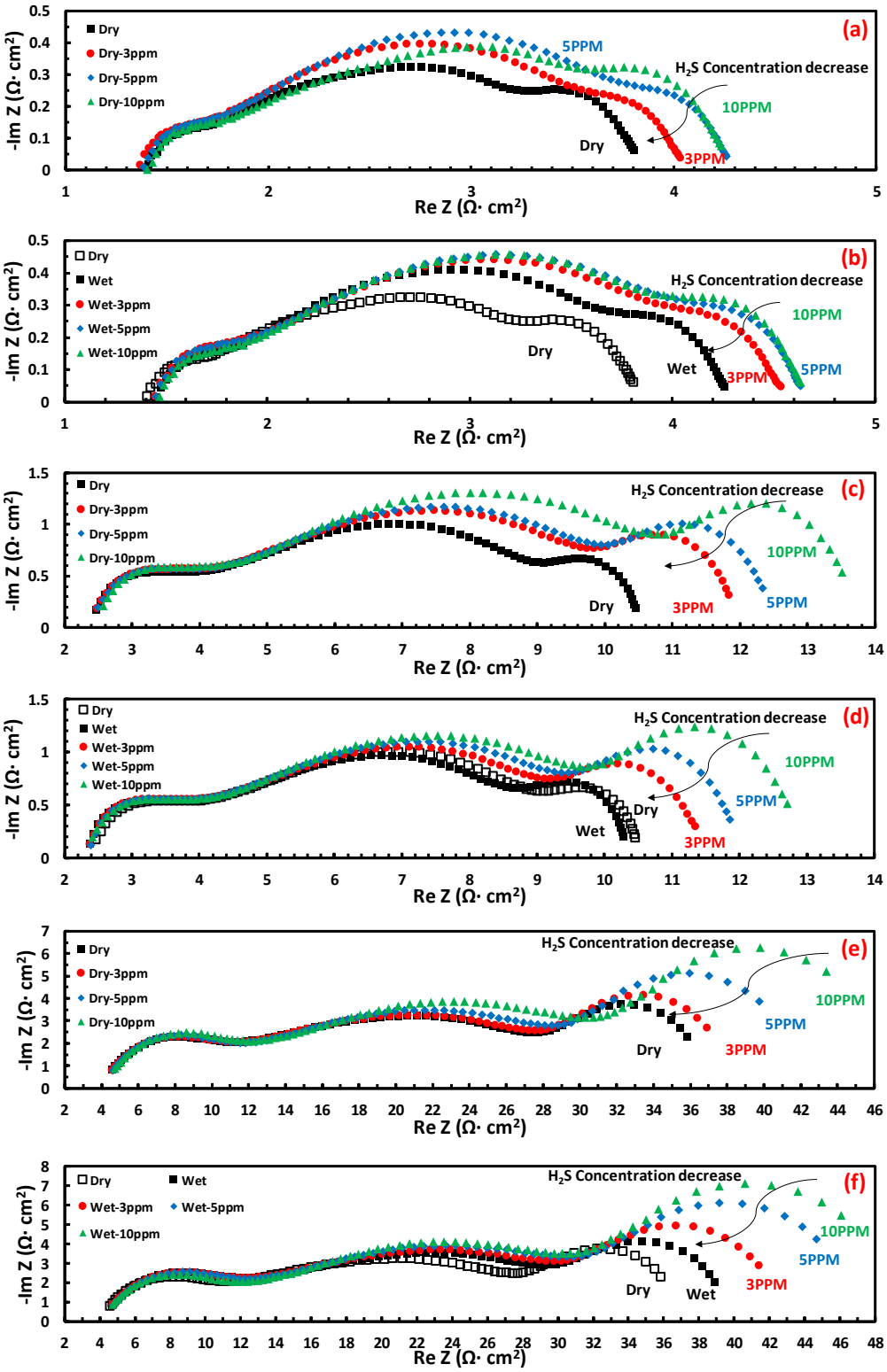
(a)
Dry
Dry-3ppm
Dry-5ppm
Dry-10ppm
5PPM
H2S Concentration decrease
10PPM
Dry
3PPM
-Im Z (Ω· cm²)
Re Z (Ω· cm²)
(b)
Dry
Wet
Wet-3ppm
Wet-5ppm
Wet-10ppm
H2S Concentration decrease
10PPM
Dry
Wet
3PPM
5PPM
-Im Z (Ω· cm²)
Re Z (Ω· cm²)
(c)
Dry
Dry-3ppm
Dry-5ppm
Dry-10ppm
H2S Concentration decrease
10PPM
Dry
3PPM
5PPM
-Im Z (Ω· cm²)
Re Z (Ω· cm²)
(d)
Dry
Wet
Wet-3ppm
Wet-5ppm
Wet-10ppm
H2S Concentration decrease
10PPM
5PPM
Dry
Wet
3PPM
-Im Z (Ω· cm²)
Re Z (Ω· cm²)
(e)
Dry
Dry-3ppm
Dry-5ppm
Dry-10ppm
H2S Concentration decrease
10PPM
5PPM
Dry
3PPM
-Im Z (Ω· cm²)
Re Z (Ω· cm²)
(f)
Dry
Wet
Wet-3ppm
Wet-5ppm
Wet-10ppm
H2S Concentration decrease
10PPM
5PPM
Dry
Wet
3PPM
-Im Z (Ω· cm²)
Re Z (Ω· cm²)

Figure 3. 6 Plots showing change of cell impedance spectra for the Ni-BZCYYb/BZCYYb/Ni-BZCYYb anode symmetrical PC-SOFC in fuels of dry H_2 (a, c, e) and ~3% humidified H_2 (b, d, f) before and after the introduction of 3, 5, and 10 ppm of H_2S at 750^{o}C (a and b), 650^{o}C (c and d), and 550^{o}C (e and f), respectively.

3.3.4 H_2S Effect on Ni-YSZ/YSZ/Ni-YSZ Anode Symmetrical OC-SOFC

Additionally, the H_2S poisoning effect on anode symmetrical OC-SOFC is also studied for comparison purposes. As shown in Figure 3. 7 (a), upon the introduction of 10 ppm H_2S into wet H_2 at 750^{o}C, R_{ai} increases by ~400% for the Ni-YSZ/YSZ/Ni-YSZ anode symmetrical OC-SOFC, which is much larger than the increase in R_{ai} (only ~10%) for the Ni-BZCYYb/BZCYYb/Ni-BZCYYb anode symmetrical PC-SOFC as shown in Figure 3. 8 (a). Similar trend, i.e., the significantly smaller relative increase in R_{ai} due to low ppm-level H_2S poisoning for PC-SOFC than for conventional OC-SOFC, was also observed at lower temperatures of 650, and 550^{o}C, as shown in Figure 3. 8(b to c) versus Figure 3. 7(b to c).

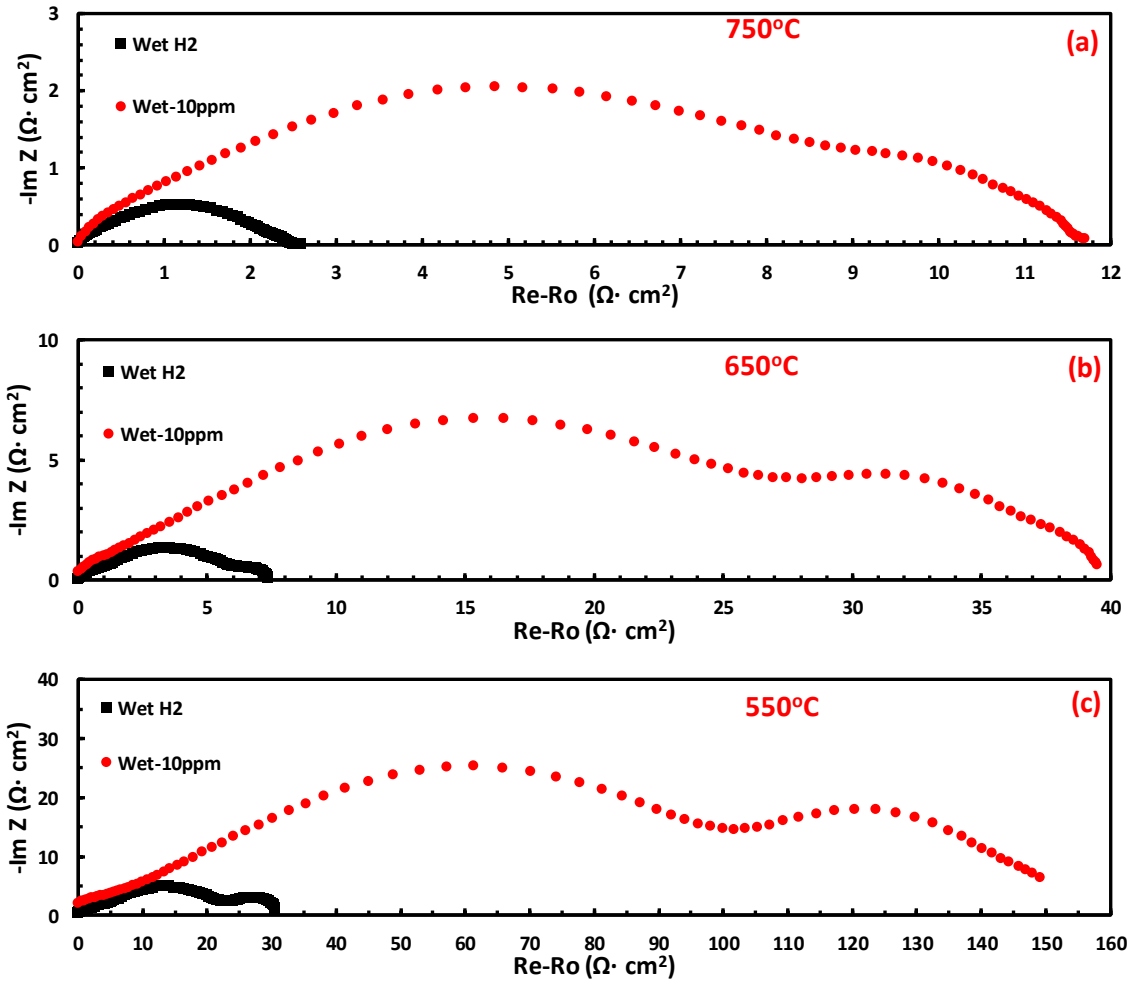

Figure 3. 7 Impedance spectra for a Ni-YSZ/YSZ/Ni-YSZ anode symmetrical OC-SOFC at (a) 750°C, (b) 650°C, (c) 550°C showing the effect of introducing 10 ppm H_2S as fuel contaminant to the wet H_2 (ohmic resistance subtracted)

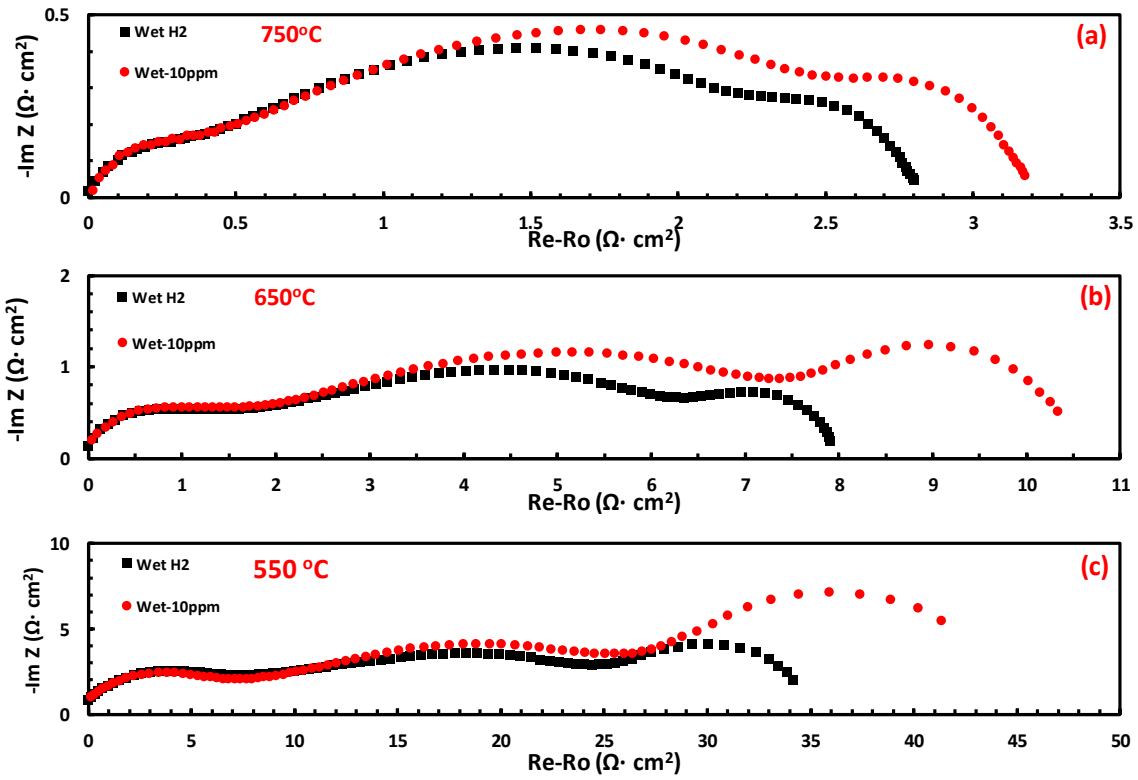

Figure 3. 8 Impedance spectra for an Ni-BZCYYb/BZCYYb/Ni-BZCYYb anode symmetrical PC-SOFC at (a) 750°C, (b) 650°C, and (c) 550°C showing the effect of introducing 10 ppm H_2S as fuel contaminant to the wet H_2 (ohimc resistance subtracted).

3.3.5 XRD and EDS Analysis on Ni-BZCYYb Powder Mixture after Exposure to H_2S

The XRD patterns for the Ni-BZCYYb loose powder mixture after exposure test to 10ppm H_2S in both dry and wet H_2 at 550°C for 24 hours are shown in Figure 3. 9. There is no obvious secondary phase formed after the exposure tests in 10 ppm H_2S balanced by either dry or wet H_2 at 550°C for 24 hours. The EDS elemental analysis of the post 10 ppm H_2S exposure samples (shown in section 3.6 supplementary materials) also shows no evidence

of sulfur accumulation in the samples. These results prove that there is no observable bulk phase reaction between Ni and BZCYYb and 10 ppm H_2S at 550°C.

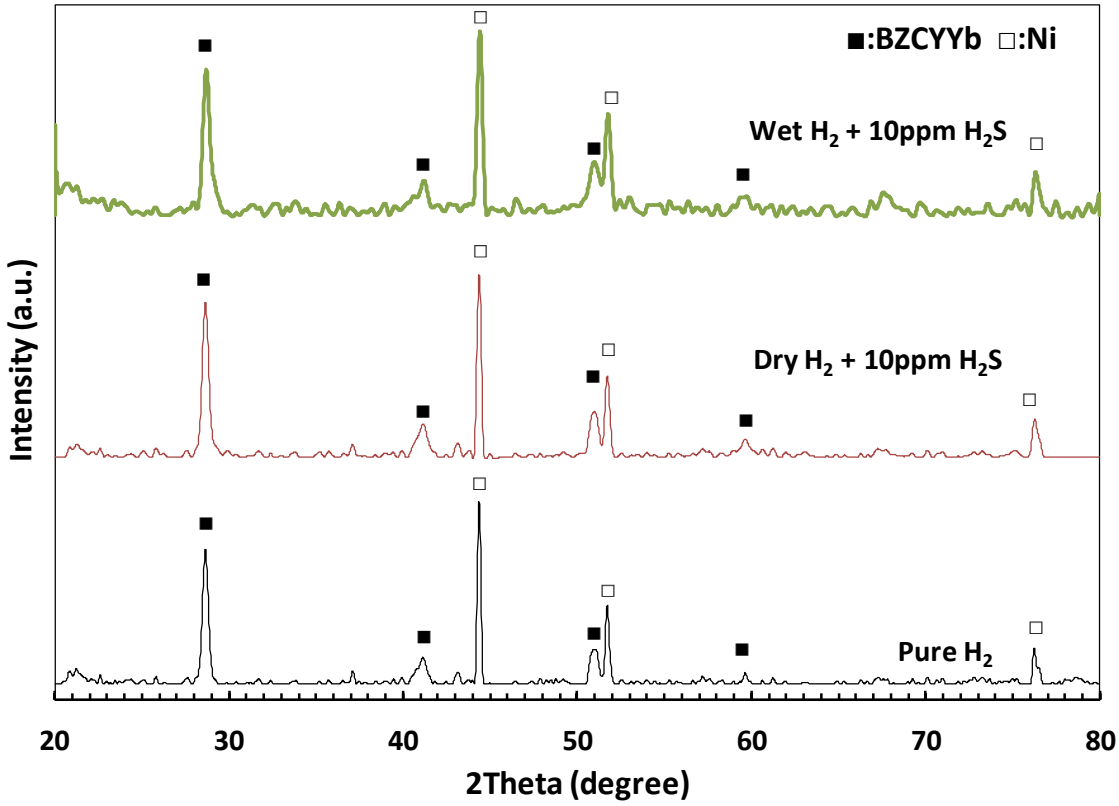

Figure 3. 9 XRD patterns for NiO-BZCYYb mixed powders after reduction in H_2 at 750°C and then exposure tests at 550°C for 24 hours in pure H_2 (as control sample) or fuel gas mixtures of dry H_2+10ppm H_2S/H_2 or wet H_2 + 10 ppm H_2S. These results prove that there is no observable bulk phase reaction between Ni and BZCYYb and 10 ppm H_2S at 550°C.

3.3.6 SIMS Analysis on Ni-BZCYYb Composite Pellet after Exposure to Low-ppm Level H_2S

Figure 3. 10 shows a representative optical microscope image of the Ni-BZCYYb composite pellet sample after sintering in 4%H_2/Argon (Ar) forming gas and subsequent grinding and polishing. The sample surface is reasonably smooth with easily identifiable bright and dark parts, which correspond to the Ni and the BZCYYb phase, respectively. The Ni regions have dimension of ~10-20 μm, while the BZCYYb regions are ~30-60 μm in size.

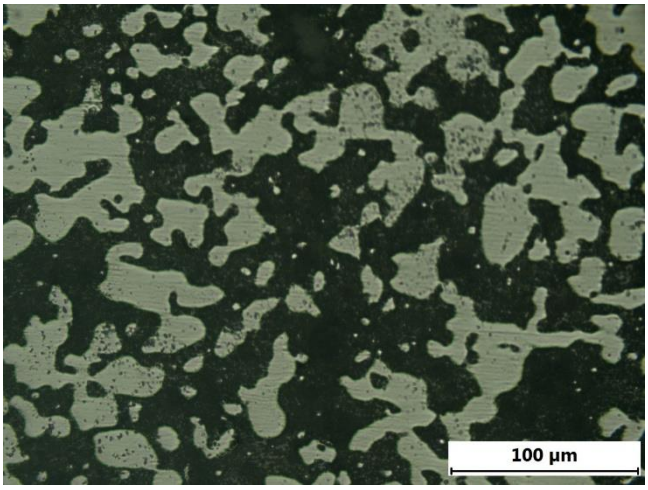

Figure 3. 10 Metallographic microscope image of the sintered and polished Ni-BZCYYb composite sample surface. The bright and dark regions correspond to the Ni and the BZCYYb phase, respectively

Figure 3. 11 shows a representative SIMS elemental mapping image of Ni and Ba species and S species from the surface of the Ni-BZCYYb dense composite pellet after it had been exposed to 10 ppm H_2S balanced by ~3% humidified H_2 at 550^oC for 24 hours

followed by rapid cooling in clean wet H_2. It's observed that Ba and S species show strong association with each other, as evidence by their overlapping distribution, while the distribution of Ni species is complementary to Ba and S species.

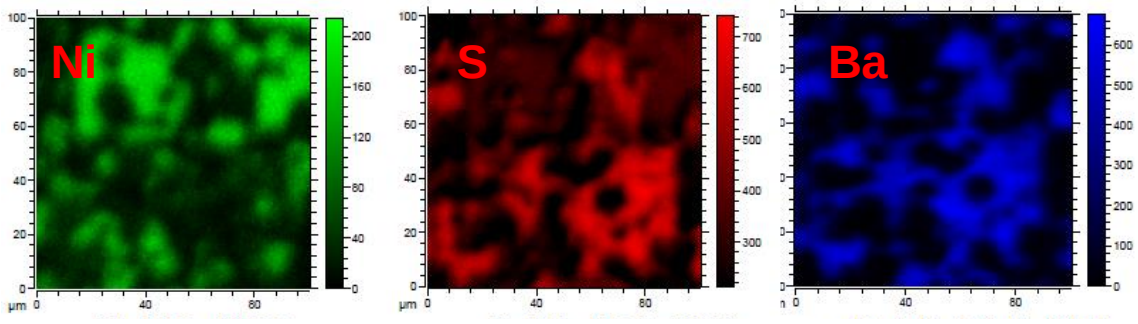

Figure 3. 11 Representative SIMS mapping results showing the distributions of Ni, S, and Ba species (including their associated oxides) as the sample was sputtered down during the analysis

3.4 Discussion

3.4.1 Electrochemical Behaviors of PC-SOFC against H_2S Poisoning

For electrolyte-supported PC-SOFC full cell and anode symmetrical cell, depending on temperature and H_2S concentration, there is an observable increase by ~10-30% in the electrode apparent interfacial resistance R_{ai}, which is largely confined to the ML to LF semicircles, while there is no obvious change in ohmic resistance R_O. (see Figure 3. 3, Figure 3. 4 and Figure 3. 6) These observations indicate that typical PC-SOFC with Ni-PCC based cermet anodes are still subjected to poisoning by low ppm-level sulfur contaminant in the hydrogen fuel at ~750 to 550^{o}C. Such a conclusion is *not* surprising consider that the typical cermet anode for a common PC-SOFC still consists of Ni metal

and highly basic PCC electrolyte such as BZCYYb, both of which have high affinity for sulfur *adsorption* and may even form bulk sulfide phases (when H_2S concentration is high in the range of hundreds of ppm or higher). [137] In addition, the results also show that as temperature drops (from ~750 to ~550^oC), the observed poisoning by low ppm-level H_2S becomes only slightly more obvious (see Figure 3. 4, Figure 3. 5, Figure 3. 6) and less reversible (Figure 3. 5), but there seems to be no fundamental change in the poisoning behavior, suggesting the underlying poisoning mechanism in that temperature range is likely to remain the same.

Comparing with earlier studies and our own study, it seems that, at elevated temperature such as 750-600^oC, the electrolyte-supported PC-SOFC as well as proton conducting anode symmetrical cell are more sensitive to H_2S poisoning than anode-supported PC-SOFC. [15, 38, 141, 142]Since all three types of electrochemical cells have the similar Ni-PCC cermet anode with doped $Ba(Ce,Zr)O_3$ (e.g., BZCYYb) based PCC electrolyte, the difference in H_2S sensitivity (i.e., the relative increase in R_{ai} due to exposure to similar low-ppm H_2S) is attributed to the large difference in the cermet anode thickness. The anode supported PC-SOFC full cell have thick anodes on the order of ~600 μm, while both electrolyte-supported PC-SOFC full cell and anode symmetrical PC-SOFC have relatively thin anode of ~30 μm, which makes the electrochemical response for those later two faster and more obvious.

3.4.2 Comparison of Electrochemical Behaviors of Anode Symmetrical PC-SOFC versus OC-SOFC

In this study, the electrochemical behavior against low-ppm level H_2S for the anode symmetrical PC-SOFC is also compared with anode symmetrical OC-SOFC with YSZ electrolyte and Ni-YSZ cermet anode at ~750^oC and lower temperatures. As summarized in However, there is also one major difference in the observed electrochemical behaviors against H_2S poisoning between the two types of SOFCs. For comparable H_2S concentration and temperature, the relative degradation in anode electrochemical reaction rate appears to be *much smaller* for a PC-SOFC comparing with a typical oxide-ion conducting SOFC. For example, for both electrolyte-supported (see Figure 3. 5) and anode-supported PC-SOFC (Figure 3. 2), when temperature was 750^oC, low ppm-level H_2S causes a very small drop (~0-2%) in cell power output under constant current operation. (Note such an observation was made for low fuel utilization condition, which might change when current density or fuel utilization is high.) In comparison, numerous earlier studies clearly show a significant drop (~10-15%) in power output for conventional oxide-ion conducting SOFC. [29, 137] The results of impedance measurement under open circuit condition are also consistent with the power output measurement. For electrolyte-supported PC-SOFC full cell, as shown in Figure 3. 4, the electrode apparent interfacial resistance R_{ai} increases due to 10 ppm H_2S is only ~20% at 750^oC, while it was ~80% for 8 ppm(v) H_2S for conventional electrolyte-supported SOFC at 800^oC. [29] Such a difference is even *more obvious* when comparison was made on the electrode interfacial resistance change *for anode symmetrical cells*. The possible explanations are discussed later.

Table 3. 1, there are several *similarities*. First, when low ppm level H_2S is used (i.e., without the concern of causing bulk phase reactions), [137] both OC-SOFC and PC-SOFC show performance degradation as evidenced by either a drop in cell power output (e.g., cell voltage drop under constant current condition) or an increase in electrode apparent interfacial resistance R_{ai} with little or no change in cell ohmic resistance R_O. Second, the extent of sulfur poisoning for both types of SOFC appears to get more significant when H_2S concentration increases or when the temperature drops. [15, 29, 33, 35, 38, 138]

However, there is also one major difference in the observed electrochemical behaviors against H_2S poisoning between the two types of SOFCs. For comparable H_2S concentration and temperature, the relative degradation in anode electrochemical reaction rate appears to be *much smaller* for a PC-SOFC comparing with a typical oxide-ion conducting SOFC. For example, for both electrolyte-supported (see Figure 3. 5) and anode-supported PC-SOFC (Figure 3. 2), when temperature was 750^{o}C, low ppm-level H_2S causes a very small drop (~0-2%) in cell power output under constant current operation. (Note such an observation was made for low fuel utilization condition, which might change when current density or fuel utilization is high.) In comparison, numerous earlier studies clearly show a significant drop (~10-15%) in power output for conventional oxide-ion conducting SOFC. [29, 137] The results of impedance measurement under open circuit condition are also consistent with the power output measurement. For electrolyte-supported PC-SOFC full cell, as shown in Figure 3. 4, the electrode apparent interfacial resistance R_{ai} increases due to 10 ppm H_2S is only ~20% at 750^{o}C, while it was ~80% for 8 ppm(v) H_2S for conventional electrolyte-supported SOFC at 800^{o}C. [29] Such a difference is even *more obvious* when comparison was made on the electrode interfacial resistance change *for anode symmetrical cells*. The possible explanations are discussed later.

Table 3. 1 Summary of poisoning effect by low-ppm level H_2S on oxide-ion conducting SOFC and PC-SOFC in hydrogen-based fuel at ~750 ºC. For electrolyte, YSZ stands for 8 mol% yttria stabilized zirconia while BZCYYb stands for $BaZr_{0.1}Ce_{0.7}Y_{0.1}Yb_{0.1}O_{3-\delta}$ proton conducting ceramic (PCC) electrolyte. ΔR_O and ΔR_{ai} are the observed *relative* increase in cell ohmic resistance and total electrode apparent interfacial resistance, respectively, measured under open circuit condition.

Cell Structure	**Electrolyte**	**Reference**	**T (ºC)**	***p*H$_2$S/*p*H$_2$ (ppm(v))**	**Poisoning behavior**		
					ΔR_O	ΔR_{ai}	Drop in cell power
Anode-supported cell	YSZ	Rasmussen[3]	850	7	0	~30%	~10% (at 1 A/cm^2)
		Yang[17]	750	10	~10%	~80% (at 200 mA/cm^2)	~11% (at 241 mA/cm^2)
	PCC	Yang[12]	750	20	0	0 (wet)	~0 (at 700 mA/cm^2)
		Sun[11]	750	5	0	~2%	~0 (at 125 mA/cm^2)
Electrolyte-supported cell	YSZ	Zha[6]	800	8	0	~80%	~15% (at 0.7 V)
	PCC	This study	750	10	0	~20%	~2% (at 35 mA/cm^2)
Anode symmetrical cell	YSZ	Matsuzaki[4]	750	0.7	0	~110%	N/A
		Zha[6]	800	8	0	~200%	
		This study	750	10	0	~400%	
	PCC	Sun[11]	750	10	0	~10%	

In addition, for the anode symmetrical PC-SOFC with the configuration of Ni-BZCYYb/BZCYYb/Ni-BZCYYb, the change of activation energy for ohmic resistance R_O

and apparent interfacial resistance R_{ai} in dry H_2 ($pH_2O \approx 10$ ppm as mentioned) and upon introduction of various concentrations of H_2S into dry H_2 is shown in Figure 3. 12 (a). The activation energy for R_O was about 0.45 eV, which matches that for typical proton conducting electrolytes. [85] The activation energy for the overall anode apparent interfacial resistance R_{ai} was about 0.92 eV, which is comparable to that for Ni-YSZ cermet H_2 electrode for oxide ion SOFC. [83, 87, 143, 144] As the impedance spectra (see Figure 3. 6) could be clearly separated into at least three semi-circles, the activation energy for each of the high, middle and low frequency part of polarization resistance (R_{HF}, R_{MF}, R_{LF}) was also analyzed. As mentioned before, with the introduction of 10 ppm H_2S, there is no obvious change in the HF semicircle. Consistently, there also appears to be no change for the activation energy for R_{HF}. This suggests that the HF process, which is most likely attributed to the charge transfer step, is not influenced by the introduction of low ppm-level H_2S for the anode symmetrical cell based on BZCYYb proton conducting electrolyte and Ni-BZCYYb cermet anode. In comparison, for the low frequency LF semicircle, the activation energy seems to increase with increasing H_2S concentration up to ~5 ppm. This means the introduction of low ppm-level H_2S makes it more difficult for the LF process and greater activation would be required. A natural hypothesis would be that the LF process might be associated with the surface diffusion process for the hydrogen electrode reaction of PC-SOFC, and the strong adsorption of sulfur interferes with the surface diffusion of adsorbed hydrogen (atoms). The sensitivity of adsorption to different low ppm-level H_2S suggests that the surface diffusion in this anode reaction is actually more likely to be over the BZCYYb surface as nickel surface should have already been saturated by parts-per-billion (ppb) level H_2S at intermediate temperature of 550^oC and no longer

sensitive to variation in low ppm-level H_2S. [25, 28] As to the mid frequency MF process, interestingly, although it seems to slow down, the activation energy actually does not change upon H_2S introduction. One possibility is that the poisoning at MF is related to physical blockage, i.e., reduced possibility of occupation but without change in the reaction mechanism. Therefore, the MF process may correspond to hydrogen adsorption onto the BZCYYb surface since at intermediate temperature such as 550^oC, Ni surface would already be completely covered by ppb-level sulfur and would not show sensitivity in low ppm-level H_2S concentration. [25, 28, 137]The H_2S poisoning behavior for proton conducting SOFC in 3% humidified hydrogen (see Figure 3. 8 and Figure 3. 12 (b)) is similar to that in dry H_2, suggesting that introduction of significantly more moisture to H_2 (i.e., 3% versus ~10 ppm in the so-called dry H_2) does not fundamentally change the sulfur poisoning behavior for Ni-proton conducting electrolyte cermet anode of PC-SOFC.

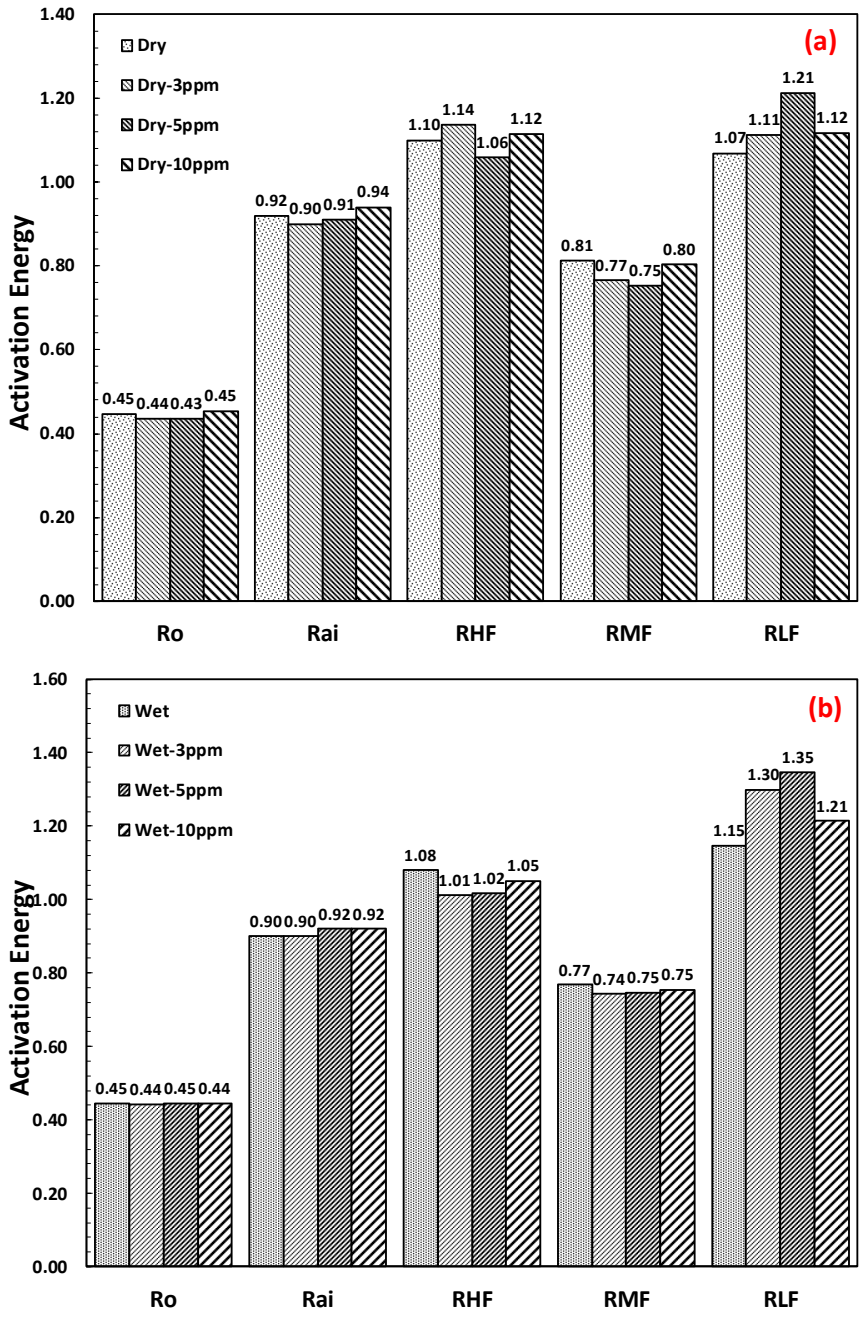

Figure 3. 12 Comparison of activation energy (calculated from 550-750^{o}C) for ohmic resistance R_O, total apparent interfacial resistance R_{ai}, and the different electrode processes at high frequency R_{HF}, mid-frequency R_{MF}, and low frequency R_{LF} in (a) dry H_2 ($pH_2O \approx 10$ ppm) and (b) 3% humidified H_2 without and with 3, 5, and 10 ppm H_2S poison for the Ni-BZCYYb/BZCYYb/Ni-BZCYYb anode symmetrical PC-SOFC.

3.4.3 Analysis of the H_2S Effect on Ni-BZCYYb Mixture

It should be mentioned that, unlike the conventional oxide ion conducting YSZ electrolyte, the highly basic proton conducting oxides such as BZCYYb are known to have strong tendency to interact with H_2S to either form bulk metal sulfides (e.g., BaS) or strongly adsorbed surface sulfur species. In fact, it had been reported that at 750^{o}C, the BZCYYb proton conducting electrolyte would not react with 50 ppm H_2S in hydrogen, [15]but it does react and form bulk BaS when H_2S concentration was increased to 100 ppm or when the balance gas was changed to argon. [89] In this study, as mentioned before, the bulk phase stability of the Ni-BZCYYb mixed powders against 10 ppm H_2S balanced by dry or wet H_2 at temperature such as 550^{o}C was confirmed in the exposure tests (see Figure 3. 9 (a)) showing no indication of observable bulk reaction between H_2S and Ni or BZCYYb. In addition, analysis using EDS did not identify the presence of bulk sulfide in the post H_2S exposure samples. On the other hand, The observed strong association between the Ba species (e.g., Ba^+, BaO^+, $BaOH^+$) and S species (e.g., S^-, SO^-, SO_2^-, SO_3^-) indicates that besides the well-known sulfur adsorption on Ni metal phase, [25, 28, 29, 137, 138] H_2S also interacts with the PCC electrolyte phase (in this study, BZCYYb) to form certain sulfur-containing species on and near the surface of the cermet including near the triple phase boundary (TPB).

However, two experimental observations also need to be taken into account here. First, in our SIMS analysis, the observed association between Ba species and S species persists even after the sample was sputtered down using ions (in this case, Bi^{3+} ions) for tens of microns and even deeper. Second, as mentioned before, no bulk BaS or other sulfur-

containing bulk phases were formed in Ni-BZCYYb powder, despite extended exposure to the low-ppm level H_2S at the testing temperature including 550^oC.

Considering all the experimental observations discussed above especially XRD, EDS and SIMS analysis of the H_2S exposed samples, the implication is that the interaction between H_2S and BZCYYb PCC electrolyte under the condition studied (low ppm H_2S at 450-750^oC) appears to be bulk in nature but not to the extent of forming a new crystalline phase. One possibility for such a scenario is that, with the presence of low ppm-level H_2S in the gas atmosphere, some sulfur atoms may get incorporated or dissolved into the BZCYYb bulk at low concentration via displacing lattice oxygen transforming the BZCYYb material into an oxysulfide, i.e. $Ba(Zr_{0.1}Ce_{0.7}Y_{0.1}Y_{0.1})O_{3-\delta-y}S_y$ with $y<<1$. This seems reasonable given that oxides such as cerium oxide (CeO_2) was observed to transform gradually to oxysulfide and eventually to sulfide depending on H_2S concentration. [141, 145-147] In comparison, no clear association between Ni and H_2S was detected by SIMS throughout the analysis including when the sample was sputtered down. This is consistent with the nature of sulfur adsorption over Ni surface and the limited sulfur solubility (on the order of 10 ppm) in solid nickel at those temperatures. [24-26, 29, 31] As the surface-adsorbed sulfur is sputtered away during SIMS analysis, very little sulfur exists within the bulk of Ni (<~10 ppm(v)), and, therefore, no clear association of sulfur and Ni was identified.

3.4.4 Proposed H_2S Poisoning Mechanism for the Anode Reaction Process of PC-SOFC

In summary, this study shows that typical PC-SOFC with Ni-PCC electrolyte cermet anode is still poisoned by low ppm-level H_2S at temperature in the range of 450-750^oC. Consistent with conventional OC- SOFC, anode sulfur poisoning of PC-SOFC is characterized by an increase in anode interfacial resistance with no change in ohmic resistance. As H_2S concentration increases or temperature decreases, the extent of sulfur poisoning (in terms of relative increase in interfacial resistance increase or drop in power output) increases, while it also becomes less reversible.

However, as stated, there is also one major difference in terms of sulfur poisoning behavior between the two types of SOFCs with different ion conducting species. The observed extent of performance degradation due to sulfur poisoning by low-ppm level H_2S for PC-SOFC is typically much less than that for conventional OC-SOFC under comparable conditions (e.g., temperature and bias condition). Such a difference is attributed primarily to the different anode reaction routes for these two types of SOFCs as shown in Figure 3. 13. In particular, as state before in section 2.2.1. , the anode reaction in conventional oxide-ion conducting SOFC with YSZ electrolyte and Ni-YSZ cermet anode involves multiple steps including (1) hydrogen adsorption, (2) hydrogen dissociation and surface diffusion, (3) charge transfer and associated water (H_2O) evolution, and finally (4) water desorption as shown in Figure 3. 13 (a). (It is recognized that hydrogen adsorption and dissociation over Ni surface is typically extremely fast at elevated temperature. [28, 138]) When sulfur (e.g., as H_2S) is present in the system, it will selectively adsorb over Ni

surface (and not much over YSZ surface), which inhibits the steps of (1) hydrogen gas adsorption, and (2) dissociation and surface diffusion as shown in Figure 3. 13 (b). In addition, due to the relatively large size of water molecules, it is also reasonable to expect that the adsorbed sulfur over Ni near TPB would also dramatically slow down step (3) of charge transfer as it requires unoccupied sites for water generation.

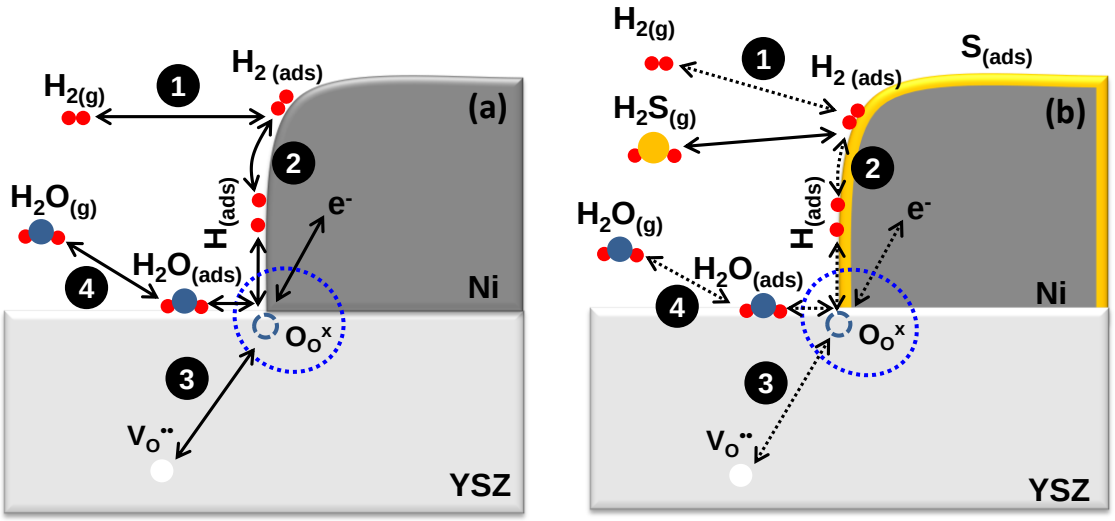

$$H_2 + O_O^x \leftrightarrow V_O^{\bullet\bullet} + H_2O + 2e^-$$

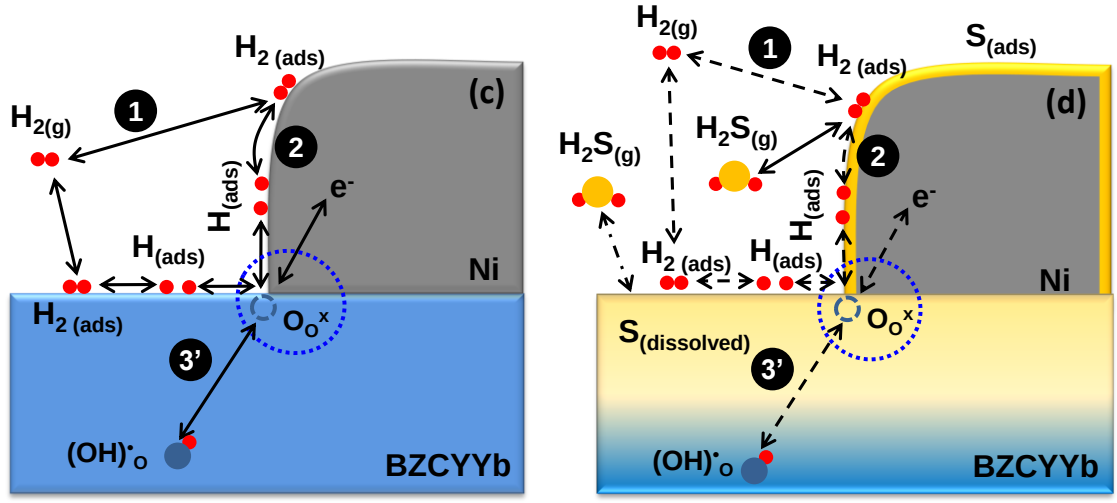

$$H_2 + 2O_O^x \leftrightarrow 2(OH)_O^{\bullet} + 2e^-$$

Figure 3. 13 Schematics showing anode reaction steps for both conventional oxide-ion conducting SOFC (a and b) and ideal pure PC-SOFC (c and d) before (a, c) and after (b, d) sulfur poisoning by low-ppm level H_2S at intermediate temperature. Note that the anode reaction mechanism for PC-SOFC is greatly simplified and the exact process including the dominating pathway still needs to be studied. In addition, BCZYYb stands for the $BaZr_{0.1}Ce_{0.7}Y_{0.1}Yb_{0.1}O_{3-\delta}$ PCC electrolyte used in this study, while BZCYYbS stands for BZCYYb with sulfur incorporation into the oxygen sublattice to form $Ba(Zr_{0.1}Ce_{0.7}Y_{0.1}Y_{0.1})O_{3-\delta-y}S_y$ oxysulfide with $y<<1$.

In comparison, for a PC-SOFC especially at relatively low temperatures such as 550 or 450^{o}C, the system would approach ideal pure proton conduction condition. The anode hydrogen electrochemical oxidation reaction in such an ideal PC-SOFC would only involve (3') hydrogen incorporation into the proton conducting electrolyte and no water evolution as shown in Figure 3. 13 (c). [15, 38, 81, 88] (It is noted that unlike conventional OC-SOFC, the exact anode reaction process for PC-SOFC, including whether it is limited to TPB or occurring over Ni or PCC surface, is not yet clear at the moment, and the schematic in Figure 3. 13 (c) is only an over-simplification of the actual processes.) Under such circumstance, if sulfur is present in the system, adsorbed sulfur would still cover both Ni metal as well the PCC electrolyte surface and interfere with (1) hydrogen adsorption and (2) dissociation and surface diffusion over Ni surface as shown in Figure 3. 13 (d). This naturally would slow down the overall anode reaction somewhat. However, it is hypothesized that, due to absence of water involvement in the anode reaction process for PC-SOFC and the relatively small size of hydrogen molecule/atom, the anode reaction could still proceed with less disruption than the circumstance when water is involved, as in conventional oxide-ion conducting SOFC.

On the other hand, one additional hypothesis from the observed much less degradation for sulfur poisoning of PC-SOFC comparing with conventional OC-SOFC is that the proton conducting ceramic (PCC) electrolyte (in this case, BZCYYb) might also play some (electro-)catalytic role in the anode hydrogen electrochemical oxidation reaction for PC-SOFC. In other words, the PCC electrolyte surface might also be active for the adsorption and dissociation of hydrogen molecules in the hydrogen anode reaction for PC-SOFC, especially at temperature of ~450-550^{o}C. The support for this hypothesis is that previous studies have shown that adsorbed sulfur would almost completely cover the Ni metal surface and dramatically slow down the adsorption and dissociation of hydrogen over the Ni surface under the relevant sulfur poisoning condition studied (e.g., 550 ^{o}C with ~10 ppm(v) H_2S). [25, 28, 137] For a PC-SOFC with Ni-PCC cermet anode, if all catalytically active sites are limited to the Ni surface, the near complete coverage of Ni surface by adsorbed sulfur would lead to very large increase in anode interfacial resistance R_{ai}, which might be the case for the >400% increase in R_{ai} for an anode symmetrical cell based on conventional oxide conducting electrolyte (see, for example, Figure 3. 7). In contrast, for a PC-SOFC, the actual observed relative increase in R_{ai} was very moderate at ~10-20% (see, for example, Figure 3. 7Figure 3. 1, Figure 3. 3, Figure 3. 4 and However, there is also one major difference in the observed electrochemical behaviors against H_2S poisoning between the two types of SOFCs. For comparable H_2S concentration and temperature, the relative degradation in anode electrochemical reaction rate appears to be *much smaller* for a PC-SOFC comparing with a typical oxide-ion conducting SOFC. For example, for both electrolyte-supported (see Figure 3. 5) and anode-supported PC-SOFC (Figure 3. 2), when temperature was 750^{o}C, low ppm-level H_2S causes a very small drop (~0-2%) in cell power

output under constant current operation. (Note such an observation was made for low fuel utilization condition, which might change when current density or fuel utilization is high.) In comparison, numerous earlier studies clearly show a significant drop (~10-15%) in power output for conventional oxide-ion conducting SOFC. [29, 137] The results of impedance measurement under open circuit condition are also consistent with the power output measurement. For electrolyte-supported PC-SOFC full cell, as shown in Figure 3. 4, the electrode apparent interfacial resistance R_{ai} increases due to 10 ppm H_2S is only ~20% at 750^{o}C, while it was ~80% for 8 ppm(v) H_2S for conventional electrolyte-supported SOFC at 800^{o}C. [29] Such a difference is even *more obvious* when comparison was made on the electrode interfacial resistance change *for anode symmetrical cells*. The possible explanations are discussed later.

Table 3. 1) even though Ni metal is still the only metal phase in the cermet anode.

Therefore, it seems likely that the surface of PCC electrolyte such as BZCYYb could also be active for hydrogen adsorption and dissociation under the condition studied, which is possible given that PCC electrolytes are known to interact with hydrogen. With the presence of low-ppm level H_2S, SIMS analysis of the Ni-BZCYYb composite suggests that sulfur atoms have got incorporated into the bulk of BZCYYb electrolyte (possibly by displacing lattice oxygen), while analysis using XRD and EDS have ruled out the formation of other crystalline bulk sulfides. We hypothesize that the similar nature of sulfur and oxygen in terms of their valence states may not lead to significant change in the defect structure of the PCC electrolyte, and hydrogen surface adsorption/dissociation might still remain active despite the PCC electrolyte surface oxygen covered-over or even (partially)

replaced by sulfur. Further detailed mechanism studies including i) analysis with more sensitive and quantitative surface analysis techniques, ii) use of patterned electrode cells with different metal electrodes that enable comparison between Ni metal and inert metal catalysts (e.g., gold or copper metal) and use of cells with different controlled microstrctures, and iii) theoretical modeling including fitting of the impedance data with better separation to equivalent circuits are all needed to test the hypotheses raised here and provide more insights about the fundamental anode reaction mechanism and sulfur poisoning processes for PC-SOFC.

3.5 Conclusions

The effect of H_2S as a fuel contaminant on PC-SOFC was studied. The results from proton conducting SOFC full cells and proton conducting anode symmetrical cells clearly show that PC-SOFC, similar to conventional OC-SOFC, is still poisoned by low-ppm level H_2S at temperatures in the range of 750 to 450^oC with increase in anode interfacial resistance R_{ai} and no change in ohmic resistance R_o. The sulfur poisoning for PC-SOFC gets more obvious and less reversible as H_2S concentration increases. On the other hand, the relative degradation in anode reaction rate due to sulfur poisoning (e.g., as measured by relative increase in anode interfacial resistance) is much smaller for PC-SOFC than for conventional OC-SOFC under comparable conditions. This is attributed to the fact that the anode reaction route for an ideal PC-SOFC only involves proton incorporation and no water evolution, which is different from conventional OC-SOFC. The displayed significantly less anode sulfur poisoning for a PC-SOFC also implies that proton

conducting ceramic (PCC) electrolyte might play an important (electro-)catalytic role (i.e., promoting hydrogen adsorption/dissociation) in the anode hydrogen oxidation reaction for PC-SOFC, which helps maintain the reaction rate upon exposure to low-ppm level H_2S. As no formation of bulk sulfide phases was revealed by bulk characterization techniques such as EDS and XRD for the post H_2S exposure sample, surface sensitive technique of SIMS mapping with depth profiling was carried out. The results suggest a strong association between Ba species and S species that persists into the bulk of the Ni-PCC composite, indicating the possible incorporation of sulfur into the barium containing PCC electrolyte. Further study using more quantitative surface analysis techniques, electrochemical testing involving patterned metal electrode cells with controlled geometry and/or electrode materials and cells with controlled microstructure, and theoretical modeling (including fitting to equivalent circuits) may help clarify the fundamental mechanism for the anode hydrogen reaction of PC-SOFC including the detailed sulfur poisoning mechanism.

3.6 Supplementary Materials

EDS results are shown as following:

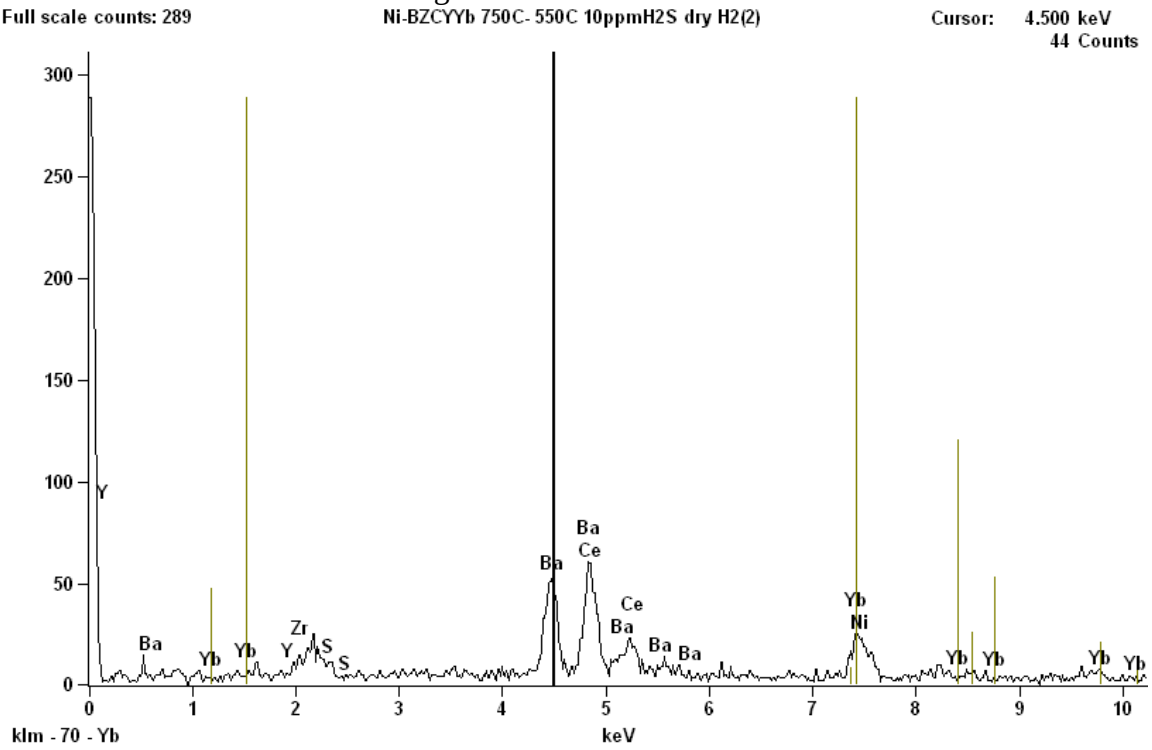

Figure S3.1 EDS map scanning of the Ni-BZCYYb mixed loose powder after exposed to 10ppm H_2S at 550°C in wet H_2 for 24 hours test showing no evidence of sulfur existence.

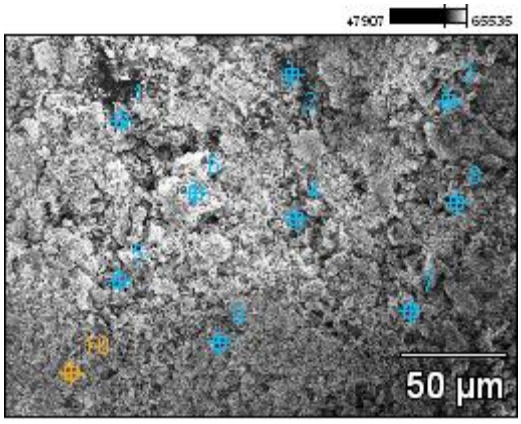

Figure S3.2 SEM image of the Points 1-10 indicating the locations for detection by EDS point scanning on the Ni-BZCYYb mixed loose powder

Table S3.1 Elements' distribution on the surface of Ni-BZCYYb mixed loose powder after H_2S exposure test by atom quantity percentage

	S-K	*Ni-K*	*Y-L*	*Zr-L*	*Ba-L*	*Ce-L*	*Yb-L*
pt1	0.00	25.37	0.00	0.00	40.82	32.18	1.64
pt2	0.00	0.00	0.00	0.00	91.74	8.26	0.00
pt3	0.00	11.41	0.00	0.00	47.67	32.32	8.60
pt4	0.00	1.25	0.00	0.00	54.82	35.11	8.82
pt5	0.00	22.62	0.00	1.82	47.12	28.17	0.27
pt6	0.00	0.91	0.00	0.00	53.79	40.11	5.18
pt7	0.00	0.00	0.00	2.33	55.15	37.21	5.31
pt8	0.00	23.90	0.00	1.96	41.71	25.30	7.14
pt9	0.00	7.56	0.00	0.00	52.93	33.76	5.75
pt10	0.00	11.67	0.00	0.00	53.12	35.22	

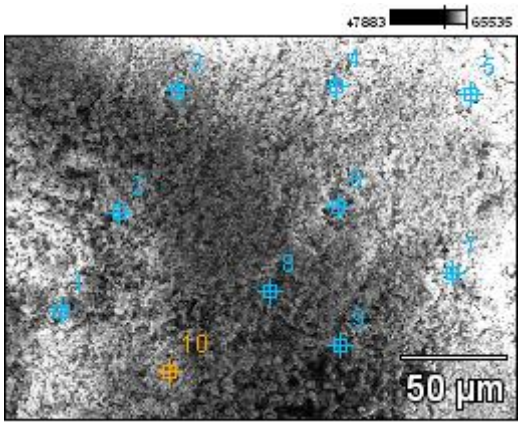

Figure S3.3 SEM image of the Points 1-10 indicating the locations for detection by EDS point scanning (2^{nd})

Table S3.2 Elements' distribution on the surface of Ni-BZCYYb mixed loose powder after H_2S exposure test by atom quantity percentage (2nd)

	S-K	*Ni-K*	*Y-L*	*Zr-L*	*Ba-L*	*Ce-L*	*Yb-L*
pt1	0.00	85.43	0.00	0.00	8.64	5.93	
pt2	0.00	2.83	3.40	2.07	54.24	29.06	8.40
pt3	4.37	2.04	0.00	1.98	46.50	40.35	4.76
pt4	0.45	0.00	0.00	0.00	55.29	39.38	4.88
pt5	0.00	0.00	0.00	0.00	56.66	38.27	5.07
pt6	0.00	5.72	0.00	0.00	60.62	33.66	
pt7	0.00	17.50	0.00	0.00	44.00	31.06	7.43
pt8	0.00	39.65	0.00	0.00	33.36	23.15	3.84
pt9	3.06	26.77	0.00	0.00	41.63	27.07	1.47
pt10	0.00	0.56	0.00	0.00	58.56	34.67	6.21

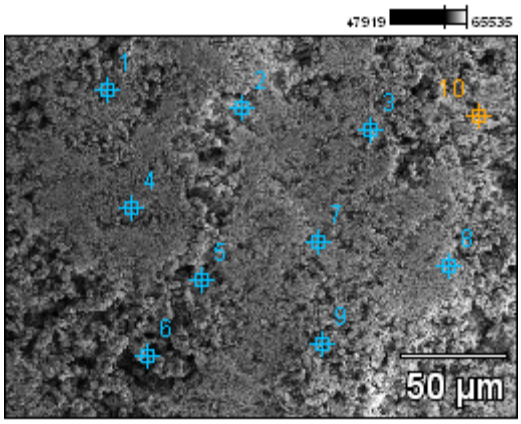

Figure S3.4 SEM image of the Points 1-10 indicating the locations for detection by EDS point scanning (3rd)

Table S3.3 Elements' distribution on the surface of Ni-BZCYYb mixed loose powder after H_2S exposure test by atom quantity percentage (3rd)

	S-K	*Ni-K*	*Y-L*	*Zr-L*	*Ba-L*	*Ce-L*	*Yb-L*
pt1	0.00	33.41	0.00	0.00	33.80	25.00	7.79
pt2	0.00	5.48	0.00	0.00	58.86	32.77	2.89
pt3	0.00	13.32	0.00	0.00	51.14	31.15	4.39
pt4	0.00	68.32	0.00	0.00	18.41	13.27	
pt5	0.00	18.02	0.00	0.00	59.03	22.96	
pt6	0.00	98.26	0.00	0.00	0.84	0.91	
pt7	0.00	13.25	0.00	5.61	48.31	27.45	5.37
pt8	0.00	18.60	0.00	0.00	50.83	28.82	1.75
pt9	0.00	72.42	0.00	0.00	14.84	12.74	
pt10	0.00	93.60	0.00	0.00	6.40		

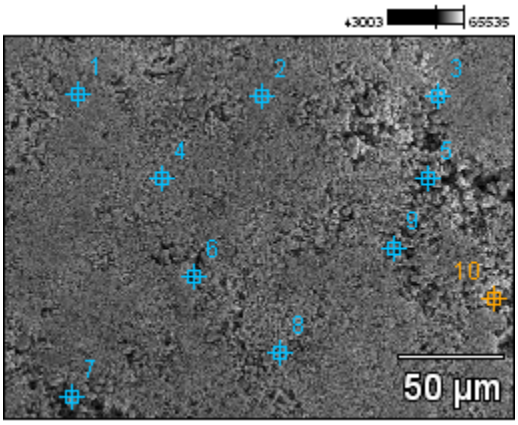

Figure S3.4 SEM image of the Points 1-10 indicating the locations for detection by EDS point scanning (4th)

Table S3.4 Elements' distribution on the surface of Ni-BZCYYb mixed loose powder after H_2S exposure test by atom quantity percentage (4^{th})

	S-K	*Ni-K*	*Y-L*	*Zr-L*	*Ba-L*	*Ce-L*	*Yb-L*
pt1	0.00	0.00	0.00	0.00	54.64	36.53	8.83
pt2	0.00	0.00	0.00	0.00	56.06	38.85	5.09
pt3	0.00	12.67	0.00	11.52	50.29	25.52	
pt4	0.00	0.00	0.00	0.00	56.99	35.68	7.33
pt5	0.00	97.61	0.00	0.00	1.44	0.95	0.00
pt6	0.00	64.09	0.00	0.00	21.12	14.80	0.00
pt7	0.00	98.66	0.00	0.00	0.90	0.45	0.00
pt8	0.00	5.74	0.00	0.00	94.26	0.00	0.00
pt9	0.00	77.55	0.00	0.00	12.29	7.13	3.03
pt10	0.00	2.23	0.00	0.00	64.42	30.04	3.31

4 Chapter IV: CO_2 Poisoning Behavior for the Anode of Proton Conducting IT-SOFC

This chapter details the study on the CO_2 poisoning behavior for the anode of proton conducting IT-SOFC. This chapter is based on published paper by Shichen Sun, Osama Awadallah, and Zhe Cheng. Title of "Poisoning of Ni-based anode for proton conducting SOFC by H 2 S, CO 2, and H 2 O as fuel contaminants." in Journal of Power Sources 378 (2018): 255-263.

4.1 Introduction

Carbon dioxide (CO_2) is deemed harmless for the anode reaction of conventional oxide-ion conducting solid oxide fuel cells (SOFC). [39] However, it is known to negatively impact proton conducting ceramics (PCC), often leading to formation of carbonates or hydroxides. [89, 121, 148-150] For proton conducting intermediate temperature SOFC (IT-SOFC) based on PCC as electrolyte and part of the cermet anode, it is necessary to investigate how carbon dioxide (CO_2) would impact the anode reaction. Therefore, the electrochemical behaviors of the anode for proton conducting IT-SOFC upon exposure to low percentage-level CO_2 in hydrogen fuel were investigated. Studies based on both anode-supported and electrolyte-supported proton conducting IT-SOFC full cell and Ni-based anode symmetrical proton conducting SOFC were carried out, using one leading proton conducting ceramics of BZCYYb. The focus was on characterizing the severity and reversibility of poisoning, if any, as caused by CO_2 as fuel contaminants including the responses in cell bulk and interfacial resistances and linking the observed electrochemical

behaviors to the electro-catalytic activity of PCC in the anode reaction using different routes. In addition, chemical stability tests regarding the exposure to CO_2 was also carried out on Ni-BZCYYb powder, followed by characterization methods such as X-Ray diffraction (XRD) and Raman spectroscopy. The implications of the observed poisoning behavior against CO_2 exposure will be discussed and analyzed to establish better understanding of the anode reaction mechanism for proton conducting IT-SOFC. Beyond that, the directions for future study will be pointed out.

4.2 Experimental

4.2.1 Powder Synthesis and Cell Fabrication

In this study, $BaZr_{0.1}Ce_{0.7}Y_{0.1}Yb_{0.1}O_{3-\delta}$ (BZCYYb) was chosen as the proton conducting ceramic (PCC) electrolyte, and it was synthesized by glycine nitrate process (GNP) followed by heat treatment to form the perovskite phase as described in 3.2.1. The cathode material used in this study is $La_{0.6}Sr_{0.4}Co_{0.2}Fe_{0.8}O_{3-\delta}$ (LSCF) and the synthesis steps are also similar to that for BZCYYb as described in 3.2.1.

Anode-supported full cells with the configuration of Ni-BZCYYb/BZCYYb/LSCF-BZCYYb were fabricated as described in 3.2.1. Briefly, anode precursor/electrolyte bilayer was first prepared via dry-pressing using 0.2 g NiO-BZCYYb-starch powder mixture with weight ratio of 5.5: 3.5: 1 and 10 mg BZCYYb electrolyte powder at a pressure of 250 MPa. Then the pellets of anode precursor/electrolyte bilayer were sintered at 1400^{o}C for 5 hours. After that, cathode slurry of LSCF and BZCYYb and polymer binder

solution with weight ratio of 7: 3: 15 were brush painted onto the electrolyte side of the sintered anode/electrolyte bilayer pellets with area of ~0.16 cm^2. The dried cathode/electrolyte/anode pellets were then calcined at 1100^oC for 2 hours in ambient air. Finally, silver mesh and wires were attached to the electrodes using pure silver paste for current collection.

Electrolyte-supported PC-SOFC full cell with the configuration of Ni-BZCYYb/BZCYYb/LSCF-BZCYYb were also fabricated by the steps as described in 3.2.1. Briefly, an electrolyte pellet was first prepared via dry-pressing 0.2 g BZCYYb powder followed by sintering at 1550^oC for 5 in a so called "protected sintering" configuration. [89] Second, the anode slurry made by mixture of NiO, BZCYYb and organic binder solution at a weight ratio of 3: 2: 5 was brushed-painted onto one side of the sintered electrolyte pellet followed by heat treatment in air at 1400 ^oC for 2 hours. Finally, LSCF-BZCYYb cathode slurry, with a LSCF: BZCYYb: organic binder solution weight ratio of 6.5: 3.5: 10 was brush-painted onto the other side of the pellet and then calcined at 1100 ^oC for 2 hours in ambient air. Both the cathode and anode area were ~0.16 cm^2. For subsequent electrochemical test, silver mesh and wires were attached to the electrodes using pure silver paste for current collection.

In addition, anode symmetrical cells with the configuration of Ni-BZCYYb/BZCYYb/Ni-BZCYYb were fabricated as described in 3.2.1 by first dry pressing 0.1 g of BZCYYb powder into 10 mm diameter pellets at a pressure of 250 MPa. The electrolyte pellets were then sintered at 1550^oC for 5 hours under "protected condition". NiO-BZCYYb slurry was made by mixing NiO, BZCYYb, and polymer binder

solution (polymer content of 8%) at weight ratio of 5.5: 3.5: 9. After that, symmetrical anodes were painted onto both sides of the sintered electrolyte pellet followed by drying in an air oven at 100^{o}C and then calcination at 1400^{o}C for 2 hours in ambient air with heating and cooling rate of 5^{o}C/min. Silver meshes were attached onto both electrodes using pure silver paste for current collection purpose.

4.2.2 Electrochemical Testing of the Effects of CO_2 as Fuel Contaminants

For electrochemical testing of anode-supported and electrolyte-supported PC-SOFC full cells, the steps are also same as described in 3.2.2. First, they were sealed onto one end of an alumina support tube using ceramic sealant (Aremco 552) and placed in the hot zone of a tube furnace. [140] The cell was then heated up to 750^{o}C during which the anode-side was purged with pure N_2 (UHP300 grade, Airgas) while the cathode side was exposed to ambient air. Then at 750^{o}C, dry hydrogen (UHP300 grade with pH_2O of ~10 ppm, Airgas) was introduced into the anode side at a flow rate of 40 mL/min and NiO in the anode was reduced to Ni.

For anode-symmetrical cells, the steps are also similar to that described in 3.2.2. First, the cells were placed in the hot zone inside a one-end closed ceramic tube with gas fed directly to the cell to obtain a rapid response. The symmetrical cells were then heated up in N_2 to 750^{o}C and reduced in pure H_2.

After anode reduction, electrochemical measurements for those cells, especially electrochemical impedance spectroscopy (EIS) measurements were carried out using a

potentiostat (Interface 1000, Gamry). To characterize the effects of CO_2 on the electrochemical responses of the full cells and anode symmetrical cells, 5% CO_2 was introduced into the H_2 fuel while keeping the total fuel flow rate the same. For anode-supported SOFC full cells, the change in cell voltage was monitored continuously at a constant current density of 125 mA/cm^2, and EIS was recorded before, after 2 hours of exposure to 5% CO_2, and after removal of CO_2 for 24 hours under both open circuit condition and biased condition of 0.7V at 750^{o}C. For electrolyte-supported and anode-symmetrical cells, EIS under open circuit condition was recorded in clean dry H_2 (UHP grade with pH_2O of ~10 ppm, labelled as *dry* in this study) and compared to those in H_2 containing 5% CO_2 after 2 hours of exposure at temperatures of 750, 650, and 550^{o}C.

4.2.3 Stability Tests of Ni-BZCYYb Mixed Powders

To study the chemical stability of Ni-BZCYYb cermet anode under relevant testing conditions and understand the observed electrochemical responses to CO_2 poisoning, a series of experiments were carried out by exposing NiO-BZCYYb powder mixtures (5.5: 3.5 weight ratio) after hydrogen reduction to low percentage-level CO_2 as fuel contaminants in both ~3% humidified and dry H_2. Similarly, as described in 3.2.3, in each set of tests, 10 mg of NiO-BZCYYb powder mixture was placed in an alumina boat in a one-end closed tube with fuel gas mixture directly fed to the sample surface. As in electrochemical testing, the samples were first heated up in N_2 to 750^{o}C. Then NiO in the mixture was reduced to Ni in dry H_2 for 30 minutes. After that, the samples were cooled down to 550^{o}C, and 5% CO_2 was introduced into the hydrogen fuel (3% humidified or

nominal *dry* with ~10 ppm H_2O) stream for 24 hours. For comparison purpose, one sample was treated in the same way without the introduction of CO_2. All post-exposure samples were cooled rapidly (by quickly removing the sample tube from the furnace) in clean N_2 to avoid any additional reaction. X-Ray diffraction (SIEMENS diffractometer D5000) was taken for all samples after the exposure tests for phase identification. Besides that, Raman spectra were also collected for selected samples using a spectrometer (HoloSpec f/l.8i, Kaiser Optical System) equipped with an air-cooled Ar ion laser system (Spectra Physics Model 177, 514 nm, 35mW, spot size 10 μm) in the range of 200 to 2000 cm^{-1} Raman shift for additional identification of the reaction products from the stability tests.

4.3 Results

4.3.1 CO_2 Poisoning of Ni-BZCYYb/BZCYYb /LSCF Anode-supported PC-SOFC Full Cell

Figure 4. 1 (a) shows the effect of 5% CO_2 on the anode-supported full cell operated at 750^{o}C under constant current condition: Upon introduction of 5% CO_2, the cell voltage dropped immediately and then seemed to reach steady state. Later, when the 5% CO_2 was removed from the fuel stream, the cell voltage increased back first quickly and then slowly and eventually fully recovered to the performance before poisoning.

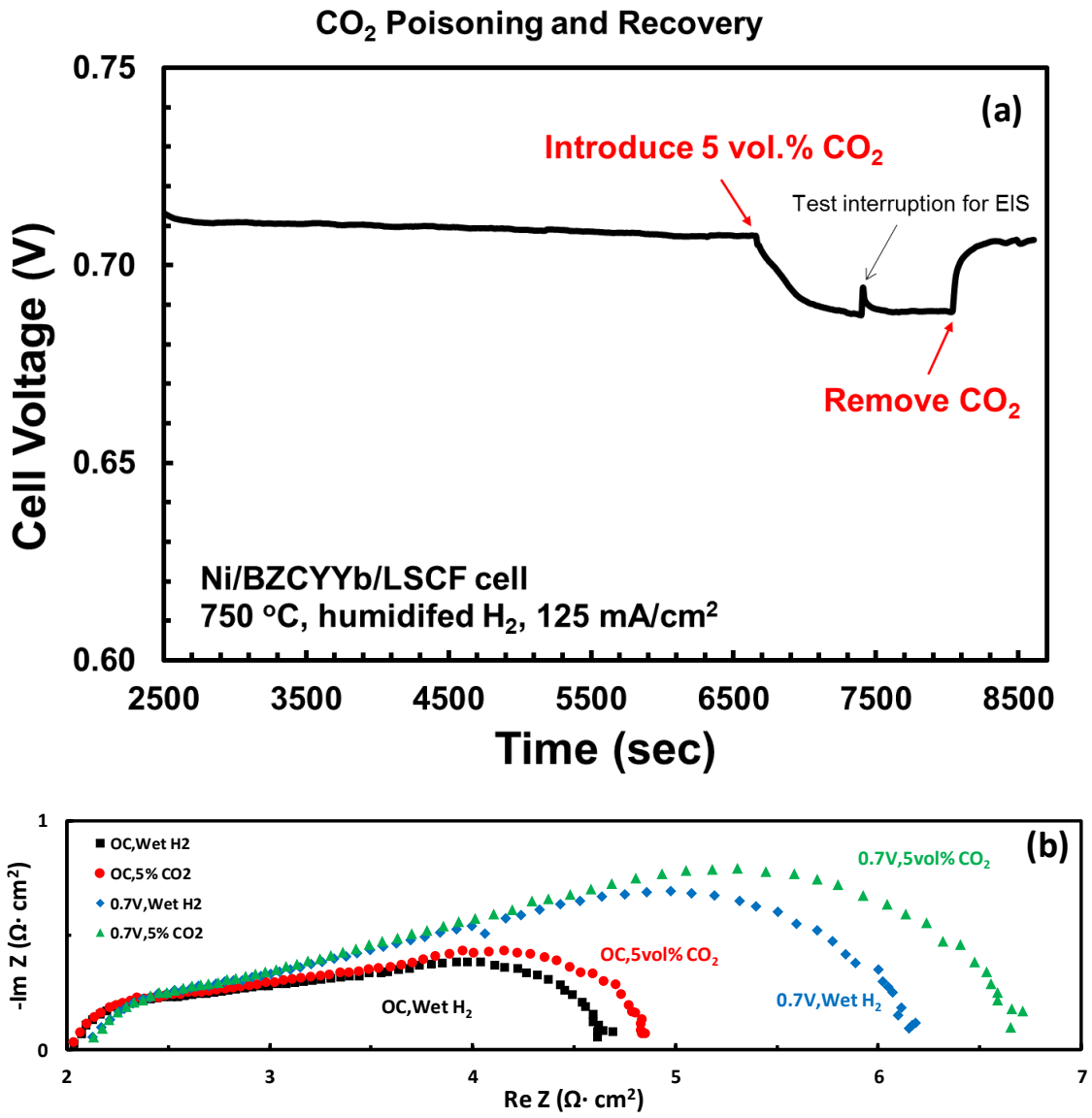

Figure 4. 1 (a) Plot of cell voltage versus time for the Ni-BZCYYb/BZCYYb/LSCF-BZCYYb anode-supported proton-conducting SOFC full cell operated under constant current density of 125 mA/cm^2 showing the poisoning and recovery as caused by introducing 5% CO_2 to the 3% humidified H_2 fuel and later remove it at 750^{o}C. (b) Impedance spectra for the Ni-BZCYYb/BZCYYb/LSCF anode-supported proton-conducting SOFC full cell operated with 3% humidified H_2 (labelled as "Wet H_2") at 750^{o}C under open circuit (OC) condition and constant cell voltage of 0.7 V showing the poisoning effect of 5% CO_2.

Figure 4. 1 (b) shows the impedance for the anode-supported full cell at 750°C under both OCV and constant cell voltage of 0.7 V before and after the introduction of 5% CO_2 into the 3% humidified H_2. Under both open circuit and biased conditions, cell interfacial resistance R_{ai} increased with the introduction of CO_2, especially in the MF-LF loops, while no change was observed in cell ohmic resistance R_O.

4.3.2 CO_2 Poisoning of Ni-BZCYYb/BZCYYb/LSCF Electrolyte-supported PC-SOFC Full Cell

Figure 4. 2 shows the change in impedance spectra for the Ni-BZCYYb/BZCYYb/LSCF electrolyte-supported PC-SOFC full cell upon the introduction of 5% CO_2 into dry H_2 fuel at 750°C, 650°C and 550°C. At 750°C, the poisoning behavior is similar to that for anode-supported cell: No change in cell ohmic resistance R_O was observed, while the MF-LF semicircles show slight increase with the introduction of 5%CO_2 (see Figure 4. 2 (a)). Similar trend was observed at 650°C, with insignificant increase in R_{ai} which is limited in MF-LF semicircles (see Figure 4. 2 (b)). As temperature goes 550°C, the increase in MF-LF semicircles get slightly larger than that at 750°C and 650°C (see Figure 4. 2 (c)).

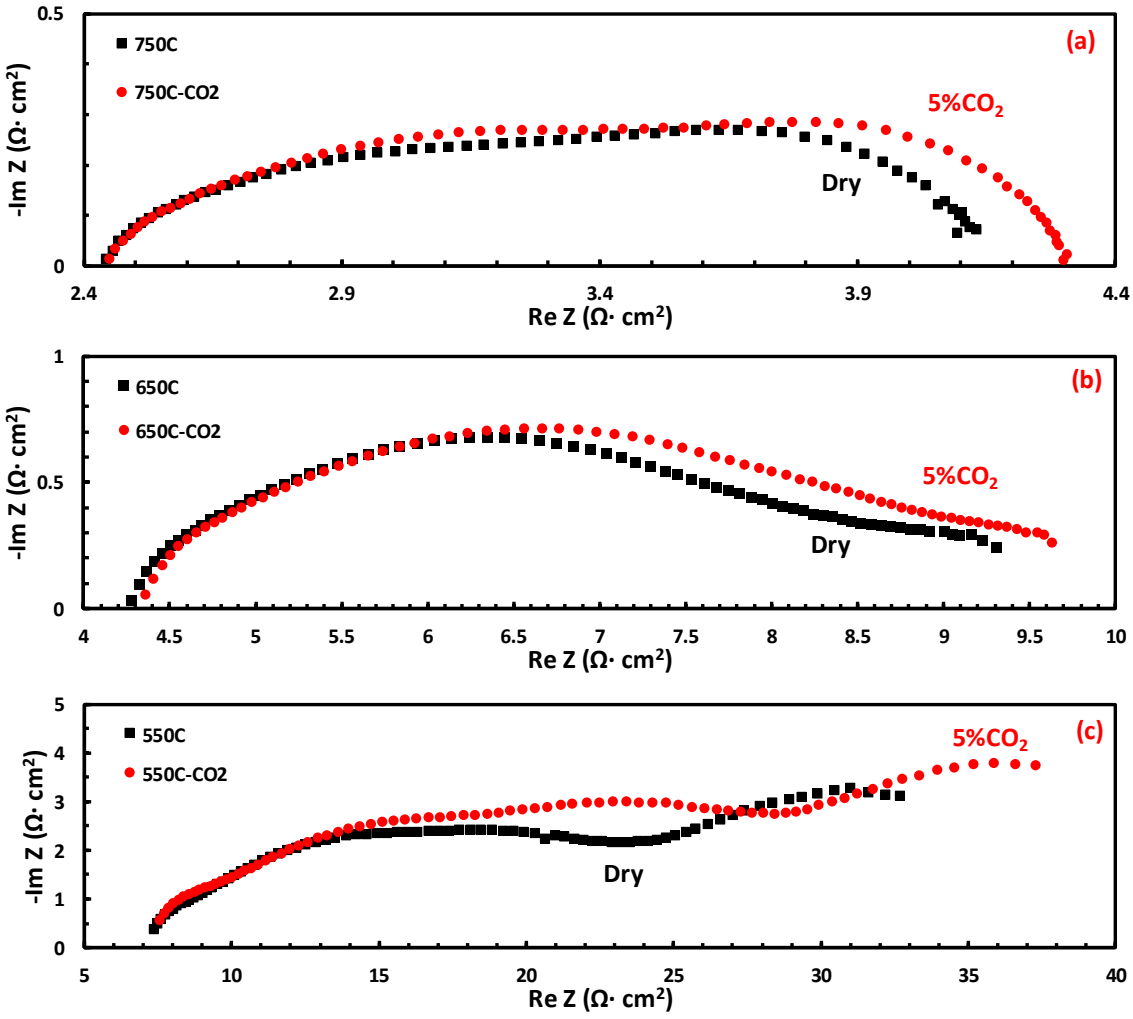

Figure 4. 2 Impedance spectra measured under open circuit condition for a Ni-BZCYYb/BZCYYb/LSCF-BZCYYb electrolyte-supported proton-conducting SOFC (PC-SOFC) at (a) 750^{o}C, (b) 650^{o}C, (c) 550^{o}C, and showing the effect of introducing 5vol% CO_2 as fuel contaminant to the dry H_2.

4.3.3 CO_2 Poisoning of Ni-BZCYYb/BZCYYb/Ni-BZCYYb Anode Symmetrical Cell

Figure 4. 3 shows the change in impedance spectra for the Ni-BZCYYb/BZCYYb/Ni-BZCYYb anode symmetrical cell upon introduction of 5% CO_2 into dry H_2 fuel at 750°C, 650°C and 550°C. At 750°C and 650°C, the poisoning behavior is similar to that for anode-supported full cell and electrolyte-supported full cell (compare Figure 4. 3 (a) and (b) versus Figure 4. 1 (b) and Figure 4. 2 (a) and (b)): No change in the HF semicircle or ohmic resistance R_O was observed, while the MF-LF semicircles show obvious increase. As temperature goes down to 550°C, very dramatic increase in MF-LF semicircles was observed with total anode apparent interfacial resistance R_{ai} more than doubled.

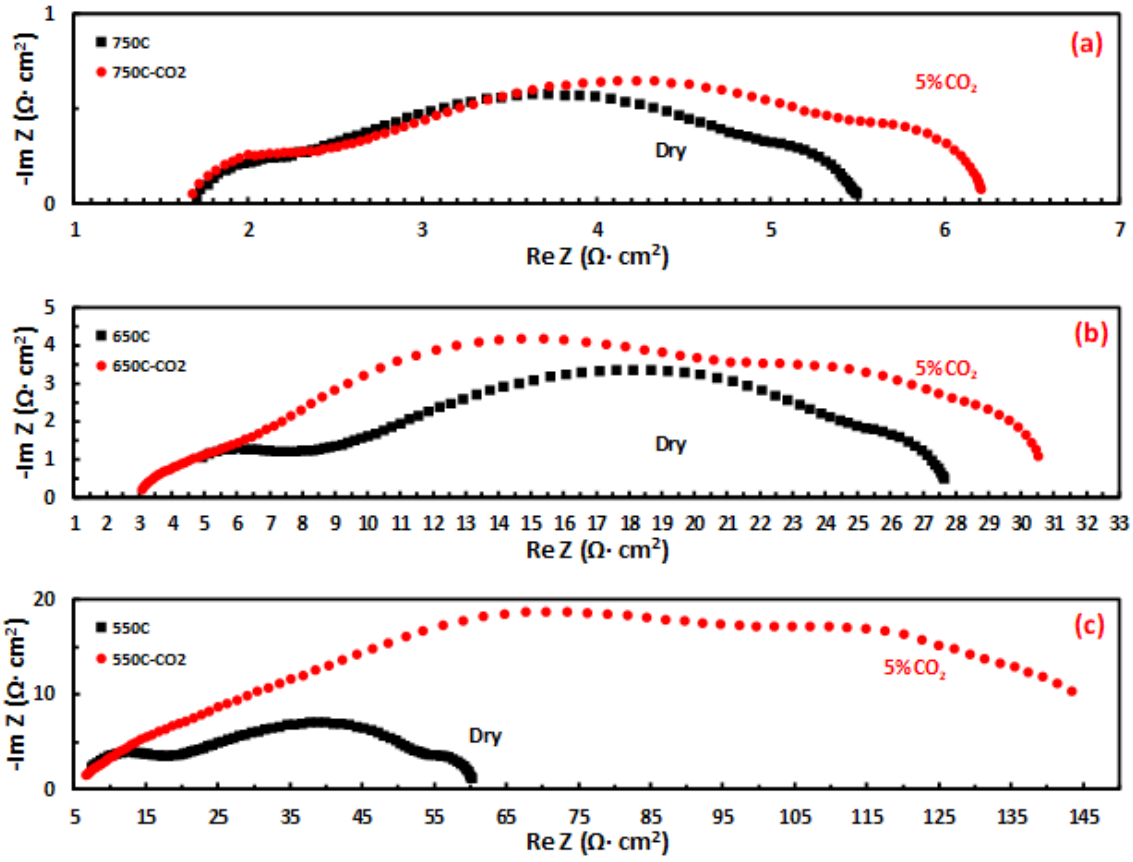

Figure 4. 3 Impedance spectra showing the effect of introducing 5% CO_2 to dry H_2 fuel on the Ni-BZCYYb/BZCYYb/Ni-BZCYYb anode symmetrical cell at (a) 750^{o}C, (b) 650^{o}C and (c) 550^{o}C, respectively.

4.3.4 CO_2 Exposure Tests on Ni-BZCYYb Mixed Powders

The XRD patterns for the Ni-BZCYYb mixed powders after various exposure tests are shown in Figure 4. 4 (a). It can be found that after exposing the Ni-BZCYYb mixed powders to 5% CO_2 at 550^{o}C in both dry and wet H_2, the diffraction peaks for BZCYYb (e.g., at 2θ of 28.7^o, 41.3^o, and 51.2^o) largely disappeared while significant amounts of new phases of barium carbonate ($BaCO_3$) *and* doped ceria (CeO_2) emerged. On the other hand, it is noted that when the CO_2 exposure test was carried out at 750^{o}C, the extent of reaction between 5% CO_2 balanced by H_2 and BZCYYb was much less obvious with no detectable doped ceria formation, which is also consistent with earlier observation. [35] These observations were further confirmed by the corresponding Raman spectra for the post CO_2-exposure samples as shown in Figure 4. 4 (b). The major peaks for BZCYYb (doublets at ~350 cm^{-1}, a small hump at ~430 cm^{-1}, and a broad peak at ~640cm^{-1}) were identified in the control sample treated in dry H_2, [35] while those peaks disappeared in the samples exposed to 5% CO_2 balanced by either dry or wet H_2 at 550^{o}C for 24 hours. On the other hand, three new major Raman peaks were identified in the CO_2-exposed samples, including two peaks at 690 and 1059 cm^{-1}, which are attributed to $BaCO_3$ [41]and one peak at ~480 cm^{-1}, which is attributed to (doped) CeO_2. [151] (It should be noted that the $BaCO_3$ Raman peaks at ~690 and 1059 cm^{-1} were also observed in the control sample that was exposed to dry H_2 only but with much lower intensities. One possible explanation is that, the

synthesized BZCYYb powder via the GNP process might contain small amount of excess Barium, which converts to $BaCO_3$ upon air exposure at room temperature.[89]) Besides that, no observable peaks for either amorphous carbon (at ~1350 cm^{-1}) or graphitic carbon (at ~1580 cm^{-1}) were detected in all the samples. [40]

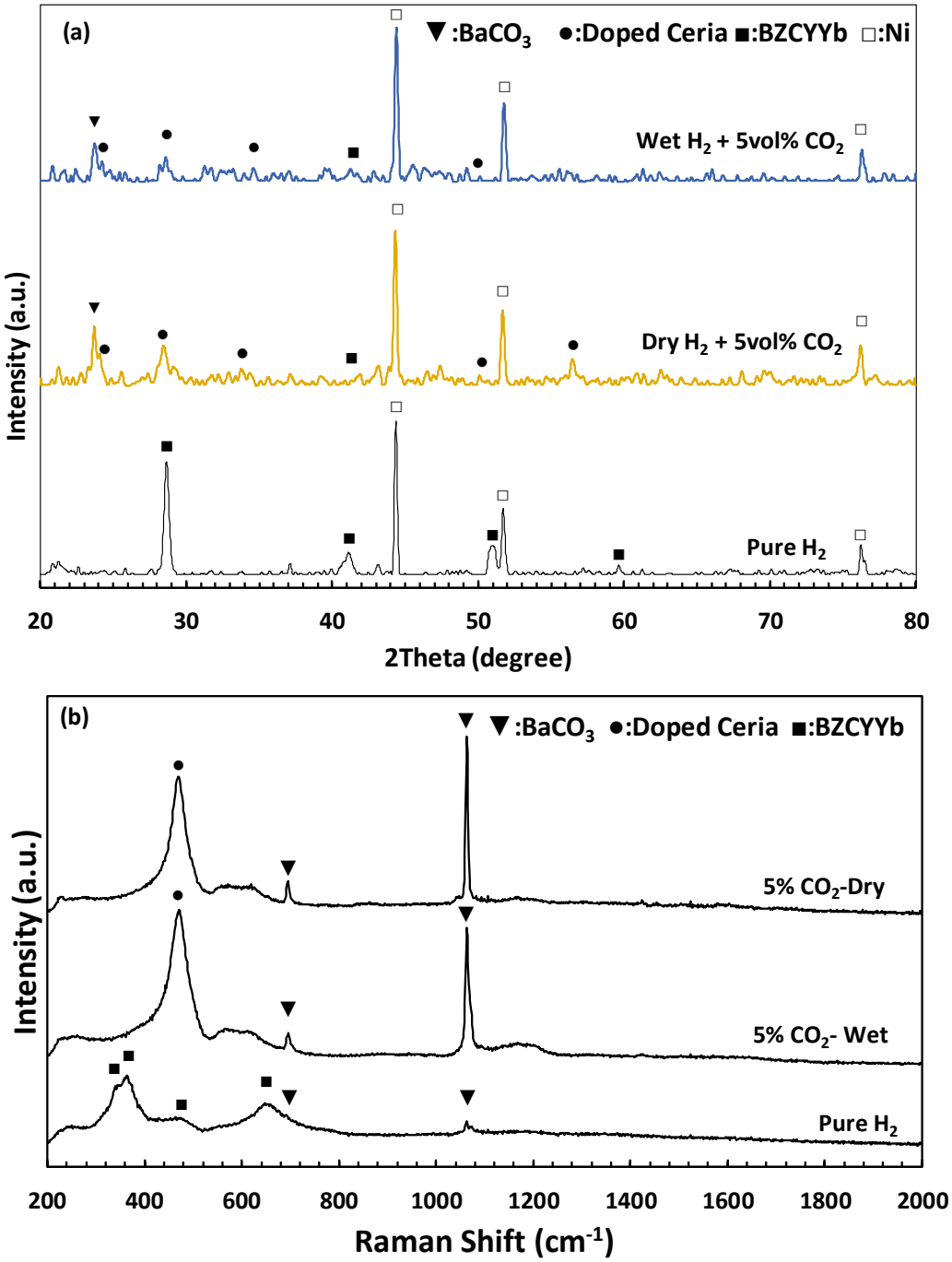

Figure 4. 4 (a) XRD patterns for NiO-BZCYYb mixed powders after reduction in H_2 at 750°C, and exposure tests at 550°C for 24 hours to pure H_2 (as control sample) and fuel gas mixtures of dry H_2 + 5%CO_2, wet H_2 + 5% CO_2, (b) Raman spectra for samples after exposure to fuel gas mixtures of dry H_2 + 5% CO_2, wet H_2 + 5%CO_2, and pure H_2 (as control sample), respectively.

4.4 Discussions

The results in Figure 4. 1, Figure 4. 2 and Figure 4. 3 for all three types of PC-SOFC clearly suggest that CO_2 behaves like a poison for the anode reaction process for PC-SOFC. This is different from conventional oxide ion conducting SOFC for which CO_2 is usually *not* regarded as harmful: CO_2 is often present in the anode chamber as the reforming/water-gas shift reaction (WGSR) product that would not harm the cell performance unless at extremely high concentration. The implication of the insensitivity of conventional oxide ion conducting SOFC with Ni-cermet anode to CO_2 fuel contaminant is that, unlike sulfur, in hydrogen atmosphere, CO_2 would *not* adsorb strongly on Ni catalyst surface to block the conventional anode hydrogen electrochemical oxidation reaction under typical SOFC operating conditions.

On the other hand, it is well known that CO_2 has very strong affinity to the highly basic proton conducting electrolyte such as BZCYYb and may even lead to bulk phase reaction. [89]In fact, it has been reported that CO_2 would react with the current BZCYYb electrolyte to form $BaCO_3$ under certain condition such as in 50% CO_2/50% Ar at 750^oC. [42, 89] In this study, as shown before in Figure 4. 3 (c), at intermediate temperature of 550^oC, the anode apparent interfacial resistance R_{ai} increases by more than 100% upon exposure to 5% CO_2 in proton conducting anode symmetrical cell. This is attributed to the bulk phase reaction between 5% CO_2 and BZCYYb proton conducting electrolyte, and it is supported by the result of stability tests at 550^oC that show disintegration of BZCYYb proton conducting electrolyte and accompanied formation of $BaCO_3$ and doped CeO_2 (see Figure 4. 4 (a)) upon exposure to 5% CO_2 in hydrogen (dry or 3% humidified). On the other hand,

the much smaller increase in R_{ai} for proton conducting electrolyte-supported cell could be possibly due to the contribution from cathode, which dominated the interfacial resistance at reduced temperature of 550°C and had no response to CO_2 introduction in the anode side.

On the other hand, when the temperature is raised to 650 or even 750°C, the relative increase in R_{ai} due to the introduction of 5% CO_2 into the H_2 fuel stream was still observable (see Figure 4. 2 and Figure 4. 3 (b) and (a)) but much less than that at 550°C. The explanation for this dramatic reduction in poisoning by 5% CO_2 at higher temperature such as 650 and 750°C is that the same fuel mixture of 5% CO_2 in H_2 at those elevated temperatures does not lead to complete bulk phase reaction and disintegration of BZCYYb proton conducting electrolyte. Instead, the exposure to the nominal 5% CO_2 balanced by H_2 mixture at those temperatures might only lead to surface CO_2 adsorption. Such an explanation was consistent with XRD for the 750°C 5% CO_2 exposed samples showing no obvious decrease in the diffraction peaks' intensity for the BZCYYb proton conducting electrolyte phase and no doped ceria formation, as typically observed when $BaCeO_3$-based proton conducting electrolyte experiences bulk phase reaction. [42, 89]

One underlying reason for the mitigation of CO_2 poisoning effect with increasing temperature to ~650 or 750°C is attributed to the fact that CO_2 and H_2 could go through reverse water gas shift (RWGS) reaction $CO_2 + H_2 = CO + H_2O$ as mentioned in section 2.2.3.

The RWGS reaction shifts towards the right (i.e., forming more CO with less remaining CO_2) at higher temperature. [152] Therefore, it is likely that at higher temperatures such as

750°C, the actual CO_2 concentration in the fuel stream could be much lower than the nominal value of 5% as introduced due to RWGS reaction. (In fact, based on equilibrium constant data for the RWGS, the equilibrium CO_2 concentration for a 5% CO_2/95% H_2 feed gas mixture will be around 0.3% at 750°C.) As a result, CO_2 poisoning was observed to be not very severe. In comparison, at a lower temperature such as 550°C, due to both *thermodynamics* (i.e., equilibrium CO_2 concentration will be higher of ~0.7% at 550°C) and *slower kinetics* for the RWGS, less amount of CO_2 is converted to CO, and severe poisoning would be observed due to bulk reaction between CO_2 and the BZCYYb proton conducting electrolytes.

Finally, it is recognized that such an explanation might still be a simplification of the actual situation. For example, as CO is also produced from RWGS, it might lead to carbon deposition or coking on the Ni-based anode for proton conducting SOFC through the disproportionation reaction, especially at lower temperature:

$$2CO = C + CO_2 \qquad \text{Equation 4.1}$$

In fact, Ishiyama had observed carbon deposition over BZCYYb in a fuel mixture of 20%CO_2 and 80% H_2 at 500°C. [103] However, no observable peaks for amorphous carbon or graphite were detected for the Ni-BZCYYb mixed powders after exposing to 5% CO_2 balanced by either wet or dry H_2 at 550°C and 450°C by Raman, as shown in Figure 4. 4 (b), suggesting formation of CO and related carbon deposition are probably not critical in explaining the observed CO_2 poisoning behavior in this study.

4.5 Conclusions

Electrochemical study on both anode-supported and electrolyte-supported PC-SOFC full cells and anode symmetrical PC-SOFC show that the anode reaction for PC-SOFC based on BZCYYb electrolyte and Ni-BZCYYb cermet anode is poisoned by low ppm-level H_2S and low percentage level of CO_2. At temperature in the range of 550 to 750^oC, CO_2 does not cause change in cell ohmic resistance R_O, but lead to observable increase in electrode interfacial resistance R_{ai}, especially in the mid-to-low frequency (MF-LF) semicircles but not in the high frequency (HF) semicircle. The observed poisoning behaviors of proton conducting SOFC by low-percentage level of CO_2 is similar to that caused by low ppm-level H_2S and can be attributed to the strong adsorption of CO_2 species on the highly basic BZCYYb electrolyte surface, which interferes with the sub-steps of hydrogen adsorption and surface diffusion in the anode reaction for PC-SOFC. The great similarity of the poisoning behaviors between CO_2 and H_2S despite their different affinity for the Ni-based metal catalyst suggests that the surface of proton conducting electrolyte such as BZCYYb might play a significant electrocatalytic role in the overall anode reaction for PC-SOFC and further experiments will be needed to test such a hypothesis and help reveal the fundamental anode reaction mechanism of hydrogen electrochemical reaction for proton conducting SOFCs. Finally, it should be mentioned that for CO_2, when their concentration increase (e.g. 5vol% to 50vol%) or when the temperature drops (750^oC-450^oC), the interactions between those contaminants and the proton conducting electrolyte (BZCYYb in this case) may change from surface adsorption to bulk phase reaction, leading to disintegration of the proton conducting electrolyte and accompanied formation of bulk

phases (e.g., $BaCO_3$ and doped CeO_2), and greater extent of poisoning would be observed accordingly.

5 Chapter V: Electrochemical Behaviors of Ag, LSCF and BSCF as Cathode for Proton Conducting IT-SOFC

This chapter details the study on the electrochemical behaviors of Ag, LSCF and BSCF as cathode for proton conducting IT-SOFC. This chapter is based on published paper by Shichen Sun, and Zhe Cheng. "Electrochemical Behaviors for Ag, LSCF and BSCF as Oxygen Electrodes for Proton Conducting IT-SOFC." in Journal of The Electrochemical Society 164.10 (2017): F3104-F3113.

5.1 Introduction

The cathode in solid oxide fuel cells (SOFC) is often considered to be the rate-limiting factor, especially for SOFCs that operated at intermediate temperature (400-700^{o}C). [44, 70] Many efforts have been put into developing cathode materials that are suitable for intermediate temperature solid oxide fuel cells (IT-SOFC). [13, 70, 153, 154] However, there has been no consensus about the ideal cathode material or architecture that enables facile oxygen electrode reaction for proton conducting IT-SOFC. In this work, the electrochemical behaviors of several model cathode materials were compared at intermediate temperature of 450-650^{o}C. Among various cathode materials available, silver (Ag), as an electronic conductor, was chosen because it could be used to represent cells with oxygen electrode reactions confined to the triple phase boundary (TPB). $La_{0.6}Sr_{0.4}Co_{0.2}Fe_{0.8}O_{3-\delta}$ (LSCF) was chosen because it is a mixed ionic and electronic conductor (MIEC) and also the state-of-the-art cathode for conventional oxide-ion conducting SOFC. [93, 155] Additionally, composite cathode made of LSCF and proton

conducting oxide is also interesting due to the concern with LSCF's limited proton conductivity and the possibility of expanded TPB for the LSCF-based composite cathode. [121]Finally, $Ba_{0.5}Sr_{0.5}Co_{0.8}Fe_{0.2}O_{3-\delta}$ (BSCF), which is regarded as one of the most active cathode materials at intermediate temperature, was also chosen because previous studies have shown BSCF displays significant weight gain and monotonic conductivity relaxation behavior in humidified atmosphere, [20, 156] suggesting possible mixed protonic and electronic conductivity. On the other hand, recent studies also show decreased electrode interfacial resistance with the introduction of moisture, especially in the high frequency range of 10^6 to 10^4 HZ, when used as the oxygen electrode on proton conducting electrolytes such as $BaCe_{0.9}Y_{0.1}O_{3-\delta}$ (BCY) [20]and $BaZr_{0.1}Ce_{0.7}Y_{0.1}Yb_{0.1}O_{3-\delta}$ (BZCYYb). [157] These observations suggest BSCF might enable the expansion of reaction sites to the entire BSCF surface thus providing high activity for cathode reaction. [20, 157] The electrochemical impedance for symmetrical cells with Ag, LSCF, LSCF-BZCYYb composite, and BSCF cathodes and a leading proton conducting electrolyte of BZCYYb were characterized. The focus was on revealing the responses to changing oxygen partial pressure (pO_2) and moisture (H_2O) content. The implications of the experimental observations to the understanding of the cathode reaction processes will be discussed, including the roles of various electrode materials (e.g. BSCF) play and the importance of being proton conducting to the oxygen electrode reaction over a proton conducting electrolyte. Finally, the directions for future development of better cathodes for proton conducting IT-SOFC are pointed out considering all things mentioned above.

5.2 Experimental

5.2.1 Powder Synthesis and Compatibility Test

All of the BZCYYb powder (nominal composition of $BaZr_{0.1}Ce_{0.7}Y_{0.1}Yb_{0.1}O_{3-\delta}$), BSCF powder (nominal composition of $Ba_{0.5}Sr_{0.5}Co_{0.8}Fe_{0.2}O_{3-\delta}$) and LSCF powder (nominal composition of $La_{0.6}Sr_{0.4}Co_{0.2}Fe_{0.8}O_{3-\delta}$) were synthesized by the glycine nitrate process (GNP). [89] The metal precursors used include $Ba(NO_3)_2$ (#10180117, Alfa Aesar, 99%), $La(NO_3)_2$ (#A11305, Alfa Aesar, 99%), $Sr(NO_3)_2$ (#SZBB0470V, Sigma-Aldrich, 99%), $Co(NO_3)_2{\cdot}6H_2O$ (#239267, Alfa Aesar, 99%), $Fe(NO_3)_3{\cdot}9H_2O$ (#216828, Alfa Aesar, 99%), $ZrO(NO_3)_2{\cdot}xH_2O$ source (#43224, Alfa Aesar, 99.9%), $Ce(NO_3)_3{\cdot}xH_2O$ (#11329, Alfa Aesar, 99.5%), $Y(NO_3)_3{\cdot}6H_2O$ (#12898, Alfa Aesar, 99.9%), and $Yb(NO_3)_3{\cdot}xH_2O$ (#12901, Alfa Aesar, 99.9%). The molar ratio between glycine and total metal ions was 1:1 for BZCYYb and 7:6 for BSCF and LSCF. The mixed solutions in 1 L glass beaker were place directly on a hotplate set at 540^{o}C and the solutions boiled and eventually self-combust. After self-combustion, the powders were calcined at 1100^{o}C for 2 hours for the BZCYYb and at 1000^{o}C for 2 hours for the BSCF and LSCF powders in ambient air to form the pure phases. [68, 89, 157, 158]The stability and compatibility between BZCYYb and BSCF at intermediate temperature have been studied before. [157] In order to verify the chemical compatibility between LSCF and BZCYYb under fabrication condition, powders of the two materials with weight ratio of 7:3 were intimately mixed and exposed to ambient air at typical LSCF-BZCYYb cathode firing temperature of 1000^{o}C for 2 hours**.** To test the stability and compatibility of the LSCF and BZCYYb mixture under subsequent

testing conditions, the powder mixtures were exposed at 750°C in dry simulated air, 3% humidified simulated air, and pure O_2 for 24 hours with the flow rate of 50 cc/min. The as-synthesized samples and samples after compatibility/stability tests were all analyzed by X-Ray diffraction (SIEMENS diffractometer D5000) for phase identification.

5.2.2 Cell Fabrication

Cathode symmetrical cells with the configuration of Ag/BZCYYb/Ag, LSCF/BZCYYb/LSCF, LSCF-BZCYYb/BZCYYb/LSCF-BZCYYb, and BSCF/BZCYYb/BSCF were fabricated. First, all electrolyte pellets with diameter of 10 mm were dry-pressed at 200 MPa using 0.2 g BZCYYb powder, followed by protected sintering at 1550°C for 5 hours. [89] Then, 4mm*4mm cathodes were brush painted onto both sides of the sintered BZCYYb pellets with pure silver paste, LSCF paste, mixed LSCF-BZCYYb paste (LSCF : BZCYYb weight ratio of 7:3), and BSCF paste, [157] respectively. All painted samples were fully dried in an air oven at 100°C and then calcined at 1000°C for 2 hours, except for the silver symmetrical cell, which was calcined at 700°C for 2 hours. The heating and cooling rates were 5°C/min.

Besides that, anode-supported full cell with the configuration of BSCF/BZCYYb/NiO-BZCYYb was fabricated. First, NiO-BZCYYb anode precursor/BZCYYb electrolyte bilayer was prepared via dry-pressing: 0.2g NiO-BZCYYb-starch powder mixture with weight ratio of 5.5: 3.5: 1 was pressed first gently in the 10 mm diameter die; then 10 mg BZCYYb electrolyte was added onto the anode substrate and the bilayer was pressed

together at a pressure of 200 MPa. The pellets of the anode precursor/electrolyte bilayer were then sintered at 1400^{o}C for 5 hours in air with heating and cooling rate of 5^{o}C/min. 4mm*4mm BSCF cathode was brush-painted onto the electrolyte side of the sintered anode/electrolyte bilayer pellets using the same BSCF slurry as described above, dried at 150^{o}C, and then calcination at 1100^{o}C for 2 hours in air with heating and cooling rate of 5^{o}C/min. Finally, silver mesh and wires were attached to the electrodes using pure silver paste for current collection. The microstructure of both the surface and the cross-section of the fabricated cathode symmetrical cells were observed using a field emission scanning electron microscope (FE-SEM, JEOL JSM 6330F).

5.2.3 Electrochemical Impedance Spectroscopy (EIS) Measurement

Electrochemical Impedance Spectroscopy (EIS) measurements were carried out using a potentiostat (Gamry Interface 1000) under open circuit condition and in the frequency range of 10^{6} to 10^{-2} HZ for the symmetrical cells and the anode-supported full cells. The symmetrical cells were connected with silver paste and silver mesh current collector and were placed in the hot zone inside a one-end closed alumina tube with gas fed directly to the cells to obtain a rapid response. Each sample was first tested in dry simulated air (Airgas AI UZ300, with nominal composition of 20% O_2/80% N_2 with <~5 parts per million or ~5 ppm of H_2O and CO_2) at a flow rate of 50 ml min^{-1} from temperature of 650^{o}C to 450^{o}C. To test the effect of pO_2 on the oxygen electrode behavior, oxygen (Airgas OX UHP300) and nitrogen (Airgas NI UHP300) were introduced to the sample testing chamber with different ratios adjusted by digital mass flow controllers. After finishing the tests in various

pO_2, water vapor with controlled concentrations (e.g., 0.6%, 3%, 10%, and 20%) was introduced into the testing chamber by passing the simulated air through a water bubbler set at different temperatures to test the effect of water vapor on the oxygen electrode behavior. For testing involving 10% and 20% water vapor, the connection tubes were heated to ~100^{o}C with heating tapes to prevent water condensation. In addition, for better control of the moisture content inside the chamber, the samples were heated to 750^{o}C before adjusting the moisture content. For the anode-supported full cell, it was sealed onto ceramic tube fixture and heated up with the anode-side exposed to nitrogen. Then, at 750^{o}C, anode gas flow was switched from nitrogen to pure hydrogen to reduce the NiO to Ni. The impedance spectra for the various symmetrical and full cells were collected at various intermediate temperatures between 450 and 650^{o}C.

5.3 Results

5.3.1 Stability, Compatibility, and Microstructure of the Electrodes

The XRD patterns for the as-synthesized LSCF and BZCYYb powders and their mixtures after compatibility/stability tests are shown in Figure 5. 1. There is no obvious secondary phase formed after the compatibility test of firing at 1000^{o}C for 2 hours in air and the three stability tests of exposing the fired LSCF-BZCYYb composite at 750^{o}C for 24 hours in ambient air, pure O_2, and 3% humidified air, suggesting no reaction occurred between LSCF and BZCYYb and their gas environment under the intended conditions. For BSCF,

previous studies have shown that BSCF is compatible with BZCYYb electrolyte for cathode firing [157] and it is also stable under typical testing condition in air. [70, 157]

Besides that, the microstructure of fabricated Ag, LSCF, LSCF-BZCYYb, and BSCF cathode symmetrical cells, all with BZCYYb electrolytes, are shown in Figure 5. 2. The thickness of the all the electrodes was around 30 μm, but the microstructure is somewhat different: The Ag electrode gives relatively dense structure with grain size significantly larger than 1 μm; both the LSCF and the LSCF-BZCYYb composite electrodes are porous with fine grain size much smaller than 1 μm; the BSCF cathode is also porous but with grain size of ~1 μm, which is between the grains size for the Ag and LSCF-based electrodes.

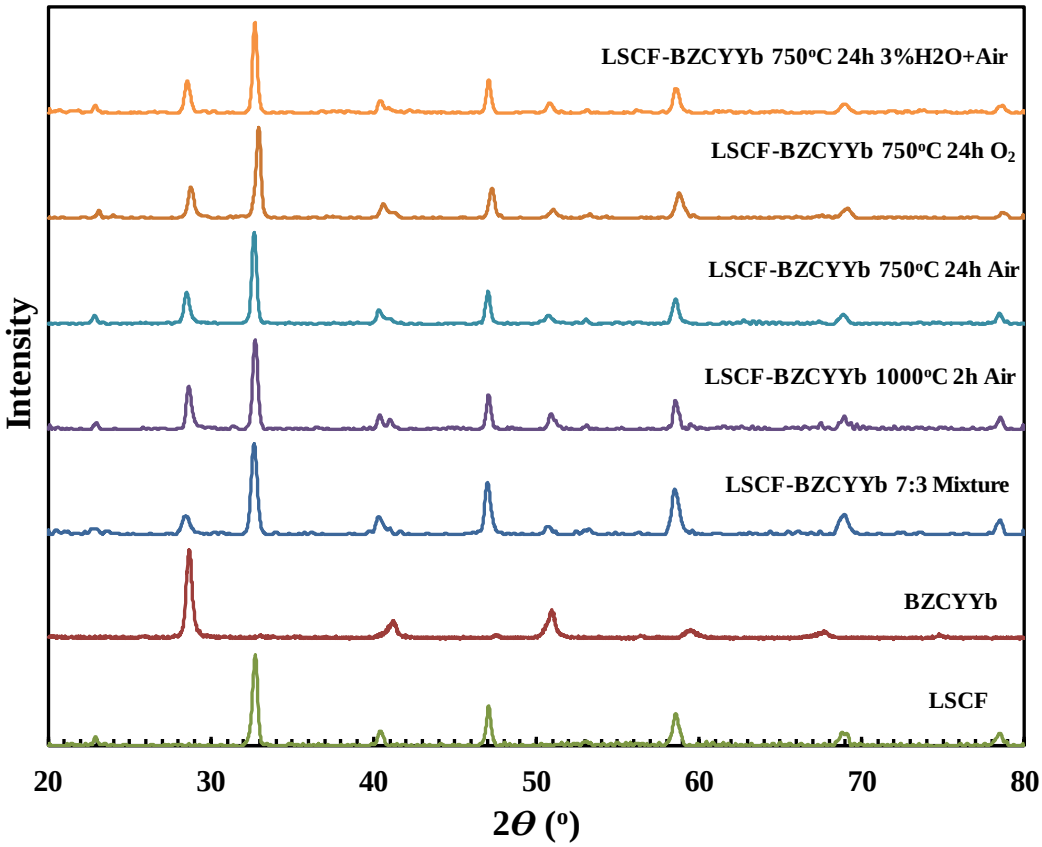

Figure 5. 1 XRD patterns of as-synthesized LSCF and BZCYYb powders and their mixtures after compatibility test of firing at 1000^{o}C for 2 hours in air and the three different stability tests of exposing the fired LSCF-BZCYYb composite at 750^{o}C for 24 hours in ambient air, pure O_2, and 3% humidified air.

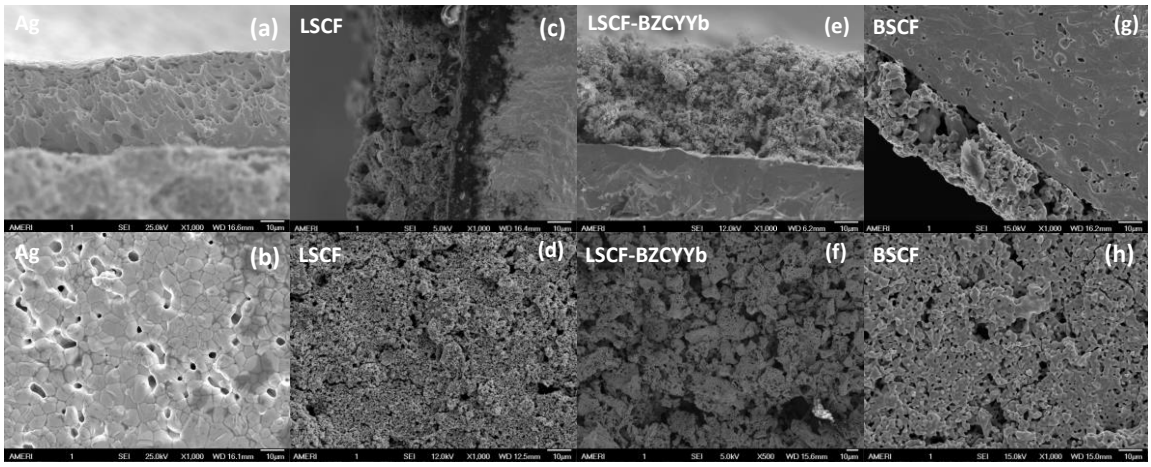

Figure 5. 2 SEM images of the cross-section and the electrode surface of the fabricated Ag/BZCYYb/Ag (a and b), LSCF/BZCYYb/LSCF (c and d), LSCF-BZCYYb/BZCYYb/LSCF- BZCYYb (e and f), and BSCF/BZCYYb/BSCF (g and h) cathode symmetrical cell, respectively.

5.3.2 Electrochemical Behavior of Different Dlectrodes under Various *p*O_2 and Moisture Content

5.3.2.1 Ag electrode

Figure 5. 3 shows the impedance spectra for an Ag/BZCYYb/Ag symmetrical cell in dry simulated air, pure oxygen, and simulated air containing 3% moisture at 650, 550, and 450 ^{o}C. Under all testing conditions, incomplete high frequency (HF) loops were observed in the impedance spectra, leading to indeterminable ohmic resistance (R_O). Additionally, there are multiple, partially overlapping loops in the mid to low frequency (MF-LF) range. The estimated total apparent electrode interfacial resistance (R_{ai}), which is the direct difference between the low frequency intercept and the high frequency

intercept on the real axis, [159] is quite high-on the order of ~50, 100, and 500 $\Omega \bullet cm^2$ at 650, 550, and 450^oC, respectively. It should be noted here that, strictly speaking, the R_{ai} defined here is *not* the electrode interfacial polarization resistance R_p due to the nature of mixed ionic and electronic conduction for the BZCYYb electrolyte. [159] However, due to the absence of precise ionic transference number, accurate R_p number *cannot* be obtained readily. As a result, only the apparent interfacial resistance R_{ai}, defined as the direct difference between the low frequency intercept and the high frequency intercept on the real axis in an impedance spectrum, is used for the analysis and discussions in this study following the practice in many previous reports. [20, 157, 159] These values are much larger than the typical values for a good cathode symmetrical cell. [20, 70, 121, 153, 157, 160, 161]In addition, for both the high frequency electrode resistance R_{HF} and the mid-to-low frequency electrode resistance R_{MF-LF}, they generally increased with decreasing pO_2 or the introduction of 3% moisture. The exception is at the relatively low temperature of 450^oC when no obvious change in R_{HF} with decreasing pO_2 was observed.

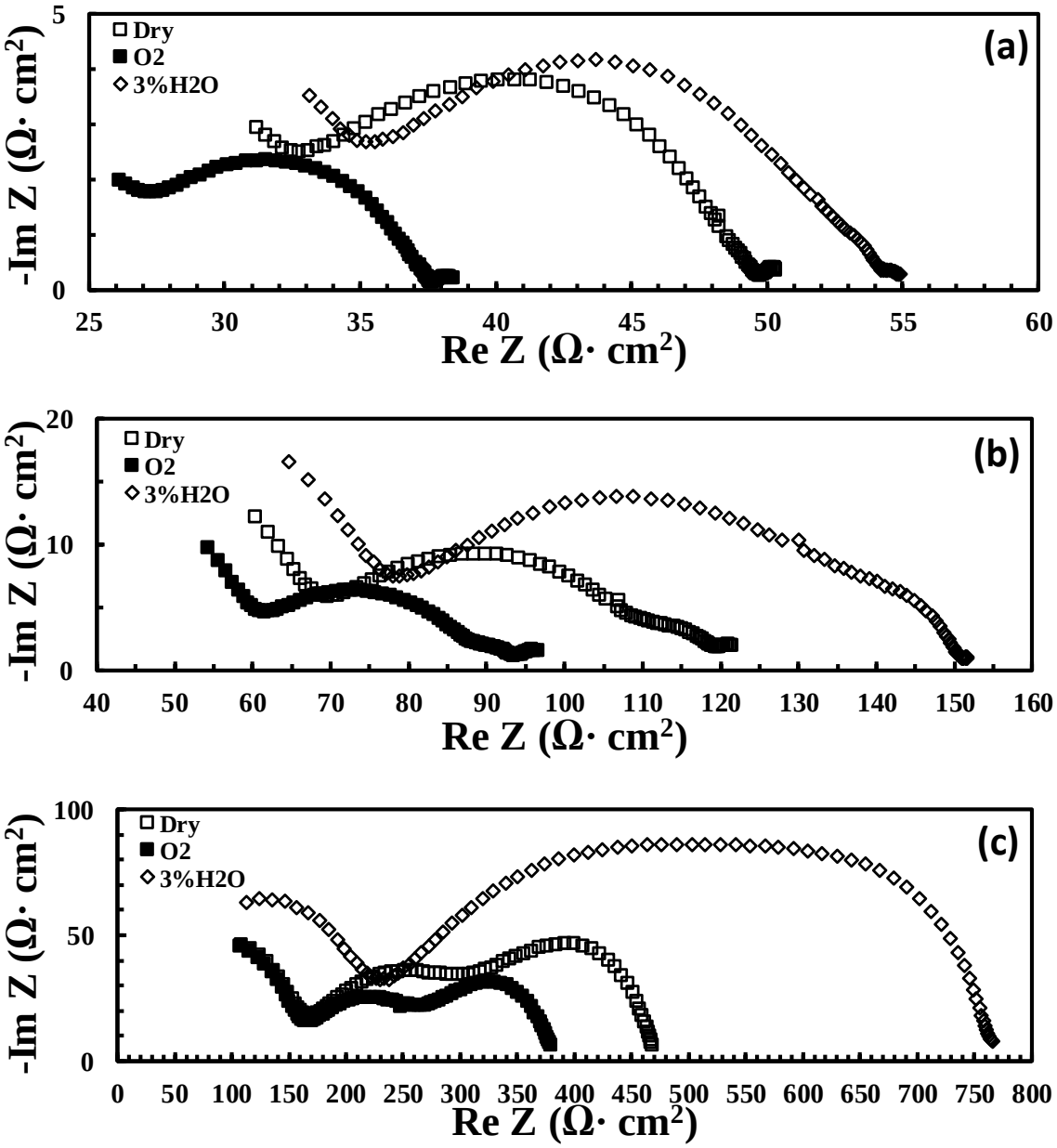

Figure 5. 3 Impedance spectra for a Ag/BZCYYb/Ag symmetrical cell in dry simulated air (20%O_2/80%N_2 with <~5ppm H_2O and CO_2), pure oxygen, and simulated air humidified with 3% H_2O at (a) 650^{o}C, (b) 550^{o}C, and (c) 450^{o}C, respectively.

5.3.2.2 LSCF Electrode

Figure 5. 4 shows the impedance spectra for the LSCF/BZCYYb/LSCF symmetrical cell under the same conditions. The electrochemical behaviors were similar to the Ag symmetrical cell in several ways: Incomplete HF loops are still observed in the impedance spectra at various temperatures, leading to indeterminable R_O. The MF-LF range also contains multiple overlapping loops at all temperatures. The estimated total electrode interfacial resistance R_{ai} appears high as well-on the order of ~30, 80, and 600 $\Omega \bullet cm^2$ at 650, 550, and 450^oC, respectively. These values are one to two orders of magnitude higher than those obtained on a LSCF symmetrical cell over $Ce_{0.9}Gd_{0.1}O_2$ (GDC) electrolyte at temperatures of 650 and 550^oC. [160] The R_{ai} also generally increased with decreasing pO_2 or introduction of 3% moisture.

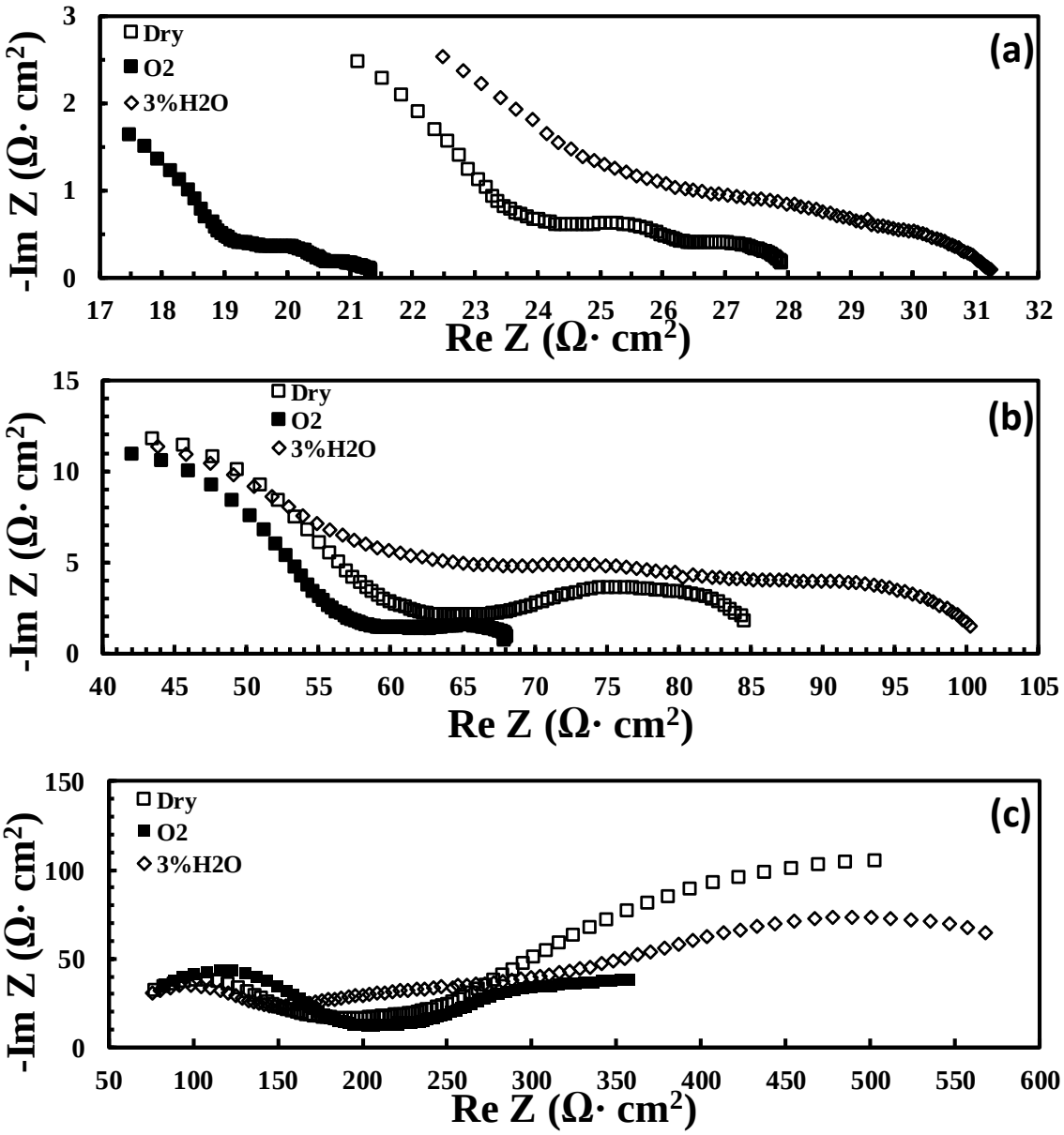

Figure 5. 4 Impedance spectra for a LSCF/BZCYYb/LSCF symmetrical cell in dry simulated air (20%O_2/80%N_2 with <~5ppm H_2O and CO_2), pure oxygen, and simulated air humidified with 3% H_2O at (a) 650^{o}C, (b) 550^{o}C, and (c) 450^{o}C, respectively.

However, comparing with the Ag electrode, there are some unique features for the LSCF electrode: In particular, temperature seems to influence the electrochemical

responses of the symmetrical cell to gas atmosphere dramatically. For example, for LSCF, at a higher temperature of 650^{o}C, both the high frequency electrode resistance R_{HF} and the mid-to-low frequency electrode resistance $R_{MF\text{-}LF}$ increased with decreasing pO_2 and the introduction of 3% moisture, which is like the Ag electrode. However, at a lower temperature of 450^{o}C, the electrochemical behavior becomes more complex: For R_{HF}, it decreased with decreasing pO_2, and did not seem to respond to the introduction of moisture; For $R_{MF\text{-}LF}$, it separated into multiple loops with the part at 10^4-10^1 Hz increased upon the introduction of 3% moisture while the part at 10^1-10^{-2} Hz decreased.

5.3.2.3 LSCF-BZCYYb Composite Electrode

Figure 5. 5 shows the impedance spectra for an LSCF-BZCYYb composite electrode symmetrical cell in dry simulated air and pure oxygen at 650, 550, and 450 ^{o}C. Unlike the Ag and the pure LSCF symmetrical cells, the HF loops now intercept with the real axis, enabling determination of the cell ohmic resistance R_O. It was observed that R_O increased with decreasing pO_2 at 650^{o}C and 550^{o}C, but didn't change significantly at 450^{o}C. The overall apparent electrode interfacial resistance R_{ai} also becomes much smaller-on the order of ~0.7, 4, and 30 $\Omega\bullet cm^2$ *in air*, and it increased with decreasing pO_2 at all temperatures. Both the high frequency contribution R_{HF} and mid-to-low frequency contribution $R_{MF\text{-}LF}$ generally followed the same trend.

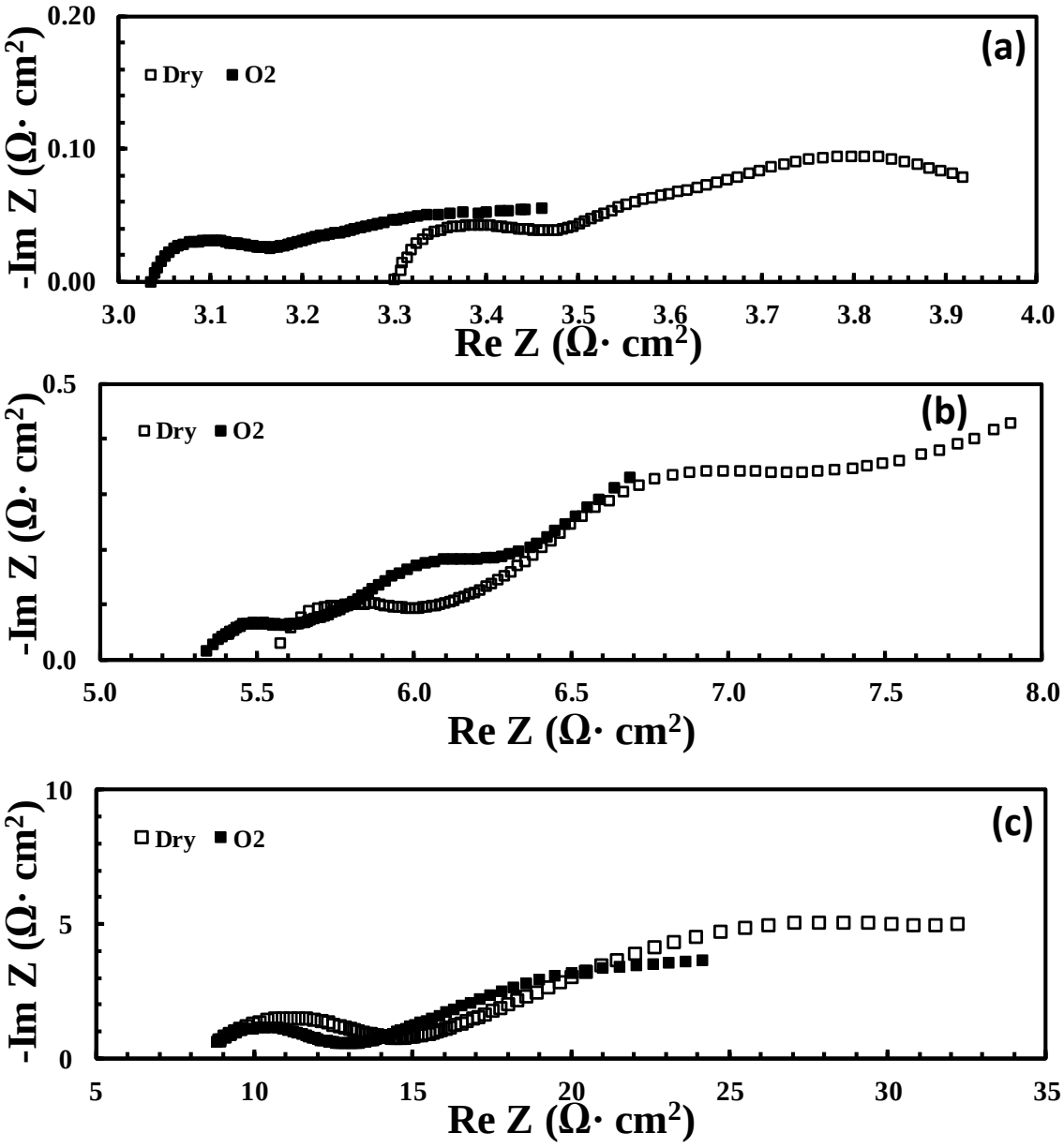

Figure 5. 5 Impedance spectra for a LSCF-BZCYYb/BZCYYb/LSCF-BZCYYb symmetrical cell in dry simulated air (20%O_2/80%N_2 with <~5ppm H_2O and CO_2) and pure oxygen at (a) 650^{o}C, (b) 550^{o}C, and (c) 450^{o}C, respectively.

Figure 5. 6 shows the impedance spectra for the same LSCF-BZCYYb composite cathode symmetrical cell in simulated air containing different moisture content.

Surprisingly, with the introduction and continued increase of moisture content, *increase* in R_O was observed, which was very dramatic at 650°C (i.e., from 3.3 Ω•cm^2 to ~12.8, ~18.0, ~23.0 and ~23.1 Ω•cm^2 with 0.6%, 3%, 10%, and 20% H_2O, respectively), still significant at 550°C (i.e., from 5.5 Ω•cm^2 to 6.7, 15.7, ~21, and ~29 Ω•cm^2 with 0.6%, 3%, 10%, and 20% H_2O, respectively), and then almost negligible at 450°C. At the same time, the total apparent interfacial resistance R_{ai} also increases accordingly, and the relative increase was very dramatic at higher temperature of 650°C and become almost negligible at lower temperature of 450°C.

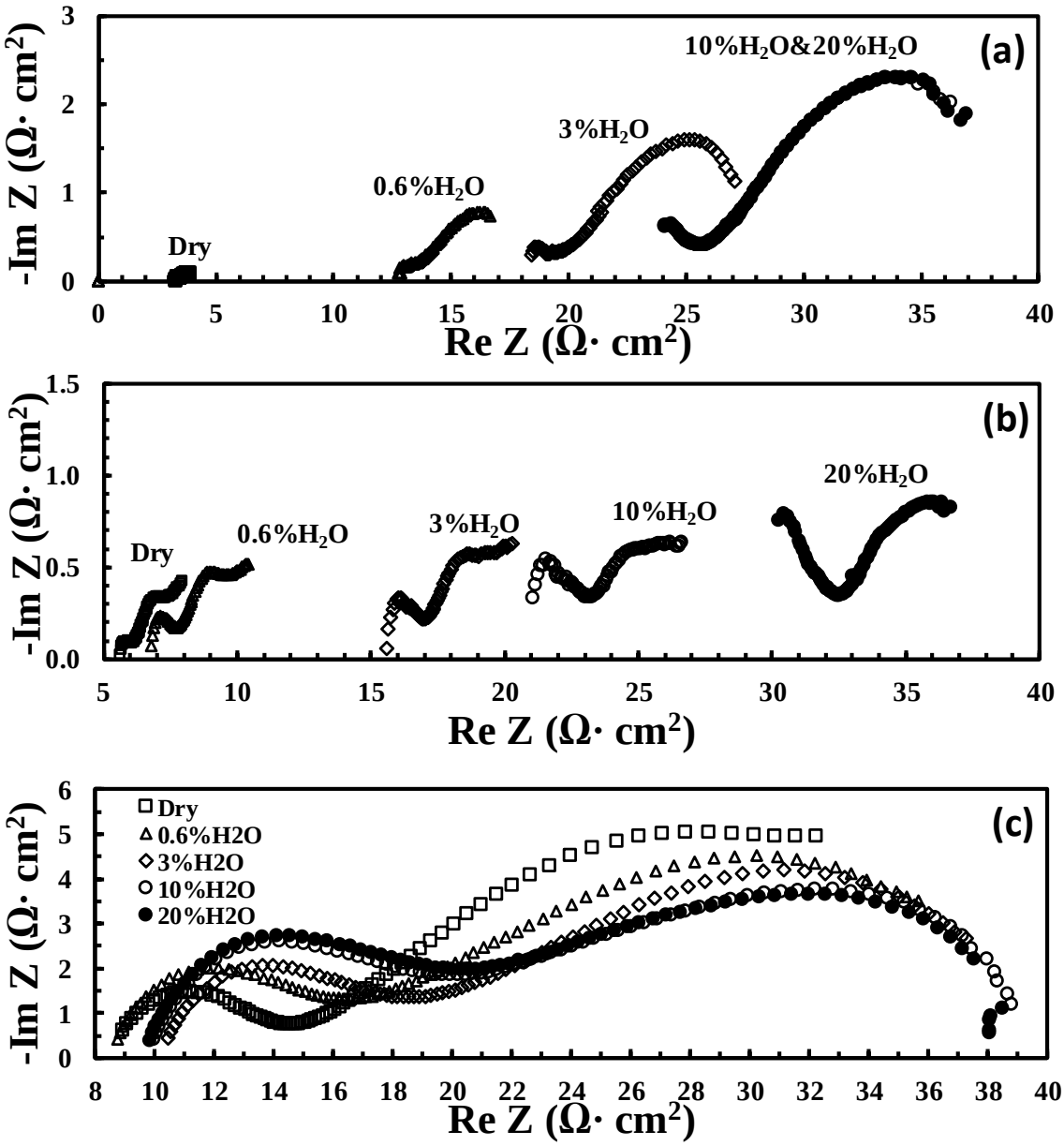

Figure 5. 6 Impedance spectra for a LSCF-BZCYYb/BZCYYb/LSCF-BZCYYb symmetrical cell in dry simulated air ($20\%O_2/80\%N_2$ with <~5ppm H_2O and CO_2) versus simulated air humidified with various concentrations of moisture at (a) 650^{o}C, (b) 550^{o}C, and (c) 450^{o}C, respectively.

5.3.2.4 BSCF Electrode

Figure 5. 7 shows the impedance spectra for the BSCF/BZCYYb/BSCF symmetrical cell in dry simulated air and dry oxygen at 650, 550, and 450 ^{o}C. Similar to the LSCF-BZCYYb composite electrode symmetrical cell, for the BSCF symmetrical cell, the HF loops still generally intercept with the real axis. Ohmic resistance R_O increased with decreasing pO_2 as well at 650 and 550^{o}C. (At lower temperature of 450^{o}C, R_O in pure O_2 did appear to be higher than that in dry simulated air.) For the total apparent electrode interfacial resistance R_{ai} of BSCF symmetrical cell, it increased with decreasing pO_2 at all temperatures under dry conditions, which is also consistent with other types of cathode symmetrical cells studied. Both the high frequency electrode resistance R_{HF} and the mid-to-low frequency electrode resistance $R_{MF\text{-}LF}$ also generally follow the same trend except for R_{HF} at lower temperature of 450^{o}C: it did not seem to change much with pO_2: Such a behavior of roughly constant R_{HF} at 450^{o}C is similar to the Ag symmetrical cell but different from the symmetrical cells with the LSCF or the LSCF-BZCYYb composite electrodes.

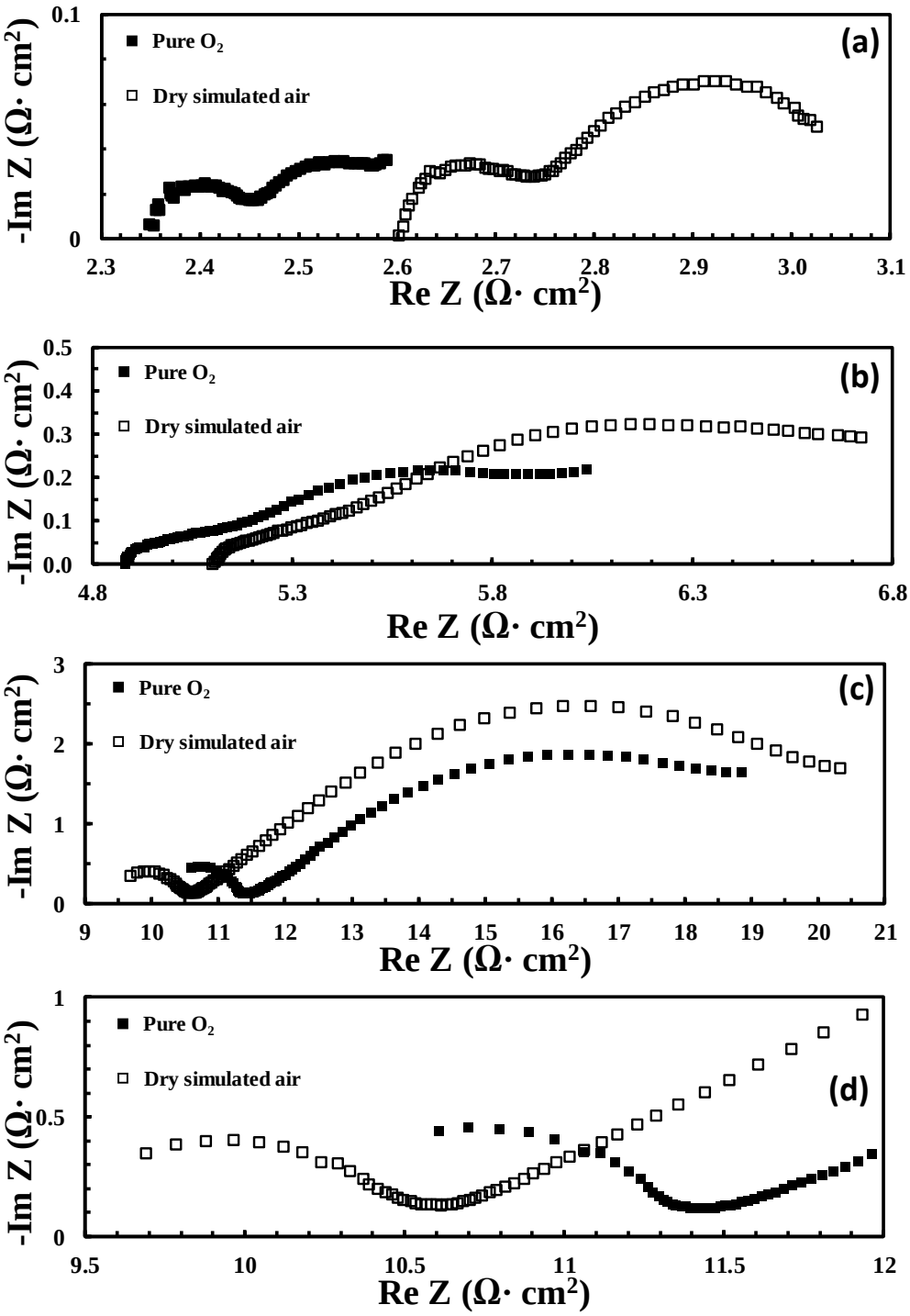

Figure 5. 7 Impedance spectra for a BSCF/BZCYYb/BSCF symmetrical cell in dry simulated air (20%O_2/80%N_2 with <~5ppm H_2O and CO_2) versus pure oxygen at (a) 650ºC, (b) 550ºC, (c) 450ºC, and (d) zoom-in of the impedance spectra at 450ºC showing the high frequency (HF) part.

Additionally, Figure 5. 8 shows the impedance spectra for the BSCF symmetrical in simulated air with different moisture content. The observations for the BSCF symmetrical cell after the introduction of moisture are as follows: R_O decreased with the introduction of moisture and further increase in moisture content. R_{ai} generally first increased with the introduction of moisture and then decreased back with further increase in moisture content. Figure 5. 9 shows the same impedance curves but with ohmic resistance subtracted, and it is consistent with the authors' previous studies: [20, 157] The mid-to-low frequency part R_{MF-LF} seems to follow the same trend as R_{ai}, while the high frequency part R_{HF} seemed to always decrease with the introduction of moisture, especially at lower temperature of 450^{o}C when the HF loop becomes clearly separated.

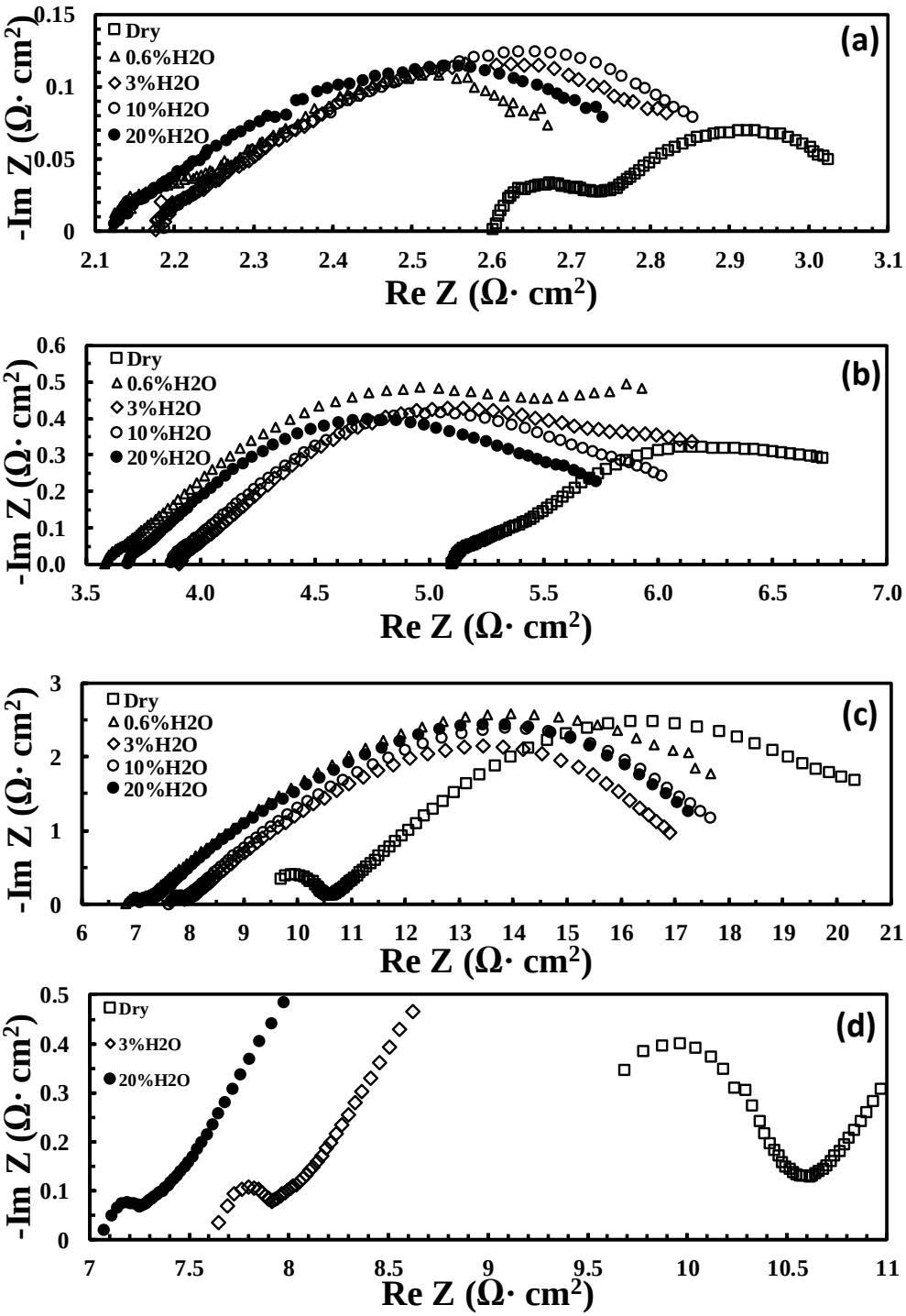

Figure 5. 8 Impedance spectra for a BSCF/BZCYYb/BSCF symmetrical cell in dry simulated air (20%O_2/80%N_2 with <~5ppm H_2O) versus simulated air with varying concentrations of moisture at (a) 650^{o}C, (b) 550^{o}C, (c)450^{o}C, and (d) zoom-in of the impedance spectra at 450^{o}C showing the high frequency (HF) part.

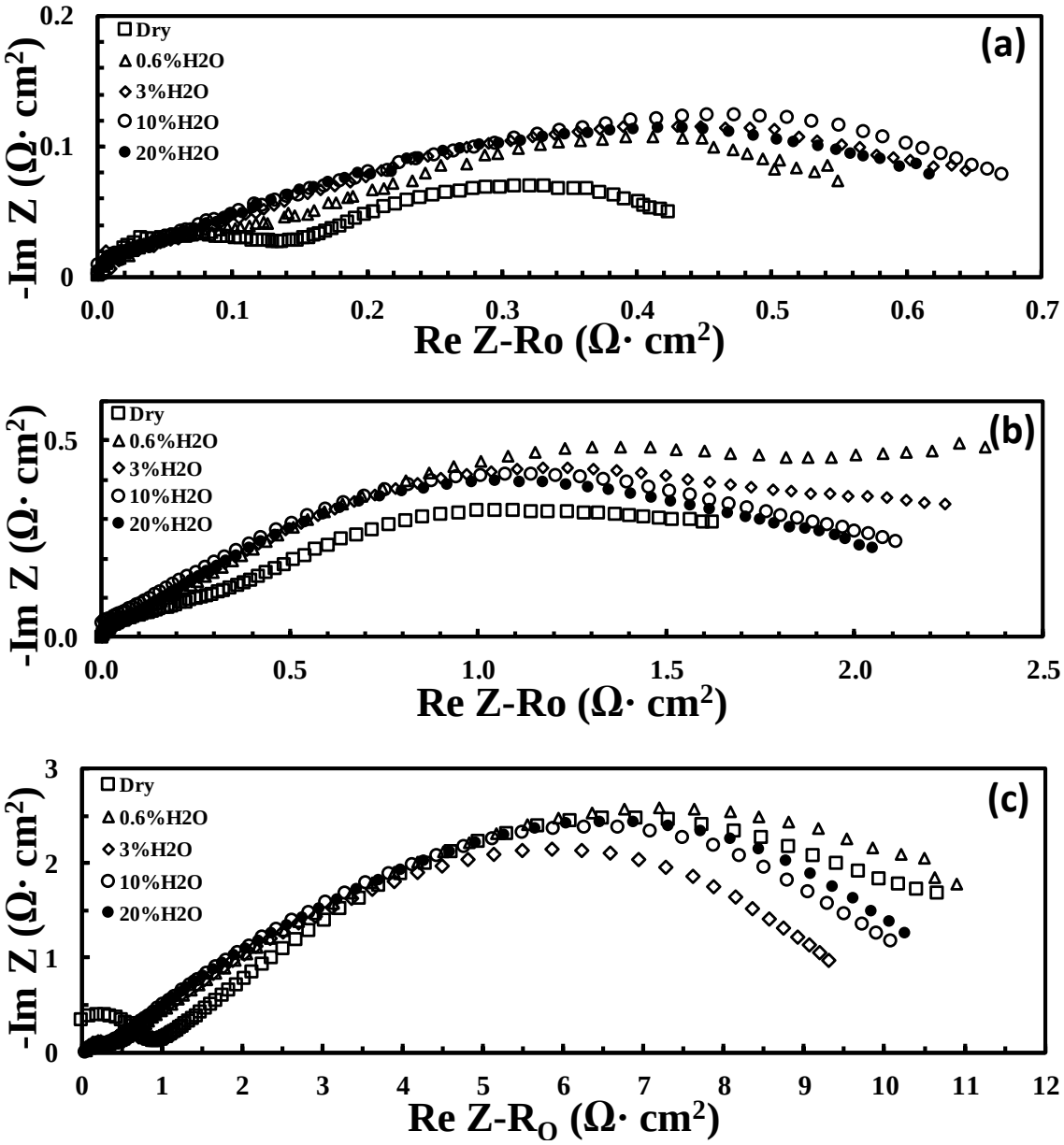

Figure 5. 9 Ohmic resistance subtracted impedance spectra for a BSCF/BZCYYb/BSCF symmetrical cell in dry simulated air (20%O_2/80%N_2 with <~5ppm H_2O) versus simulated air with various concentrations of moisture at (a) 650^{o}C, (b) 550^{o}C, and (c) 450^{o}C, respectively.

5.4 Discussions

As discussed in section 1.1 and published paper, [157] the overall cathode or oxygen electrode reaction process based on a conventional oxide ion conducting electrolyte proceeds via

$$O_2 + 2V_O^{\bullet\bullet} + 4e^- \leftrightarrow 2O_O^{\times}\ , \qquad \text{Equation 5.1}$$

while the cathode reaction based on an ideal, "pure" proton conducting electrolyte proceeds via

$$O_2 + 4(OH)_O^{\bullet} + 4e^- \leftrightarrow 4O_O^{\times} + 2H_2O. \qquad \text{Equation 5.2}$$

The elementary steps for both reaction pathway (1) and (2) are summarized in Table 5. 1 and also illustrated in Figure 5. 10 and Figure 5. 11 for the different electrodes used.

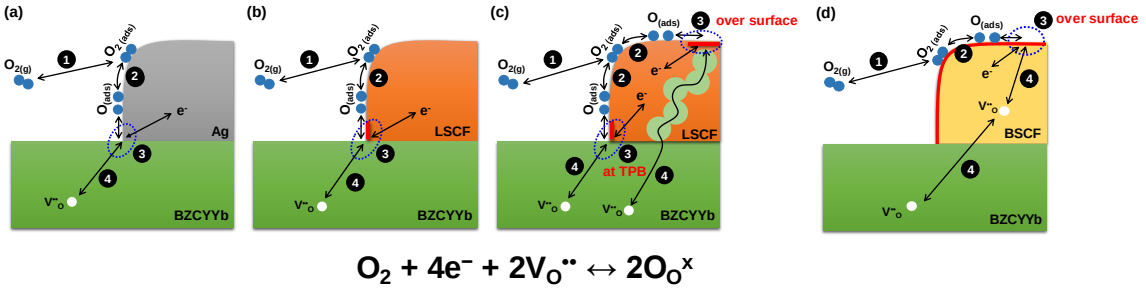

Figure 5. 10 Schematics showing the reaction species involved and the elementary steps (also refer to Table 5. 1) for the reversible oxygen electrode reactions for an ideal oxide-ion based SOFC with (a) Ag, (b) pure LSCF, (c) LSCF-BZCYYb composite, and (d) BSCF as the cathode (oxygen electrode) on BZCYYb electrolyte in a dry simulated air atmosphere.

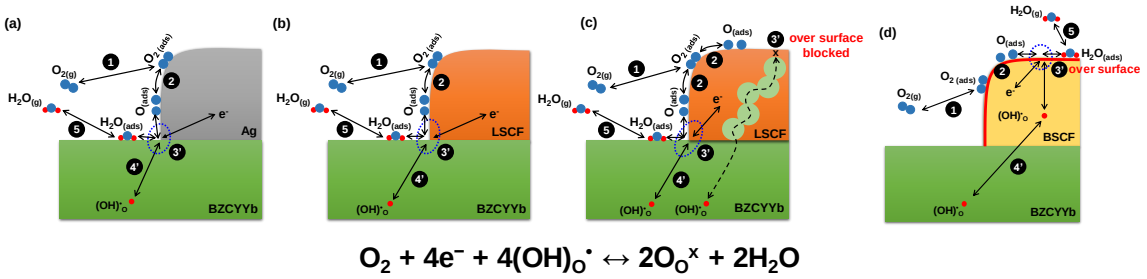

Figure 5. 11 Schematics showing the reaction species involved and the elementary steps (also refer to Table 5. 1) for the reversible oxygen electrode reactions for an ideal proton-conducting electrolyte based SOFC with (a) Ag, (b) pure LSCF, and (c) LSCF-BZCYYb composite, and (d) BSCF as the cathode (oxygen electrode) on proton conducting BZCYYb electrolyte in simulated air in a humidified atmosphere assuming full hydration for the electrolyte.

Table 5. 1 Elementary steps (and their reverse steps) of the oxygen electrode reaction for the reversible oxygen electrode reactions for ideal oxide-ion based SOFC (step 1,2,3,4) and ideal proton conducting SOFC (step 1,2,3',4',5). [157]

Elementary Steps		Frequency range
1 Mass transfer of O_2 molecule in gas phase and adsorption on electrode surface	$O_2(g) \leftrightarrow O_2\ (ads)$	LF
2 Adsorbed O_2 molecule dissociation	$O_2\ (ads) \leftrightarrow 2O\ (ads)$	MF
3 Charge transfer for ideal oxide ion electrolyte	$O(ads) + V_O^{\cdot\cdot} + 2e^- \leftrightarrow O_O^X$	HF
3' Charge transfer for ideal pure proton electrolyte	$O\ (ads) + 2e^- + 2OH_O^{\cdot} \leftrightarrow H_2O(ads) + 2O_O^X$	HF
4 Mass transfer of oxide ion in the bulk of electrode and/or electrolyte	$V_{O(electrode)}^{\cdot\cdot} \leftrightarrow V_{O(electrolyte)}^{\cdot\cdot}$	Very HF (>> 10^6 Hz)
4' Mass transfer of proton in the bulk of electrode and/or electrolyte	$OH_{O(electrode)}^{\cdot} \leftrightarrow OH_{O(electrolyte)}^{\cdot}$	Very HF (>> 10^6 Hz)
5 (or **5'**) H_2O transport and desorption	$H_2O(ads) \leftrightarrow 2H_2O(g)$	LF

Among those processes, the steps of oxygen adsorption (step 1) and dissociation (step 2) always exist no matter whether the atmosphere contains water or not. For the charge transfer step, for a proton conducting electrolyte such as BZCYYb used in this study, if the atmosphere is dry and the temperature is high (>~700°C), it is expected to proceed primarily via the oxide ion (or $V_O^{\cdot\cdot}$) route as shown in step 3; (19) On the other hand, if the atmosphere is humidified and the temperature is relatively low (~450°C), most if not all

oxygen vacancy can be assumed to be protonated, and the charge transfer step is expected to proceed primarily via the proton ($(OH)_O^{\bullet}$) route as shown in step 3'. Consequently, depending on the atmosphere as well as temperature, the bulk phase ion transport step, in the electrode and/or the electrolyte, would proceed either via oxide ion (step 4) or proton (step 4'). Finally, if the charge transfer step is based on proton, there must also be the additional step of water desorption (or adsorption for the reverse reaction) (step 5'). With this in mind, the electrochemical behaviors of different oxygen electrodes over the BZCYYb proton conducting electrolyte are discussed here below.

5.4.1 Ag Electrode

Based on the observations above, Ag, as an electron conducting cathode, behaves rather poorly on the proton conducting BZCYYb electrolyte, giving very large apparent interfacial resistance R_{ai} at intermediate temperature of 450 to 650^{o}C. This is understandable from two aspects: First, Ag is not expected to be an effective oxide-ion or proton conductor, which would limit the cathode oxygen electrochemical reaction to the triple-phase boundary (TPB) region, and the electrode process on the Ag electrode over an ideal oxide ion conducting electrolyte in air is represented in the schematic in Figure 5. 10 (a). Second, the fired Ag electrode has relatively coarse microstructure, as shown in the SEM images of Figure 5. 2 (a) and (b), which would severely limit the total length of triple-phase boundary (TPB). In fact, it is probably for these two reasons that the oxygen electrode process becomes so sluggish that high frequency loop does not even intercept with the real axis.

Nevertheless, for the Ag electrode, the displayed increase of R_{ai} with respect to reducing pO_2 under dry atmosphere appears reasonable: With reduction of pO_2 from 100% to 20%, the oxygen gas phase transport [48] as well as surface adsorption and dissociation processes are expected to slow down significantly. Due to the complexity of the cathode process, the exact interpretation of the various overlapping semi-circles observed (e.g., as many of 4 semi-circles from high frequency to low frequency were observed at 550°C) is *not* straightforward except at the lower temperature of 450°C when the reduction of pO_2 does not seem to impact the HF semi-circle (see Figure 5. 3 (c)), suggesting that, at 450°C, the HF semi-circle most likely represents the charge transfer step, while the MF-to-LF semicircles should represent the various processes including gas phase transport, oxygen molecule adsorption and dissociation, and surface diffusion.

With respect to the moisture effect on the Ag electrode, the process is conceptually illustrated in Figure 5. 11 (a). Due to very sluggish electrode process, the ohmic resistance R_O cannot be accurately determined in this study in the temperature range of 450 to 650°C. Nevertheless, an earlier study on a Pt/$BaCe_{0.8}Gd_{0.2}O_3$(BCG)/Pt symmetrical cell at 722°C clearly showed decrease in R_O upon introduction of 3% moisture. [159] In addition, as mentioned before and will be discussed later, similar reduction in R_O upon the introduction of moisture for BZCYYb proton conducting electrolyte was clearly observed for the BSCF cathode symmetrical cell (see Figure 5. 8), indicating the change of ion conducting species from oxide ion to proton and the acceleration of the bulk transport process. As to the oxygen electrode reaction process, Figure 5. 3 suggests that all HF and MF-LF loops seem to increase upon the introduction of 3% moisture into dry air at temperatures from 650 to

450^{o}C. Such an observation is consistent with the previous study on the Pt/BCG/Pt symmetrical cell. [162] Part of the increase could be attributed to the strong adsorption of water molecules over the BZCYYb electrolyte surface including near the TPB, which would interfere with the processes of oxygen adsorption (step 1) and dissociation and surface diffusion (step 2). These steps, as stated before for 450^{o}C, are represented by the mid-to-low frequency loops. As to the charge transfer step at the TPB, with the introduction of moisture to the testing chamber, the ion conducting species is expected to change from oxygen vacancy to proton, and the charge transfer step would change from the oxide ion route (step 3) to the proton route (step 3'). The observed increase in R_{HF} upon moisture introduction to dry air for the Ag electrode seems to suggest that, for the Ag electrode (and the Pt electrode as in the earlier study), the charge transfer step via the proton route *appears to be slower* than via the oxide ion route. One possible explanation for this is that the very strongly adsorbed water molecules at the TPB reduces the concentration of adsorbed oxygen, which slows down the overall charge transfer step despite the acceleration of ion transport in the bulk phase(s). Another possibity is that the proton conducting electrolytes (e.g. BZCYYb in this study and BCG [121] in the earilier study) have certain electronic conductivity in dry atmospheres, which means the measured impedance would be subjected to *shortage* effect, leading to *underestimation* of the apparent electrode interfacial resistance R_{ai} under dry condition. [163] With the introdution of moisture, the electronic conduction would get suppressed for the proton conducting electrolyte. As a result, the measured R_{ai} would suffer less from the shortage effect and appear to be larger comparing with the dry condition. Further study is needed to clarify the exact origin for

this phenomenon (i.e., the reduction of R_{HF} for Ag or Pt electrode over proton conducting electrolyte when moisture is introduced into dry air).

5.4.2 Pure LSCF Electrode

For the pure LSCF cathode, the observation of very large total apparent electrode interfacial resistance R_{ai} on the order of ~30 Ω•cm^2 at 650^{o}C and ~80 Ω•cm^2 at 550^{o}C in dry simulated air or dry oxygen was rather surprising. Given that LSCF is known to be a very good mixed oxide ion and electron conductor (MIEC), [68, 74] and the BZCYYb electrolyte should also conduct primarily oxide ion with high conductivity in *dry* atmosphere, the expectation was that such an LSCF/BZCYYb/LSCF symmetrical cell should give much better interfacial resistance in dry atmosphere. In fact, as mentioned before, for pure LSCF cathode symmetrical cells over oxide ion conducting electrolyte (e.g., yttria stabilized zirconia YSZ or GDC), the interfacial resistance reported was measured to be only ~0.4-1 Ω•cm^2 at 650^{o}C and ~3-10 Ω•cm^2 at 550^{o}C in air. [69, 160, 164] Nevertheless, the experimental observation of LSCF electrode over proton conducting electrolyte (e.g., BZCYYb) giving much larger interfacial resistance in dry atmosphere similar to the Ag electrode suggests that there is certain *complexity* involved when matching the pure LSCF cathode with the BZCYYb electrolyte: The LSCF behaves as if oxide ion could *not* effectively transport between the BZCYYb electrolyte and the LSCF cathode and, as a result, LSCF behaves more like an electronic conductor as Ag or $La_{1-x}Sr_xMnO_3$ (LSM). Thus, as illustrated in Figure 5. 10 (b), the active reaction sites become limited to the LSCF-BZCYYb-air TPB and its very vicinity region, while most of the surface of the LSCF electrode is *not* active unlike in typical oxide ion SOFCs with LSCF

cathode. Related to this, at a lower temperature of 450°C, despite that the high frequency semi-circle seems to intercept with the real axis at ~50 Ω•cm^2, this value is unlikely to represent the actual electrolyte ohmic resistance but is attributed to the very sluggish electrode process due to limited TPB and active LSCF surface.

As to the pO_2 and moisture effects on the LSCF cathode, despite the complex shapes of the impedance spectra, the responses are also similar to the Ag electrode: With the introduction of moisture, R_{ai} generally increases. This is understandable because strong adsorption of water molecules on the BZCYYb surface is expected to slow down the oxygen adsorption and dissociation and, maybe, the charge transfer step, as illustrated in Figure 5. 11 (b). The situation is expected to be somewhat similar with decreasing pO_2. It is worth noting that, as mentioned before, for the LSCF cathode at 450°C (see Figure 5. 4 (c)), the high frequency loop seems to *decrease* with both decreasing pO_2 and increasing pH_2O. Although the exact reason for such behaviors is not clear, one possible explanation is that this HF loop may *not* represent the charge transfer step as for the Ag electrode. Instead, it may represent O_2 and H_2O *gas diffusion* through the highly porous electrode with pore size <~1 μm at that temperature to access the TPB sites right at the interface of the LSCF electrode and BZCYYb electrolyte. This seems possible given that the LSCF over BZCYYb electrolyte here behaves more like the Ag electrode with electrode reaction confined at the electrode/electrolyte interface, which is buried deeply beneath a cathode with very fine pores. As a result, the gas phase transport limitation may show up. Further study is needed to verify such a hypothesis.

5.4.3 LSCF-BZCYYb Composite Electrode

When mixing LSCF with BZCYYb to make a composite electrode, as shown before in Figure 5. 5 and Figure 5. 6, such an electrode is much more active comparing with the pure LSCF electrode: The high frequency semicircle now intercepts with the real axis, giving good estimate of the ohmic resistance R_O that would reflect the conductivity of the BZCYYb electrolyte materials: For example, considering electrolyte thickness of ~600 μm, the estimated conductivity in dry simulated air is ~0.03 S/cm at 650^{o}C, ~0.016 S/cm at 550^{o}C and ~0.01 S/cm at 450^{o}C, which matches well with previous results. [88]

In addition, the overall apparent electrode interfacial resistance R_{ai} in dry air as well as pure oxygen decreases by ten times or even more comparing with the pure LSCF cathode. This dramatic improvement of electrode activity provides additional support to the earlier hypothesis that LSCF behaves more like an electronic conductor with very limited oxide ion conductivity when it is matched with a proton conducting electrolyte such as BZCYYb in the dry atmosphere. As depicted in Figure 5. 10 (c), when making a LSCF-BZCYYb composite electrode, the TPB in the LSCF-BZCYYb composite is expanded comparing with the pure LSCF cathode due to fine mixing of submicron-scale (see Figure 5. 11Figure 5. 10 (e) and (f)) ion conducting BZCYYb electrolyte phase and the LSCF phase, which only conducts electrons here. On the other hand, by providing a porous BZCYYb network in close contact with LSCF, the oxide-ions from the BZCYYb electrolyte could transport through the BZCYYb network over much of the composite cathode to larger regions with LSCF surface close to the LSCF/BZCYYb two phase boundary. The result is that more surface area of the LSCF now also becomes active for oxygen electrode reaction. The

added TPB and expanded surface area of LSCF that become active together help accelerate the oxygen electrode processes, which are illustrated in Figure 5. 10 (c). As a result of the greatly accelerated electrode reaction, the obtained R_O from impedance spectra reduce dramatically reflecting the actual conductivity of the BZCYYb electrolyte used.

On the other hand, as stated, Figure 5. 9 shows that when such an LSCF-BZCYYb composite electrode symmetrical cell over BZCYYb electrolyte is subject to humidified air, dramatic increase in R_O (by almost 6 times in 3% moisture!) with the introduction of moisture was observed at 650^{o}C and, to a less extent, 550^{o}C. Such a behavior is attributed to the reduction of reaction sites upon humidification for the composite cathode. As stated before and shown in Figure 5. 10 (c), electrode reaction in the LSCF-BZCYYb composite cathode symmetrical cell under *dry* condition can occur at the TPB sites as well as *over LSCF surface* where BZCYYb network is close enough to deliver oxide-ions (see the schematic in Figure 5. 10 (c)). However, after the introduction of moisture, the electrode reaction for the composite cathode again becomes limited only to the TPB sites presumably due to the inability of LSCF to conduct protons when the major ionic species changes from oxide-ion to proton: This effectively blocks the reactions going through the LSCF surface near the BZCYYb network, making processes 3', 4' and 5' almost impossible to happen. In addition, this explanation could be supported by the observation that the R_O for the LSCF-BZCYYb composite symmetrical cell seems to increase to values comparable to those for the pure LSCF cathode symmetrical cell after the introduction of moisture at 650^{o}C and 550^{o}C (see Figure 5. 4), suggesting dramatically slowed down oxygen electrode reaction with moisture introduction.

In comparison, at lower temperature such 450°C, such "blocking effect" or the increases in R_{ai} as well as R_O due to moisture introduction to air for the LSCF-BZCYYb composite cathode symmetrical cell is much smaller. This might be because that although moisture still covers the BZCYYb surface and TPB at lower temperature, due to faster bulk ionic transport for proton (step 4') compared to the ionic transport via oxygen vacancy route (step 4) and the fact that moisture is now part of the charge transfer step (step 3'): despite certain parts of the oxygen electrode reaction (e.g., O_2 adsorption (step 1) and dissociation (step 2)) got hindered, other part may actually accelerate (e.g., H_2O splitting over the electrode surface (step 3')), and the net effect is no longer obvious. Another factor, which might be more important, is that for the BZCYYb electrolyte, both the reaction route via oxide-ion (reaction (1)) and via proton (reaction (2)) would co-exist and compete with each other. At a higher temperature such as 650°C, the difference in the actual extent of BZCYYb hydration is large between "dry simulated air" and the 3% humidified air. This means in "dry" air, most of the reaction would go through the oxide ion route. Then, after 3% moisture is introduced, a significant portion of the oxide ion route is blocked due to hydration of the BZCYYb electrolyte and shut off the route over LSCF surface near BZCYYb and confinement of the active region to strictly TPB. In comparison, at a lower temperature of 450°C, due to strong bonding of the BZCYYb electrolyte with moisture at that temperature, even for the so-called "dry" condition, very significant portion of the electrode reaction already goes through the proton route. As a result, when 3% moisture is introduced, the actual difference in impedance spectra between "dry simulated air" and 3% humidified air appear to be much less dramatic. [88] Further study is needed to verify this.

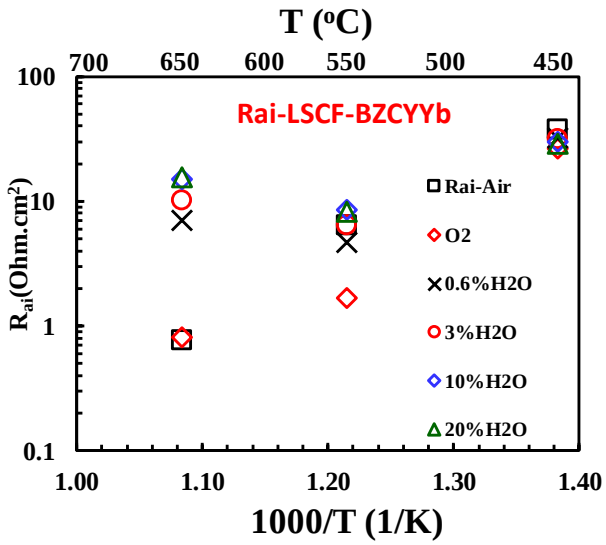

Figure 5. 12 Total apparent electrode interfacial resistance R_{ai} in dry simulated air, pure oxygen and simulated air containing up to 20% moisture for LSCF-BZCYYb composite electrode symmetrical cells at temperatures from 650 to 450°C.

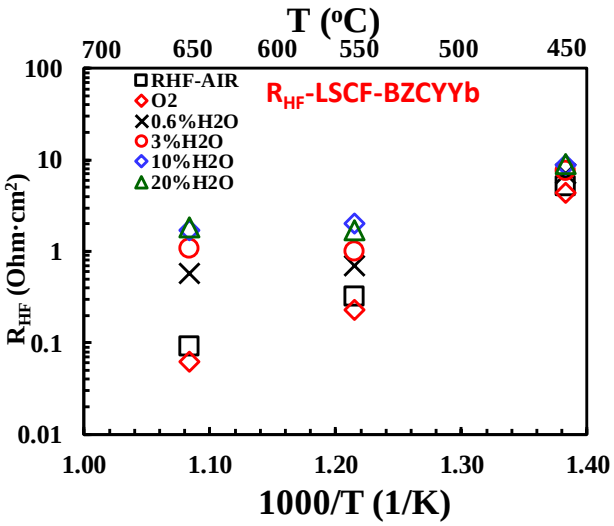

Figure 5. 13 High frequency resistance R_{HF} in dry simulated air, pure oxygen and simulated air containing up to 20% moisture for LSCF-BZCYYb composite electrode symmetrical cells at temperatures from 650 to 450°C.

Finally, for the LSCF-BZCYYb symmetrical cell, equivalent circuit fitting was carried out to *roughly* evaluate the total apparent electrode interfacial resistance R_{ai} and the high frequency resistance R_{HF}, and the values are plotted against inverse temperature (1/T), as in Figure 5. 12 and Figure 5. 13. Besides, the ASR vs. pH_2O dependence of the LSCF-BZCYYb symmetric cell cathode response was also examined (not shown here). It is observed that, between 650°C and 550°C, both R_{ai} and R_{HF} *decrease* with decreasing temperature under humidified condition; in comparison, under dry condition, both R_{ai} and R_{HF} *increase* with decreasing temperature. This may also be related to the explanation before about the large difference in moisture response with respect to temperature for the LSCF-BZCYYb composite electrode. However, no more definitive insight into the cathode reaction process could be extracted so far as no consistent trend in behavior based on the ASR vs. pH_2O dependence was observed at various temperatures.

5.4.4 BSCF Electrode

Comparing with the Ag, pure LSCF, and also LSCF-BZCYYb composite electrodes, the impedance data in Figure 5. 7 shows that BSCF behaves like a good MIEC electrode in a symmetrical cell with BZCYYb electrolyte: The overall R_{ai} was the lowest among all those electrodes tested under both dry and humidified conditions. The decrease in R_O with increasing pO_2 is attributed to the increased electronic conduction, especially at higher temperature of 650°C, which matches that reported in literature. [165] The decrease in R_O with the introduction of moisture is expected and can be attributed to faster mass transfer process via proton (step 4') than via oxide ion (step 4) at all temperatures, which is

consistent with previous studies. [12, 72, 157, 166] In addition, as discussed elsewhere, the high frequency semicircle in the impedance spectra for the BSCF symmetrical cell has been attributed to the charge transfer process. [157] Such an assignment is rational as R_{HF} does not seem to change with changing pO_2, yet it decreases continuously with introduction and increasing moisture content, and it was particularly obvious at lower temperature. This has been attributed to *faster* charge transfer step via the proton route (step 3') than via the oxide ion route (step 3), especially at lower temperature of 450°C, because BSCF seems to behave like a MIEC with the entire BSCF surface as well as TPB active for oxygen electrode reactions, which is not expected to be severely limited by available sites for oxygen adsorption/dissociation and charge transfer.

Besides that, the observation of the increase in R_{MF-LF} with decreasing pO_2 (see Figure 5. 14) or the introduction of H_2O (see Figure 5. 8 and Figure 5. 9), which is more obvious at higher temperature of 650°C and 550°C, but less so at low temperature of 450°C, suggests that these parts of resistance can be attributed to the adsorption/desorption (step 1) and dissociation/association (step 2), both which are limited by reduced surface area due to adsorption of water molecules. Moreover, the increase in R_{MF-LF} with the introduction and increase of moisture content is generally consistent with most other types of symmetrical cells, suggesting such an increase does not seem to depend on the specific oxygen electrode material but more reflects the intrinsic strong water adsorption property of the BZCYYb electrolyte.

5.4.5 Electrochemical Behavior of BSCF Anode-supported Full Cell at 450ºC

The comparison of these different electrodes suggests that, despite the higher ionic conductivity of the proton conducting electrolyte like BZCYYb, simply borrowing a good MIEC material (e.g., LSCF) for an oxide ion conducting SOFC does *not* guarantee excellent performance when it is used as the cathode for a proton conducting IT-SOFC. In fact, this has been confirmed by previous studies. For example, Yang *et al.* compared the performance for the pure LSCF cathode versus the LSCF-BZCYYb composite cathode at 750^{o}C and arrived at the same conclusion that the composite cathode delivers significantly higher activity than the pure LSCF cathode. [121]

On the other hand, cathode material of BSCF does behave like a good MIEC both in dry atmosphere and in humidified atmosphere. Given that BSCF is a good oxide ion conductor and has been shown to be able to take up significant amount of moisture, [20] the result here strongly suggests the possibility that BSCF is a *mixed proton-oxide ion-electron triple conducting oxide* in humidified atmosphere at lower temperature and would serve as a good cathode for proton conducting IT-SOFC. This can also be supported by comparison of R_{ai} between the BSCF symmetrical cell versus the LSCF-BZCYYb composite symmetrical cell, showing significantly lower values for the BSCF electrode, especially under humidified condition. Another piece of evidence comes from the comparison with data for an LSCF-$Ba(Zr_{0.1}Ce_{0.7}Y_{0.2})O_{3-\delta}$ (BZCY) composite cathode/BZCY electrolyte/NiO-BZCY anode-supported full cell reported in a previous study: [121] At 450^{o}C, that cell was expected to yield total electrode interfacial resistance as high as ~10 Ω•cm^2, while a BSCF/BZCYYb/NiO-BZCYYb anode supported cell in this

study gave a much lower value of ~2.7 Ω•cm^2, as shown in Figure 5. 15. Additionally, the R_O and R_{ai} values obtained in this study for the anode-supported cell is ~1.5 Ω•cm^2 and ~2.7 Ω•cm^2 at 450^{o}C, respectively. These values are consistent with those obtained for a BSCF cathode/$BaCe_{0.9}Y_{0.1}O_{2.95}$ (BCY) electrolyte anode-supported full cell giving R_O and R_{ai} values of ~0.75 Ω•cm^2 and ~0.4 Ω•cm^2 at 500^{o}C. [72]

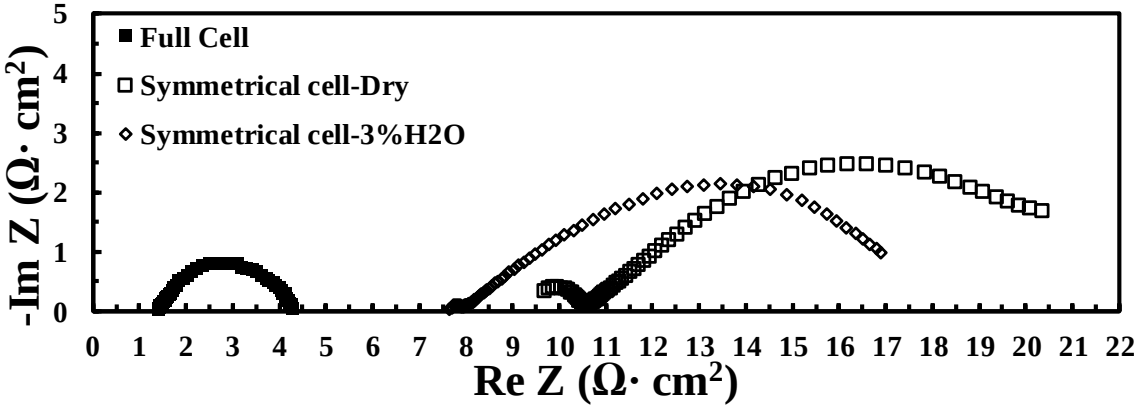

Figure 5. 15 Impedance spectra for a BSCF/BZCYYb/BSCF symmetrical cell in dry simulated air (20%O_2/80%N_2 with <~5ppm H_2O) and simulated air with 3%H2O versus BSCF/BZCYYb/Ni-BZCYYb full cell at 450^{o}C

Considering that the BSCF cathode microstructure prepared in this study was by convention printing and firing approach, leading to rather coarse microstructures (Figure 5.2 (g) and (h)) comparing with the LSCF-based electrodes (see Figure 5. 2 (c to f)), it seems there is still significant room for improvement in terms of optimizing the microstructure of the BSCF electrode. For example, the BSCF cathode microstructure might be optimized with better tuning of the firing process and/or introduction of nanostructured catalysts into the BSCF cathode via methods such as infiltration. [160] These would help further increase electrode active surface area and may significantly improve the cathode performance for proton conducting IT-SOFC, and will be studied in

future. In addition, it is noted that BSCF was still developed as a "traditional" SOFC cathode materials for conventional oxide-ion conducting SOFC, while some proton-oxide ion-electron "triple conducting" cathode materials have been specifically developed recently for proton-conducting SOFCs and seem to show dramatically improved proton conductivity and electrochemical activity over BSCF. For example, $Ba_{0.5}Sr_{0.5}Fe_{0.8}Zn_{0.2}O_{3-\delta}$ (BCFZ) showed proton conductivity of 0.9 to 3×10^4 *S* cm^{-1} at 600 to 350°C; [122] $NdBa_{0.5}Sr_{0.5}Co_{1.5}Fe_{0.5}O_{5+\delta}$ (NBSCF) achieved outstanding maximum power densities of 1.71, 1.37, 1.05, and 0.69 W cm^2 over BZCYYb electrolyte at 750, 700, 650, and 600°C; [127] $BaCo_{0.4}Fe_{0.4}Zr_{0.2-x}Y_xO_{3-\delta}$ (BCFZY) exhibited significantly reduced cathode interfacial resistance of only 0.12 $\Omega\cdot cm^2$ at 500°C over BZCYYb electrolyte. [167] These studies suggest that partial doping or substituting for the A or B site elements in BSCF could be another way to further tailor the properties for improved cathode performance for proton conducting IT-SOFC.

Finally, it should be noted that for the BSCF electrode, there appears to be a very *large difference between the impedance measured in anode-supported full cell configuration versus in a cathode symmetrical cell configuration*. To illustrate this, the impedance for the impedance spectra for the BSCF/BZCYYb/BSCF symmetrical cell in both dry air and 3% humidified air are also plotted together with that of the BSCF/BZCYYb/Ni-BZCYYb anode-supported full cell, as in Figure 5. 15. It can be observed that the R_{ai} for the anode-supported full cell, which include contributions from both the Ni-BZCYYb cermet anode and the BSCF cathode, is only about one tenth (1/10) of the value from the cathode symmetrical cell! Such a large difference was *not* observed when BSCF was matched with the samaria-doped ceria (SDC) electrolyte with the oxygen electrode interfacial resistance

giving the same value in full cell and in cathode symmetrical cell. [70] The underlying reason for this large discrepancy is *not* clear at this moment. According to the previous study by Merkle et al, [163] for the apparent cathode interfacial resistance from a cathode symmetrical cell with proton conducting electrolyte should be *smaller* than that when measured from a full cell due to the electronic shortage in relatively thick electrolyte for the symmetric cell. However, *this prediction seems to be opposite to the current observation* that the apparent cathode interfacial resistance as determined from the symmetrical cell with proton conducting electrolyte is much larger than from an anode-supported full cell. The underlying reason for this observation and the discrepancy from prediction is not clear. One hypothesis is related to the possible difference in the actual extent of hydration within the BZCYYb electrolyte: In the anode-supported cell configuration, due to the thin electrolyte (~20 μm) and anode side hydrogen supply, the BZCYYb electrolyte is presumably better hydrolyzed, which might ensure full proton conduction at intermediate temperature. In comparison, for the cathode symmetrical cell in humidified air, due to the thick electrolyte (~600 μm) used, the electrolyte may not stay fully hydrated in impedance measurement, especially for the cathodic part (water evolution size) due to slow diffusion of proton. Further studies will be needed to test such a hypothesis and understand the origin for the discrepancy when BSCF cathode is used over a proton conducting electrolyte.

5.5 Conclusions

In summary, different oxygen electrodes of Ag, LSCF, LSCF-BZCYYb composite, and BSCF have been evaluated using cathode symmetrical cells based on BZCYYb proton conducting electrolyte. Generally, most cells show increased electrode interfacial resistance with decreasing pO_2 or introduction of moisture. Pure LSCF does *not* behave like a good MIEC but more like Ag over the BZCYYb electrolyte, giving very high interfacial resistance and high ohmic resistance, suggesting very sluggish electrode reaction in both dry and humidified conditions. This indicates that the oxide-ion transfer between LSCF and BZCYYb electrolyte is *not* very ineffective even in dry atmosphere, but the underlying reason is not clear at the moment. Nevertheless, when LSCF was mixed with BZCYYb electrolyte to make a composite electrode, its activity becomes much better under dry conditions, which might be attributed to the extended TPB area and BZCYYb networks in the electrode that transfer oxide-ion to places near the LSCF surface. In comparison, BSCF electrode behaves like a MIEC giving low interfacial resistance and ohmic resistance than the other electrode materials studied under both dry and humidified conditions. The high frequency resistance R_{HF} of BSCF does not change with pO_2 but decreases with increasing pH_2O, which is attributed to intrinsically faster charge transfer step for the oxygen electrode reaction via the proton route than the oxide ion route. Full cell impedance data confirms that BSCF appears to be a better cathode for IT-proton conducting SOFC than the LSCF-BZCYYb composite cathode. Further study aimed at refining the cathode microstructure via techniques such as firing optimization and infiltration [168] into the BSCF cathode as well as proper doping to enhance the proton-

oxide ion-electron triple conduction appears attractive to obtain high performance cathode for proton conducting IT-SOFCs. Finally, study also needs to be carried out to understand the large difference in BSCF cathode interfacial resistance measured in full cell versus cathode symmetrical cell configuration when using a proton conducting electrolyte and also reconcile the difference with theoretical predictions in the literature.

6 Chapter VI: Effects of H_2O and CO_2 on Electrochemical Behaviors of BSCF Cathode for Proton Conducting IT-SOFC

This chapter details the study on the electrochemical behaviors of Ag, LSCF and BSCF as cathode for proton conducting IT-SOFC. This chapter is based on published paper by Shichen Sun, and Zhe Cheng. Title of "Effects of H2O and CO2 on electrochemical behaviors of BSCF cathode for proton conducting IT-SOFC." in Journal of The Electrochemical Society 164.2 (2017): F81-F88.

6.1 Introduction

In recent years, intermediate temperature (400-700^{o}C) solid oxide fuel cells (IT-SOFC) have drawn increasing interest due to the possibility of achieving slower degradation during long-term operation, cheaper sealing and interconnect material choices, as well as higher overall thermodynamic efficiency compared to conventional high temperature (≥ ~750^{o}C) solid oxide fuel cells (HT-SOFC). [12, 94] For IT-SOFC, conventional oxide ion electrolyte of yttria-stabilized zirconia (YSZ) suffers from low ionic conductivity,[78, 81] which dictates unreasonably thin electrolyte and high cost,[169, 170] while alternative oxide ion electrolytes, such as gadolinium doped ceria (GDC) or samarium doped ceria (SDC), suffer from high electronic transport number, which lowers open circuit voltage (OCV) and system efficiency despites their significantly improved ionic conductivity at intermediate temperature.[21, 171, 172] In comparison, proton conducting oxides, many of which are perovskite-structured, offer higher ionic conductivity with low electronic transport number as well as lower activation energy at intermediate temperature.[15, 79,

82, 86, 89, 173, 174] As a result, they are regarded as the preferred electrolyte for IT-SOFC.[175]

For IT-SOFC, cathode process is generally regarded as the rate-limiting step due to its high activation energy compared to the electrolyte. In particular, for proton conducting IT-SOFC, there have been a number of perovskite oxides employed as potential cathodes such as $La_{0.6}Sr_{0.4}Co_{0.2}Fe_{0.8}O_{3-\delta}$ (LSCF), $Sm_{0.5}Sr_{0.5}CoO_{3-\delta}$ (SSC), and $BaCo_{0.4}Fe_{0.4}Zr_{0.1}Y_{0.1}O_{3-\delta}$ (BCFZY).[121, 167, 176-178] $Ba_{0.5}Sr_{0.5}Co_{0.8}Fe_{0.2}O_{3-\delta}$ (BSCF), which is considered to be one of the most active cathode materials for oxide ion conducting IT-SOFC, [70] could also be a promising cathode material for proton conducting IT-SOFC because of its capability of undertaking significant amount of water and becoming proton conductive at intermediate temperature of ~600^{o}C and below.[20, 72, 156, 179] In fact, various researchers have already explored BSCF as the cathode for proton conducting IT-SOFC and obtained varying degrees of success. [163, 166, 176, 177, 180]However, there are still many unknown aspects left. For example, the exact influence of water vapor on the cathodic process for such proton conducting SOFC, especially at even lower temperatures of ~400-500^{o}C is still not clear. On the other hand, the influence of carbon dioxide (CO_2), which is always present in air, on the cathode electrochemical behavior for such proton conducting IT-SOFC is also uncertain despite evidence showing questionable stability of BSCF against CO_2 in SOFC operation at intermediate temperature.[21] In addition, how would the co-presence of H_2O and CO_2, which is a more realistic situation for practical SOFC operation, influence the electrochemical behavior for proton conducting SOFC with BSCF cathode has never been studied to the best of the authors' knowledge.[22, 23]

In this work, the chemical stability and compatibility of the BSCF cathode with one of the leading proton conducting electrolytes $BaZr_{0.1}Ce_{0.7}Y_{0.1}Yb_{0.1}O_{3-\delta}$ (BZCYYb) [79, 82, 86, 89] under various conditions were studied. More importantly, BSCF/BZCYYb/BSCF cathode symmetrical cells were used to investigate the influence of water vapor and CO_2 on the electrochemical behaviors for the proton conducting IT-SOFC at various temperatures ranging from 650°C to 400°C. The implication of the experimental observations on the underlying oxygen electrode reaction mechanism for proton conducting IT-SOFC versus conventional oxide ion conducting SOFC is discussed, and the direction for future research on designing better cathode for proton conducting IT-SOFC is pointed out.

6.2 Experimental

6.2.1 Powder Synthesis

Both BZCYYb powder with nominal composition of $BaZr_{0.1}Ce_{0.7}Y_{0.1}Yb_{0.1}O_{3-\delta}$ and BSCF powder with nominal composition of $Ba_{0.5}Sr_{0.5}Co_{0.8}Fe_{0.2}O_{3-\delta}$ were synthesized by glycine nitrate process (GNP).(33) For BZCYYb, stoichiometry amounts of $Ba(NO_3)_2$ (#A11305, Alfa Aesar, 99%), $ZrO(NO_3)_2 \cdot xH_2O$ (#43224, Alfa Aesar, 99.9%), $Ce(NO_3)_3 \cdot 6H_2O$ (#11329, Alfa Aesar, 99.5%), $Y(NO_3)_3 \cdot 6H_2O$ (#12898, Alfa Aesar, 99.9%), and $Yb(NO_3)_3 \cdot xH_2O$ (#12901, Alfa Aesar, 99.9%) powders were dissolved in DI water. Then glycine (#G8898, Sigma Aldrich, 99+ %) was added to the solution with molar ratio between glycine and total metal ions of 1:1. The solution was stirred for about 30 minutes

in a 2-liter beaker on a hot plate at ~100^{o}C in order to dissolve the various salts completely. The obtained transparent solution was then heated up on the hot plate set at ~540^{o}C. Rapid self-combustion process occurred after water was evaporated, and the very fine white powder generated after combustion was collected and calcined in ambient air at 1100^{o}C for 5 hours to form pure BZCYYb perovskite phase. (It is noted that right after combustion, the powder obtained was not BZCYYb, but doped CeO_2 and amorphous phases, as reported elsewhere. [89]) In the case of BSCF powder, the major steps for powder synthesis are similar to that for BZCYYb, except the starting materials now also include $Fe(NO_3)_3 \cdot 9H_2O$(#216828, Alfa Aesar, 99%) and $Co(NO_3)_2 \cdot 6H_2O$ (#239267, Alfa Aesar, 99%), while the molar ratio between glycine and total metal ions was changed to 7:6 for complete combustion. After self-combustion, the powder was calcined at 1000^{o}C for 2 hours in ambient air to form the pure phase. [180]

6.2.2 Chemical Compatibility and Stability Test

For chemical compatibility test between BSCF and BZCYYb in typical cell fabrication process, intimately mixed powders of the two materials with weight ratio of 1:1 were exposed to ambient air at typical BSCF cathode firing temperature of 1000^{o}C for 5 hours. To test the stability and compatibility of the BSCF and BZCYYb mixture under typical IT-SOFC operation conditions, the powder mixtures were exposed at 450^{o}C in ambient air, humidified nitrogen with nominal composition of 3% H_2O/97% N_2 (gas compositions are all by volume in this study), and gas mixture of ~1% CO_2/99% N_2 for various time from 24 to 72 hours. Furthermore, the chemical stability of the BZCYYb electrolyte against

1%CO_2/99% N_2 was also investigated at 750^{o}C by exposing BZCYYb powder to that gas mixture for 24 hours. The samples after various chemical stability/compatibility tests were analyzed by X-Ray diffraction (SIEMENS diffractometer D5000) for phase identification.

6.2.3 BSCF/BZCYYb/BSCF Symmetrical Cells Fabrication

Cathode symmetrical cells with the configuration of BSCF/BZCYYb/BSCF were fabricated. First, electrolyte pellets with diameter of 10 mm were dry-pressed at 200 MPa using 0.2 g BZCYYb powder followed by protected sintering at 1550^{o}C for 5 hours. [89] Then, the BSCF slurry was prepared by mixing BSCF powder with alpha-terpineol (#16285, Alfa Aesar, 96%) solvent and organic binder at weight ratio of ~65: 34: 1, and ball-milled for 24 hours. 4×4 mm^2 BSCF electrodes were brush painted onto both sides of the sintered electrolyte pellets using the prepared slurry, fully dried in an air oven at 100^{o}C, and calcined at 1000^{o}C for 2 hours in ambient air with heating and cooling rate of 5^{o}C/min. (It is noticed that the BSCF cathode fired at 900^{o}C showed weak bonding to the electrolyte, while the cathode fired at 1000^{o}C showed better bonding to the electrolyte. Thus, only symmetrical cells with cathode firing temperature of 1000^{o}C were used for electrochemical testing in this study.) The microstructure of the cross-section in the fabricated symmetrical cell was observed using a field emission scanning electron microscope (FE-SEM, JEOL JSM 6330F).

6.2.4 Electrochemical Impedance Spectroscopy (EIS) Measurements

Electrochemical Impedance Spectroscopy (EIS) measurements were carried out using a potentiostat (Gamry Interface 1000) under open circuit condition for the symmetrical cells. The symmetrical cell with silver paste and silver mesh current collector was placed in the hot zone of a sealed quartz tube furnace. Dry simulated air (with the composition of 20% O_2/80% N_2 with <~5 parts per million or ~5 ppm of CO_2 or H_2O) at a flow rate of 200 ml min^{-1} was used as the baseline. To test the effect of water vapor on the oxygen electrode behavior, 3%, 10%, and 20% water vapor was introduced into the test chamber by passing the dry simulated air through a water bubbler set at different temperatures. And the connection tubes were heated to ~100^oC to prevent condensation. Before the tests, the symmetrical cell was heated to 750^oC in dry simulated air and held for 24 hours to stabilize it. The sequence of the electrochemical experiments for evaluating the moisture effect is described as following: i) The cell was cooled from 750^oC to the testing temperature (e.g., 650^oC) in dry simulated air, held for 12 hours and then the impedance spectrum was collected. ii) After that, moisture was introduced into the simulated air first at 3% then increased to 10% and finally to 20%, and the impedance spectrum for each level of humidity was collected 2 hours after the adjustment of the moisture content. iii) The cell was then heated back up to 750^oC in dry simulated air and held for 12 hours or longer to fully dehydrate the system (including both the cell and testing chamber). This sequence of step i) to ii) and then iii) was repeated for each testing temperature such as 650^oC, 550^oC, and 450^oC to obtain electrochemical responses of the cell to different atmospheres. Similarly, to test the influence of CO_2 on the oxygen electrode behavior, 1% CO_2 was

introduced into the simulated air through a mass flow controller and the impedance spectra for the cell were collected at a given temperature before and after 2 hours of the introduction of 1% CO_2, as well as after the removal of CO_2 for 24 hours. Before changing to a different testing temperature for CO_2 response, the sample was always recovered in the dry simulated air (with < 5 ppm CO_2 as mentioned before) at 750 ^oC for 24 hours to ensure a complete recovery and a clean surface of both the electrode and the electrolyte. To test the behaviors when the electrode is exposed to both H_2O and CO_2, which is a more realistic situation for fuel cell operation, the simulated air was passed through the water bubbler at room temperature and then mixed with CO_2 to give a gas mixture with nominal composition of ~1% CO_2/3% H_2O/20% O_2/76% N_2, and the sequence of these tests was similar to that for tests in 1% CO_2 alone. All impedance data were collected with zero DC bias and AC amplitude of 0.1 mA.

6.3 Results

6.3.1 Compatibility and Stability of BSCF and BZCYYb in Various Atmospheres

The XRD patterns for the as synthesized BSCF and BZCYYb powders and their mixtures after various compatibility/stability tests are summarized in Figure 6. 1. (It's noted that the synthesized BSCF contains some minor unidentified secondary phase as evidenced by the extra peak at~31^o.) The chemical compatibility between BSCF and BZCYYb was verified with XRD, showing no change for both BSCF and BZCYYb materials after heat treatment

at 1000 °C for 5 hours. (Similar result was also obtained for compatibility test at 900°C.) In addition, as shown in Figure 6. 1, the chemical stability of the BSCF-BZCYYb powder mixture in both ambient air (i.e., containing ~1-3% H_2O and ~400 ppm CO_2) and in N_2 containing up to 3% H_2O and 1% CO_2 at targeted IT-SOFC operating temperature of 450°C was also demonstrated, which is supported by the absence of impurity peaks in the XRD patterns after long time exposure to the various gas mixtures for 24-72 hours. It is worth mentioning that when the BZCYYb electrolyte with Zr doping at 0.1 level was exposed to the gas mixture of 1% CO_2/99% N_2 at 750 °C for 24 hours, some $BaCO_3$ did form, as shown in Figure 6. 1.

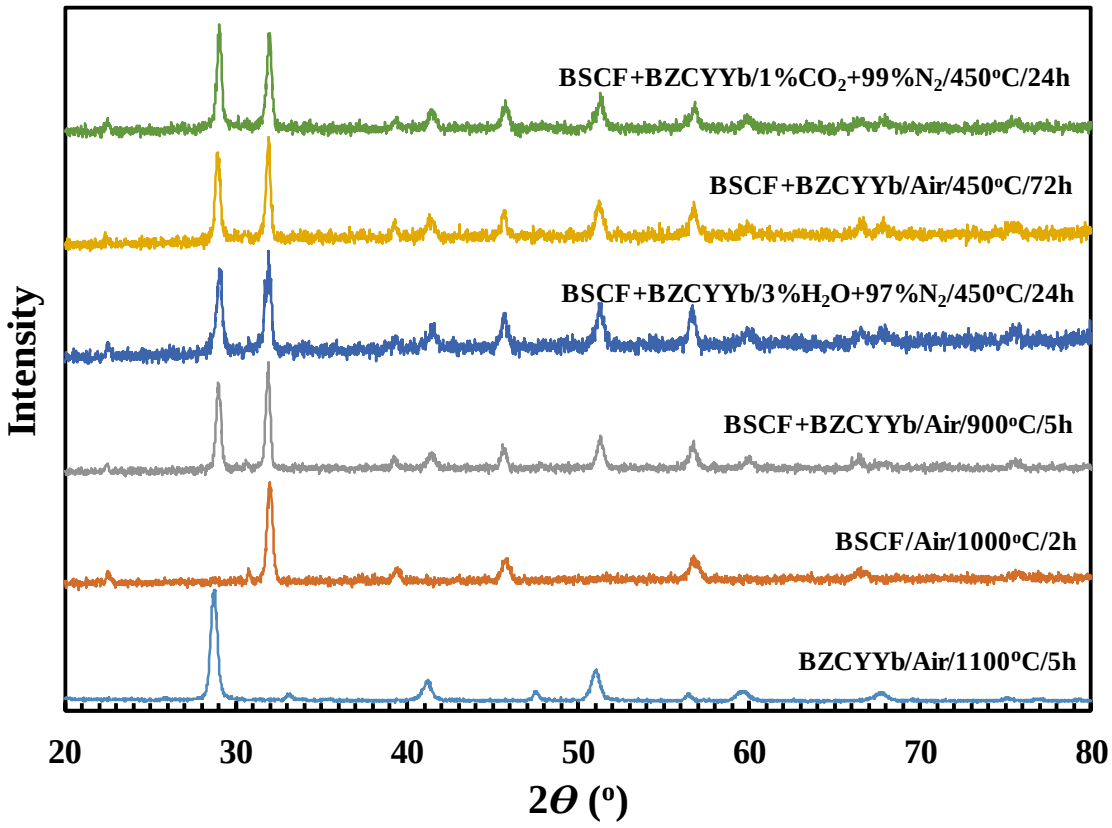

Figure 6. 1 XRD patterns of as synthesized BSCF and BZCYYb powders and their mixtures after different compatibility/stability tests.

Apart from testing for the compatibility and stability of the materials, the microstructure of a fabricated BSCF/BZCYYb/BSCF cathode symmetrical cell is shown in Figure 6. 2. The thickness of the BSCF electrode layer was around 30 μm. Relatively large particle size of ~1-3 μm for the BSCF electrode was observed, which may be attributed to the high surface energy of BSCF and the strong tendency to coarsen.[70, 162, 181] The porosity of the BSCF electrode was estimated to be ~22% based on the analysis of SEM image using the software of ImageJ (version 1.50i).

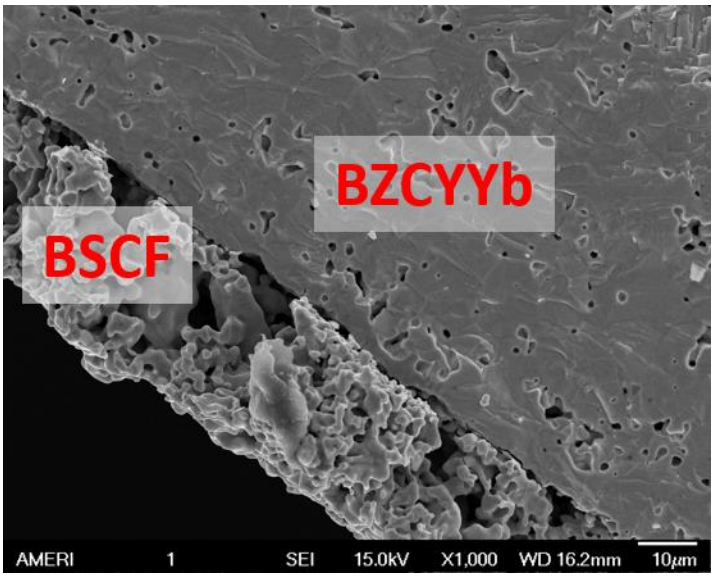

Figure 6. 2 SEM image of cross-section of fabricated BSCF/BZCYYb/BSCF symmetrical cell.

6.3.2 Effect of Moisture on BSCF Cathode Electrochemical Behavior

Figure 6. 3 (a), (b), and (c) show the impedance spectra for the BSCF/BZCYYb/BSCF cathode symmetrical cell in the dry simulated air (as explained, it is a gas mixture of 20% O_2 and 80% N_2 with <~5ppm H_2O and CO_2 as supplied from Airgas) and simulated air

humidified with ~3%, ~10%, and ~20% of moisture at 650^{o}C, 550^{o}C, and 450^{o}C, respectively. At 650^{o}C, as shown in Figure 6. 3 (a), with the introduction of 3% H_2O, the ohmic resistance R_O decreases from 2.11 Ohm•cm^2 to 2.04 Ohm•cm^2. As the moisture content increases further to 10% and 20%, a continued decreasing of R_O was observed. On the other hand, for the electrode interfacical polarization resistance R_p, due to the nature of mixed ionic and electronic conduction for the BZCYYb electrolyte and the absence of precise ionic transference number, [88] accurate R_p number cannot be obtained readily. As a result, only the apparent interfacial resistance $R_{ai,}$ which is the direct difference between the low frequency intercept and the high frequency intercept on the real axis in an impedance spectrum, is used for the analysis and discussions in this study as in many previous reports. [20, 159] It can be seen from Figure 6. 3 (a) that comparing with dry simulated air, R_{ai} increases from ~0.6 Ohm•cm^2 to ~0.7 Ohm•cm^2 with the introduction of 3% moisture. However, with further increase of H_2O concentration to 10% and beyond, R_{ai} starts to decrease back to ~0.64 Ohm•cm^2 and stabilizes. It is noted that the observation of the decrease of R_{ai} with increasing moisture content beyond 3% H_2O for BSCF cathode over $BaCe_{0.9}Y_{0.1}O_{3-\delta}$ (BCY10) proton conducting electrolyte had been reported before. [20] Nevertheless, to the best of the authors' knowledge, the initial increase in R_{ai} from dry simulated air to 3% humidified air for proton conducting IT-SOFC with BSCF cathode has not been reported before, and such an observation implies that the introduction of moisture seems to slow down at least certain part(s) of the oxygen electrode reaction for the BSCF/BZCYYb/BSCF cathode symmetrical cell.

At reduced temperature of 550^{o}C, which is shown in Figure 6. 3 (b), when 3% moisture was introduced, R_O still decreases; however, no continued decreasing of R_O was observed with the further increase in moisture content beyond 3%, suggesting saturation of the hydration effect by 3% of moisture at that temperature. On the other hand, an increase in R_{ai} was observed with the introduction of 3% moisture compared with dry simulated air, and, in contrast to the observations at 650^{o}C, total R_{ai} does not show a decrease when moisture concentration was further increased to 10% and beyond.

When the temperature was further reduced to 450^{o}C, the overall impedance spectra (shown in Figure 6. 3 (c)) clearly separate into one semicircle at the high frequency (HF, 10^6~10^4 Hz) range and one large depressed semicircle, which most likely represents two overlapped arcs-one at the middle frequency (MF, ~10^4 to ~10^0 Hz) range and the other at the low frequency (LF, ~10^0 to 10^{-2} Hz) range. At this temperature, when 3% moisture was introduced, the change in R_O becomes negligible. On the other hand, for R_p, the HF part decreases significantly, while the MF and LF parts show an obvious increase with the introduction of moisture. In addition, the effect of moisture seems to reach saturation at 3%, as further increase in moisture content does not produce significant differences at 450^{o}C.

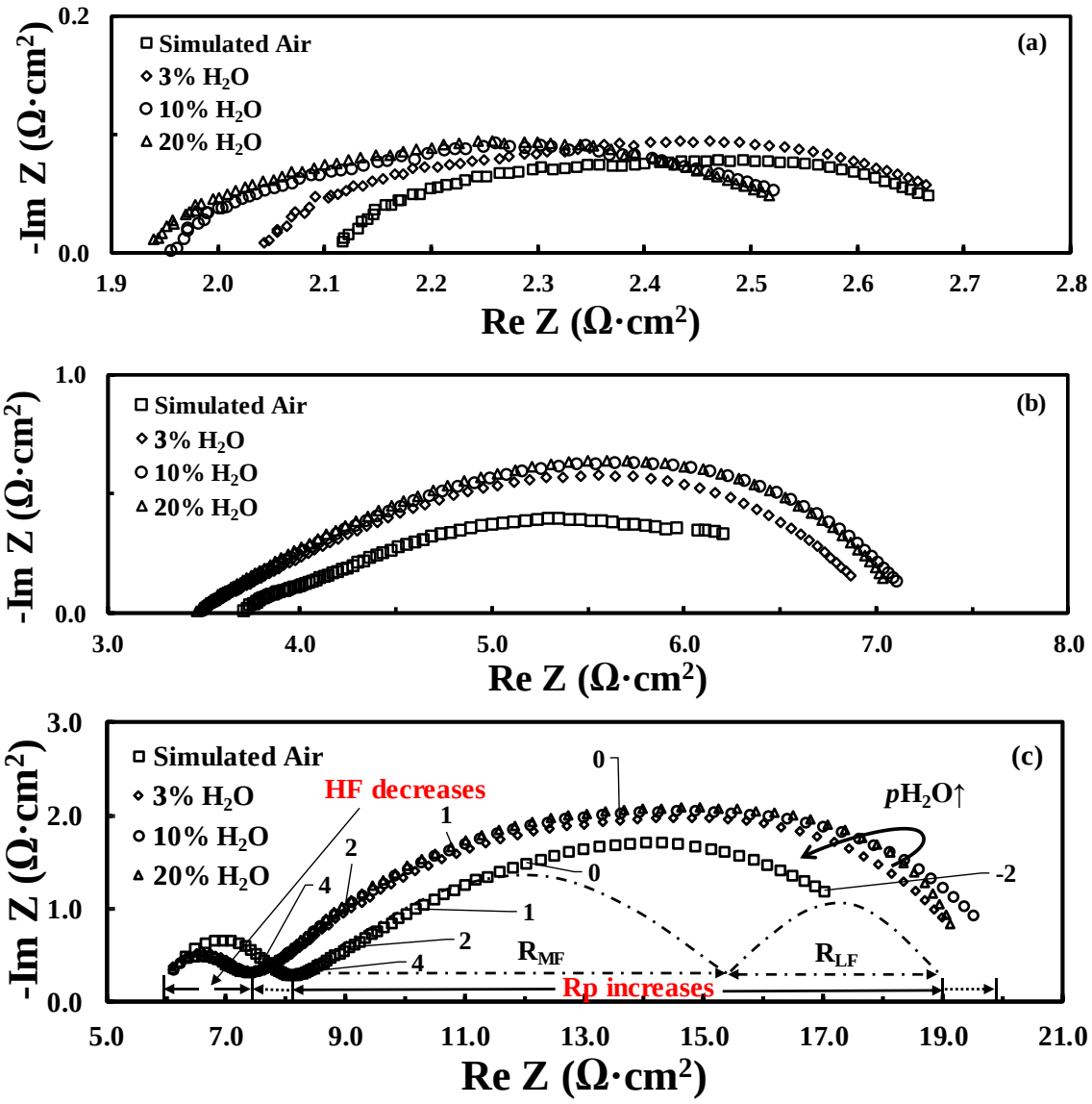

Figure 6. 3 Impedance spectra for a BSCF/BZCYYb/BSCF symmetrical cell in simulated air (20%O_2/80%N_2 without H_2O or CO_2) versus simulated air humidified with various pH_2O at (a) 650ºC, (b) 550ºC, and (c) 450ºC, respectively.

Additional EIS measurements were conducted at 500-400ºC because of the clear separation of impedance spectra into two semicircles (HF and MF-LF) in that temperature range. Gradual decrease in the HF semicircle was observed with increasing concentration

of moisture as shown, for example, in Figure 6. 4 for 475ºC. For comparison, impedance spectra for another symmetrical cell in both pure O_2 and dry simulated air at 450ºC are given in Figure 6. 5 (a), which shows almost no difference in the size of the HF semicircle, while a significant increase was observed in the MF-LF semicircle in dry simulated air versus in pure O_2. On the other hand, as in Figure 6. 5 (b), when moisture content was increased in O_2, the HF semicircle shows the similar gradual decrease.

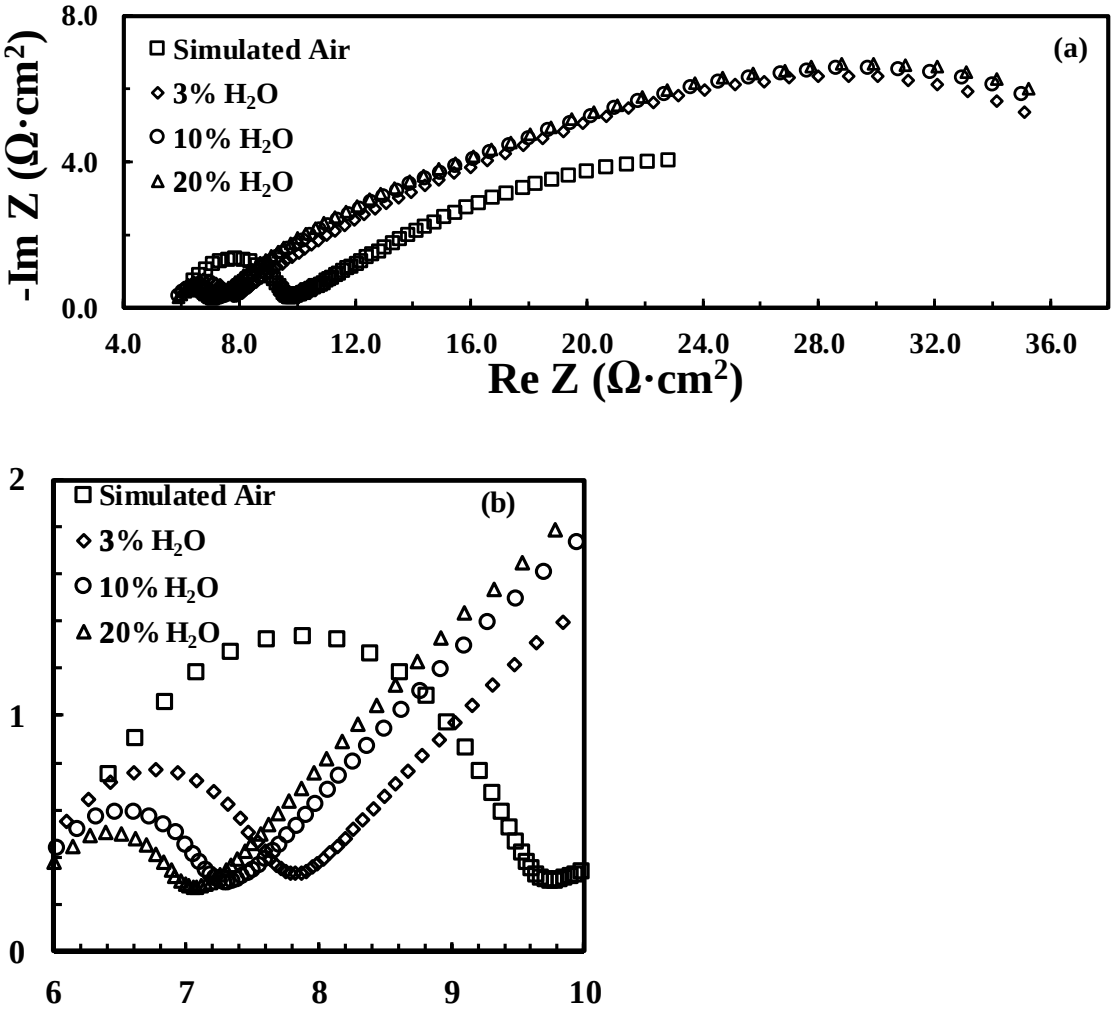

Figure 6. 4 Impedance spectra for BSCF/BZCYYb/BSCF symmetrical cell at 475ºC in dry and wet (with various pH_2O) "simulated air" (a) the full impedance spectra, (b) zoom in to show the changes at the high frequency (HF) portion.

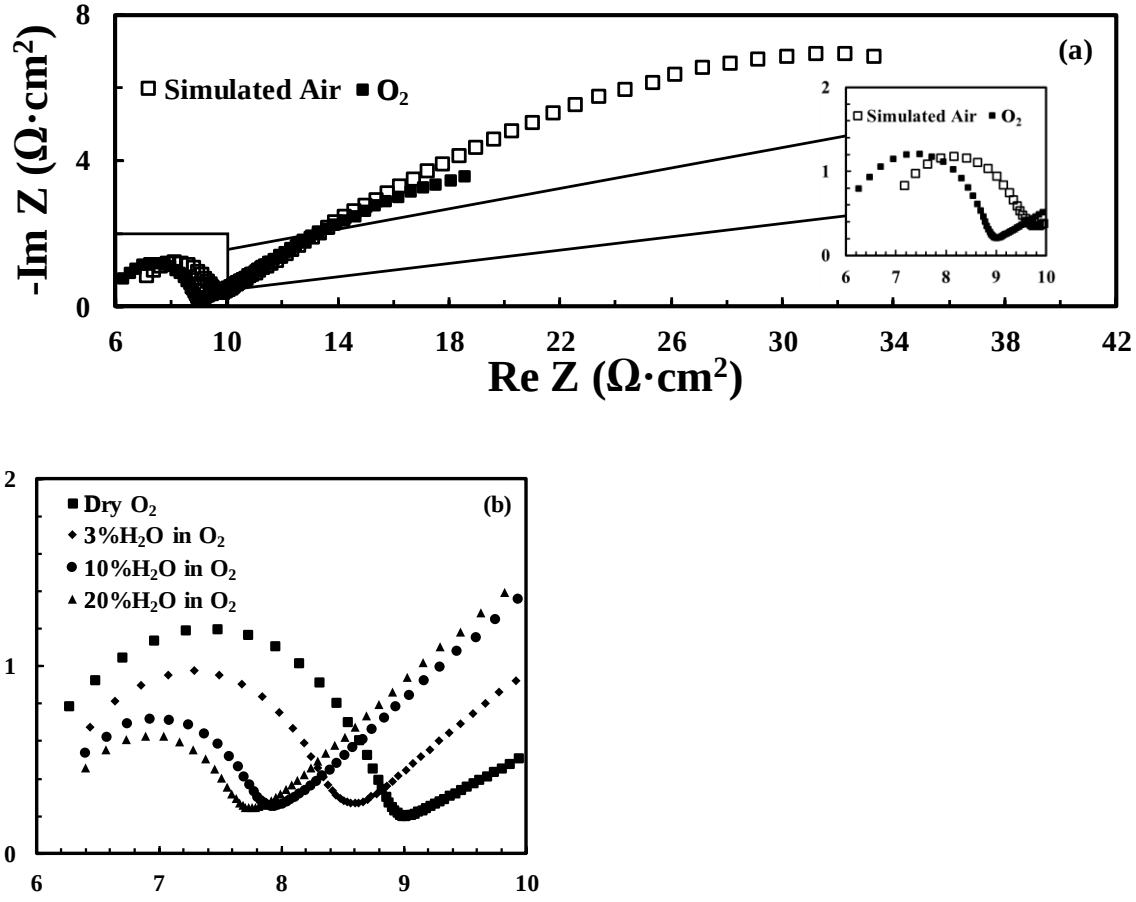

Figure 6. 5 Comparison of the impedance spectra for BSCF/BZCYYb/BSCF symmetrical cell at 450°C (a) entire impedance spectra comparing dry "simulated air" and dry pure O_2 and zoom-in of the high frequency (HF) part, (b) zoom-in of pure O_2 with different concentration of moisture at the high frequency (HF) part.

6.3.3 Effect of CO_2 on BSCF Cathode Electrochemical Behavior

The effect of CO_2 alone (i.e., without the presence of moisture) on the BSCF/BZCYYb/BSCF symmetrical cell at 650°C, 550°C, and 450°C is shown in Figure 6. 6. At 650°C, as shown in Figure 6. 6 (a), increase in R_O from 2.21 ohm·cm^2 to 2.39

ohm·cm^2 and in R_{ai} from 0.49 ohm·cm^2 to 0.72 ohm·cm^2, respectively, were observed after the introduction of 1% CO_2 into the dry simulated air for 2 hours. After the removal of CO_2 for 24 hours, almost complete recovery in both R_O and R_{ai} was observed. At 550^{o}C, as shown in Figure 6. 6 (b), both R_O and R_{ai} increased after the introduction of 1% CO_2, and the relative increase in R_{ai} due to CO_2 poisoning becomes larger comparing with 650^{o}C. Also, only incomplete recovery was observed with the removal of CO_2 even after 24 hours. At further reduced temperature of 450^{o}C, little change in R_O was observed with the introduction of 1% CO_2, while large increase in R_{ai} was still observed. In addition, because of the clear separation of the impedance spectra into one semicircle at the HF range and another at the MF-LF range, the increase in R_{ai} due to CO_2 at 450^{o}C occurs almost exclusively to the MF-LF part. At this temperature, very little recovery was observed after the removal of CO_2 for 24 hours.

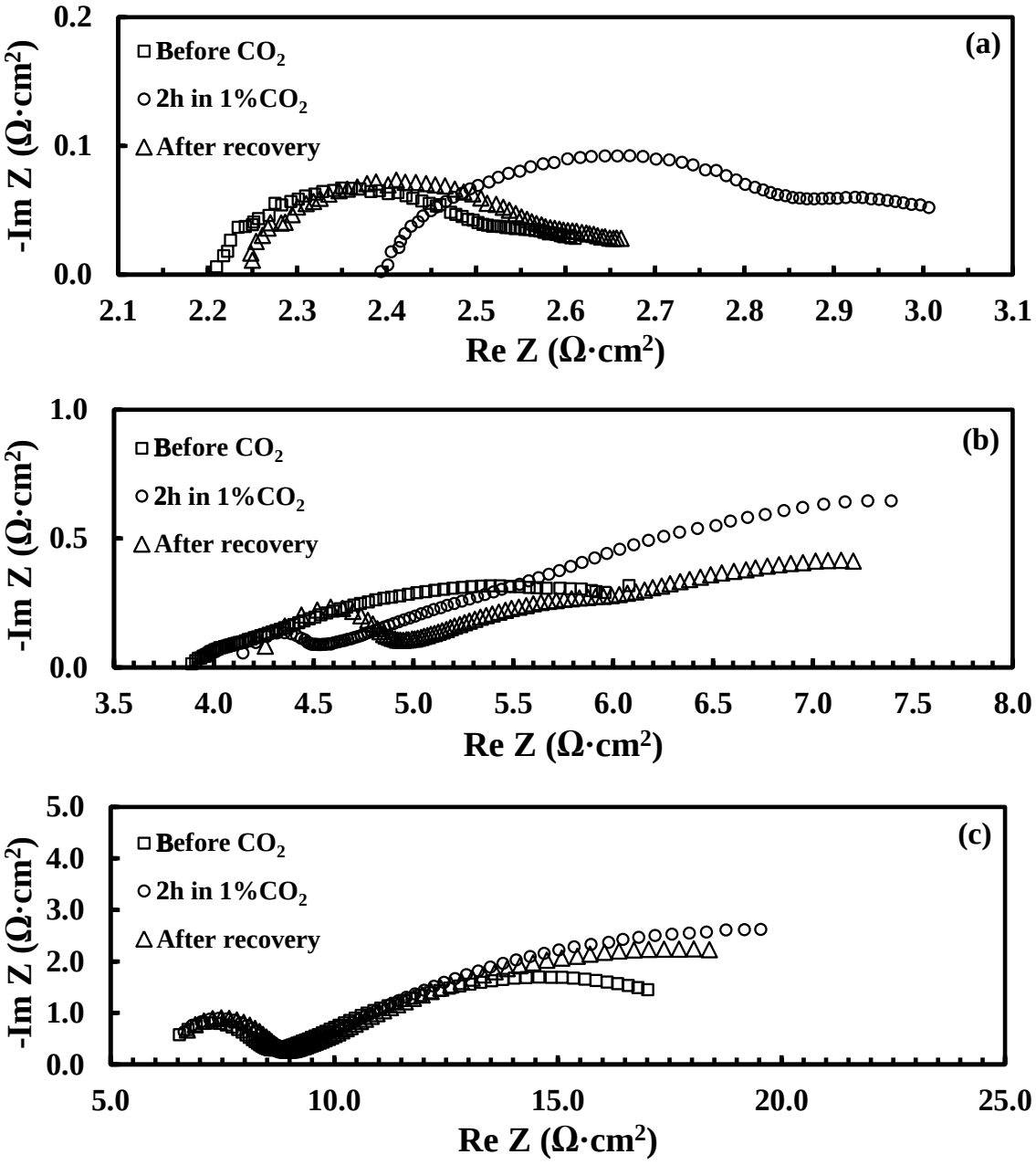

Figure 6. 6 Plots showing the change in impedance spectra for BSCF/BZCYYb/BSCF symmetrical cell in dry "simulated air" (20% O_2/80% N_2) before exposure to CO_2, after exposure to 1% CO_2 for 2 h, and after recovery (i.e., removal of 1% CO_2) for 24 hours at (a) 650^{o}C, (b) 550^{o}C and (c) 450^{o}C, respectively.

In comparison, the effect of 1% CO_2 for 3% humidified simulated air on the BSCF/BZCYYb/BSCF symmetrical cell at 650, 550, and 450^oC is shown in Figure 6. 7. At 650^oC, almost the same behavior was observed as both R_O and R_{ai} increase with the introduction of 1% CO_2, and they are largely recoverable with the removal of CO_2. However, at lower temperatures of 550 and 450^oC, it is seen that the presence of moisture significantly improves the reversibility for CO_2 poisoning. In fact, at 450^oC, the presence of 3% moisture makes the cathode much less sensitive to 1% CO_2. To illustrate the results better, based on the collected impedance spectra (as shown in Figure 6. 6 and Figure 6.), the estimated value of R_O and R_{ai} are summarized in Table 6. 1, as well as their relative changes after being poisoned for 2hours and after the recovery by removing 1% CO_2 for 24 hours in both dry and 3% humidified simulated air.

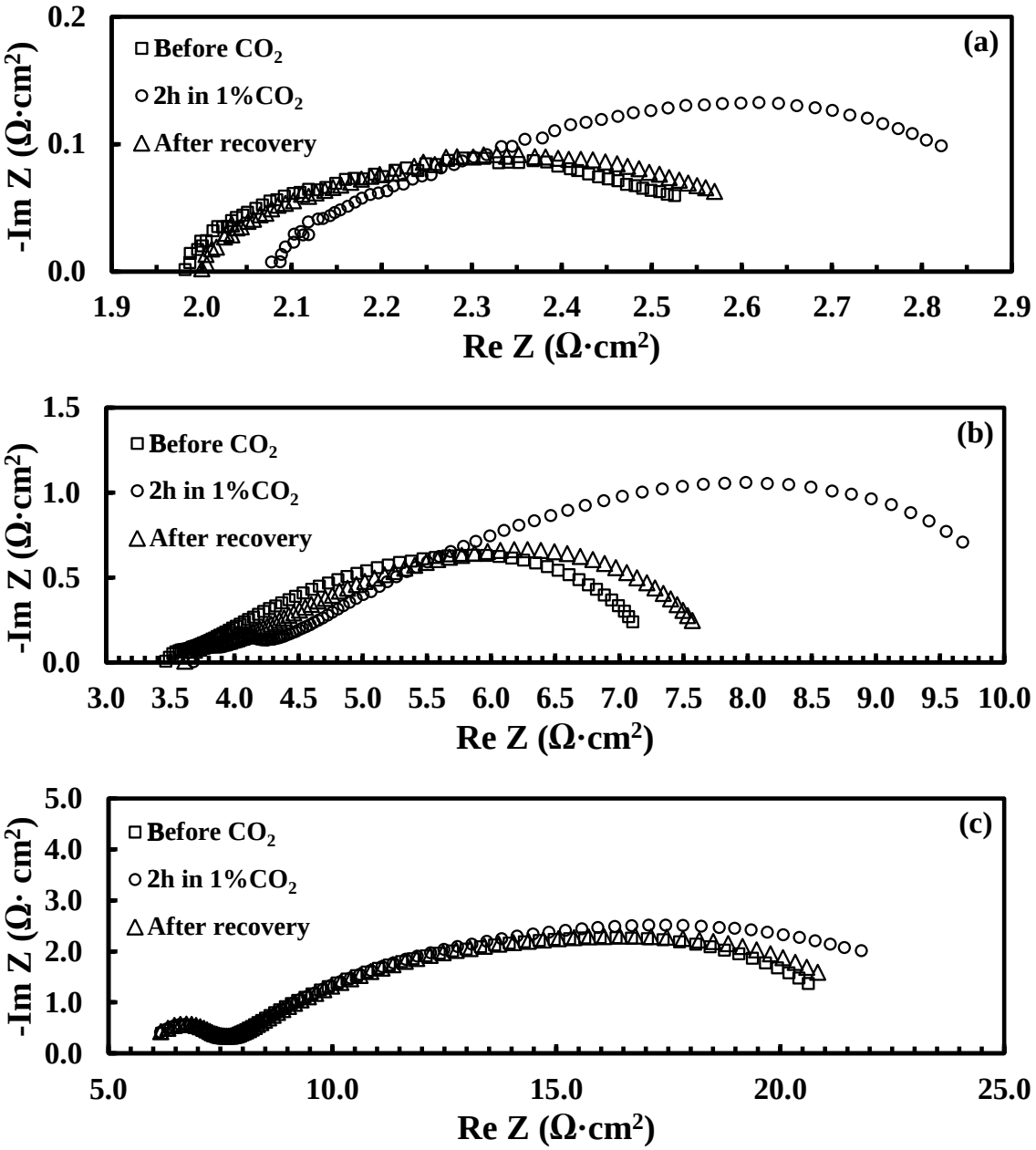

Figure 6. 7 Impedance curve for BSCF/BZCYYb/BSCF symmetrical cell in humidified simulated air (3% H_2O/20% O_2/77% N_2) before exposure, after exposure to 1% CO_2 for 2 hours, and after recovery (i.e., removal of 1% CO_2) for 24 hours at (a) 650^oC, (b) 550^oC and (c) 450^oC, respectively.

Table 6. 1 Elementary steps of the oxygen electrode reaction for BSCF electrode over BZCYYb electrolyte without the presence of H_2O under ideal oxide ion conduction condition and under ideal, fully hydrated condition which only conduct proton and not oxide ion.

Elementary Steps	Elemental step	Frequency range
1 Mass transfer of O_2 molecule in gas phase and adsorption and desorption on electrode surface	$O_2(g) \leftrightarrow O_2\ (ads)$	LF
2 Adsorbed O_2 molecule dissociation/association	$O_2\ (ads) \leftrightarrow 2O\ (ads)$	MF
3 Charge transfer for pure oxide ion electrolyte	$O(ads) + V_O^{\cdot\cdot} + 2e^- \leftrightarrow O_O^X$	HF
3' Charge transfer for pure proton electrolyte	$O\ (ads) + 2e^- + 2OH_O^{\cdot} \leftrightarrow H_2O(ads) + 2O_O^X$	HF
4 Mass transfer of oxide ion in bulk of electrode and electrolyte	$V_{O(electrode)}^{\cdot\cdot} \leftrightarrow V_{O(electrolyte)}^{\cdot\cdot}$	Very HF (>> 10^6 Hz)
4' Mass transfer of proton in bulk of electrode and electrolyte	$OH_{O(electrode)}^{\cdot} \leftrightarrow OH_{O(electrolyte)}^{\cdot}$	Very HF (>> 10^6 Hz)
5 H_2O transport and adsorption/desorption	$H_2O(ads) \leftrightarrow 2H_2O(g)$	LF

6.4 Discussions

The results from compatibility and chemical exposure tests show that at the targeted proton conducting IT-SOFC operating temperature of ~450 ^oC, the combination of BSCF cathode and BZCYYb electrolyte has demonstrated the desired compatibility in processing and stability to practical air. However, the observation of reactivity of BZCYYb electrolyte to 1% CO_2/99% N_2 to form $BaCO_3$ seems to contradict the earlier study showing stability of BZCYYb against a gas mixture of 50% CO_2/50% H_2 at 750 ^oC. [121] Whether such a discrepancy is due to the different balance gas (N_2 versus H_2) used, or the variation in

sample stoichiometry (e.g., Ba to (Ce+Zr+Y+Yb) molar ratio), or other factors is not clear at the moment.

Besides that, in order to understand the various observed phenomena concerning the effects of moisture and CO_2 on the electrochemical behaviors for the BSCF/BZCYYb/BSCF symmetrical cell, fundamental oxygen electrode reaction processes are first summarized. Shown in Figure 6. (a) is the conventional cathode reaction pathway for an ideal oxide ion based SOFC with a mixed ionic and electronic conductor (MIEC) electrode. In comparison, shown in Figure 6. (b) is the ideal cathode reaction pathway for a "pure" proton conducting SOFC with MIEC electrode, which means electrolyte is fully hydrated and conducts only proton while the electrode conducts electron (hole) and proton upon hydration. The elementary steps corresponding to the illustrated pathways are summarized in Table 6. 2.

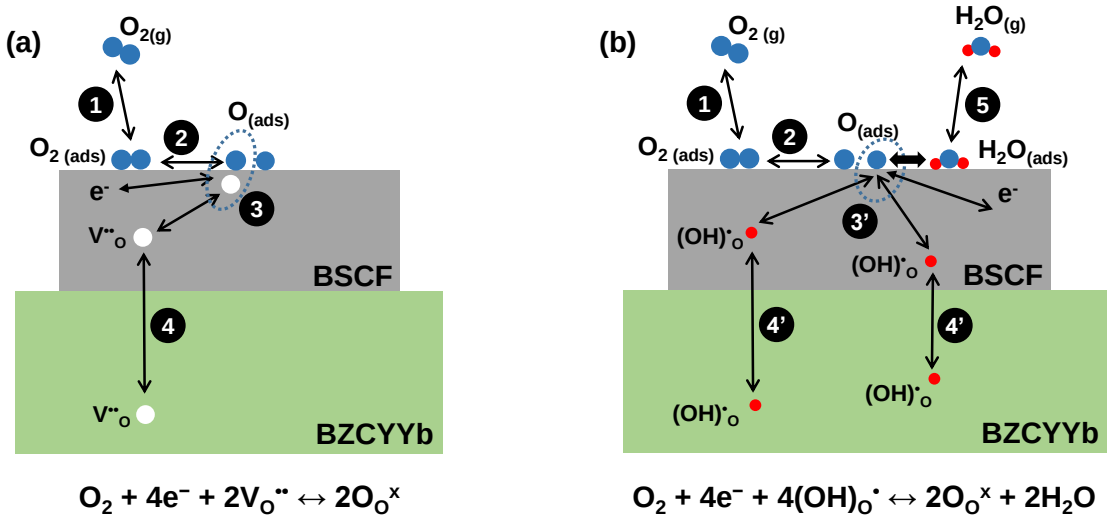

$O_2 + 4e^- + 2V_O^{\bullet\bullet} \leftrightarrow 2O_O^x$

$O_2 + 4e^- + 4(OH)_O^{\bullet} \leftrightarrow 2O_O^x + 2H_2O$

Figure 6. 8 Schematics showing the reaction species involved and the elementary steps (also refer to Table 5.1) for the reversible oxygen electrode reaction for (a) ideal pure oxide-ion based SOFC and (b) ideal pure proton conducting SOFC.

Table 6. 2 Relative change of Ohmic resistance R_O and interface polarization resistance R_p for the BSCF/BZCYYb/BSCF cathode symmetrical cell after being poisoned by 1% CO_2 for 2 hours and the recovery by then removing 1% CO_2 for 24 hours in both dry and 3% H_2O humidified simulated air

	Temperature	650°C		550°C		450°C	
	Condition	Dry	3% H_2O	Dry	3% H_2O	Dry	3% H_2O
$\Delta R_O/R_O$	After CO_2 poisoning	7.3%	3.2%	8.4%	10.3%	1.7%	-0.3%
	After recovery	1.9%	0.6%	13.5%	5.4%	2.7%	-0.2%
$\Delta R_p/R_p$	After CO_2 poisoning	69.1%	48.3%	61.8%	102%	68.4%	15.9%
	After recovery	5.0%	-7.6%	83.8%	5.6%	46.1%	8.3%

For the conventional ideal oxide ion based SOFC, the overall oxygen electrode reaction follows:

$$O_2 + 4e^- + 2V_O^{\bullet\bullet} \leftrightarrow 2O_O^x \qquad \text{Equation 6.1}$$

When the electrode is MIEC, the overall oxygen electrode reaction consists of elementary steps (and their reverse steps) of 1) mass transport of O_2 molecule in the gas phase and adsorption on the electrode surface; 2) dissociation of adsorbed O_2 molecule into adsorbed oxygen atoms; 3) charge transfer and combining of lattice oxygen vacancy with surface adsorbed oxygen atom and electrons to form lattice oxygen; and 4) mass transport of oxide ion (oxygen vacancy) in the bulk of electrode and electrolyte.

In comparison, for the ideal pure proton conducting SOFC, in principle, the oxygen electrode reaction would follow a different pathway:

$$O_2 + 4e^- + 4(OH)_O^{\bullet} \leftrightarrow 4O_O^x + 2H_2O \qquad \text{Equation 6.2}$$

When the electrode is MIEC with proton as the sole ionic charge carrier, apart from the common elementary steps of O_2 molecules gas phase transport and adsorption (step 1) and adsorbed O_2 molecule dissociation (step 2), alternative elementary steps of 3') charge transfer and combining of proton with adsorbed oxygen atom and electrons to form water, and 4') mass transport of proton in the bulk of electrode and electrolyte, as well as 5) water molecule transport in the gas phase and adsorption/desorption on the electrode surface also need to be taken into consideration.

The actual system considered here would approach the ideal oxide-ion based system (Figure 6. (a)) in dry condition. On the other hand, when significant concentration of moisture is present, proton is generated in the BZCYYb electrolyte as following:

$$H_2O + V_O^{\bullet\bullet} + O_O^x \leftrightarrow 2(OH)_O^{\bullet} \qquad \text{Equation 6.3}$$

The system would then approach the ideal "pure" proton-based system (Figure 6. (b)) in humidified condition especially when the moisture content is high (≥3%) and at lower temperature (e.g., ~450^{o}C and below) when the BZCYYb electrolyte and the BSCF electrode become fully hydrated with oxygen vacancy $V_O^{\cdot\cdot}$ replaced by proton $OH_O^{\cdot}$.

As shown in Figure 6. 3 (a) and (b), the decrease in R_O at 650 and 550^{o}C with the introduction of moisture into the simulated air could be attributed to the hydration of the BZCYYb electrolyte and the change of conducting species from oxide ion to proton yielding higher ionic conductivity.[88, 121] However, at temperature below ~500^{o}C, almost negligible reduction in R_O was observed (see Figure 6. 3 (c) and Figure 6. 4). Such a phenomenon could be attributed to the enhanced affinity of proton conducting oxide

electrolyte (BZCYYb here) for water below the temperature of ~450^{o}C, [84, 182] which is supported by the TGA from previous reports suggesting that the dehydration of proton conducting oxides and associated weight loss only occur significantly at temperature above ~450^{o}C. [20] The implication is that despite the dry simulated air used, which is supposed to give moisture content of only ~5 ppm, the actual moisture content in the system due to various leakage might be sufficient to hydrate the electrolyte and make it proton conductive at temperature of ~450^{o}C and below. Therefore, strictly speaking, the so-called "dry simulated air" is only a loosely used term to indicate that the moisture content is, qualitatively, much lower than the 3% used for comparison. Though the difference in actual moisture content between the so-called "dry simulated air" and 3% humidified air may not be large enough to influence the Ohmic resistance at ~450^{o}C and below, it is, however, adequate to significantly impact the oxygen electrode processes, as discussed below.

For the apparent interfacial resistance R_{ai}, in the temperature range of 650^{o}C to 450^{o}C, as shown in Figure 6. 3 and Figure 6. 4, the overall R_{ai} seems to increase with the introduction of moisture, especially for the middle to low frequency (MF-LF) semicircle. Generally, the MF-LF semicircle is believed to be associated with the mass transport process of oxygen molecules and the oxygen adsorption/dissociation process on the BSCF electrode. [183] The observed increase in that part upon moisture introduction could be attributed to the strong adsorption of H_2O on the surface of BSCF electrode and the BZCYYb electrolyte, both of which have high affinity for water. This would result in the reduced number of active sites for the adsorption/dissociation of oxygen molecules. In addition, strongly adsorbed water molecules on the BSCF surface could also greatly

impede the transport (or diffusion) of oxygen species on the electrode surface. Both effects would slow down the overall cathode reaction process, leading to the increased R_{ai}, especially in the MF-LF range.

On the other hand, as shown in Figure 6. 3 (c) and Figure 6. 4, an opposite trend with respect to the moisture effect was observed in the high frequency (HF) part of the impedance spectra. Figure 6. summarizes the HF resistances obtained from 500^{o}C to 400^{o}C for a symmetrical cell in both dry simulated air and humidified air with different moisture content. It is observed that the decrease in HF resistance due to the introduction of moisture is more significant at higher temperature (e.g., 500 and 475^{o}C) than at lower temperature (e.g., 450^{o}C or below). Such results suggest that the activation energy for the HF resistance is significantly different in dry simulated air from those in humidified air. (It is noted that there appears to be a deviation at 475^{o}C in Figure 6. . Whether it is due to experimental error or other factors is not clear at this moment and will be investigated in the future.) Therefore the HF semicircle is attributed to the resistance from the charge transfer step and not the grain boundary (GB), because previous study suggests that the activation energy for the GB resistance remains almost the same in humidified versus dry atmosphere.[184] Such assignment of the HF semicircle at temperature below ~500^{o}C to the charge transfer step is also consistent with literature.[20, 183]

It should be noted that similar behavior of decrease in HF semicircle with increase of moisture content from 3, 10, and 20% in simulated air had been reported before for the system of $Sm_{0.5}Sr_{0.5}CoO_{3-\delta}$ (SSC)-$BaCe_{0.8}Sm_{0.2}O_{3-\delta}$ (BCS) composite cathode over BCS proton conducting electrolyte at 500^{o}C, [185] while in another study on the system of BSCF

over $BaCe_{0.9}Y_{0.1}O_{3-\delta}$ (BCY10) electrolyte at 600^{o}C, [20] the total apparent interfacial resistance decreases with increasing moisture content from 3% to 30%. Nevertheless, to the best of the authors' knowledge, no previous study has systematically compared the cathode behavior over proton conducting electrolyte between dry and humified conditions, as reported here. The significant decrease in the HF semicircle for the oxygen electrode upon the introduction of moisture in the current study is hypothesized to be due to i) the intrinsically faster kinetics for the charge transfer step 3') via proton (Figure 6. (b)) comparing with the conventional charge transfer step 3) via oxide ion (Figure 6. (a)) and/or ii) the greater concentration of $H_2O_{(ads)}$ reactant for the reverse reaction of step 3'). Both explanations are consistent with the observation of a continued decrease of high frequency resistance R_{HF} with increasing concentration of H_2O, especially at temperatures of 475^{o}C and 500 ^{o}C (see Figure 6. 4 (b) and Figure 6.): As moisture content increases, the BSCF electrode and the BZCYYb electrolyte can become more and more hydrated, leading to the continued increase in proton conduction and decrease in oxide ion conduction. On the other hand, the concentration of surface $H_2O_{(ads)}$ would increase as well. Either way, the overall charge transfer process 3') would become faster with greater moisture content. Further study will be needed to clarify the exact origin for such a phenomenon.

Furthermore, such explanations could also be supported by the comparison of the impedance spectra obtained in simulated air versus in pure O_2 at 450^{o}C, as shown in Figure 6. 5 (a). The HF semicircles in simulated air and in pure O_2 are essentially the same, which suggests that they are not sensitive to the amount of O_2 available and should represent the charge transfer step of the electrode reaction. On the other hand, the MF-LF semicircle is

significantly smaller in pure O_2 comparing with that in dry simulated air, which is consistent with the attribution of the MF-LF semicircle to the oxygen adsorption/mass transport of oxygen molecules in the gas phase. With the introduction of moisture to O_2, R_{HF} becomes smaller and smaller with increasing moisture content, as shown in Figure 6. 5 (b), while the MF-LF semicircle becomes significantly larger, which is similar to the behavior in simulated air. In addition, as shown in Figure 6. 5 (c), the impedance spectra in 3% humidified air and in humidified O_2 are very similar including the MF-LF part, and this can be understood as significant surface sites over BSCF electrode are now occupied by adsorbed water, which leads to limited reaction sites for O_2 adsorption, making the overall electrode reaction less sensitive to the oxygen gas concentration.

For the effect of CO_2 on the cathode electrochemical behavior, adding CO_2 to the dry simulated air obviously poison the BSCF electrode as evidenced by the increase in R_{ai} (shown in Figure 6. 6 and Table 6. 1). In addition, 1% CO_2 also seems to cause increase in R_O for the BZCYYb electrolyte at higher temperature such as 650^{o}C and 550^{o}C (as shown in Table 6. 1). This is most likely due to the bulk reaction between CO_2 and the BZCYYb electrolyte, as evidenced by the XRD pattern in Figure 6. 1 showing the existence of $BaCO_3$ impurity after the exposure of the BZCYYb powder to 1%CO_2/99%N_2 at 750^{o}C for 24 hours. In comparison, at lower temperature of 450^{o}C, no obvious change in R_O was observed, which is consistent with the XRD pattern for the BSCF+BZCYYb powder mixture after 24 hours of exposure to 1%CO_2/99%N_2 in Figure 6. 1, suggesting sufficient chemical stability against 1%CO_2 for the BSCF electrode and BZCYYb electrolyte at that temperature.

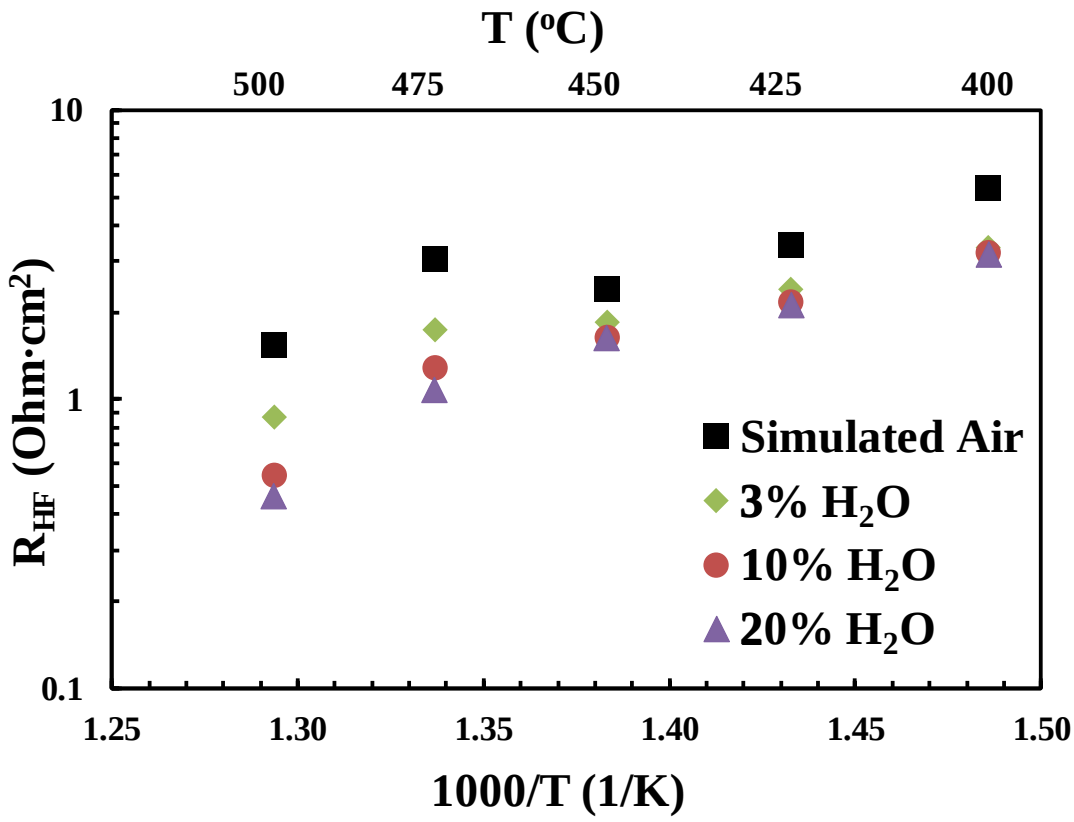

Figure 6. 9 High frequency resistance R_{HF} in dry simulated air versus that contains up to 20% moisture at temperatures from 500 to 400°C.

In addition, the increase of R_{ai} upon the introduction of 1% CO_2 into the dry simulated air, especially for the MF-LF semicircle (shown in Figure 6. 6 (b) and (c)) could be attributed to the adsorption of CO_2 on the BSCF and BZCYYb surfaces, which would substantially occupy the active surface sites for oxygen adsorption and slow down the overall reaction. On the other hand, when the oxygen electrode process shows clear separation into HF and MF-LF semicircles at lower temperature such as 450°C, the HF semicircle does not appear to be influenced much by the adsorption of CO_2 (Figure 6. 6 (c)). This is also consistent with the attribution that the HF semicircle represents the charge

transfer process. Furthermore, as summarized in Table 6.2, the CO_2 poisoning is largely recoverable upon the removal of 1% CO_2 in the dry simulated air at 650^oC, but it gets less reversible at lower temperature of 550^oC and 450^oC. This is likely due to the relative strong adsorption and high desorption temperature (>600^oC) for CO_2 on BSCF surface as reported before.[21-23]

With the presence of 3% moisture, the extent of poisoning caused by 1% CO_2 reduces and the recovery becomes much more complete, especially at lower temperature of 550^oC and 450^oC, as shown in Figure 6. and in Table 6. 1. The less extent of CO_2 poisoning, faster and more complete recovery in the presence of moisture comparing with dry condition could be attributed to the strong adsorption of moisture on the BSCF and BZCYYb surfaces, especially at lower temperature of 550^oC and 450^oC, which leads to the formation of adsorbed surface bicarbonate species (i.e., adsorbed -HCO_3) apart from typical surface carbonate (adsorbed -CO_2) on the electrode and electrolyte. According to Yan et al., the surface bicarbonate species have weaker bonding and much lower desorption temperature of ~400^oC comparing with the desorption temperature of ~600^oC for surface carbonate species. [22]

Finally, considering that the CO_2 concentration in ambient air is much lower than the 1% used in this study and there will always be some moisture in air, the results observed suggest that proton conducting IT-SOFC with BSCF cathode might be insensitive to typical CO_2 poisoning for operation at reduced temperature of ~450^oC. On the other hand, the observed apparent interfacial resistance on the order of 10-15 $\Omega \bullet cm^2$ at this temperature is still much higher than ideal. Therefore, alternative SOFC cathodes that have relatively

lower affinity for water adsorption, high activity for oxygen dissociative adsorption, as well as high proton conductivity would be promising candidates for proton conducting IT-SOFC.

6.5 Conclusions

BSCF cathode demonstrates chemical compatibility with BZCYYb proton conducting electrolyte up to 1000^{o}C and stability at 450^{o}C in air containing 3% H_2O and 1% CO_2. For a BSCF/BZCYYb/BSCF symmetrical cell, ohmic resistance R_O decreases with the introduction of moisture, which is consistent with typical hydration behavior of the BZCYYb proton conducting electrolyte. For the apparent interfacial resistance R_{ai}, the middle and low frequency (MF-LF) semicircle increases with the introduction of moisture. [20, 118, 185] Such an increase is attributed to the occupation of the BSCF electrode surface active sites by water molecules that inhibit oxygen adsorption/dissociation and surface diffusion. On the other hand, the high frequency (HF) semicircle, which corresponds to the charge transfer process in the oxygen electrode reaction, could be clearly separated at $\leq$~500^{o}C and it shows significant reduction with the introduction of moisture. Such a phenomenon is hypothesized to be related to the intrinsically faster charge transfer process involving proton vs the conventional pathway involving only oxide ion and/or the greater availability of reactant, in particular adsorbed water $H_2O_{(ads)}$, for the reverse reaction of the charge transfer step in the oxygen electrode reaction over the proton conducting electrolyte. On the other hand, introducing 1% CO_2 to simulated air causes obvious poisoning for the BSCF/BZCYYb/BSCF symmetrical cell. While CO_2 poisoning

becomes less reversible at lower temperature, the presence of moisture helps reduce the extent of CO_2 poisoning and improves the reversibility especially at reduced temperatures of 450^oC. This is attributed to the co-adsorption of H_2O and CO_2 on BSCF and BZCYYb surfaces, as well as the formation of bicarbonates on surfaces, which tend to bond weaker and desorb at lower temperature comparing with surface carbonate species. Considering water molecules adsorb strongly on BSCF at ~450^oC and below, which tends to interfere with the oxygen adsorption as shown in this study, designing alternative cathodes with reduced tendency for water adsorption while maintaining fast oxygen adsorption and high proton conductivity appears to be a promising direction in the future development of cathodes for proton conducting IT-SOFC.

7 Chapter VII: Summary

7.1 Anode for Proton Conducing IT-SOFC

The present study investigated the H_2S and CO_2 poisoning effects on the Ni-BZCYYb cermet anode of proton conducting IT-SOFC, and the major conclusions are listed below:

- PC-SOFC, especially the electrolyte-supported full cell and anode symmetrical cell with thin anode, show small but observable poisoning effect with increase in interfacial resistance R_{ai} and no change in ohmic resistance R_O upon the introduction of low-ppm level H_2S to H_2 in the range of 750 to 450^oC
- The extent of anode H_2S poisoning is much smaller for PC-SOFC compared to conventional OC-SOFC, and this is attributed to the fact that the anode reaction route for PC-SOFC involves only proton incorporation and no water evolution, which is very different from conventional OC-SOFC
- The displayed significantly less anode sulfur poisoning for PC-SOFC also implies that proton conducting ceramic (PCC) electrolyte might play an important (electro-) catalytic role in the anode reaction for PC-SOFC, and helps maintain the reaction rate upon exposure to low-ppm level H_2S
- No bulk sulfide phases was revealed by characterization techniques such as XRD and EDS for the post low ppm-level H_2S exposure sample, while surface sensitive technique of SIMS suggests a strong association between Ba species and S species that persists into the bulk of the Ni-BZCYYb mixture, indicating the possible incorporation or dissolution of sulfur into the BZCYYb

- Low-percentage level CO_2 shows similar poisoning effect as low-ppm level H_2S on all three types of PC-SOFC at temperature in the range of 550 to 750^oC, with no change in electrolyte ohmic resistance R_O while observable increase in electrode interfacial resistance R_{ai} was limited to the mid-to-low frequency (MF-LF) semicircles.

- The observed poisoning behaviors of proton conducting SOFC by low-percentage level of CO_2 at higher temperature can be attributed to the strong adsorption of CO_2 species on the highly basic BZCYYb electrolyte surface, which interferes with the sub-steps of hydrogen adsorption and surface diffusion in the anode reaction for PC-SOFC. On the other hand, with decrease in temperature, the same low percentage-level CO_2 would cause bulk phase reaction with the BZCYYb electrolyte and greater poisoning effect.

- The great similarity of the electrochemical behaviors of proton conducting SOFC upon exposure to H_2S and CO_2 fuel contaminants, despite their different affinity to Ni catalyst, suggest PCC (BZCYYb in this study) might play an electrocatalytic role ed in the anode reaction for PC-SOFC

- Future studies using different tools such as anode patterned electrode cells and more in-depth materials characterizations will be needed to fully reveal the H_2S and CO_2 poisoning mechanism and the exact roles of PCC for proton conducting SOFC.

7.2 Cathode for Proton Conducting IT-SOFC

Ag, LSCF, LSCF-BZCYYb composite, and BSCF were evaluated as cathodes for PC-SOFC using cathode symmetrical cells under various pO_2 and pH_2O at 650-450^oC. In addition, the H_2O and CO_2 effect on the BSCF cathode was also studied based on PC-SOFC cathode symmetrical cells. The major conclusions are listed below:

- For Ag, LSCF, LSCF-BZCYYb, and BSCF cathode symmetrical cells based on BZCYYb proton conducting ceramic electrolyte, electrode interfacial resistance R_{ai} increased with decreasing pO_2 or introduction of moisture.
- Pure LSCF does *not* behave like a good MIEC but more like an electronic conductor as Ag over the BZCYYb electrolyte, giving very high R_{ai} and R_o, suggesting sluggish cathode reaction in both dry and humidified conditions. This indicates that the oxide-ion transfer between LSCF and BZCYYb electrolyte is *not* very effective even in dry atmosphere.
- LSCF-BZCYYb composite cathode shows much lower interfacial resistance under dry conditions, which is attributed to the extended TPB area and BZCYYb networks in the electrode that transfer oxide-ion to places near the LSCF surface. However, the interfacial resistance of LSCF-BZCYYb composite cathode increased dramatically with the introduction of moisture
- BSCF electrode behaves like a good cathode in proton conducting IT-SOFC showing low R_{ai} and R_o under both dry and humidified conditions. The high frequency resistance R_{HF} of BSCF does not change with pO_2 but decreases with increasing pH_2O, which is attributed to the intrinsically faster charge transfer step for the oxygen electrode

reaction via the proton route than the oxide ion route. On the other hand, the overall R_{ai}, especially the MF-LF semicircles increase with the introduction of moisture. Such increase was attributed to the occupation of the BSCF electrode surface active sites by water molecules that inhibit oxygen adsorption/dissociation and surface diffusion steps in cathode reaction

- BSCF cathode shows obvious poisoning effect upon the introduction of 1% CO_2 and the poisoning effect becomes less reversible at lower temperature. On the other hand, the presence of moisture helps reduce the extent of CO_2 poisoning and improves the reversibility, which is attributed to the co-adsorption of H_2O and CO_2 on BSCF and BZCYYb surfaces, as well as the formation of bicarbonates on surfaces that tends to bond weaker and desorb at lower temperature

- Future work focusing on improving cathode microstructure for the proton conducting cathode is needed. On the other hand, research aimed at designing of cathodes with reduced tendency for water adsorption while maintaining fast oxygen adsorption and high proton conductivity should be carried out.

References

1. Badwal, S.P.S. and K. Foger, *Solid oxide electrolyte fuel cell review.* Ceramics International, 1996. **22**(3): p. 257-265.

2. Hammou, A. and J. Guindet, *Solid oxide fuel cells.* The CRC Handbook of Solid State Electrochemistry, 1997: p. 407.

3. Singhal, S.C., *Advances in solid oxide fuel cell technology.* Solid State Ionics, 2000. **135**(1-4): p. 305-313.

4. Yamamoto, O., *Solid oxide fuel cells: fundamental aspects and prospects.* Electrochimica Acta, 2000. **45**(15-16): p. 2423-2435.

5. Singhal, S.C., *Solid oxide fuel cells for stationary, mobile, and military applications.* Solid State Ionics, 2002. **152**: p. 405-410.

6. Stambouli, A.B. and E. Traversa, *Solid oxide fuel cells (SOFCs): a review of an environmentally clean and efficient source of energy.* Renewable and sustainable energy reviews, 2002. **6**(5): p. 433-455.

7. Ormerod, R.M., *Solid oxide fuel cells.* Chemical Society Reviews, 2003. **32**(1): p. 17-28.

8. Minh, N.Q., *Solid oxide fuel cell technology—features and applications.* Solid State Ionics, 2004. **174**(1-4): p. 271-277.

9. Mahato, N., et al., *Progress in material selection for solid oxide fuel cell technology: A review.* Progress in Materials Science, 2015. **72**: p. 141-337.

10. Fergus, J., et al., *Solid oxide fuel cells: materials properties and performance*. 2016: CRC press.

11. Singhal, S.C. and K. Kendall, *High-temperature solid oxide fuel cells: fundamentals, design and applications*. 2003: Elsevier.

12. Wachsman, E.D. and K.T. Lee, *Lowering the temperature of solid oxide fuel cells.* Science (New York, N.Y.), 2011. **334**(6058): p. 935-939.

13. Brett, D.J.L., et al., *Intermediate temperature solid oxide fuel cells.* Chemical Society Reviews, 2008. **37**(8): p. 1568-1578.

14. Jacobson, A.J., *Materials for solid oxide fuel cells.* Chemistry of Materials, 2009. **22**(3): p. 660-674.

15. Yang, L., et al., *Enhanced sulfur and coking tolerance of a mixed ion conductor for SOFCs: BaZr(0.1)Ce(0.7)Y(0.2-x)Yb(x)O(3-delta).* Science (New York, N.Y.), 2009. **326**(5949): p. 126-129.

16. Hirabayashi, D., et al., *Solid oxide fuel cells operating without using an anode material.* Solid State Ionics, 2004. **168**(1-2): p. 23-29.

17. Tomita, A., et al., *Chemical and redox stabilities of a solid oxide fuel cell with BaCe0. 8Y0. 2O3− α functioning as an electrolyte and as an anode.* Solid State Ionics, 2006. **177**(33-34): p. 2951-2956.

18. Goodenough, J.B. and Y.-H. Huang, *Alternative anode materials for solid oxide fuel cells.* Journal of Power Sources, 2007. **173**(1): p. 1-10.

19. Li, M., et al., *BaZr0. 1Ce0. 7Y0. 1Yb0. 1O3− δ as highly active and carbon tolerant anode for direct hydrocarbon solid oxide fuel cells.* International Journal of Hydrogen Energy, 2014. **39**(28): p. 15975-15981.

20. Grimaud, A., et al., *Hydration properties and rate determining steps of the oxygen reduction reaction of perovskite-related oxides as H -SOFC cathodes.* Journal of the Electrochemical Society, 2012. **159**(6): p. B694.

21. Yan, A., et al., *Investigation of a Ba 0.5 Sr 0.5 Co 0.8 Fe 0.2 O 3− δ based cathode IT-SOFC: I. The effect of CO2 on the cell performance.* Applied Catalysis B: Environmental, 2006. **66**(1): p. 64-71.

22. Yan, A., et al., *Investigation of a Ba 0.5 Sr 0.5 Co 0.8 Fe 0.2 O 3− δ based cathode SOFC: II. The effect of CO2 on the chemical stability.* Applied Catalysis B: Environmental, 2007. **76**(3): p. 320-327.

23. Yan, A., et al., *A temperature programmed desorption investigation on the interaction of Ba 0.5 Sr 0.5 Co 0.8 Fe 0.2 O 3− δ perovskite oxides with CO 2 in the absence and presence of H 2 O and O 2.* Applied Catalysis B: Environmental, 2008. **80**(1): p. 24-31.

24. Brigham, R.J., H. Neumayer, and J.S. Kirkaldy, *Solubility limit for sulphur in nickel between 637 and 1400 C.* Canadian Metallurgical Quarterly, 1970. **9**(4): p. 525-529.

25. Bartholomew, C.H., P.K. Agrawal, and J.R. Katzer, *Sulfur poisoning of metals.* Advances in catalysis, 1982. **31**: p. 135-242.

26. Sasaki, K., et al., *H2S poisoning of solid oxide fuel cells.* Journal of the Electrochemical Society, 2006. **153**(11): p. A2029.

27. Cheng, Z., S. Zha, and M. Liu, *Influence of cell voltage and current on sulfur poisoning behavior of solid oxide fuel cells.* Journal of Power Sources, 2007. **172**(2): p. 688-693.

28. Wang, J.-H. and M. Liu, *Computational study of sulfur–nickel interactions: A new S–Ni phase diagram.* Electrochemistry Communications, 2007. **9**(9): p. 2212-2217.

29. Zha, S., Z. Cheng, and M. Liu, *Sulfur poisoning and regeneration of Ni-based anodes in solid oxide fuel cells.* Journal of the Electrochemical Society, 2007. **154**(2): p. B206.

30. Hansen, J.B.g., *Correlating sulfur poisoning of SOFC nickel anodes by a Temkin isotherm.* Electrochemical and Solid-State Letters, 2008. **11**(10): p. B180.

31. Lussier, A., et al., *Mechanism for SOFC anode degradation from hydrogen sulfide exposure.* International Journal of Hydrogen Energy, 2008. **33**(14): p. 3945-3951.

32. Offer, G.J., et al., *Thermodynamics and kinetics of the interaction of carbon and sulfur with solid oxide fuel cell anodes.* Journal of the American Ceramic Society, 2009. **92**(4): p. 763-780.

33. Rasmussen, J.F.B. and A. Hagen, *The effect of H2S on the performance of Ni–YSZ anodes in solid oxide fuel cells.* Journal of Power Sources, 2009. **191**(2): p. 534-541.

34. Rasmussen, J.F.B. and A. Hagen, *The effect of H2S on the performance of SOFCs using methane containing fuel.* Fuel Cells, 2010. **10**(6): p. 1135-1142.

35. Yang, L., et al., *New insights into sulfur poisoning behavior of Ni-YSZ anode from long-term operation of anode-supported SOFCs.* Energy & Environmental Science, 2010. **3**(11): p. 1804-1809.

36. Papurello, D., et al., *Sulfur poisoning in Ni-anode solid oxide fuel cells (SOFCs): deactivation in single cells and a stack.* Chemical Engineering Journal, 2016. **283**: p. 1224-1233.

37. Papurello, D. and A. Lanzini, *SOFC single cells fed by biogas: Experimental tests with trace contaminants.* Waste Management, 2018. **72**: p. 306-312.

38. Sun, S., O. Awadallah, and Z. Cheng, *Poisoning of Ni-Based anode for proton conducting SOFC by H 2 S, CO 2, and H 2 O as fuel contaminants.* Journal of Power Sources, 2018. **378**: p. 255-263.

39. Abudula, A., et al., *Oxidation mechanism and effective anode thickness of SOFC for dry methane fuel.* Solid State Ionics, 1996. **86**: p. 1203-1209.

40. Ferrari, A.C. and J. Robertson, *Interpretation of Raman spectra of disordered and amorphous carbon.* Physical review B, 2000. **61**(20): p. 14095.

41. Tu, C.S., et al., *Thermal stability of Ba (Zr 0.8− x Ce x Y 0.2) O 2.9 ceramics in carbon dioxide.* Journal of Applied Physics, 2009. **105**(10): p. 103504.

42. Ishiyama, T., et al., *Decomposition reaction of BaZr0. 1Ce0. 7Y0. 1Yb0. 1O3− δ in carbon dioxide atmosphere with nickel sintering aid.* Journal of the Ceramic Society of Japan, 2017. **125**(4): p. 247-251.

43. Badwal, S. *Materials for solid oxide fuel cells*. in *Materials Forum*. 1997.

44. Brandon, N.P., S. Skinner, and B.C.H. Steele, *Recent advances in materials for fuel cells.* Annual Review of Materials Research, 2003. **33**(1): p. 183-213.

45. Zhu, W.Z. and S.C. Deevi, *Development of interconnect materials for solid oxide fuel cells.* Materials Science and Engineering: A, 2003. **348**(1-2): p. 227-243.

46. Fergus, J.W., *Lanthanum chromite-based materials for solid oxide fuel cell interconnects.* Solid State Ionics, 2004. **171**(1-2): p. 1-15.

47. Minh, N.Q., *Ceramic fuel cells.* Journal of the American Ceramic Society, 1993. **76**(3): p. 563-588.

48. Tsai, T. and S.A. Barnett, *Effect of LSM-YSZ cathode on thin-electrolyte solid oxide fuel cell performance.* Solid State Ionics, 1997. **93**(3-4): p. 207-217.

49. Yokokawa, H., et al., *Fundamental mechanisms limiting solid oxide fuel cell durability.* Journal of Power Sources, 2008. **182**(2): p. 400-412.

50. Lefebvre-Joud, F., G. Gauthier, and J. Mougin, *Current status of proton-conducting solid oxide fuel cells development.* Journal of Applied Electrochemistry, 2009. **39**(4): p. 535-543.

51. Männer, R., et al., *CHARACTERISATION OF YSZ ELECTROLYTE MATERIALS WITH VARIOUS YTTRIA CONTENTS.* 1991. **3**: p. 2085-2089.

52. Minh, N.Q. and T. Takahashi, *Science and technology of ceramic fuel cells*. 1995: Elsevier.

53. Baumard, J. and P.i. Abelard, *Defect structure and transport properties of ZrO 2-based solid electrolytes*, in *Science and technology of zirconia II*. 1983.

54. Rühle, M., N. Claussen, and A.H. Heuer, *Science and technology of zirconia II*. Vol. 12. 1984: American Ceramic Society.

55. Murakami, S., et al. *A study on Composite Anode of Solid Oxide Fuel Cells*. in *Proc. of the International Symposium on Solid Oxide Fuel Cells, Science House, Tokyo, Japan*. 1990.

56. Easler, T., et al., *Electrode Development for Monolithic Fuel Cells.* 1986: p. 72-5.

57. MAJUMDAR, S., T. CLAAR, and B.J.J.o.t.A.C.S. FLANDERMEYER, *Stress and fracture behavior of monolithic fuel cell tapes.* 1986. **69**(8): p. 628-633.

58. Dees, D., et al., *Conductivity of Porous Ni/ZrO2 ‐ Y 2 O 3 Cermets.* 1987. **134**(9): p. 2141-2146.

59. Yamamoto, O., et al., *Perovskite-type oxides as oxygen electrodes for high temperature oxide fuel cells.* 1987. **22**(2-3): p. 241-246.

60. Inoue, T., et al., *Cathode and anode materials and the reaction kinetics for the solid oxide fuel cell.* 1990. **40**: p. 407-410.

61. Princivalle, A. and E. Djurado, *Nanostructured LSM/YSZ composite cathodes for IT-SOFC: A comprehensive microstructural study by electrostatic spray deposition.* Solid State Ionics, 2008. **179**(33-34): p. 1921-1928.

62. Hammouche, A., E. Schouler, and M.J.S.S.I. Henault, *Electrical and thermal properties of Sr-doped lanthanum manganites.* 1988. **28**: p. 1205-1207.

63. KATAYAMA, K., et al., *Sintering and Electrical Conductivity of La1-XSrXMnO3.* 1989. **97**(1131): p. 1327-1333.

64. Hashimoto, T., et al., *Electrical resistivity and Seebeck coefficient of La 1− x M x MnO 3 (M= Ca, Sr) single crystals.* 1988. **23**(3): p. 1102-1105.

65. Kertesz, M., et al., *Structure and electrical conductivity of La0. 84Sr0. 16MnO3.* 1982. **42**(2): p. 125-129.

66. Kuo, J., H. Anderson, and D.J.J.o.s.s.c. Sparlin, *Oxidation-reduction behavior of undoped and Sr-doped LaMnO3: Defect structure, electrical conductivity, and thermoelectric power.* 1990. **87**(1): p. 55-63.

67. Hwang, H.J., et al., *Electrochemical performance of LSCF-based composite cathodes for intermediate temperature SOFCs.* Journal of Power Sources, 2005. **145**(2): p. 243-248.

68. Tietz, F., et al., *Performance of LSCF cathodes in cell tests.* Journal of Power Sources, 2006. **156**(1): p. 20-22.

69. Liu, M., et al., *Enhanced performance of LSCF cathode through surface modification.* International Journal of Hydrogen Energy, 2012. **37**(10): p. 8613-8620.

70. Shao, Z. and S.M. Haile, *A high-performance cathode for the next generation of solid-oxide fuel cells.* Nature, 2004. **431**(7005): p. 170-173.

71. Lee, S., et al., *Ba 0.5 Sr 0.5 Co 0.8 Fe 0.2 O 3− δ (BSCF) and La 0.6 Ba 0.4 Co 0.2 Fe 0.8 O 3− δ (LBCF) cathodes prepared by combined citrate-EDTA method for IT-SOFCs.* Journal of Power Sources, 2006. **157**(2): p. 848-854.

72. Lin, Y., et al., *Evaluation of Ba 0.5 Sr 0.5 Co 0.8 Fe 0.2 O 3− δ as a potential cathode for an anode-supported proton-conducting solid-oxide fuel cell.* Journal of Power Sources, 2008. **180**(1): p. 15-22.

73. Zhao, H., et al., *Preparation and properties of Ba x Sr 1− x Co y Fe 1− y O 3− δ cathode material for intermediate temperature solid oxide fuel cells.* Journal of Power Sources, 2008. **182**(2): p. 503-509.

74. Zhou, W., et al., *Evaluation of A-site cation-deficient (Ba0. 5Sr0. 5) 1− xCo0. 8Fe0. 2O3− δ (x> 0) perovskite as a solid-oxide fuel cell cathode.* Journal of Power Sources, 2008. **182**(1): p. 24-31.

75. Zhu, B., et al., *Intermediate-temperature proton-conducting fuel cells—present experience and future opportunities.* Solid State Ionics, 1999. **125**(1-4): p. 439-446.

76. Iwahara, H., *Technological challenges in the application of proton conducting ceramics.* Solid State Ionics, 1995. **77**: p. 289-298.

77. Iwahara, H., *Proton conducting ceramics and their applications.* Solid State Ionics, 1996. **86**: p. 9-15.

78. Kreuer, K.D., *On the development of proton conducting materials for technological applications.* Solid State Ionics, 1997. **97**(1-4): p. 1-15.

79. Katahira, K., et al., *Protonic conduction in Zr-substituted BaCeO 3.* Solid State Ionics, 2000. **138**(1): p. 91-98.

80. Hassan, D., S. Janes, and R. Clasen, *Proton-conducting ceramics as electrode/electrolyte materials for SOFC's—part I: preparation, mechanical and thermal properties of sintered bodies.* Journal of the European Ceramic Society, 2003. **23**(2): p. 221-228.

81. Kreuer, K.D., *Proton-conducting oxides.* Annual Review of Materials Research, 2003. **33**(1): p. 333-359.

82. Fergus, J.W., *Electrolytes for solid oxide fuel cells.* Journal of Power Sources, 2006. **162**(1): p. 30-40.

83. Ding, H., Y. Xie, and X. Xue, *Electrochemical performance of BaZr 0.1 Ce 0.7 Y 0.1 Yb 0.1 O 3− δ electrolyte based proton-conducting SOFC solid oxide fuel cell with layered perovskite PrBaCo 2 O 5 δ cathode.* Journal of Power Sources, 2011. **196**(5): p. 2602-2607.

84. Tauer, T., R. O'Hayre, and J.W. Medlin, *A theoretical study of the influence of dopant concentration on the hydration properties of yttrium-doped barium cerate.* Solid State Ionics, 2011. **204**: p. 27-34.

85. Nguyen, N.T.Q. and H.H. Yoon, *Preparation and evaluation of BaZr 0.1 Ce 0.7 Y 0.1 Yb 0.1 O 3− δ (BZCYYb) electrolyte and BZCYYb-based solid oxide fuel cells.* Journal of Power Sources, 2013. **231**: p. 213-218.

86. Yoo, Y. and N. Lim, *Performance and stability of proton conducting solid oxide fuel cells based on yttrium-doped barium cerate-zirconate thin-film electrolyte.* Journal of Power Sources, 2013. **229**: p. 48-57.

87. Zhou, X., et al., *Ionic conductivity, sintering and thermal expansion behaviors of mixed ion conductor BaZr 0.1 Ce 0.7 Y 0.1 Yb 0.1 O 3− δ prepared by ethylene diamine tetraacetic acid assisted glycine nitrate process.* Journal of Power Sources, 2011. **196**(11): p. 5000-5006.

88. Rainwater, B.H., *Electrical properties of BaZr0. 1Ce0. 7Y0. 1Yb0. 1O3-δ and its application in intermediate temperature solid oxide fuel cells.* 2012.

89. VahidMohammadi, A. and Z. Cheng, *Fundamentals of Synthesis, Sintering Issues, and Chemical Stability of BaZr0. 1Ce0. 7Y0. 1Yb0. 1O3-δ Proton Conducting Electrolyte for SOFCs.* Journal of the Electrochemical Society, 2015. **162**(8): p. F811.

90. Dahl, P.I., et al., *Synthesis, densification and electrical properties of strontium cerate ceramics.* Journal of the European Ceramic Society, 2007. **27**(16): p. 4461-4471.

91. Münch, W., et al., *A quantum molecular dynamics study of proton conduction phenomena in BaCeO3.* Solid State Ionics, 1996. **86**: p. 647-652.

92. Zhou, W. and Z.J.N.E. Shao, *Fuel cells: hydrogen induced insulation.* 2016. **1**(6): p. 16078.

93. Fabbri, E., et al., *Composite cathodes for proton conducting electrolytes.* 2009. **9**(2): p. 128-138.

94. Kilner, J.A. and M. Burriel, *Materials for intermediate-temperature solid-oxide fuel cells.* Annual Review of Materials Research, 2014. **44**: p. 365-393.

95. Jiang, S.P. and S.P.S. Badwal, *Hydrogen oxidation at the nickel and platinum electrodes on yttria‐tetragonal zirconia electrolyte.* Journal of the Electrochemical Society, 1997. **144**(11): p. 3777-3784.

96. Jiang, S.P. and S.P.S. Badwal, *An electrode kinetics study of H 2 oxidation on Ni/Y 2 O 3–ZrO 2 cermet electrode of the solid oxide fuel cell.* Solid State Ionics, 1999. **123**(1): p. 209-224.

97. Holtappels, P., L.G.J. De Haart, and U. Stimming, *Reaction of Hydrogen/Water Mixtures on Nickel‐Zirconia Cermet Electrodes: I. DC Polarization*

Characteristics. Journal of the Electrochemical Society, 1999. **146**(5): p. 1620-1625.

98. Holtappels, P., et al., *Reaction of Hydrogen/Water Mixtures on Nickel - Zirconia Cermet Electrodes: II. AC Polarization Characteristics.* Journal of the Electrochemical Society, 1999. **146**(8): p. 2976-2982.

99. Norby, T., et al., *Hydrogen in oxides.* Dalton transactions, 2004(19): p. 3012-3018.

100. Fang, S., et al., *Chemical stability and hydrogen permeation performance of Ni–BaZr0. 1Ce0. 7Y0. 2O3− δ in an H2S-containing atmosphere.* Journal of Power Sources, 2008. **183**(1): p. 126-132.

101. Fang, S., et al., *H2S poisoning and regeneration of Ni–BaZr0. 1Ce0. 7Y0. 2O3− δ at intermediate temperature.* 2009. **475**(1-2): p. 935-939.

102. Li, J., et al., *Chemical stability of Y-doped Ba (Ce, Zr) O3 perovskites in H2S-containing H2.* 2008. **53**(10): p. 3701-3707.

103. Wang, J.-H., M. Liu, and Z. Cheng, *Anodes*, in *Solid Oxide Fuel Cells: Materials Properties and Performance*. 2008, CRC Press. p. 73-129.

104. Wang, S.-G., et al., *Chemisorption of CO2 on nickel surfaces.* The Journal of Physical Chemistry B, 2005. **109**(40): p. 18956-18963.

105. Zuo, C., et al., *Hydrogen Permeation and Chemical Stability of Cermet [Ni–Ba (Zr0. 8− x Ce x Y0. 2) O3] Membranes.* 2005. **8**(12): p. J35-J37.

106. Zuo, C., et al., *Effect of Zr-doping on the chemical stability and hydrogen permeation of the Ni− BaCe0. 8Y0. 2O3-α mixed protonic− electronic conductor.* 2006. **18**(19): p. 4647-4650.

107. Fang, S., et al., *Unprecedented CO2-Promoted Hydrogen Permeation in Ni-BaZr0. 1Ce0. 7Y0. 1Yb0. 1O3− δ Membrane.* 2013. **6**(1): p. 725-730.

108. Fang, S., K.S. Brinkman, and F.J.J.o.M.S. Chen, *Hydrogen permeability and chemical stability of Ni–BaZr0. 1Ce0. 7Y0. 1Yb0. 1O3− δ membrane in concentrated H2O and CO2.* 2014. **467**: p. 85-92.

109. Lee, H.Y., et al., *Active reaction sites for oxygen reduction in La0. 9Sr0. 1MnO3/YSZ electrodes.* Journal of the Electrochemical Society, 1995. **142**(8): p. 2659-2664.

110. Siebert, E., A. Hammouche, and M. Kleitz, *Impedance spectroscopy analysis of La1− xSritxMnO3-yttria-stabilized zirconia electrode kinetics.* Electrochimica Acta, 1995. **40**(11): p. 1741-1753.

111. Adler, S.B., J.A. Lane, and B.C.H. Steele, *Electrode kinetics of porous mixed‐conducting oxygen electrodes.* Journal of the Electrochemical Society, 1996. **143**(11): p. 3554-3564.

112. Mizusaki, J., T. Saito, and H. Tagawa, *A Chemical Diffusion‐Controlled Electrode Reaction at the Compact La1−x Sr x MnO3/Stabilized Zirconia Interface in Oxygen Atmospheres.* Journal of the Electrochemical Society, 1996. **143**(10): p. 3065-3073.

113. Sasaki, K., et al., *Microstructure‐property relations of solid oxide fuel cell cathodes and current collectors cathodic polarization and ohmic resistance.* Journal of the Electrochemical Society, 1996. **143**(2): p. 530-543.

114. Tanner, C.W., K.Z. Fung, and A.V. Virkar, *The effect of porous composite electrode structure on solid oxide fuel cell performance I. Theoretical analysis.* Journal of the Electrochemical Society, 1997. **144**(1): p. 21-30.

115. Van Heuveln, F.H. and H.J.M. Bouwmeester, *Electrode Properties of Sr‐Doped LaMnO3 on Yttria‐Stabilized Zirconia II. Electrode Kinetics.* Journal of the Electrochemical Society, 1997. **144**(1): p. 134-140.

116. Van Heuveln, F.H., H.J.M. Bouwmeester, and F.F. van Berkel, *Electrode Properties of Sr‐Doped LaMnO3 on Yttria‐Stabilized Zirconia I. Three‐Phase Boundary Area.* Journal of the Electrochemical Society, 1997. **144**(1): p. 126-133.

117. Horita, T., et al., *Active Sites Imaging for Oxygen Reduction at the La0. 9Sr0. 1MnO3− x/Yttria‐Stabilized Zirconia Interface by Secondary‐Ion Mass Spectrometry.* Journal of the Electrochemical Society, 1998. **145**(9): p. 3196-3202.

118. Peng, R., et al., *Cathode processes and materials for solid oxide fuel cells with proton conductors as electrolytes.* Journal of Materials Chemistry, 2010. **20**(30): p. 6218-6225.

119. Sun, C., R. Hui, and J. Roller, *Cathode materials for solid oxide fuel cells: a review.* Journal of Solid State Electrochemistry, 2010. **14**(7): p. 1125-1144.

120. Choi, Y., M.e.C. Lin, and M. Liu, *Computational study on the catalytic mechanism of oxygen reduction on La0. 5Sr0. 5MnO3 in solid oxide fuel cells.* Angewandte Chemie International Edition, 2007. **46**(38): p. 7214-7219.

121. Yang, L., et al., *A mixed proton, oxygen ion, and electron conducting cathode for SOFCs based on oxide proton conductors.* Journal of Power Sources, 2010. **195**(2): p. 471-474.

122. Poetzsch, D., R. Merkle, and J. Maier, *Proton conductivity in mixed-conducting BSFZ perovskite from thermogravimetric relaxation.* Physical Chemistry Chemical Physics, 2014. **16**(31): p. 16446-16453.

123. Hu, H. and M. Liu, *Interfacial studies of solid-state cells based on electrolytes of mixed ionic–electronic conductors.* Solid State Ionics, 1998. **109**(3): p. 259-272.

124. Fleig, J., *Solid oxide fuel cell cathodes: Polarization mechanisms and modeling of the electrochemical performance.* Annual Review of Materials Research, 2003. **33**(1): p. 361-382.

125. Zhao, H., et al., *New cathode materials for ITSOFC: phase stability, oxygen exchange and cathode properties of La2− xNiO4 δ.* Solid State Ionics, 2008. **179**(35-36): p. 2000-2005.

126. Hibino, T., et al., *A solid oxide fuel cell using Y-doped BaCeO3 with Pd-loaded FeO anode and Ba0. 5Pr0. 5CoO3 cathode at low temperatures.* Journal of the Electrochemical Society, 2002. **149**(11): p. A1508.

127. Kim, J., et al., *Triple‐conducting layered perovskites as cathode materials for proton‐conducting solid oxide fuel cells.* ChemSusChem, 2014. **7**(10): p. 2811-2815.

128. Taherparvar, H., et al., *Effect of humidification at anode and cathode in proton-conducting SOFCs.* 2003. **162**: p. 297-303.

129. Potter, A. and R.J.S.S.I. Baker, *Impedance studies on Pt| SrCe0. 95Yb0. 05O3| Pt under dried and humidified air, argon and hydrogen.* 2006. **177**(19-25): p. 1917-1924.

130. Akimune, Y., et al., *Nano-Ag particles for electrodes in a yttria-doped BaCeO3 protonic conductor.* 2007. **178**(7-10): p. 575-579.

131. Lim, D.-K., et al., *Performance of proton-conducting ceramic-electrolyte fuel cell with BZCY40 electrolyte and BSCF5582 cathode.* 2016. **42**(3): p. 3776-3785.

132. Shang, M., J. Tong, and R.J.R.A. O'Hayre, *A promising cathode for intermediate temperature protonic ceramic fuel cells: BaCo 0.4 Fe 0.4 Zr 0.2 O 3− δ.* 2013. **3**(36): p. 15769-15775.

133. Duan, C., et al., *Readily processed protonic ceramic fuel cells with high performance at low temperatures.* Science, 2015. **349**(6254): p. 1321-1326.

134. Sammells, A.F., et al., *Rational selection of advanced solid electrolytes for intermediate temperature fuel cells.* Solid State Ionics, 1992. **52**(1-3): p. 111-123.

135. Park, S., J.M. Vohs, and R.J. Gorte, *Direct oxidation of hydrocarbons in a solid-oxide fuel cell.* Nature, 2000. **404**(6775): p. 265-267.

136. Steele, B.C.H., *Appraisal of Ce 1− y Gd y O 2− y/2 electrolytes for IT-SOFC operation at 500 C.* Solid State Ionics, 2000. **129**(1): p. 95-110.

137. Cheng, Z., et al., *From Ni-YSZ to sulfur-tolerant anode materials for SOFCs: electrochemical behavior, in situ characterization, modeling, and future perspectives.* Energy & Environmental Science, 2011. **4**(11): p. 4380-4409.

138. Matsuzaki, Y. and I. Yasuda, *The poisoning effect of sulfur-containing impurity gas on a SOFC anode: Part I. Dependence on temperature, time, and impurity concentration.* Solid State Ionics, 2000. **132**(3): p. 261-269.

139. Zhou, W., et al., *LSCF Nanopowder from Cellulose‐Glycine‐Nitrate Process and its Application in Intermediate‐Temperature Solid‐Oxide Fuel Cells.* Journal of the American Ceramic Society, 2008. **91**(4): p. 1155-1162.

140. Cheng, Z., *No title.* Investigations into the interactions between sulfur and anodes for solid oxide fuel cells, 2008.

141. He, H., R.J. Gorte, and J.M. Vohs, *Highly sulfur tolerant Cu-ceria anodes for SOFCs.* Electrochemical and Solid-State Letters, 2005. **8**(6): p. A280.

142. Duan, C., et al., *Highly durable, coking and sulfur tolerant, fuel-flexible protonic ceramic fuel cells.* Nature, 2018. **557**(7704): p. 217.

143. Xia, C., F. Chen, and M. Liu, *Reduced-temperature solid oxide fuel cells fabricated by screen printing.* Electrochemical and Solid-State Letters, 2001. **4**(5): p. A54.

144. Leng, Y.J., et al., *Low-temperature SOFC with thin film GDC electrolyte prepared in situ by solid-state reaction.* Solid State Ionics, 2004. **170**(1): p. 9-15.

145. Gorte, R.J., H. Kim, and J.M. Vohs, *Novel SOFC anodes for the direct electrochemical oxidation of hydrocarbon.* Journal of Power Sources, 2002. **106**(1): p. 10-15.

146. Devianto, H., et al., *The effect of a ceria coating on the H2S tolerance of a molten carbonate fuel cell.* Journal of Power Sources, 2006. **159**(2): p. 1147-1152.

147. Gong, M., et al., *Sulfur-tolerant anode materials for solid oxide fuel cell application.* Journal of Power Sources, 2007. **168**(2): p. 289-298.

148. Jiang, S.P. and S.H. Chan, *A review of anode materials development in solid oxide fuel cells.* Journal of Materials Science, 2004. **39**(14): p. 4405-4439.

149. McIntosh, S. and R.J. Gorte, *Direct hydrocarbon solid oxide fuel cells.* Chemical reviews, 2004. **104**(10): p. 4845-4866.

150. Zuo, C., et al., *Ba (Zr0. 1Ce0. 7Y0. 2) O3‐δ as an Electrolyte for Low‐Temperature Solid‐Oxide Fuel Cells.* Advanced Materials, 2006. **18**(24): p. 3318-3320.

151. Weber, W.H., K.C. Hass, and J.R. McBride, *Raman study of CeO 2: second-order scattering, lattice dynamics, and particle-size effects.* Physical Review B, 1993. **48**(1): p. 178.

152. Ratnasamy, C. and J.P. Wagner, *Water gas shift catalysis.* Catalysis Reviews, 2009. **51**(3): p. 325-440.

153. Dusastre, V. and J.A. Kilner, *Optimisation of composite cathodes for intermediate temperature SOFC applications.* Solid State Ionics, 1999. **126**(1-2): p. 163-174.

154. Zhou, W., R. Ran, and Z. Shao, *Progress in understanding and development of Ba 0.5 Sr 0.5 Co 0.8 Fe 0.2 O 3− δ-based cathodes for intermediate-temperature solid-oxide fuel cells: a review.* Journal of Power Sources, 2009. **192**(2): p. 231-246.

155. Bi, L., et al., *Proton-conducting solid oxide fuel cells prepared by a single step co-firing process.* 2009. **191**(2): p. 428-432.

156. Lim, D.-K., et al., *Study of Hydration/Dehydration Kinetics of SOFC Cathode Material Ba0. 5Sr0. 5Co0. 8Fe0. 2O3-δ by Electrical Conductivity Relaxation Technique.* Journal of the Electrochemical Society, 2013. **160**(8): p. F768.

157. Sun, S. and Z. Cheng, *Effects of H2O and CO2 on Electrochemical Behaviors of BSCF Cathode for Proton Conducting IT-SOFC.* Journal of the Electrochemical Society, 2017. **164**(2): p. F88.

158. Chick, L., *Novel Glycine-Nitrate Process Produces Ultrafine Oxide Ceramic Powders.* Materials and Processing Report, 1990. **5**(8): p. 1-3.

159. Hu, H. and M. Liu, *Interfacial Polarization Characteristics of Pt| BaCe0. 8Gd0. 2 O 3| Pt Cells at Intermediate Temperatures.* Journal of the Electrochemical Society, 1997. **144**(10): p. 3561-3567.

160. Lou, X., et al., *Improving La 0.6 Sr 0.4 Co 0.2 Fe 0.8 O 3− δ cathode performance by infiltration of a Sm 0.5 Sr 0.5 CoO 3− δ coating.* Solid State Ionics, 2009. **180**(23): p. 1285-1289.

161. Nie, L., et al., *La 0.6 Sr 0.4 Co 0.2 Fe 0.8 O 3− δ cathodes infiltrated with samarium-doped cerium oxide for solid oxide fuel cells.* Journal of Power Sources, 2010. **195**(15): p. 4704-4708.

162. Baumann, S., et al., *Influence of sintering conditions on microstructure and oxygen permeation of Ba 0.5 Sr 0.5 Co 0.8 Fe 0.2 O 3− δ (BSCF) oxygen transport membranes.* Journal of Membrane Science, 2010. **359**(1): p. 102-109.

163. Poetzsch, D., R. Merkle, and J. Maier, *Oxygen Reduction at Dense Thin-Film Microelectrodes on a Proton-Conducting Electrolyte I. Considerations on Reaction Mechanism and Electronic Leakage Effects.* Journal of the Electrochemical Society, 2015. **162**(9): p. F950.

164. Jamale, A.P., C.H. Bhosale, and L.D. Jadhav, *Electrochemical behavior of LSCF/GDC interface in symmetric cell: An application in solid oxide fuel cells.* Journal of Alloys and Compounds, 2015. **623**: p. 136-139.

165. Virkar, A.N. and H.S. Maiti, *Oxygen ion conduction in pure and yttria-doped barium cerate.* Journal of Power Sources, 1985. **14**(4): p. 295-303.

166. Ranran, P., et al., *Electrochemical properties of intermediate-temperature SOFCs based on proton conducting Sm-doped BaCeO 3 electrolyte thin film.* Solid State Ionics, 2006. **177**(3): p. 389-393.

167. Duan, C., et al., *Readily processed protonic ceramic fuel cells with high performance at low temperatures.* Science (New York, N.Y.), 2015. **349**(6254): p. 1321-1326.

168. Ding, D., et al., *Enhancing SOFC cathode performance by surface modification through infiltration.* Energy & Environmental Science, 2014. **7**(2): p. 552-575.

169. Leng, Y.J., et al., *Performance evaluation of anode-supported solid oxide fuel cells with thin film YSZ electrolyte.* International Journal of Hydrogen Energy, 2004. **29**(10): p. 1025-1033.

170. Moon, H., et al., *Development of IT-SOFC unit cells with anode-supported thin electrolytes via tape casting and co-firing.* International Journal of Hydrogen Energy, 2008. **33**(6): p. 1758-1768.

171. Matsui, T., et al., *Effects of mixed conduction on the open-circuit voltage of intermediate-temperature SOFCs based on Sm-doped ceria electrolytes.* Solid State Ionics, 2005. **176**(7): p. 663-668.

172. Chiodelli, G. and L. Malavasi, *Electrochemical open circuit voltage (OCV) characterization of SOFC materials.* Ionics, 2013. **19**(8): p. 1135-1144.

173. Ling, Y., et al., *A cobalt-free Sm 0.5 Sr 0.5 Fe 0.8 Cu 0.2 O 3− δ–Ce 0.8 Sm 0.2 O 2− δ composite cathode for proton-conducting solid oxide fuel cells.* Journal of Power Sources, 2011. **196**(5): p. 2631-2634.

174. Zhao, F., et al., *Fabrication and characterization of anode-supported micro-tubular solid oxide fuel cell based on BaZr 0.1 Ce 0.7 Y 0.1 Yb 0.1 O 3− δ electrolyte.* Journal of Power Sources, 2011. **196**(2): p. 688-691.

175. Malavasi, L., C.A.J. Fisher, and M.S. Islam, *Oxide-ion and proton conducting electrolyte materials for clean energy applications: structural and mechanistic features.* Chemical Society Reviews, 2010. **39**(11): p. 4370-4387.

176. Dailly, J., et al., *Perovskite and A 2 MO 4-type oxides as new cathode materials for protonic solid oxide fuel cells.* Electrochimica Acta, 2010. **55**(20): p. 5847-5853.

177. Fabbri, E., et al., *Electrode materials: a challenge for the exploitation of protonic solid oxide fuel cells.* 2010. **11**(4): p. 044301.

178. Fabbri, E., et al., *Towards the Next Generation of Solid Oxide Fuel Cells Operating Below 600 ° C with Chemically Stable Proton‐Conducting Electrolytes.* Advanced Materials, 2012. **24**(2): p. 195-208.

179. Jeon, S.-Y., et al., *Effectiveness of Protonic Conduction in Ba0. 5Sr0. 5Co0. 8Fe0. 2O3− δ Cathode in Intermediate Temperature Proton-Conducting Ceramic-Electrolyte Fuel Cell.* Journal of the Electrochemical Society, 2014. **161**(6): p. F760.

180. Liu, B. and Y. Zhang, *Ba 0.5 Sr 0.5 Co 0.8 Fe 0.2 O 3 nanopowders prepared by glycine–nitrate process for solid oxide fuel cell cathode.* Journal of Alloys and Compounds, 2008. **453**(1): p. 418-422.

181. Zhou, W., et al., *A novel efficient oxide electrode for electrocatalytic oxygen reduction at 400–600 C.* Chemical Communications, 2008(44): p. 5791-5793.

182. Andersson, A.K.E., et al., *Chemical Expansion Due to Hydration of Proton‐Conducting Perovskite Oxide Ceramics.* Journal of the American Ceramic Society, 2014. **97**(8): p. 2654-2661.

183. Mauvy, F., et al., *Electrode properties of Ln2NiO4 δ (Ln= La, Nd, Pr) AC impedance and DC polarization studies.* Journal of the Electrochemical Society, 2006. **153**(8): p. A1553.

184. Ryu, K.H. and S.M. Haile, *Chemical stability and proton conductivity of doped BaCeO 3–BaZrO 3 solid solutions.* Solid State Ionics, 1999. **125**(1): p. 355-367.

185. He, F., et al., *Cathode reaction models and performance analysis of Sm 0.5 Sr 0.5 CoO 3− δ–BaCe 0.8 Sm 0.2 O 3− δ composite cathode for solid oxide fuel cells with proton conducting electrolyte.* Journal of Power Sources, 2009. **194**(1): p. 263-268.

VITA

SHICHEN SUN

2007-2011	B.S., Materials Physics Fudan University Shanghai, China
2011-2014	Physics editor Wangxiangsiwei Publication Coporation Beijing, China
2014-2018	Research Assistant Florida International University Miami, Florida

PUBLICATIONS

1. Sun, Shichen; Cheng, Zhe. "H2S poisoning of proton conducting solid oxide fuel cell and comparison with conventional oxide-ion conducting solid oxide fuel cell," Journal of the Electrochemical Society (2018), 165 (10), F836-F844. DOI: 10.1149/2.0841810jes

2. Sun, Shichen; Awadallah, Osama; Cheng, Zhe. "Poisoning of Nickel-Based Anode for Proton Conducting SOFC by H2S, CO2, and H2O as Fuel Contaminants," Journal of Power Sources (2018), 378, 255-263. DOI:10.1016/j.jpowsour.2017.12.056

3. Sun, Shichen; Cheng, Zhe. "Electrochemical Behaviors for Ag, LSCF and BSCF as Oxygen Electrodes for Proton Conducting IT-SOFC," Journal of the Electrochemical Society (2017), 164(10), F3104-F3113. DOI:10.1149/2.0121710jes

4. Sun, Shichen; Cheng, Zhe. "Effects of H2O and CO2 on Electrochemical Behaviors of BSCF Cathode for Proton Conducting IT-SOFC," Journal of the Electrochemical Society (2017), 164(2), F81-F88. DOI:10.1149/2.0611702jes.